WOOD RESEARCH
e-ISSN 2729-8906
66(3):2021 331-340 pp.
doi.org/10.37763/wr.1336-4561/66.3.331340

EFFECTS OF POLYMER ADDITIVES ON SOME MECHANICAL AND PHYSICAL PROPERTIES OF CEMENT BONDED PARTICLEBOARDS

HASAN HÜSEYİN TAŞ
Isparta University Of Applied Sciences
Turkey

BİLGE ARSLAN
Süleyman Demirel University
Turkey

HÜLYA KALAYCIOĞLU
Karadeniz Technical University
Turkey

(Received June 2020)

ABSTRACT

The effects of some polymer additives, also called super plasticizers, on selected physical and mechanical properties of cement bonded particle board were investigated. Two different kinds of poly carboxylic ether (PF300, DX40) and a melamine based polymer (300M) were added to the wood cement mixture. The ratios of polymer additives to the wood cement mixture were 1%, 1.2% and 1.4%. Cement bonded particleboards were manufactured with wood/cement (w/w) ratio of 1:3; target density of 1300 $kg \cdot m^{-3}$, and $CaCl_2$ content of 5%. The cement bonded particleboards were tested for water absorption (2 and 24 hour), thickness swelling (2 and 24 hour), bending stiffness and strength and internal bond strength. Results of the study showed that most of the polymer addition decreased water absorption and thickness swelling of the boards. Replacement of cement with polymers increased internal bond strength and bending stiffness of the boards while bending strength was slightly reduced. Use of small amount of super plasticizers significantly improves most of the board properties.

KEYWORDS: Cement-bonded particleboard, polymer, physical , mechanical properties.

INTRODUCTION

Wood-cement boards are usually made of wood fibers or particles blended with cement and water. In order to speed up the bonding process some additives may be added to the mixture (Marteinsson and Gudmundsson 2018). They have been already in use for most of the world (Na et al. 2014). They are utilized in roofs, floors and walls as mainly replacement of adhesive bonded wood based panels. They have some peculiar advantages compared to these composites such as durability, dimensional stability, acoustic and thermal properties and low cost (Lee 1984, Ramirez-Coretti 1998, Savastano et al. 2003, Okino et al. 2005, Del Menezzi 2007). These properties make them still attractive as building materials.

Cement-bonded particleboards have been subjected to different investigations concerning utilization of different cellulosic materials, chemicals and pretreatments in order to boost cement hydration (Davies and Davies 2017). Investigations have shown that mechanical interlocking and hydrogen bonds hold wood and cement together (Frybort et al. 2008, Tonoli et al. 2013). Extractives and polysaccharides of wood are mostly responsible for the inhibition between wood and cement resulting low quality boards (Del Menezzi 2007). To overcome inhibitions, some accelerators are usually used in the mixture or some pretreatments may be applied (Moslemi et al. 1983, Lee 1984, Zhengtian and Moslemi 1985, Simatupang et al. 1987, Lee and Short 1989). The replacement of parts of cement by fumed silica in combination with super plasticizers is another approach to solve the inhibitory problem (Frybort et al. 2008). Most of the physical and mechanical properties of cement- bonded particleboards are adequate for indoor and outdoor applications (Ashori et al. 2012). Mechanical properties of cement bonded particleboard are the lowest among cement bonded wood products with comparable density which used in structural applications. Thus, its mechanical properties are intended to improve by application of reinforcement in the literature. Fibers or continuous reinforcements in a fabric form are usually utilized as the reinforcements. An industrial and cost-effective production process has not been developed for practical use of fabric reinforcements (Peled and Mobasher 2005).

Super plasticizers are chemicals used for well-dispersed particle suspension. Their addition to concrete lowers water to cement ratio, thus producing high performance concrete. In this study, some polymer additives were considered in order to improve properties of cement bonded particleboard.

MATERIAL AND METHODS

Experimental cement bonded particleboard (CBPB) measuring 13 mm x 500 mm x 500 mm with target density of 1.30 $g{\cdot}cm^{-3}$ were prepared in the laboratory. The ratio between the wood particles and cement by mass was 1:3. Amount of 5% CaCl2 based on the cement weigh was used as an accelerator. Water/cement ratio of the mixture was 0.4.

The cement used in the mixture was commercial portland cement (CEM I 42.5). Red pine (*Pinus brutia*) coarse particles which were used as core layers of commercial adhesive bonded particleboard were obtained from a local particleboard factory. Aqueous two different kinds of poly carboxylic ether super plasticizers, PF300 and DX40, and a melamine based polymer, 300M, (Draco Construction Products, Turkey) were used as a water reducer to improve cement hydration. Levels of super plasticizers were maintained at 1%, 1.2% and 1.4%, respectively, based on the weight of cement. The required amount of super plasticizer dissolved in distilled water.

Production of experimental cement bonded particleboard started with spraying water on the wood particles. Then, cement was added and mixing continued until a homogeneous

distribution. After mixing, fresh mixtures were placed within a metal frames where cured for 2 days. The amount of pressure provided during curing of the mixture was 1.8–2.0 $N \cdot mm^{-2}$. The cured boards were then left for conditioning in the laboratory climate at approximately +20°C, relative humidity 65%. Cement bonded particleboards were cut down after curing to required size in order to determine some physical and mechanical properties.

In order to determine the effects of super plasticizers on some physical and mechanical properties of the experimental boards the following tests were conducted: Water absorption and thickness swelling properties (2 and 24 hours) of the boards were determined on 50 x 50 mm samples according to EN 317. Bending stiffness (MOE) and strength (MOR) were evaluated using a three point bending test following EN 310. MOE and MOR were determined for each specimen using load–deformation curves. Internal bond strength of the 50 mm x 50 mm samples was also determined according to EN 319. Five replicates were used for each test and obtained data were subjected to an analysis of variance. Experimental results were analyzed using ANOVA tests to identify their statistical significance. Duncan's multiple range tests were performed in order to find the least significant difference between all the variables.

RESULTS AND DISCUSSION

Tab.1 shows density and moisture content (MC) of the laboratory manufacture cement bonded particleboard samples. Density of the manufactured boards ranged from 1.31 to 1.44 $g \cdot cm^{-3}$ and varied with the polymer type and amount. DX40 and PF300 yielded significantly higher densities than 300M and control groups. The amount of polymers had more profound effects on the density. Final moisture content of the manufactured boards varied between 13.43 and 15.44%. Final moisture contents of the manufactured boards were also significantly influenced by the polymer types and amount. Cement bonded particleboards manufactured without any polymer and 300M had the lower moisture content while boards manufactured with PF300 had the highest moisture content. Although small amount of cement in the mixture was replaced by polymer addition, an increase in the densities of the experimental boards has been observed. This can be explained by the inert water molecules captivated in the voids of the boards or in the cavities of the wood cells. Higher moisture content of the polymer added boards supports this idea.

Tab. 2 presents water absorption (WA) and thickness swelling (TS) values of sample boards. Water absorption (%) values of the manufactured boards was significantly affected by the type and different proportions of polymers used in the study. Water absorption values after 2 hours of soaking decreased significantly ($P < 0.001$) as the amount of polymers was increased from 1% to 1.4% (Tab. 1). PF300 had the lower water absorption while 300M had the highest. For 300M, use of higher proportion resulted lower water absorption values. Water absorption values after 24 hours of soaking are not significantly ($P < 0.001$) effected by the amount of polymers. PF300 had the lowest 24 hour water absorption values than other polymers and control group. All water absorption values of the manufactured boards are lower than those of most commercial cement bonded particleboards.

2 hour thickness swelling values of the boards was significantly influenced by polymer types, but not by the proportion of the polymers used ($P < 0.001$). Among the tested treatments, 300 M had the highest thickness swelling value. 1.5% or less of thickness swelling value is required for commercial cement bonded particleboards.

Tab 1: Density and the moisture content of the CBPB manufactured.

Polymer type	Polymer amount (%)	Density (g·cm^{-3})	MC (%)
Control	-	1.31 (0.02)*	13.99 (0.18)
PF300	1	1.36 (0.02)	14.62 (0.13)
	1.2	1.41 (0.04	14.81 (0.52)
	1.4	1.36 (0.04)	15.44 (0.66)
DX40	1	1.35 (0.02)	14.00 (0.28)
	1.2	1.34 (0.01)	15.24 (0.66)
	1.4	1.44 (0.02)	13.43 (0.17)
300M	1	1.32 (0.02)	13.68 (0.22)
	1.2	1.35 (0.03)	13.80 (0.21)
	1.4	1.32 (0.02)	13.44 (0.47)

*Values in parenthesis are standard deviations.

Tab. 2: Some physical properties of the CBPB manufactured.

Polymer type	Polymer amount (%)	Density (g.cm^{-3})	WA (2 hour) (%)	WA (24 hour) (%)	TS (2 hour) (%)	TS (24 hour) (%)
Control	-	1.31 (0.02)*	5.48 (0.42)	8.48 (1.35)	1.28 (0.17)	2.15 (0.68)
PF300	1	1.36 (0.02)	3.35 (1.40)	6.47 (3.23)	1.14 (0.17)	1.10 (0.05)
	1.2	1.41 (0.04	2.86 (0.69)	7.07 (1.65)	1.40 (0.24)	1.66 (0.31)
	1.4	1.36 (0.04)	5.44 (0.83)	9.86 (1.28)	0.79 (0.11)	1.57 (0.22)
DX40	1	1.35 (0.02)	2.74 (0.59)	6.75 (1.02)	1.31 (0.25)	1.51 (0.35)
	1.2	1.34 (0.01)	4.56 (0.20)	7.34 (0.60)	1.30 (0.30)	1.55 (0.27)
	1.4	1.44 (0.02)	5.50 (0.48)	9.15 (0.73)	1.38 (0.29)	1.63 (0.33)
300M	1	1.32 (0.02)	6.66 (1.35)	10.52 (1.10)	1.47 (0.37)	1.55 (0.30)
	1.2	1.35 (0.03)	4.64 (3.25)	10.74 (1.07)	1.63 (0.10)	1.91 (0.23)
	1.4	1.32 (0.02)	4.59 (0.34)	8.24 (1.55)	2.31 (0.24)	2.34 (0.09)

*Values in parenthesis are standard deviations.

24 hour thickness swelling (%) values of the manufactured boards was significantly affected by the type and different proportions of polymers used in the study ($P < 0.001$). Thickness swelling values after 24 hours of soaking lowered significantly as 1% use of polymers was yielded the lowest thickness swelling in general. 1% PF300 treatment may be pronounced as the most effective treatment to prevent the thickness welling of the boards.

The polymers had significantly influenced on the water absorption capacity of the cement bonded particleboards. This effect may be due to polymers capable of forming chemical bonds with the wood particles and the surface of the cement matrix. The polymers used may act as the interface bridging between wood and cement to improve adhesion. Excessive use of polymers may also blocks potential engagement of water and cement, by surrounding wood particles, thus yielding higher water absorption.

The use of 1% PF300 and DX40 lowered the 2 hour water absorption values of manufactured cement bonded boards by approximately 38% and 50%, respectively. 24 hour water absorption values of the boards were also decreased more than 20% by addition of same amount of additives. 24 hour thickness swelling values were also diminished nearly 50% by the use of 1% PF300.

According to Savastano et al. (2003) water absorption and particle content are positively

correlated. Water affinity of cement-bonded particleboards decreased with increase in cement content (Moslemi and Pfister 1987, Olorunnisola 2009). Since wood particle content held constant and cement proportion was slightly decreasing in this study, the declination in water absorption can be attributed to utilization of polymers.

In general, a higher cement content of the boards diminishes thickness swelling (Moslemi and Pfister 1987). Olorunnisola (2009) pointed out that chemical additives significantly effects water absorption capacity of the boards besides type of wood particle and wood-cement ratio. Huang and Cooper (2000) claims that more spring back during immersion in water for denser boards can be expected because of the higher compression exposed during production.

The mechanical test results including the bending and internal bond strength of cement bonded particleboard are presented in Tab. 3. In general, the bending stiffness of the cement bonded particleboards significantly affected by application of super plasticizer polymers ($P < 0.001$). While all polymers significantly increase the bending stiffness, PF300 has the greatest effect on the bending stiffness. When the proportion of polymer increases the increase of bending stiffness is higher. Use of polymers increases the bending stiffness values of the boards above the standard value of 4500 $N{\cdot}mm^{-2}$ (EN 634-2). Only treatment that lowers the bending stiffness of the cement bonded particleboard was 1% 300M.

The average bending stiffness of reference boards was 4192 $N{\cdot}mm^{-2}$ while the highest average bending stiffness of 5796 $N{\cdot}mm^{-2}$ was achieved with the application of 1.4% PF300. An increase of 38% in bending stiffness was reached with the application of polymer although the difference between the densities of the corresponding boards was only 3.8%. When an increase of 19.2% for internal bond strength of the corresponding boards also considered it can be concluded that application of polymers increases the number of hydrogen bonds within the mixture. In general, the stiffness of cement bonded boards increase with decreasing wood content (Al Rim et al. 1999) or density increase. Due to the density increase, frictional forces may also be developed between particles and the cement matrix.

Tab. 3: Some mechanical properties of the CBPB manufactured.

Polymer type	Polymer amount (%)	Density ($g{\cdot}cm^{-3}$)	MOR ($N{\cdot}mm^{-2}$)	MOE ($N{\cdot}mm^{-2}$)	IB ($N{\cdot}mm^{-2}$)
Control	-	1.31 (0.02)*	9.98 (0.36)	4192 (318)	0.83 (0.04)
PF300	1	1.36 (0.02)	9.10 (0.56)	4609 (169)	1.27 (0.05)
	1.2	1.41 (0.04	9.24 (0.54)	5368 (296)	0.99 (0.07)
	1.4	1.36 (0.04)	8.24 (0.31)	5796 (388)	0.99 (0.07)
DX40	1	1.35 (0.02)	7.09 (0.54)	4742 (435)	0.89 (0.12)
	1.2	1.34 (0.01)	6.85 (0.38)	4742 (387)	0.66 (0.10)
	1.4	1.44 (0.02)	9.85 (0.73)	5039 (379)	1.19 (0.04)
300M	1	1.32 (0.02)	7.83 (0.25)	3875 (284)	0.47 (0.05)
	1.2	1.35 (0.03)	9.37 (0.34)	5777 (862)	1.14 (0.17)
	1.4	1.32 (0.02)	7.60 (0.26)	4742 (527)	0.82 (0.03)

*Values in parenthesis are standard deviations.

In general, the bending strength of the cement bonded particleboards significantly influenced by application of super plasticizer polymers ($P < 0.001$). While PF300 nearly causes 20% bending strength reduction, 300M and DX40 cause far more significant strength loss (31% and 45%, respectively). The loss of strength is not proportional to the amount of polymer

used. Use of polymers lowers the bending strength of the boards but some of the values are still above the accepted standard value of 9 $N \cdot mm^{-2}$ (EN 634-2).

According to Bejo et al. (2005) density and mechanical properties are interrelated and densification will lead to higher mechanical properties. Since densities of polymer added boards are slightly higher, better bending strength values may be expected. Lower bending strength of the cement bonded particleboards with super plasticizer could be due to captivated water molecules that are not reacted with the cement. Higher moisture content up to 2% may cause reduction in bending strength of the boards. Simatupang and Geimer (1990) reported that excessive water causes porosity thus reduced board strength.

The effect of super plasticizers on the properties of cement bonded products is contradictory. Hospodarova et al. (2018) reported that addition of 0.5% super plasticizer to cement bonded boards containing 0.5% recycled paper fibers significantly improve mechanical properties including bond strength in addition to workability. According to Kumar et al. (2010) use of super plasticizer reduces the pores in both size and number and results higher compressive strength. Hamoush and El-Hawary (1994) claims that high levels of plasticizer delays cement hydration and lowers the strength properties of feather-cement bonded composites. It is known that higher cement content in the wood cement mixture lowers bending strength (Moslemi and Pfister 1987, Oyagade 1990). A possible contributory factor to the relatively low bending strength of the boards is the use of coarse particles.

Generally, internal bond strength of the cement bonded particleboards significantly altered by application of super plasticizer polymers ($P < 0.001$). PF300 and DX40 nearly doubled internal bond strength of control boards. Use of 1% 300M and 1.2% DX40 significant reduced the internal bond strength compared to the reference boards. Bond strength can be affected by several factors including density, water/cement ratio, type of cement, use and ratio of accelerators, type and dimensions of the wood particles (Ashori et al. 2012, Davies and Davies 2017). The increase in bond strength could be attributed to higher density and higher number of hydrogen bonding between wood and cement.

CONCLUSIONS

This study explored the effects of the use of polymer additives, also called super plasticizers, in cement-bonded particleboard production, under laboratory conditions, on their physical and mechanical properties. Based on the findings of the study, it is evident that addition of small amount of super plasticizer to wood cement mixture improves most of the properties of cement bonded particleboard tested. Use of super plasticizers in general resulted in better dimensional stability compared to control boards. More than 20 % decrease in thickness swelling and nearly 50 % reduction in water absorption were achieved by the use of polymers. Utilization of super plasticizer polymers also significantly improved bending stiffness which means treated boards will deform less in actual loading conditions in service. Gain in stiffness could be up to 38 % by the addition of additives. Deformation is more important than strength because the strength can be controlled by using larger cross sectional areas. Reduction in bending strength of the cement bonded particleboards may be prevented by use of lower water contents. Further investigations are, however, required on the effects of lower proportion of additives and lower water ratios and other fabrication variables such as fine particles on board properties.

REFERENCES

1. Al Rim, K., Ledhem, A., Douzane, O., Dheilly, R.M., Queneudec, M., 1999: Influence of the proportion of wood on the thermal and mechanical performance of clay-cement-wood composites. Cement Concrete Composites 21: 269-276.
2. Ashori, A., Tabarsa, T., Sepahv, S., 2012: Cement-bonded composite boards made from poplar strands. Construction and Building Materials 26: 131–134.
3. Bejo, L., Takats, P., Vass, N., 2005: Development of cement bonded composite beams. Acta Silva Lignaria Hungary 1: 111-119.
4. Del Menezzi, C.H.S., De Castro, G.H., De Souza, M.R., 2007: Production and properties of a medium density wood-cement boards produced with oriented strands and silica fume. Maderas. Ciencia y tecnología 9(2): 105-115.
5. Davies, I.O.E., Davies, O.O.A., 2017: Agro-waste-cement particleboards: A review. MAYFEB Journal of Environmental Science 2: 10-26.
6. EN 310, 1993: Wood-based panels - Determination of modulus of elasticity in bending and of bending. European Committee for Standardization, Bruxelas.
7. EN 317, 1993: Particleboards and fiber boards. Determination of swelling in thickness after immersion in water. European Committee for Standardization, Bruxelas.
8. EN 319, 1993: Particleboards and fiber boards. Determination of tensile strength perpendicular to the plane of the board. European Committee for Standardization, Bruxelas.
9. EN 634-2, 2007: Cement-bonded particleboards. Specifications. Part 2: Requirements for OPC bonded particleboards for use in dry, humid and external conditions. European Committee for Standardization, Bruxelas.
10. Frybort, S., Mauritz, R., Teischinger, A., Müller, U., 2008: Cement bonded composites. A mechanical Review. BioResources 3(2): 602-626.
11. Hamoush, S.A., El-Hawary, M.M., 1994: Feather fiber reinforced concrete. Concrete International 16: 33-35.
12. Hospodarova, V., Stevulova, N., Briancin, J., Kostelanska, K., 2018: Investigation of waste paper cellulosic fibers utilization into cement based building materials. Buildings 8: 43-55.
13. Huang, C., Cooper, P.A., 2000: Cement-bonded particleboard using CCA-treated wood removed from service. Forest Products Journal 50(6): 49-56.
14. Jorge, F.C., Pereira, C., Ferreira, J.M.F., 2004: Wood-cement composites: A review. Holz als Roh und Werkstoff 62(5): 370-377.
15. Kumar, M., Singh, N.P., Singh, S.K., Singh, N.B., 2010: Combined effect of sodium sulphate and superplasticizer on the hydration of fly ash blended Portland (R) cement. Material Research 13: 177–183.
16. Lee, A.W.C., 1984: Physical and mechanical properties of cement bonded southern pine excelsior. Forest Products Journal 34(4): 30-34.
17. Lee, A.W.C., Short, P.H., 1989: Pretreating hardwood for cement-bonded excelsior board. Forest Products Journal 39(10): 68-70.
18. Marteinsson, B., Gudmundsson, E., 2018: Cement bonded particle boards with different types of natural fibers using carbon dioxide injection for increased initial bonding. Open Journal of Composite Materials 8: 28-42.
19. Moslemi, A.A., Garcia, J.F., Hofstrand, A.D., 1983: Effect of various treatments and additives on wood-portland cement-water systems. Wood and Fiber Science 15(2): 164-176.
20. Moslemi, A.A., Pfister, S.C., 1987: The influence of cement wood ratio and cement type on bending strength and dimensional stability of wood cement composite panels. Wood Fiber Science 19: 165-175.

21. Na, B., Wang, Z., Wang, H., Lu, X., 2014: Wood-cement compatibility review. Wood Research 59(5): 813-826.
22. Okino, E.Y.A., De Souza, M.R., Santana, M.A.E., Alves, M.V.D.S., De Sousa M.E., Teixeira, D.E., 2004: Cement-bonded wood particleboard with a mixture of eucalypt and rubberwood. Cement and Concrete Composites 26(6): 729–734.
23. Okino, E.Y.A., Souza, M.R., Santana, M.A.E., Alves, M.V.S., Sousa M.E., Teixeira, D.E., 2005: Physico-mechanical properties and decay resistance of *Cupressus* spp. cement-bonded particleboards. Cement and Concrete Composites 27(2): 333-338.
24. Olorunnisola, A.O., 2009: Effects of husk particle size and calcium chloride on strength and sorption properties of coconut husk–cement composites. Industrial Crop Production 29(2/3): 495–501.
25. Oyagade, A.O., 1990: Effect of cement/wood ratio on the relationship between cement bonded particleboard density and bending properties. Journal of Tropical Forest Science 2(2): 211-219.
26. Peled, A., Mobasher, B., 2005: Pultruded fabric-cement composites. ACI Materials Journal 102(1): 15-23.
27. Ramirez-Coretti, A., Eckelman, C.A., Wolfe, R.W., 1998: Inorganic-bonded composite wood panel systems for low-cost housing: a Central American perspective. Forest Products Journal 48: 62-68.
28. Tonoli, G.H.D., Santos, S.F., Teixeira, R.S., Pereira-Da-Silva, M.A., Rocco Lahr, F.A., Pescatori, S.F.H., Savastano Jr, H., 2013: Effects of eucalyptus pulp refining on the performance and durability of fiber–cement composites. Journal of Tropical Forest Science 25(3): 400–409.
29. Savastano, H., Warden, P.G., Coutts, R.S.P., 2003: Potential of alternative fiber cements as building materials for developing areas. Cement and Concrete Composites 25: 585-592.
30. Simatupang, M.H., Lange, H., Neubauer, A., 1987: Einfluß der Lagerung von Pappel, Birke, Eiche und Lärche sowie des Zusatzes von SiO_2-Feinstaub auf die Biegefestigkeit zementgebundener Spanplatten. Holz als Roh- und Werkstoff 45(4): 131-136.
31. Simatupang, M.H., Geimer, R.L., 1990: Inorganic binder for wood composites: feasibility and limitations. Wood Adhesives 1990. Pp 169-176, Forest Products Research Society, Madison, Wisconsin.
32. Wolfe, R.W., Gjinolli, A., 1996: Cement bonded wood composites as an engineering material. The use of recycled wood and paper in building applications. Pp 84-91, Madison, Wisconsin.
33. Zhengtian, L., Moslemi, A.A., 1985: Influence of chemical additives on the hydration characteristics of western larch wood-cement- water mixtures. Forest Products Journal 35(7): 37-43.

HASAN HÜSEYİN TAŞ*
Isparta University Of Applied Sciences
Faculty Of Technology
Department Of Civil Engineering
32260 Isparta
Turkey
*Corresponding author: huseyintas@isubu.edu.tr

BİLGE ARSLAN
Süleyman Demirel University
Institute Of Science
Department Of Building Education
32260 Isparta
Turkey

HÜLYA KALAYCIOĞLU
Karadeniz Technical University
Forestry Faculty
Department Of Forest Industry Engineering
Trabzon
Turkey

WOOD RESEARCH
e-ISSN 2729-8906
66(3):2021 341-352 pp.
doi.org/10.37763/wr.1336-4561/66.3.341352

STUDY AND ANALYSIS ON SOUND ABSORBING AND NOISE REDUCING PERFORMANCE OF TIMBER CONSTRUCTION WALL BASED ON ACOUSTIC SPIRAL MATASURFACE

Haiyan Fu, Xinyue Zhao, Patrick Adjei, Zheng Wang, Xiaoli Wu
Nanjing Forestry University
China

(Received June 2020)

ABSTRACT

Based on acoustic spiral metasurface, a spiral structural layer was designed to apply to timber construction interior wall. The sound absorption coefficient was measured by impedance tube method and compared with Helmholtz resonance structural layer, solid structural layer and air layer in traditional wall. The results show that the combination of the spiral structural layer and the wall can optimize the sound absorption performance of the wall in the medium and low frequency. Without reducing the overall sound-absorbing performance of the wall, can achieve perfect sound absorption in some medium and low frequency sound bands.

KEYWORDS: Acoustic metasurface-based, timber construction, sound absorption performance, interior wall, spiral metasurface.

INTRODUCTION

In recent years, due to the national attention to environmental protection and energy conservation, green buildings (Haitao et al. 2019, Azkorra et al. 2015) are more and more popular. Timber or bamboo (Xin et al. 2019, Xin et al. 2020, Cheng et al. 2019) construction not only meets people's basic requirements for buildings, but also meets people's requirements for living environmental comfort and protection, as well as energy saving environment (Ying-Yang et al. 2018, Valachova et al. 2019). The application of this phenomenon is more extensive in China. The timber construction has advantages in physical and mechanical properties, but it still has shortcomings in low frequency noise reduction and sound absorption in wall structure. Generally, in the case of relatively low surface density, it is difficult to calculate the weight of sound insulation R_W (weighted sound reduction index) to reach more than 50 dB, or even less than 40 dB. In the low frequency region of the sound frequency band (100-500 Hz), acoustic resonance phenomenon is prone to occur, which affects the overall acoustic performance of the wall (Caniato et al. 2017). Previous studies have generally improved the sound-absorbing

properties of walls by changing the internal materials of walls, such as reasonably filling pores with sound-absorbing materials (Zhong-Bin et al. 2015), using composites with high sound-absorbing properties (Bo-Seung et al. 2016, Cao-Ping 2006), or changing the spacing and sizes of wooden keel (Belakroum et al. 2017, Ljunggren et al. 2011). But in the actual control, through these methods and measures, the effect of sound absorption and noise reduction of the wall is not significantly actualize, especially with low and medium frequency noise. Low frequency noise has the characteristics of strong penetration, slow attenuation, long propagation. And low-frequency noise will have a bad impact on the functionalities of some vital organs of the human body. In acoustics, a variety of resonance structures can be used for sound absorption, but the most widely used structure is a Helmholtz resonator. Acoustic metasurface plays a significant role in solving low-frequency vibration and noise reduction (Zhu et al. 2019, Ali et al. 2020, Krupali et al. 2020). Based on the acoustic metasurface, researchers studied the spiral acoustic metasurface, a perfect low-frequency sound absorber (Huang et al. 2018, Li et al. 2016, Huang et al. 2019, Assouar et al. 2018). The purpose of this experimental study is to solve the problem of poor acoustic performance in timber construction. To improve the acoustic performance of wall structure of timber construction, the acoustics metasurface structure combined with wall structure of timber construction. Through optimizing the exterior structure of wall, it is improved the wall of sound absorption performance and the overall structure of the sound insulation performance.

MATERIAL AND METHODS

Material

Design principle

As shown in Fig. 1, the spiral structural layer is composed of a perforated plate and a coplanar spiral chamber.

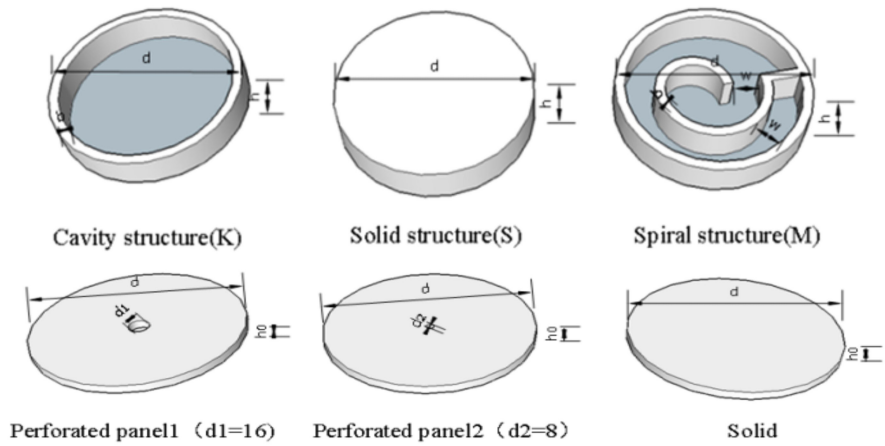

**Note: The solid structure and solid are the traditional structure (control group).*

Fig. 1: Design drawing of structural layer.

The plane sound wave propagates along the "z" direction. The sound wave enters the coplanar spiral chamber through the hole in the perforated plate. It is completely reflected

at the end of the spiral chamber and then emitted from the hole, forming a reflected wave. The structure is actually a resonant sound absorption structure composed of a perforated plate and a cavity behind the plate. Its acoustic impedance Z_s is formed by the equivalent acoustic resistance x_s and acoustic reactance y_s of the perforated plate and the coplanar spiral cavity in series (Li et al. 2016, Dah-You et al. 1998, Ingard et al. 1953), which can be expressed as follows:

$$z_s = x_s + iy_s$$

When the plane sound wave is vertically incident, the sound absorption coefficient of the perforated plate absorber is:

$$\alpha = \frac{4x_s}{(1+x_s)^2 + y_s^2} = \frac{4x_h}{(1+x_h)^2 + (y_h + y_c)^2}$$

where: $\alpha=1$: $x_h = 1$, $y_h + y_c = 0$. l corresponds to the length of the crimp cavity. The spiral structural layer can be adjusted to obtain the appropriate acoustic reactance by adjusting the spiral structure. On this basis, the diameter of the hole in the perforated plate can be adjusted to match its overall acoustic resistance with the air layer, and finally achieve perfect sound absorption (Li 2017):

$$l = \frac{cS'}{\omega S}\cot^{-1} y_h$$

where: c is the propagation velocity of sound waves in air, which is 340 m.s^{-1} at room temperature; S is the area of the incident side plate of sound wave, $S = \pi d^2/4$ (mm^2); S' is the cross sectional area of the dorsal cavity, $S' = w^2$ (mm2); l is the equivalent length of the crimped back cavity (mm); d is the diameter of the perforated plate (mm); w is the width of the groove (mm).

Specimen structure

Based on the acoustic ultra-surface low-frequency perfect absorber, the spiral structural layer designed in this study is composed of spiral structure and perforated plate, and is adjusted by combining the theory (Ming-Ming et al. 2018) with the actual interior wall structure size. To test in a larger size, the spiral structural layer whether still have low frequency sound absorption effect, was compared with Helmholtz resonance structural layer, solid structural layer and air layer in traditional wall. The main test of the study is focused on the sound absorption coefficient of medium and low frequency, which used impedance tubes for testing. Due to the impedance tube suite in the low and medium frequency used fill a diameter of 100 mm diameter, specimen are designed (Fig. 1), and combination of concrete specimen are shown in Tab. 1. In Fig. 1, d is the external diameter of the specimen, d=100 mm; d_1 and d_2 are the apertures of perforated plate 1 and 2 respectively, d_1=16 mm, d_2=8 mm; h is the thickness of the structure, h = 20 mm; h_0 is the thickness of the cover plate, h_0=5 mm; b is the edge width, b=5 mm; w is the width of the groove, and w=15 mm. The material of the structural layer (structure + cover) is ethoxyline resin, and the material parameters are shown in Tab. 2.

Tab. 1: Specimen combinations.

Specimen	Mark	Combination	Quantity
Spiral structural layer	M08	Perforated panel 2 + Spiral structure	3
	M16	Perforated panel 1 + Spiral structure	3

Helmholtz resonance structural layer	G08	Perforated panel 2 + Cavity structure	3
	G16	Perforated panel 1 + Cavity structure	3
Air layer	K	Solid + Cavity structure	3
Solid structural layer	S	Solid + Solid structure	3

**The solid structural layer (S) is a combination of traditional structures (control group).*

Tab. 2: Material parameters structural layer.

Material	E (GPa)	v ($m \cdot s^{-1}$)	ρ ($kg \cdot m^{-3}$)
Ethoxyline resin	4.35	368	1180

Based on the structural layer test, the structural layer is combined with the wall structure, as shown in Fig. 2. The wall structure from outside to inside are orderly arranged with structural layer, OSB, insulation cotton, and OSB (material parameters are shown in Tab. 3).

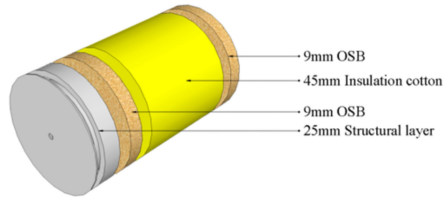

Fig. 2: Design drawing of composite wall.

Tab. 3: Wall material parameters.

Material	ρ ($kg \cdot m^{-3}$)	v ($m \cdot s^{-1}$)
Oriented strand board (OSB)	593	1.8×10^3

The specific wall combination is shown in Tab. 4, and the sound absorption coefficient of the wall structure is measured.

Tab. 4: Wall combination.

Specimen	Mark	Combination (outside-inside)	Quantity
Spiral structural layer- Wall	M08OBO	M08 + OSB + Insulated cotton + OSB	3
	M16OBO	M16 + OSB + Insulated cotton + OSB	3
Helmholtz resonance structural layer- Wall	G08OBO	G08 + OSB + Insulated cotton + OSB	3
	G16OBO	G16 + OSB + Insulated cotton + OSB	3
Air layer- Wall	KOBO	K + OSB + Insulated cotton + OSB	3
Solid structural layer- Wall	SOBO	S + OSB + Insulated cotton + OSB	3

*OBO is OSB (O), insulation cotton (B), and OSB (O). The solid structural layer- wall (SOBO) is a combination of traditional structures (control group).

Methods

Test methods

In this study, the impedance tube is used to measure the sound absorption coefficient, and the main principle is the transfer function method. The transfer function method is one

of the common methods to measure the acoustic characteristics of materials and structures. The pipe and the dynamic acoustic characteristics of the specimen were used to measure the acoustic characteristics of the material structure (Zheng et al. 2018).

Test procedures

There were six sets of specimen combinations and six sets of wall combinations. Then three specimens in each group were tested repeatedly in three groups and averaged to output the corresponding sound absorption coefficient data at 150-1600 Hz. At last, OriginPro 2016 was used for data processing and analysis, and the test value curve of sound absorption coefficient was drawn. According to the curve drawing, the influence of spiral acoustic metasurface on the sound absorption of timber construction wall was investigated and the results were obtained.

RESULTS AND DISCUSSION

Results

Through theoretical calculation and experimental test, the theoretical and experimental values of sound absorption coefficient of spiral structural layer are obtained. The theoretical value is compared with the actual value to obtain the curve graph, as shown in Fig. 3. The acoustic absorption coefficient curves obtained by testing the six structural layers are shown in Fig. 4. Based on the sound absorption coefficient test of the structural layer, the structural layer is combined with the wall structure to measure the sound absorption coefficient curve of six wall structures, as shown in Fig. 5.

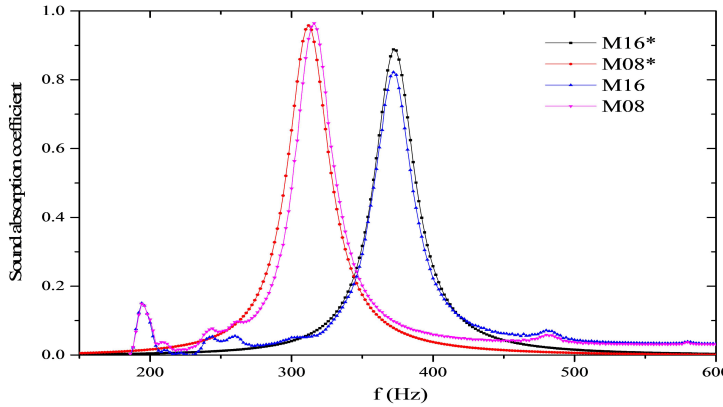

* is the theoretical value, and without * is the experimental value.

Fig. 3: Theoretical and experimental values of sound absorption coefficient of spiral structural layer.

According to the standards of ISO 354 (2003) and ISO 140-18 (2006), in the frequency range of 150-1600 Hz, the average value obtained by calculating the sound absorption coefficient of the specimen is the average sound absorption coefficient, and the formula is expressed as Eq. 4. According to Eq. 4, the average sound absorption coefficients of six kinds of test piece structural layers and six kinds of wall structures are calculated, as shown in Tabs. 5 and 6.

$$\alpha = \left(\alpha_{160Hz} + \alpha_{200Hz} + \cdots + \alpha_{1600Hz}\right) / 11$$

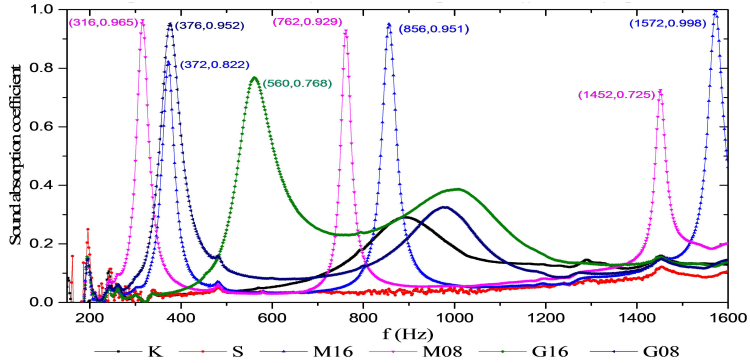

Fig. 4: Test value curves of sound absorption coefficient of six structural layers.

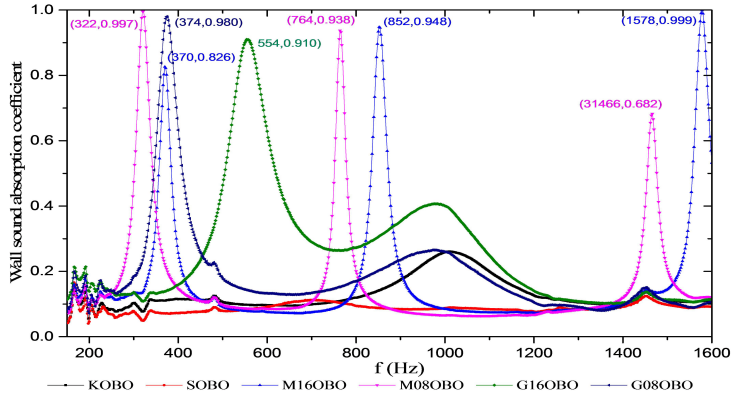

Fig. 5: Test value curves of sound absorption coefficient of six wall structures.

Tab. 5: Average sound absorption coefficient of the six structural layers.

Combination / f(Hz)	K	S	G08	M08	G16	M16
160	0.00	0.07	0.08	0.08	0.08	0.07
200	0.01	0.16	0.10	0.10	0.10	0.09
250	0.05	0.05	0.05	0.07	0.02	0.04
316	0.00	0.01	0.12	0.96	0.01	0.06
400	0.03	0.03	0.57	0.06	0.04	0.22
500	0.04	0.03	0.12	0.04	0.25	0.04
630	0.06	0.03	0.08	0.03	0.39	0.03
800	0.18	0.03	0.13	0.16	0.24	0.12
1000	0.19	0.05	0.31	0.06	0.39	0.06
1250	0.12	0.06	0.09	0.09	0.14	0.06
1600	0.13	0.11	0.15	0.20	0.14	0.46
Average sound absorption coefficient	0.07	0.06	0.15	0.15	0.15	0.10

Tab. 6: Average sound absorption coefficient of six wall structures.

Combination / f(Hz)	KOBO	SOBO	M16OBO	M08OBO	G16OBO	G08OBO
160	0.07	0.08	0.11	0.10	0.14	0.12
200	0.06	0.05	0.10	0.09	0.14	0.07
250	0.08	0.07	0.12	0.13	0.14	0.14
316	0.08	0.05	0.13	0.94	0.11	0.22
400	0.11	0.07	0.26	0.15	0.16	0.63
500	0.11	0.08	0.09	0.10	0.46	0.18
630	0.10	0.10	0.07	0.09	0.45	0.13
800	0.12	0.09	0.15	0.20	0.27	0.17
1000	0.26	0.09	0.08	0.07	0.40	0.26
1250	0.11	0.08	0.08	0.08	0.12	0.10
1600	0.11	0.09	0.53	0.12	0.11	0.11
Average sound absorption coefficient	0.11	0.08	0.16	0.19	0.23	0.19

Analysis of sound absorption performance of structural layer

It can be seen from Fig. 3 that the frequency of the first peak of the experimental value and the theoretical value is basically consistent. The influence of the change of perforated plate aperture on the sound absorption coefficient of the structural layer is also mutually satisfied by the experimental results and the theoretical results, but the numbers are slightly different. The possible reason is that both the sound field and external conditions designed in the theoretical calculation are ideal environments, while the effect of environmental sound waves during the field measurement is ignored. In addition, the materials used in the specimen are homogeneous materials in theoretical calculation, while there may be gaps in the structural layer during actual processing. In the case of sound absorption, the structural material itself may cause vibration, causing certain losses to sound waves. In general, the experimental results meet the theoretical results to a certain extent.

Based on the results obtained in Fig. 3, sound absorption coefficients of six structural layers of specimens were compared, as shown in Fig. 4. Within the frequency range of 150-1600 Hz, the sound absorption coefficient curve of the solid structural layer is gentle. The value does not exceed 0.2, and there is basically no peak value. Although the air layer structure has a peak value at about 850 Hz, the peak value is only around 0.3. In the whole frequency band, the sound absorption performance is not strong. According to Tab. 5, the average sound absorption coefficient of the solid structural layer and the air layer are 0.07, 0.06 respectively, indicating that the two structures basically do not absorb sound in the medium and low frequency bands. The reason for this phenomenon may be that the sound waves are transmitted to the solid structural layer, and most of the sound waves are reflected, while some medium and low frequency sound waves have strong penetrability, which cannot be absorbed by the solid structural layer, and the sound waves are transmitted. However, there is air impedance in the air layer; there is certain absorption of sound waves, but less consumption, especially for the medium and low frequency waves.

Compared with the solid structural layer and the air layer, the Helmholtz structural layer and the spiral structural layer have obvious sound absorption performance in the frequency range of 150-1600 Hz. According to Tab. 5, the average sound absorption coefficient of the two structural layers are within the range of 0.15 respectively. Compared with sound absorption

performance of Helmholtz layer structure, spiral structural layer on the average absorption coefficient has no significant advantages. However, it can be seen from Fig. 3 that within the range of the test frequency band, there are three obvious peaks in the spiral structural layer. The three peaks occurred at about 350 Hz, 800 Hz and 1500 Hz respectively, and the peak sound absorption coefficient was between 0.71-1.0. The Helmholtz structure layer of perforated plate with the same aperture only has two peaks. The peak values are about 500 Hz and 1000 Hz respectively, and the peak values are smaller than the corresponding peak values in the spiral structural layer. The lower peak sound absorption coefficient is only 0.35. In addition, it is found that compared with the first and second peaks of Helmholtz structural layer, the first and second peaks of spiral structural layer not only increase in value, but also move to low frequency and narrow the absorption band. This shows that the spiral structure does have a significant advantage in the absorption of medium and low frequency sound waves. The reason for this phenomenon is that airborne sound is a scalar wave and propagates freely without a cut-off frequency inside a waveguide with rigid walls. Because there is a large impedance difference between air and solid, the propagating path of the wave can be greatly extended by using coiling-up space with labyrinthine configuration (Assouar et al. 2018). Thus, with a longer propagating path from the coiling effect, the spiral structure has a lower resonant frequency and absorption peak. Compared with Helmholtz structure, the appropriate acoustic reactance can be obtained by adjusting the length of the spiral structure. On this basis, the diameter of the hole of the perforated plate can be adjusted to match the overall acoustic resistance with the air layer to achieve the perfect sound absorption in a certain frequency band.

At the same time, by comparing the spiral structural layers of different perforated plates, it was found that M08 with small aperture had three peaks of about 316 Hz, 762 Hz and 1452 Hz in the test frequency band. The sound absorption coefficients were 0.96, 0.93 and 0.72, respectively, and the sound absorption coefficients were gradually decreasing. In the range of the test frequency band, the three peaks of M16 with larger aperture were around 372 Hz, 856 Hz and 1572 Hz, respectively. The sound absorption coefficients were 0.82, 0.95 and 0.99, respectively. The sound absorption coefficient was gradually increasing, and the peak value moved towards high frequency as compared with M08. The main reason is that as the perforated plate aperture increases, the corresponding cross-sectional area of the hole also increases. However, the volume of the spiral air cavity structure does not change and the length of the holes does not change, so the peak value will move to the high frequency, which is determined by the resonance principle formula of Helmholtz sound absorption.

Therefore, compared with the traditional structure (solid structural layer and air layer), the spiral structure layer has obvious sound absorption performance in the range of 150-1600 Hz. And the perforated plate aperture can affect the sound absorption performance of the spiral structure layer.

Analysis of sound absorption performance of wall

It can be seen from the comparison between Fig. 4 and Fig. 5 that the variation curve of sound absorption coefficient obtained by applying the structural layer to the wall structure is basically consistent with the trend and value of the curve of sound absorption coefficient, measured by the structural layer itself. This shows that changing the structural form of the structural layer can indeed optimize the sound absorption performance of the wall. In addition, the combination of the spiral structural layer and the wall structure can indeed optimize the sound absorption performance of the wall in the medium and low frequency band. Without reducing the overall sound absorption performance, it can achieve perfect sound absorption in some medium and low

acoustic frequency bands.

At the same time, it can be roughly seen from Figs. 4, 5 and Tabs. 5, 6 that the peak value of sound absorption coefficient measured by the composite wall structure is basically consistent with the peak value of sound absorption coefficient of the structural layer in position, but slightly increased in value. According to the data in Tabs. 5 and 6, the comparison diagram of the average sound absorption coefficient of six groups of structural layers and walls are drawn (Fig. 6).

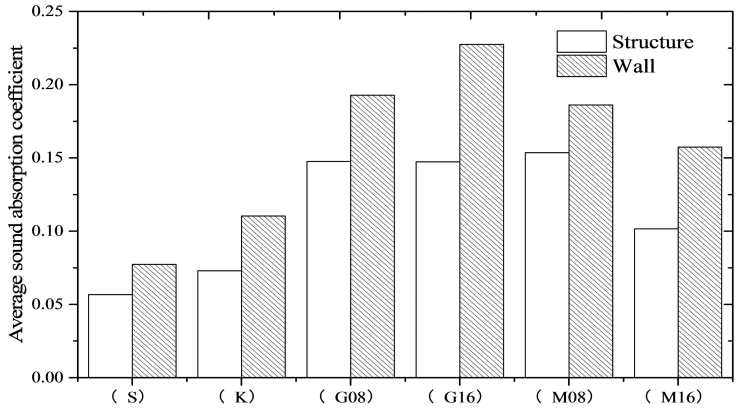

Fig. 6: Comparison of average sound absorption coefficient between six groups of structural layers and wall.

The average sound absorption coefficient measured by the wall composite structure are indeed higher than those measured by the structural layer. The main reason may be the absorption of sound waves by other structural materials in the wall, such as insulation cotton.

CONCLUSIONS

(1) The frequency of the first peak value of acoustic absorption coefficient of spiral structural layer is basically consistent with that of the theoretical value. *(2)* Analysis and comparison for six kinds of structural layer in the 150-1600 Hz frequency range of the absorption coefficient, the spiral structural layer had the best sound absorption performance in the test frequency range , which is obviously better than the traditional structure. *(3)* Within the range of the test frequency band, there were three obvious peaks in the spiral structural layer and the peak sound absorption coefficient was between 0.71-1.0. *(4)* The perforated plate aperture can affect the sound absorption performance of the spiral structure layer. *(5)* It shows that changing the structural form of the structural layer can optimize the sound-absorbing performance of the wall, especially in the medium and low frequency bands. *(6)* By using the acoustic spiral metasurface structure's efficient absorption performance of low-frequency sound waves and combining with the absorption performance of the timber construction wood wall's own absorption performance of medium-high frequency sound waves, the sound-absorbing and noise reduction performance of the timber construction wood wall, especially the low-frequency noise reduction performance, is effectively increased without affecting the mechanical and other physical properties of the wall.

ACKNOWLEDGMENT

This study was funded by the Co-Innovation Center of Efficient Processing and Utilization of Forest Resources, Nanjing Forestry University, Nanjing 210037, China.

REFERENCES

1. Assouar, B., Liang, B., Wu, Y., Li, Y., Cheng, J.C., Jing, Y., 2018: Acoustic metasurfaces. Nature Reviews Materials (3): 460–472.
2. Ali, I., Mosa, A., Putra, R.R., Al-Ameri, E., 2020: Wideband sound absorption of a double-layer microperforated panel with inhomogeneous perforation. Applied Acoustics 161: 107167.
3. Azkorra, Z., Pérez, G., Coma, J., Luisa, F.C., 2015: Evaluation of green walls as a passive acoustic insulation system for buildings. Applied Acoustics 89: 46-56.
4. Bo-Seung, K., Sung-Jin, C., Dong-Ki, M., Park, J., 2016: Experimental study for improving sound absorption of a composite helical-shaped porous structure using carbon fiber. Composite Structures 145: 242-247.
5. Belakroum, R., Gherfi, A., Bouchema, K., Gharbi, A., 2017: Hygric buffer and acoustic absorption of new building insulation materials based on date palm fibers. Journal of Building Engineering 12: 132-139.
6. Caniato, M., Bettarello, F., Ferluga, A., Marsich, L., Schmid, C., Fausti, P., 2017: Acoustic of lightweight timber buildings: A review. Renewable and Sustainable Energy Reviews 80: 585-593.
7. Cao-ping, W., 2006: Study on sound absorption and sound insulation of gypsum board structure and its application. New Building Materials (8): 46-49.
8. Cheng, T., Hai-Tao, L., Dong-Dong, W., Rodolfo, L., Cong-Gan, Y., 2019: Mechanical performance of parallel bamboo strand lumber columns under axial compression: Experimental and numerical investigation. Construction and Building Materials 231: 117168.
9. Dah-You, M., 1998: Potential of microperforated panel absorber. Journal of Acoustical Society 104(5): 2861.
10. Hai-Tao, L., Gang, W., Zhen-Hua, X., Ileana, C., Ottavia, C., Xiao-Hong, X., Hui-Zhong, Z., Zhen-Yu, Q., 2019: Length and orientation direction effect on static bending properties of laminated Moso bamboo. European Journal of Wood and Wood Products 77(4): 547-557.
11. Huang, S., Fang, X., Wang, X., Badreddine, A., 2018: Acoustic perfect absorbers via spiral metasurfaces with embedded apertures. American Institute of Physics 113(2): 254-262.
12. Huang, S., Fang, X., Wang, X., Badreddine, A., 2019: Acoustic perfect absorbers via Helmholtz resonators with embedded apertures. Acoustical Society of America 145(1): 254-262.
13. Ingard, U., 1953: On the theory and design of acoustic resonators. The Journal of the Acoustical Society of America 25: 1037-1061.
14. ISO 354(E), 2003: Acoustics. Measurement of sound absorption in reverberation room.
15. ISO 140-18(E), 2006: Acoustics. Measurement of sound insulation in buildings and of building elements. Part 18: Laboratory measurement of sound generated by rainfall on building elements.
16. Krupali, D., Yi-Fan, Z., Shi-Wang, F., Li-Yun, C., 2019: Extreme low-frequency ultrathin acoustic absorbing metasurface. Applied Physics Letters 115: 173506.

17. Ljunggren F., Ågren, A., 2011: Potential solutions to improved sound performance of volume based lightweight multi-storey timber buildings. Applied Acoustics 72(04): 231-240.
18. Li, Y., Assouar B.M., 2016: Acoustic metasurface-based perfect absorber with deep subwavelength thickness. Applied Physics Letters 108 (6): 063502.
19. Li, Y., 2017: Acoustic metasurfaces. Physical (11): 14-23.
20. Valachova, D., Skotnicova, I., 2019: Using the finite element method to predict heat dissipation in a timber frame building construction. Wood Research 64(5): 859-870.
21. Xin, L., Mahmud, A., Hai-Tao, L., Xiao-Yan, Z., Hong-Xu, W., Al-Deen, S., Paul, J.H., 2019: An experimental investigation on parallel bamboo strand lumber specimens under quasi static and impact loading. Construction and Building Materials 228: 116724.
22. Xin, L., Mahmud, A., Hai-Tao, L., Xiao-Yan, Z., Al-Deen, S., Hong-Xu, W., Paul, J.H., 2020: Experimental study on the deformation and failure mechanism of parallel bamboo strand lumber under drop-weight penetration impact. Construction and Building Materials 242: 118135.
23. Ying-Yang, L., Hai-Bei, X., Jia-Hua, K., 2018: Seismic evaluation of wood frame construction based on all connection deflection status. Wood Research 63(6): 979-992.
24. Zhong-Bin, X., Bai-Cun, W., San-Ming, Z., Rong-Jun, C., 2015: Design and acoustical performance investigation of sound absorption structurebased on plastic micro-capillary films. Applied Acoustics 89:152-158.
25. Zheng, W., Wen-Bo, X., Yao, L., Hai-Tao, Li., Zhi-Heng, W., Zhong, L., 2019: Dynamic and static testing methods for shear modulus of oriented strand board. Construction and Building Materials (216) 542–551
26. Zhu, Y.F., Donda, K., Fan, S.W., Cao, L.Y., Assouar, B., 2019: Broadband ultra-thin acoustic metasurface absorber with coiled structure. Applied Physics Express 12(11): 114002.

Haiyan Fu, Xinyue Zhao
College Of Materials Science And Engineering
Nanjing Forestry University
210037 Nanjing
China

Patrick Adjei
College Of Civil Engineering
Nanjing Forestry University
210037 Nanjing
China

Zheng Wang*
College Of Materials Science And Engineering
Nanjing Forestry University
210037 Nanjing
China
*Corresponding author: wangzheng63258@163.com

Xiaoli Wu
College Of Mechanical And Electrical
Nanjing Forestry University
210037 Nanjing
China

WOOD RESEARCH
e-ISSN 2729-8906
66(3):2021 353-364 pp.
doi.org/10.37763/wr.1336-4561/66.3.353364

EFFECT OF DIFFERENT PRE-TREATMENTS ON THE PERMEABILITY OF GLUE-LAMINATED BAMBOO

Chunyan Lv, Caijuan Zhang, Xinjie Zhou, Mingyu He, Lili Yu
Tianjin University Of Science And Technology
Faculty Of Light Industry Science And Engineering
P. R. China
Q. R. China

Zhenzhong Tang
China Timber & Wood Products Distribution Association
R. R. China

(Received June 2020)

ABSTRACT

In this study, hydrothermal treatments (duration: 2 h, 5 h, 8 h; temperature: 60°C, 80°C, 100°C), ultrasonic treatments (duration: 60 min, 90 min, 120 min; temperature: 40°C, 50°C, 60°C; ultrasonic power: 400 W, 600 W, 800 W) and freeze-drying treatments (vacuum degree: 0.05 mbar, 0.1 mbar, 0.5 mbar, 1.0 mbar, 1.7 mbar) were performed respectively to improve the permeability of glue-laminated bamboo. The effects of different pre-treatments on the permeability were compared according to the water absorption test and the mercury intrusion porosimetry test. The microstructure change of the samples was observed by scanning electron microscope (SEM). The results showed that freeze-drying treatment was an effective way to increase the permeability of the samples, in which the water absorption rate can be increased by 47%, and the porosity can be increased by 10% at 0.5 mbar vacuum. From SEM analysis, some small holes appeared in the cell wall of the freeze-dried samples, because he free water inside the samples was changed into ice, and the volume became larger, and the pore diameter of the bamboo was enlarged.

KEYWORDS: Glue-laminated bamboo, permeability, hydrothermal treatment, freeze-drying, porosity.

INTRODUCTION

With the rapid development of China, the wooden resources cannot meet the increasing needs of the market, as the result, bamboo has been widely considered as the best substitute for wood because of the shorter growth cycle, the better mechanical properties and

the rich accumulation (Ge et al. 2012, Seo et al. 2016, Kaur et al. 2016). However, the permeability of bamboo is very poor, which has obstructed the processing and modification treatments, such as dyeing, preservation, and flame-retardant treatment (Wen et al. 2017, Chen et al. 2019). As bamboo contains almost no lateral structure such as wood rays, the liquid flow can only pass through the pits (Ilic 1995, Sernek et al 1999), which is the main reason for the poor permeability of bamboo. When the bamboo-based material is subjected to permeation treatment, the pore diameter will increase and the quantity will increase. Therefore, improving the permeability of bamboo has become the key step for promoting the application of bamboo.

From the previous researches, some effective measures have been successfully performed to improve the permeability of bamboo including physical and chemical methods. The shortcomings of the chemical method are very obvious. For example, the mechanical properties of the material are greatly reduced, the color of the material is deepened, and the equipment is corroded. (Hass et al. 2012, Lu et al. 2017, Haase et al. 2018). The main physical methods include hydrothermal treatment, ultrasonic treatment, and freeze drying. The main purpose of hydrothermal treatment is to reduce the extract in bamboo (Xiao et al. 2017), thereby increasing the liquid circulation channel and improving the permeation. The principle is that some terpenoids in the extract which can be azeotroped in water at about 100°C, resulting in the extracts leaching out from bamboo (Li et al. 2011, Kaur et al. 2013). Rao et al. (2013) showed that when bamboo was boiled at 80°C hot water for 2 h, the penetration depth can be increased by 67% compared to the untreated samples. During ultrasonic treatment, water is used as the medium to generate shock waves inside the sample, so that the internal structure of the bamboo is destroyed and some weak tissues are also destroyed (Huang et al. 2017, Guan et al. 2019). Yong et al. (2013) have showed that the starch content in the bamboo with ultrasonic treatment at 70°C and 1400 W for 150 min has decreased significantly, and the average penetration depth was also increased from 431.33 μm to 820.64 μm. Freeze-drying treatment has been proved as the most effective physical method at present, and the principle is involve in the three-phase morphological change of water. In the early phase, the water inside the sample began to freeze resulting in the pore size of bamboo enlarged in the second phase. In the third phase, the ice is directly sublimated and the pore diameter changed irreversibly (Lv et al. 2005). The similar results also can be found in the research of Xu et al. (2018), which showed the porosity of bamboo with vacuum freeze-drying could increase to 73% and the mechanical properties have no noticeable change.

In this study, hydrothermal treatment, ultrasonic treatment, and freeze drying were also performed to improve the permeability of bamboo. The orthogonal test and single factor test were used to screen and compare the conditions of each method, and the optimal conditions of these three processes were obtained and compared. The mechanisms of permeability change were analyzed by the observations of the internal structure of the bamboo using a scanning electron microscope (SEM) and the pore size and pore size distribution of the specimen before and after treatment obtained from the mercury intrusion porosimeter (MIP).

MATERIAL AND METHODS

Samples

Glue-laminated bamboo hot pressed with bamboo strips was obtained from Ganzhou, Jiangxi Province and the moisture content was 8-10%. The experimental specimens were cut from the glue-laminated bamboo with three dimensions of 20 mm (length) × 20 mm (width) × 7 mm (thickness) for water absorption test, 10 mm (length) × 10 mm (width) × 3 mm (thickness) for SEM analysis

and 15 mm (length) × 15 mm (width) × 7 mm (thickness) for MIP analysis. The glue-laminated bamboo with epoxy resin was manufactured by Jiangxi Anzhu Science and Technology Company and the cross section of the samples were sanded smooth enough although with the adhesive joints.

Hydrothermal experiment

The orthogonal experimental conditions of the glue-laminated bamboo with hydrothermal treatment were set in the following conditions: the treatment time was set in three levels of 2 h, 5 h and 8 h, and the treatment temperature was set in three levels of 60°C, 80°C and 100°C.

Ultrasonic experiment

The orthogonal experimental conditions of the glue-laminated bamboo with ultrasonic treatment were set in the following conditions: the treatment time was set in three levels of 60 min, 90 min and 120 min, the temperature was set in three levels of 40°C, 50°C and 60°C and the ultrasonic power was set in three levels of 400 W, 600 W and 800 W.

Vacuum freeze-drying experiment

Before vacuum freeze-drying treatment, the samples were immersed in water for several days to adjust the moisture content to 50-60%. The vacuum freeze-drying method was performed using the vacuum freeze-drying machine (ALPHA 1-2 LD plus; Christ company of Germany) to dry the bamboo specimens and the condensation temperature was -50°C. In this experiment, the vacuum degree during vacuum drying was selected as the single variable, and was set in five levels of 1.7 mbar (170 Pa), 1.0 mbar (100 Pa), 0.5 mbar (50 Pa), 0.1 mbar (10 Pa), 0.05 mbar (5 Pa). During the drying process, the drying time is 15 h, and the drying temperature is -15°C, -20°C, -27°C, -42°C, -48°C according to these five different vacuum degrees.

Evaluation of permeability

Before the water absorption test, the oven-dried method was performed in accordance with the national standard (GB/T 17657-2013) to determine the moisture content of glue-laminated bamboo. After different treatments, the samples were immersed in a beaker containing deionized water, and after 6 h, each sample was weighed for the first time, and then weighed every 24 h, 48 h, 96 h, and 128 h, and the experimental results were recorded. The water absorption of the sample was calculated by using Eq. 1. This method was performed in accordance with the national standard (GB/T 1934.1 (2009):

$$WAR = \frac{W_1 - W}{W} \times 100\% \quad (1)$$

where: W and W1 were the weights of each sample before and after water absorption measurement, WAR is the water absorption ratio.

Orthogonal experiment analysis

This orthogonal experiment uses the L9 design table, and the factors for each condition are selected in three levels. According to the size of the K value in the range, the optimal conditions of the process are selected, and the influence of each factor on the experimental results is analyzed by the R value.

SEM analysis

Scanning electron microscopy (JSM-IT300LV, Japan) were used to observe the microstructure of the experimental specimens. The samples (10 x 10 x 3 mm) with the best permeability performance in each treatment were selected and coated with gold under an environment of a vacuum of 5 Pa before the observation.

Pore size analysis

The mercury intrusion porosimetry experiment was performed using an automated mercury porosimeter (AutoPore IV 9510; USA) and the sample size is 15 x 15 x 7 mm. The principle of MIP test is to use the characteristics of mercury to press the mercury into the interior of the bamboo under pressure conditions, so that the pore size and pore size distribution of the sample can be measured by the relationship between the total amount of mercury intrusion and the pore size.

RESULTS AND DISCUSSION

Permeability analysis

Hydrothermal treatment

The optimal conditions for the hydrothermal treatment were obtained by the analysis of the range and variance of the orthogonal experiments. As showed in Tab. 1, the Rang value (R) of the temperature is much larger than the R value of the time, which indicated that during hydrothermal treatment, temperature has greater impact on the permeability of the treated glue-laminated bamboo. The reason may be attributed to the extracts in the samples much more easily removed out during hydrothermal treatment with higher temperature. For example, some terpene compounds can be azeotroped with water at 100°C and glycans and polyphenols are soluble in hot water (Li et al. 2011).

Tab. 1: The range results of hydrothermal treatment.

Test No.	Temperature (°C)	Time (h)	Water absorption ratio (%)
1	60	2	56.1
2	60	5	56.8
3	60	8	56.8
4	80	2	60.0
5	80	5	58.7
6	80	8	57.9
7	100	2	59.6
8	100	5	61.8
9	100	8	61.1
K1	56.567	58.567	
K2	58.867	59.1	
K3	60.833	58.6	
R	4.266	0.533	

According to the sum of the identified column with the correspondent factor (K) based on the variance analysis as showed in Tab. 2, the optimum conditions were 100°C, 5 h, which were the same as the results of the range analysis. The temperature had a significant effect at the 0.05 level, which also confirmed the importance of temperature during the hydrothermal treatment process. The water absorption ratio of the samples would significantly increase as the temperature increased. The results were similar with some previous results that Gao et al. (2015) processed the poplar by hydrothermal treatment. As the temperature increased, the reaction of poplar increased, and the permeability also increased.

Tab. 2: The variance results of hydrothermal treatment.

Factors	Sum of squares	DF	F – value	Sig.
Temperature	27.362	2	19.323	**
Time	0.536	2	0.379	/
Error	1.42	2		

Note: / is referred to the factor insignificant at the 0.1 level, *, **, *** are referred to the factor significant at the 0.1, 0.05, and 0.01 levels respectively.

Ultrasonic treatment

Based on the range analysis of ultrasonic experiments (Tab. 3), the order of influence factors on water absorption ratio during the ultrasonic treatment process was: time > ultrasonic power > temperature, which demonstrated that time was the most important factor on the permeability of bamboo laminated timber.

Tab. 3: The range results of ultrasonic experiment.

Test no.	Temperature (°C)	Time (h)	Ultrasonic power	WAR (%)
1	1	1	1	62.7
2	1	2	2	61.8
3	1	3	3	57.2
4	2	1	2	59.6
5	2	2	3	58.2
6	2	3	1	57.4
7	3	1	3	59.1
8	3	2	1	65.8
9	3	3	2	59.1
K1	60.567	60.467	61.967	
K2	58.4	61.933	60.167	
K3	61.333	57.9	60.867	
R	2.933	4.033	3.8	

Guan et al. (2012) used ultrasonic treatment of bamboo, and the results showed that the higher the power, the longer the time, the more substances were extracted from the bamboo. The difference in this experiment is that the maximum power of the ultrasonic instrument used

is much smaller than the power level selected for the above experiment, and the main effect is not the power level but the time. Based on the variance analysis of ultrasonic experiments (Tab. 4), the optimal conditions were 60°C, 90 min, and 400 W. However, the three factors selected in the experiment were not significant, and the influence order of each factor was the same as that in the range analysis.

Tab. 4: The range results of ultrasonic experiment.

Factors	Sum of squares	Degree of Freedom	F-value	Sig.
Temperature	13.887	2	4.441	/
Time	25.007	2	7.997	/
Ultrasonic power	21.680	2	6.933	/
Error	3.13	2		

Vacuum freeze-drying experiment

Percentages of water absorption in the glue-laminated bamboo increased as the duration prolonged during vacuum freeze-drying treatment under 0.05, 0.1, 0.5, 1.0, and 1.7 mbar, respectively as showed in Fig. 1a.

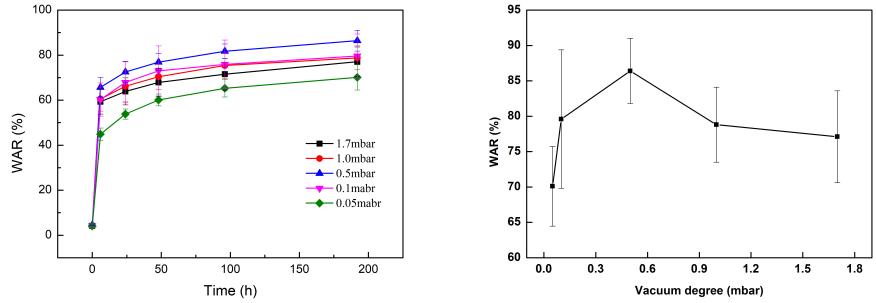

(a) (b)

Fig. 1: Percentage of water absorption of the treated bamboo after different vacuum freeze-drying experiments: (a)the treatment process, (b) the maximum water absorption ratio.

The water absorption ratios under these five vacuum degrees were higher in the first 10 h, and then the growth rate became slow. In the first 6 h, the water absorption rate of each group was larger, and the water absorption rate increased rapidly. Then, with the passage of time, the water absorption rate gradually decreased. At 192 h, the water absorption rate of the 0.5 mbar group was the highest, and the water absorption rate was 5%-16% higher than that of the other groups. In the subsequent experiments, 0.5 mbar was selected as the vacuum degree when the bamboo was dried. The reason for this phenomenon may be that too low a vacuum will make the sublimation process difficult to carry out, and too high a vacuum, the drying temperature is higher, so that the pore diameter of the bamboo material rebounds.

The comparison of the maximum water absorption ratio in the glue-laminated bamboo under these five vacuum degrees were shown in Fig. 1b. It can be seen that the water absorption ratio in the glue-laminated bamboo was increased as the vacuum degree increased from 0.05-0.5 mbar during vacuum freeze-drying treatment, and began to decrease when the vacuum degree was higher than 0.5. When the vacuum degree between 0.05 mbar and 0.5 mbar,

as the vacuum degree increased, the vapor pressure on the surface of the dried layer of treated bamboo was decreased, so that the crystallization inside the bamboo can be directly sublimated in a large volume, and the permeation effect is increased. From 0.5-1.7 mbar, when the vacuum degree increased, the surface of sublimation temperature would be lowered significantly, which has resulted in the decrease of the internal crystallization of the treated bamboo, and the originally enlarged pore size was rebounded, as the result the permeability became poor.

Comparison of different treatments on the water permeability

The optimal conditions of these three methods, hydrothermal experiment (HE), ultrasonic experiment (UE), vacuum freeze-drying experiment (VE) and the untreated sample (US) were showed in Fig. 2.

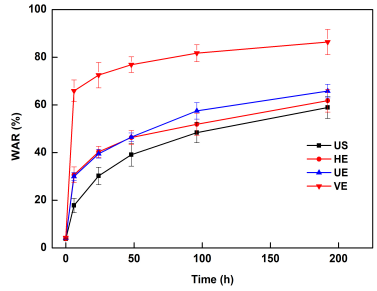

Fig. 2: Water absorption rate under four conditions: hydrothermal experiment (HE), ultrasonic experiment (UE), vacuum freeze-drying experiment (VE) and the untreated sample (US).

It was noted that the water absorption rate of the treated wood after different treatments was improved significantly compared to the control group. Among of these three treatments, the freeze-drying group had the best performance for improving the permeability of treated wood, and the water absorption rate could be increased by 47% compared to the control group. While hydrothermal and ultrasound treatments were not very promising, only increased by 5% and 12% resp. From the growth trend of the water absorption rate during 200 h, in the first 10 h, the water absorption rate of each group was increased sharply, then it would become gradually reduced, and after 150 h, the water content in the samples gradually became saturated.

In the hydrothermal treatment, due to the decrease in the extract, the obstruction substance in the passage inside the bamboo is reduced, and the permeation effect is improved. However, the disadvantage of this method is that, in addition to the extract which is soluble in boiling water, other types of extracts cannot be removed, resulting in an infiltration effect (Bao and Zhou 2017). Ultrasonic method relies on external force to cause cell wall damage and increase the penetration channel of bamboo. According to the observation results of SEM, the instrument used has less damage to the cell wall, which leads to poor penetration. The freeze-drying method uses the principle that the same mass of water becomes ice, and the volume becomes larger, and the pore diameter is enlarged inside the permeation channel, thereby increasing the permeation channel. From the experiment, compared with the former two methods, the effect is very obviously (Han 2007).

Mercury intrusion porosimeter analysis

According to Tab. 5, the total intrusion volume of the control sample was only 0.48 $mL \cdot g^{-1}$, while it would be increased by about 83% of the sample with freeze drying treatment. The reason was that a series of holes appeared on the freeze-dried sample as observed by SEM (Fig. 3), which became the channels to the bamboo inside, as the result more mercury could be pressed into the glue-laminated bamboo.

Tab. 5: MIP analysis of glue-laminated bamboo with different treatment conditions.

Sample	Total intrusion volume ($mL \cdot g^{-1}$)	Porosity (%)	Median pore diameter (nm)	Bulk density ($g \cdot cm^{-3}$)
Control	0.48	41.20	26.30	0.87
Freeze drying	0.87	51.80	50.40	0.60
Ultrasound	0.57	50.10	38.60	0.79
Hydrothermal	0.53	36.60	45.40	0.69

From the porosity results, compared with the control group, the median pore size of the three methods has increased. It can be seen that the porosity of untreated samples was quite low, which was the main reason for the poor permeability of bamboo, and the biggest porosity was only increased to 51.8% observed in the samples with the promising freeze drying treatment. The mercury intrusion volume of the ultrasound and the hydrothermal samples also increased with respect to the control samples, but the porosity of the hydrothermal group was lower than that of the control samples. The reason may be attributed that the porosity was derived from the volume of mercury injected/sample volume (Plötze et al. 2011, Yang et al. 2013). When the sample was selected, the sample may be selected from the bamboo plate at a different position. The selected sample has a larger volume, which results in a smaller porosity. Compared with the control group, hydrothermal methods and ultrasonic methods increased the volume of mercury by 11% and 20%.

The pore diameters of the freeze-dried samples were mainly about 40-50 nm as observed in Tab. 5, and the median diameter of the group was 50.40 nm. The ultrasound group had the largest difference from the control group at around 50 nm and 7 nm, and its general trend was similar to that of the freeze-dried group. The difference between the hydrothermal group and the control group was the most obvious at 25 nm, which indicated that the hydrothermal treatment increased the number of pores around 25 nm, but the amount was still less than that of the freeze-dried group. It was further verified that the permeation effect was not as good as that of the freeze-drying group. It shows that in the range of 40-50 nm, the distribution of the pore size is the most extensive. At a pore size after 76 nm, the volume difference of the pressed mercury is small, which is about 75% lower than the range of the previous mesopores (2-50 nm), and then the curve tends to be moderated. The relationship between the cumulative mercury intrusion volume and pore size of glue-laminated bamboo with different treatments were shown in Fig. 3.

In general, the samples with different modification treatments could improve the total intrusion volume significantly compared to control samples. As observed in Fig. 3, the pore diameters of the samples with different treatments for mercury intrusion were mainly 10-100 nm, and the cumulative mercury intrusion volume would decrease to a low level and change gently until the end when the pore size exceeded 100 nm.

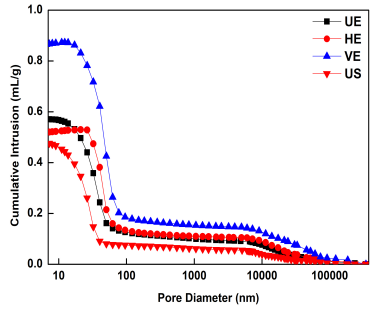

Fig. 3: Relationship between cumulative intrusion volume and pore diameter of glue-laminated bamboo with different treatment conditions.

It seemed that the cumulative mercury intrusion volume was bigger in the samples with different modification treatments compared to the control samples during mercury intrusion, and the promising result was observed in the freeze-dried samples, in which the cumulative intrusion volume was about 0.19-0.85 $mL \cdot g^{-1}$ in the range of 10-100 nm, while it was only about 0.09-0.45 $mL \cdot g^{-1}$.

Analysis of microstructure

Microstructures of the samples before and after different treatments were evaluated by SEM as showed in Figs. 4a-d. The structure of bamboo was mainly composed of some thin-walled tissues and tube bundle structures. It can be seen that the parenchyma cells of the untreated samples were relatively intact, and the structures were relatively dense as observed in Fig. 4a. While the other samples with different modification treatments behaved different structural changes.

For the freeze-dried samples as showed in Fig. 4b, some small holes appeared on the cell wall, which was due to that after freezing treatment the internal free water of the samples could be turned into ice, and the volume became larger, as the result the pore diameter of the glue-laminated bamboo could be enlarged, and then it was dried, and directly sublimated to ice, ensuring that the enlarged aperture does not rebound and return to its original state (Ilic et al. 1995).

For the ultrasonically treated samples as showed in Fig. 4c, it can be clearly seen that the cracks appeared on the cell wall of glue-laminated bamboo, and some holes with different sizes appeared on the parenchyma cells, which indicated that using water as a medium, ultrasonic waves can break the parenchyma tissue of glue-laminated bamboo. As the result, the perforated film provided channels for water intrusion.

For the hydrothermally treated samples as showed in Fig. 4d, it can be seen that the whole cell does not change at all compared to the control samples. The hydrothermal treatment was generally in the higher temperature condition, and used water as the medium to enlarge the pore size of the glue-laminated bamboo (Bao and Zhou 2017). During the treatment, the extracts were boiled out or evaporated. However, the effect of hydrothermal treatment on the enlarging pore size or increasing the number of pores was less than the other two modification treatments.

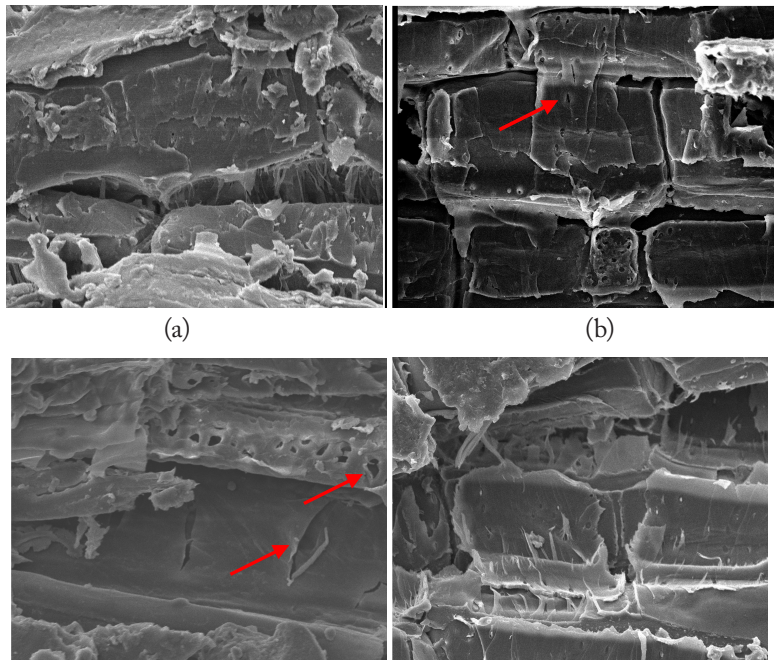

Fig. 4: Microstructure of bamboo before and after treatment: a) HS-1000×, b) VE-1000×, c) UE-1000×, d) HE-1000×.

CONCLUSIONS

The treatment effect of hydrothermal method is limited to the fact that many extracts cannot be extracted in the boiling water. The ultrasonic treatment effect is limited to the lower ultrasonic power of the selected instrument. The freeze-drying method has a good effect on the treatment of bamboo laminated materials. When the degree is 0.5 mbar, the water absorption rate can be optimized.

The mercury intrusion porosimetry relates the pore size distribution to the water absorption rate. The media pore size of the hydrothermal method (45.40 nm), the ultrasonic method (38.60 nm), and the freeze-drying method (50.40 nm), compared with the control group (26.3nm), have increased by 73%, 47%, 92%. Under the scanning electron microscope, both the ultrasonic method and the freeze-drying method can see the permeation channel after the external force is destroyed, and a series of micropores appear.

ACKNOWLEDGMENT

The authors are grateful for the financial support of the Subjects of National Natural Science Foundation of China (NSFC No. 31400499), the National College Students Innovation and

entrepreneurship training program (201910057047), and the Science and Technology of Tianjin University College Students Innovation and entrepreneurship training program (202110057013).

REFERENCES

1. Bao, Y., Zhou, Y., 2017: Comparison between superheated steam drying and conventional drying of Chinese cedar lumber. Scientia Silvae Sinicae 53(1): 88-93.
2. Chen, H., Zhang, Y.T., Xue, Y., Han, J., Zhong, T.H., Wang, G., 2019: A comparative study of the microstructure and water permeability between flattened bamboo and bamboo culm. Journal of Wood Science 65(1): 1-14.
3. Emaminasab, M., Tarmian, A., Pourtahmasi, K., Avramidis, S., 2016: Improving the permeability of Douglas-fir (*Pseudotsuga menziesii*) containing compression wood by *Physisporinus vitreus* and *Xylaria longipes*. International Wood Products Journal 7(3): 110-115.
4. Ge, H., 2012: A research on the apply of bamboo elements in packing design. Pp 24-32, China Academy of Art, Hangzhou, China.
5. Gao C., 2015: Study on the process and properties of hydrothermally treated poplar wood raw materials and its plate making. Master's thesis. Pp 25-34, Nanjing Forestry University, Nanjing, China.
6. Guan, M.J., Zhang, Z.W., Yong, C., Du, K.K., 2019: Interface compatibility and mechanisms of improved mechanical performance of starch/poly (lactic acid) blend reinforced by bamboo shoot shell fibers. Journal of Applied Polymer Science 136(35): 47899.
7. Hass, P., Wittel, F.K., Mendoza, M., 2012: Adhesive penetration in beech wood: experiments. Wood Science and Technology 46(1-3): 243-256.
8. Haase, J., Leung, L., Evans, P., 2018: Plasma pre-treatments to improve the weather resistance of polyurethane coatings on Black spruce wood. Coatings 9(1): 8-22.
9. Han, N., 2007: Progress of study on vacuum freeze-drying technology. Food Engineering (03): 28-29+47.
10. Huang, Z., 2017: Effect of ultrasonic treatment on surface properties and bonding properties of bamboo. Pp 49-55, Nanjing Forestry University, Nanjing, China.
11. Ilic, J., 1995: Advantages of prefreezing for reducing shrinkage-related degrade in eucalyptus: General considerations and review of the literature. Wood Science & Technology 29(4): 277-285.
12. Kaur, P.J., Pant, K.K., Naik, S.N., 2016: Field investigations of selectively treated bamboo species. European Journal of Wood and Wood Products 74(5): 771-773.
13. Kaur, P., Kardam, V., Pant, K.K., 2013: Scientific investigation of traditional water leaching method for bamboo preservation. Bamboo science and culture. Journal of the American chemical society, 23(1): 27-32.
14. Li, Y., Liu, Y., Wang, F., 2011: Control factors and improvement measures of wood permeability. Scientia Science and Technology 47(5): 131-139.
15. Lu, C., Jiang, T., Liu, Y., 2017: Research progress on the influence factors of eucalyptus wood permeability and its improvement methods. Journal of Southwest Forestry University (Natural Science) 37(1): 214-220.
16. Lv, J.X., Li, Z.Y., Jiang, J.L., 2005: Liquid penetration of freeze-drying and air-drying wood of plantation Chinese fir. Forestry Study 16(4): 293-295.
17. Plötze, M., Niemz, P., 2011: Porosity and pore size distribution of different wood types as determined by mercury intrusion porosimetry. European Journal of Wood and Wood Products 69(4): 649-657.

18. Rao, S., Yu, L., 2013: Effect of pretreatment on fluid permeability of bamboo. Forestry Machinery & Woodworking Equipment 41(8): 26-29.
19. Sernek, M., Resnik, J., Kamke, F.A., 1999: Penetration of liquid urea-formaldehyde adhesive into beech wood. Wood and Fiber Science 31(1): 41-48.
20. Seo, H.J., Kim, S., Huh, W., 2016: Enhancing the flame-retardant performance of wood-based materials using carbon-based materials. Journal of Thermal Analysis and Calorimetry 123(3): 1935-1942.
21. Wen, X., 2017: Study on the penetration and influence factors of preservatives in bamboo. Pp 43-49, Chinese Academy of Forestry, Beijing, China.
22. Xu, J., He, S., Li, J., 2018: Effect of vacuum freeze-drying on enhancing liquid permeability of Moso bamboo. BioResources 13(2): 4159-4174.
23. Xiao, H., 2017: Microwave treatment of *Pinus sylvestris* var. Mongolica. Pp 89-92, Chinese Academy of Forestry, Beijing, China.
24. Yang, F., Ning, Z., Kong, D., Liu, H., 2013: Analysis of shale pore structure by high pressure mercury intrusion and nitrogen adsorption. Natural Gas Geosciences 3: 450-455.
25. Yong, C., Chan, X., Guan, M., 2013: Effect of ultrasonic wall breaking effect on transverse permeability of bamboo. Bamboo Research Summary 32(4): 33-36+41.

Chunyan Lv, Caijuan Zhang, Xinjie Zhou, Mingyu He, Lili Yu*
Tianjin University Of Science And Technology
P. R. China
Zhenzhong Tang*
China Timber & Wood Products Distribution Association
P. R. China

Chunyan Lv, Caijuan Zhang, Xinjie Zhou, Mingyu He, Lili Yu*
Tianjin University Of Science And Technology
Faculty Of Light Industry Science And Engineering
Dagu Southroad 1038, Hexi District, P. O. Box 546
300222 Tianjin
Q. R. China

Zhenzhong Tang*
China Timber & Wood Products Distribution Association
R. R. China
Lugu Road 74, Shijingshan District
100040 Beijing

*Corresponding author: yulilucky@tust.edu.cn
*Corresponding author: zhenzhongtang@hotmail.com

WOOD RESEARCH
e-ISSN 2729-8906
66(3):2021 365-378 pp.
doi.org/10.37763/wr.1336-4561/66.3.365378

CHARACTERISTIC FEATURES OF THE OIL-HEAT TREATED WOODS FROM TROPICAL FAST GROWING WOOD SPECIES

Intan Fajar Suri, Byantara Darsan Purusatama, Seung Hwan Lee, Nam Hun Kim
Kangwon National University
Republic Of Korea

Wahyu Hidayat, Shalehudin Denny Ma'ruf
University Of Lampung
Indonesia

Fauzi Febrianto
IPB University
Indonesia

(Received July 2020)

ABSTRACT

This study aimed to evaluate the effect of oil-heat treatment on the anatomical, physical, and chemical properties of the tropical fast-growing wood species as gmelina (*Gmelinaarborea*) and mindi (*Melia azedarach*) wood. Vessel lumen area and diameter in radial and tangential direction of both species increased with increasing temperature. The fiber lumen areas in both woods were remarkably decreased by oil-heat treatment, and the fiber wall area increased considerably with increasing temperature. Both woods tended to gain weight after heat treatment at 180°C and 200°C, and then lose weight after heat treatment at 220°C. The density of mindi increased greatly at 180°C and 200°C and slightly decreased at 220°C. The dimension of the specimens in tangential direction increased with heat treatment, but the rate decreased with increasing temperature. The relative crystallinity and crystallite width of the heat-treated woods were greater than those of the untreated wood. In the Fourier transform infrared analyses, the peaks from the carbohydrates were changed after oil-heat treatment, mainly due to the degradation of hemicellulose. Consequently, it was revealed that the heat treatment affected various properties of gmelina and mindi woods. Differing characteristics between the species were also noted.

KEYWORDS: Anatomical properties, chemical composition, *Gmelinaarborea*, *Melia azedarach*, oil-heat treatment, physical properties.

INTRODUCTION

The potential supply and utilization of wood from plantation forests continue to increase. The wood harvested from plantation forests in Indonesia mostly belongs to fast-growing wood species as well as gmelina (*Gmelinaarborea*) and mindi (*Melia azedarach*). Gmelina has raised interest because of its rapid growth and rapid return on investment that can be used for many products ranging from pulp to furniture (Dvorak 2004). Mindi is considered as a fast-growth and drought-resistant species and widely used for construction, furniture, or interior decoration because it is quite durable and termite resistant (Bui et al. 2019). However, wood from most fast-growing species is generally low in quality, and its properties need to be improved, due to inferior quality with low density, low durability, and low mechanical properties, rendering them not suitable as structural materials(Febrianto et al. 2015).

Modification by heat treatment is one of the recent technologies used to improve some properties of woods (Biziks et al. 2013,Hidayat et al. 2016). Heat treatment of wood can be applied to achieve the desired improvement in dimensional stability and hydrophobicity (Tjeerdsma and Militz 2006), and biological durability (Welzbacher et al. 2008). Welzbacher et al. (2011) also reported that thermal treatment leads to substantial loss of the strength of heat-treated woods. Heat-treated wood also had lower equilibrium moisture content than untreated wood (Hidayat et al. 2015) and increased in hydrophobicity with increasing contact angle on wettability (Kocaefe et al. 2008). Meanwhile, heat treatment affects the anatomical structure of wood, as evidenced by the destruction of tracheid walls and ray tissues, as well as pit deaspiration (Awoyemi and Jones 2011), but this depends on the wood species, heat treatment process, and the conditions used (Boonstra et al. 2006).

With regard to cost, environmental-friendliness, and sustainability of chemistry, oil-heat treatment is considered one of the most practical approaches to eliminating the inferior features of wooden materials (Tang et al. 2019). Another related study on oil-heat treatment also explained that oil uptake also contributes to the dimensional stability and hydrophobicity (Wang and Cooper 2005) as well as fungal resistance and darkening (Dubey et al. 2011) of wood. Lee et al. (2018) demonstrated that oil-heat-treated wood showed superior dimensional stability to that of wood treated in hot air and nitrogen. Oil heat treatment can also be used to upgrade wood for outdoor uses and uniformly color its surface (Sailer et al. 2000).

To date, information on the improvement of the wood quality of fast-growing wood species using oil-heat treatment has been lacking. Therefore, in the present study, oil heat treatment was applied to improve the wood quality of two fast-growing wood species, gmelina and mindi, growing in Indonesia

MATERIAL AND METHODS

Materials

Gmelina (*Gmelinaarborea*) and Mindi (*Melia azedarach*) woods were harvested from PerumPerhutaniKesatuanPemangkuanHutan (KPH) Bogor and KPH Purwakarta in Java, Indonesia. Logs of woods were converted into quarter-sawn boards with dimensions of 200 mm (L) x 90 mm (R) x 20 mm (T). Boards were selected that were free of natural defects and straight grain. Then the selected boards were air-dried and conditioned at 25˚C ± 5˚C under a relative humidity of 70–80% until they reached the equilibrium moisture content.

Methods

Oil-heat treatment

Boards were heat-treated in a lab-scale oil bath using commercial cooking palm oil. The heat treatment was started at an initial temperature of 25°C - 30°C. The temperature was then raised to the target of 180°C, 200°C, and 220°C at the rate of 2°C·min^{-1}. The target temperature was maintained over a period of 1 h. In the final stage of heat treatment, the oil bath was allowed to cool naturally until it reached ± 30°C. The boards were then taken out and stored in a room with the relative humidity of 70–80% and a temperature of 25 ± 5°C for two weeks until further testing.

Scanning electron microscopy

The smooth transversal section of the block with a dimension of 10 mm (L) x 10 mm (T) x 10 mm (R) was prepared with a microtome, and then oven-dried and a Cressington sputter coater (ULVAC G-50DA, Japan) used to coat the sample. Microscopic observation was performed with a scanning electron microscope (JSM-5510, JEOL, Japan, 15kV). The micrographs of each sample were analyzed for measuring vessel lumen area (μm^2), diameter of vessel lumen in the radial (RD) and tangential (TD) direction (μm), fiber lumen area (μm^2), and fiber wall area (μm^2). The measurements for each parameter were examined 90 times. The change of cell lumen area in vessel and fiber was calculated using the following formula (Biziks et al. 2013):

$$SEM\ (\%) = \frac{SEM_1 - SEM_0}{SEM_0} \times 100 \quad (1)$$

where: SEM (%) is the change in the cell lumen area in the vessel and the fiber (%), SEM_1 is the cell lumen area after heat treatment, and SEM_0 is the cell lumen area before heat treatment. Measurements were performed using the freely-available ImageJ software package (University of Wisconsin, Madison, USA).

Measurements of physical properties

Weight change before and after the heat treatment was intended according to the following formula:

$$WC\ (\%) = \frac{m_1 - m_0}{m_0} \times 100 \quad (2)$$

where: $m_0$is the weight of samples before oil-heat treatment (g) and m_1 is the weight of samples after oil-heat treatment (g). Density (D) of samples before and after heat treatment was intended according to the following formula:

$$D = \frac{m}{v} \quad (3)$$

where: m is the weight (g) and vis the volume of samples (cm^3). Swelling in tangential direction of samples before and after heat treatment was intended according to the following formula:

$$S\ (\%) = \frac{S_1 - S_0}{S_0} \times 100 \quad (4)$$

where: S_0 is the swelling of samples before oil-heat treatment (mm) and S_1 is the swelling of samples after oil-heat treatment (mm). Three samples were measured for each physical property after each treatment and mean values were determined.

Crystalline characteristic analyses

An X-ray diffractometer (DMAX2100V, Rigaku, Tokyo, Japan) was used to measure crystalline characteristics as relative crystallinity and crystallite width. Segal's equation

(Segal et al. 1959) was used to calculate the relative crystallinity:

$$Relative\ crystallinity = \frac{I_{200} - I_{am}}{I_{200}} \times 100 \quad (5)$$

where: I_{200} is the diffraction intensity of (200) (2θ = 22.8°) and I_{am} is the diffraction intensity of the non-crystalline portion (2θ = 18°). The crystallite width was calculated using the Scherer's equation (Burton et al. 2009):

$$L = \frac{K\lambda}{\beta cos\theta} \quad (6)$$

where: L is the crystallite width, K is the Sherrer constant (0.9), λ is the X-ray wave length (λ = 0.1542 nm), and β is half-width in radians. Three samples were measured for each treatment and average values were determined.

Chemical composition analyses

To investigate the chemical composition of gmelina and mindi woods before and after oil-heat treatment, wood powders for each treatment were prepared. The spectra were measured using the attenuated total reflection (ATR) method in the range of 4000-400 cm^{-1} with Fourier transform infrared spectrometer (Perkin Elmer Inc., USA) set in the main laboratory of Kangwon National University.

Statistical analysis

All multiple comparisons were analyzed with multivariate analysis of variance. Significant ($\alpha \leq 0.05$) differences between values of the untreated and treated samples were determined using Duncan's multiple range tests. All statistics were performed using SPSS ver. 24, IBM Corp., New York, USA.

RESULTS AND DISCUSSION

Anatomical properties

As shown in Tab. 1, the vessel lumen area and diameter of vessel lumen in a radial (RD) and tangential (TD) direction increased with increasing temperature. Gmelina wood increased up to 5.6% in the vessel lumen area and 24.7% and 18.3% in the diameter of vessel lumen in radial and tangential directions, respectively, at 220°C. While in mindi wood, there was an increase of up to 59.9% in vessel lumen area, 37.4% in the radial diameter, and 17.1% in the tangential diameter of vessel lumen at 220°C. Comparing both species, it can be explained that mindi wood showed a greater change in the dimension of the vessel than in gmelina wood during heat treatment. Fig. 1 shows the vessels on the transverse section of the gmelina and mindi woods with the same magnification before and after oil-heat treatment; the vessel dimension in both the wood species increased with heat treatment. Batista et al. (2015) reported that the vessel diameter of *Eucalyptus grandis* wood increased after heat treatment at 140°C, but this increase was not significant. However, Biziks et al. (2013) reported opposite results, that in *Betula pendula*, lumen area and diameter of the vessels slightly decreased, and the wall area and wall thickness of the vessels considerably decreased after hydrothermal treatment. A significant change in fiber dimension was observed, as shown in Tab. 1. The fiber lumen area of gmelina wood decreased by 36.2%, fiber wall area increased by 60.1%, and fiber total area decreased by 1.37% at 220°C. The fiber lumen area in mindi greatly decreased by 61.9%, the fiber wall area increased by 61.1%, and fiber total area decreased by 11.58% at 220°C. The fiber lumen area and fiber total area decreased, while the fiber wall area increased with increasing temperature. This shows that the fiber wall swelled as a result of oil uptake during heat treatment and that the heat temperature affected the swelling of the cell wall. Scanning

electron micrographs of the fibers of gmelina and mindi before and after oil-heat treatment are shown in Fig.2. The fiber lumen area of the treated wood clearly decreased to less than that of the untreated wood, but the fiber wall area increased with increasing temperature. Ling et al. (2016) reported similar results in *Populuscathayaha* sapwood, in which the fiber walls thickened and fiber lumen size shrank during and after heat treatment. Biziks et al. (2013) observed structural changes in *Betula pendula* wood: the fiber lumen area, fiber total area, and fiber wall area decreased during hydrothermal treatment. They described that the degradation of hemicelluloses in cell wall, which is known as the most unstable wood component, causes the change in cell dimension by heat treatment. Awoyemi and Jones (2011) also explained that changes in wood anatomy might be affected by wood properties with chemical degradation during the process of heat treatment. In this study, the oil-heat treatment led to anatomical changes in the wood cells. This phenomenon could be explained as follows: *(1)* The cell wall in the wood fiber and vessel might be softened and become more flexible following oil uptake, *(2)* The increased size of the vessel lumen can also be attributed to the tension force induced by the change of fiber dimension in the swollen state due to oil uptake, *(3)* The space created due to changes in fiber dimensions allowed the vessel dimension to increase in oil-heat-treated wood as compared to that of untreated wood. Bernabei and Salvatici (2016) demonstrated that the tracheid cell dimensions decreased, but in certain cases, it increased after treatment, because of the power given to the lumen by surrounding cells. Boonstra et al. (2006) also explained that the dimensions of vessels and rays were changed due to the contraction of the cell walls and the shrinkage of the surrounding cells, such as the wood fibers or tracheid.

Tab. 1: Dimensional changes in vessels and fibers before and after oil-heat treatment.

Wood species	Cell type	Vessel			Fiber		
	Measurements	Lumen area (μm²)	RD (μm)	TD (μm)	Lumen area (μm²)	Wall area (μm²)	Total area of fiber (μm²)
Gmelina	Initial sizes	11455 (1524)	112.1 (1.53)	92.2 (3.30)	97.6 (1.74)	59.4 (4.74)	158 (2.45)
Mindi	Initial sizes	24126 (7008)	164.6 (3.72)	143.5 (1.52)	87.7 (1.18)	61.4 (1.59)	149 (1.47)
	Temperature (°C)	Changes (%)					
Gmelina	180	2.3 (2.28)	14.4 (3.82)	4.7 (2.70)	-2.2 (1.32)	1.6 (3.24)	-0.84 (1.73)
	200	4.9 (2.35)	23.2 (3.33)	10.1 (5.24)	-23.0 (0.55)	37.0 (1.52)	-0.86 (1.15)
	220	5.6 (2.39)	24.7 (2.10)	18.3 (2.51)	-36.2 (0.65)	60.1 (3.94)	-1.37 (3.74)
Mindi	180	19.0 (7.53)	19.9 (4.05)	1.2 (3.72)	-12.9 (1.16)	12.5 (1.11)	-2.39 (1.98)
	200	30.7 (3.81)	24.6 (1.52)	13.7 (6.08)	-34.5 (2.58)	42.5 (1.76)	-2.75 (2.02)
	220	59.9 (6.92)	37.4 (4.65)	17.1 (2.64)	-61.9 (6.14)	61.1 (2.75)	-11.58 (2.65)

Notes: The numbers in parenthesis are the standard deviations. RD: diameter of vessel in radial direction, TD: diameter of vessel in tangential direction.

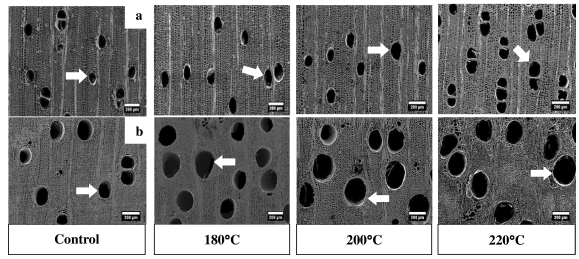

Fig.1: Vessels on the transverse sections of gmelina (a) and mindi (b) before and after oil-heat treatment. White arrows indicate the change in vessel lumen size before and after oil-heat treatment.Scale bars: 200μm.

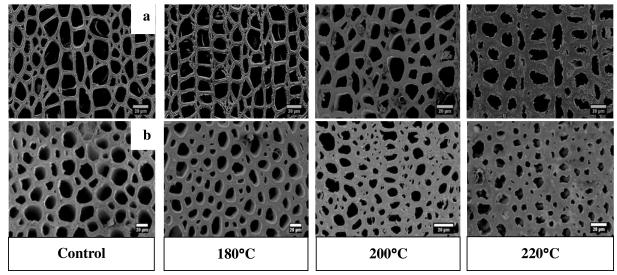

Fig.2: Fibers on the transverse sections of gmelina (a) and mindi (b) before and after oil-heat treatment. Scale bars: 20μm.

Physical properties

The physical properties of gmelina and mindi woods before and after oil-heat treatment are shown in Tab. 2. A higher degree of weight change was observed in mindi, showing a great increase in the weight after heat treatment at 180°C and 200°C and a decrease in the weight at 220°C. Gmelina wood gained weight slightly at 180°C and 200°C and rapidly lost weight at 220°C. This result agreed with the study conducted by Dubey et al. (2011) that observed an increase in specimen weight due to oil absorption during heat treatment and a weight decrease with increasing temperature and time. Sailer et al. (2000) also reported that the weight of *Pinussylvestris* and *Piceaabies* increased by about 50 ± 70% after oil-heat treatment. Dubey et al. (2011) also stated that the weight decrease after heat treatment indicated the change of chemical composition in wood, particularly, the degradation of the hemicellulose content up to 70%. Hidayat et al. (2015) and Mburu et al. (2007) also explained that the weight loss of wood was due to the degradation of hemicelluloses during heat treatment.

Tab. 2: Weight change, density, and swelling after heat treatment.

Wood species	Temperature (°C)	Weight change* (%)	Density ($g \cdot cm^{-3}$)	Swelling in tangential direction (%)
Gmelina	Control	-	0.43 (0.02)	-
	180	1.98 (0.02)	0.45 (0.01)	3.46 (0.65)
	200	2.50 (0.06)	0.43 (0.01)	2.32 (0.58)
	220	-5.73 (1.04)	0.42 (0.02)	2.09 (0.29)
Mindi	Control	-	0.51 (0.03)	-
	180	24.61 (4.38)	0.66 (0.02)	5.77 (1.36)
	200	15.03 (0.98)	0.59 (0.02)	4.20 (1.02)
	220	-7.39 (0.74)	0.48 (0.01)	0.66 (1.06)

Note: *minus (-) values mean weight loss and vice versa. The numbers in parenthesis are the standard deviations.

The density of mindi wood after heat treatment was changed as shown in Tab. 2. The density increased greatly at 180°C and 200°C and slightly decreased at 220°C. However, the density of gmelina wood before and after treatment was scarcely changed. Wang et al. (2014) observed similar result as the density of *Eucalyptus pellita* wood decreased slowly with increasing the temperature at 200°C and 240°C. They stated the two possible factors for the decrease in density during heat treatment as the degradation of hemicellulose and volatile components.

The specimen's thickness in tangential direction increased with heat treatment as shown in Tab. 2. The degree of swelling decreased with increasing temperature. The woods treated at 220˚C appeared more stable than those treated treated at 180˚C and 200˚C. This result agreed with the study of Bal (2015) that the swelling values of wood treated with oil-heat treatment decreased with increasing temperature. Lee et al. (2018) stated that oil absorption and oil deposits in the cell walls of wood also act as factors, which contribute to the improvement of the dimensional stability of wood.

Crystalline characteristics

The relative crystallinityof the heat-treated woods was slightly larger than that of the untreated woods, as shown in Tab. 3. It could be suggested that the relative crystallinity increased with heat treatment. Kim et al. (2018) reported that heat treatment increased the relative crystallinity of Paulownia wood. Yun et al. (2015) also reported that the relative crystallinity of Eucalyptus urophylla and E. camaldulensis increased as the temperature increased. The increase in crystallinity can probably be attributed to the degradation of hemicelluloses and the realignment of cellulose (Tang et al. 2019).

Tab 3: Crystalline properties of gmelina and mindi woods before and after oil-heat treatment.

Wood species	Temperature (°C)	Relative crystallinity (%)	Crystallite width (nm)
Gmelina	Control	57.3^{a} (1.5)	2.69^{a} (0.14)
	180	58.2^{a} (3.4)	2.84^{a} (0.16)
	200	60.9^{b} (1.7)	2.97^{a} (0.14)
	220	69.3^{c} (0.5)	3.22^{b} (0.11)
Mindi	Control	57.8^{a} (2.8)	2.85^{a} (0.07)
	180	58.4^{a} (2.0)	2.91^{a} (0.14)
	200	61.4^{b} (2.0)	3.03^{a} (0.28)
	220	68.5^{c} (2.3)	3.45^{b} (0.38)

Note: The numbers in parenthesis are the standard deviations. The different letters beside the mean value show the significance at 5% level between untreated and treated wood using Duncan's multiple range tests.

The heat-treated woods showed slightly larger crystallite width than that of the untreated one, as shown in Tab. 3. It seems that the crystallite width could be increased after oil-heat treatment. Kubojima et al. (1998) also reported that the crystallite length of the heat-treated Sitka spruce seemed to be increased. The same tendency was also observed by Andersson et al. (2005), stating that the increase in the size of cellulose crystallites was due to the changes in porosity of the cell wall by the degradation of the amorphous part of wood during heat treatment.

Chemical composition analyses

Fig.3 shows the FTIR spectra of gmelina and mindi before and after oil-heat-treatment, and the appropriate peak assignment is summarized in Tab. 4. The spectral differences before and after oil-heat treatment were more considerable for mindi wood than for gmelina wood. The heat-treated wood showed the decreased characteristics of carbohydrates as compared to the untreated wood. The peak at 1740 cm^{-1} corresponding C=O stretch decreased greatly in both gmelina and mindi with increasing temperature. Lin et al. (2018) reported that the peaks at 1730–1740 cm^{-1} of poplar and fir wood decreased with increasing temperature. They explained that the decrease was caused by the cleavage of acetyl side chains of hemicellulose

after heat treatment. Ling et al. (2016) also reported that the peak at 1740 cm^{-1} on heat-treated *Populuscathayaha* wood decreased. Similarly, Cheng et al. (2016) reported that the peak at 1734 cm^{-1} of Chinese fir wood changed slightly at 190°C and considerably decreased at 230°C. Esteves et al. (2013) also reported that the peaks at 1740 cm-1 assigned to the division of acetyl or acetoxy groups in xylan of eucalypt wood decreased, showing the degradation of hemicelluloses. The peak at the range of 1105 and 1050 cm^{-1}, corresponding to C-O-C stretching in cellulose and hemicellulose, in mindi also slightly decreased at 220°C. Mburu et al. (2007) reported that the peaks at 1058 cm^{-1} in heat-treated *Grevillea robusta* wood slightly decreased as temperature increased. They also stated that the decrease of the band confirmed the degradation of hemicelluloses.

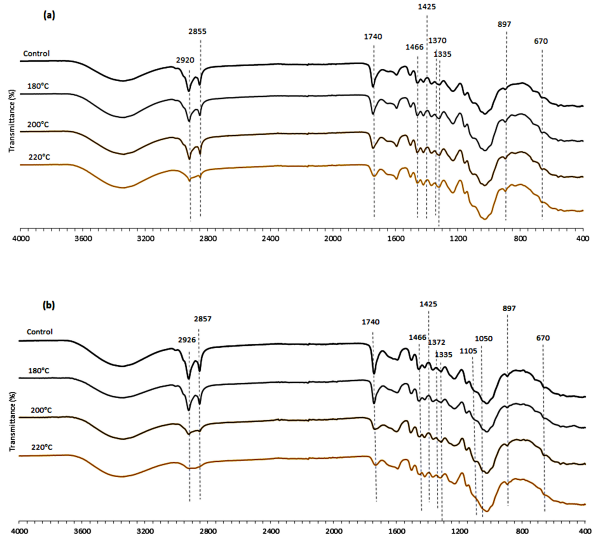

Fig. 3: FTIR spectra of gmelina (a) and mindi (b) wood before and after oil-heat treatment.

Tab. 4: Peak assignment for FTIR spectra of gmelina and mindi before and after oil-heat treatment.

Wave number (cm^{-1})	Peak assignment
2926	C-H stretching in cellulose (Esteves et al. 2013, Schwanninger et al. 2004)
2857	
1740	C=0 stretch (unconjugated) in esters, ketones, aldehydes and acids (Esteves et al. 2013, Schwanninger et al. 2004, Lin et al. 2018)
1466	C-H deformations; asymmetric in $-CH_3$ and $-CH_2-$ (Huang et al. 2012, Schwanninger et al. 2004)
1425	Aromatic skeletal vibrations (lignin) and C H deformation in plane (cellulose) (Schwanninger et al. 2004)
1372	C H deformation in cellulose and hemicellulose (Schwanninger et al. 2004)
1105	C-O-C stretching in cellulose and hemicellulose (Traoré et al. 2018)
1050	C-O stretching of secondary alcohols (Mburu et al. 2007, Traoré et al. 2018)
897	C H deformation in cellulose (Schwanninger et al. 2004)
670	C-OH out-of-plane bending mode (Schwanninger et al. 2004)

In addition to the characteristics of carbohydrates, heat-treated wood and untreated wood were also pronounced well by the peak of lignin at 1466 cm^{-1}. The peak in gmelina and mindi decreased scarcely as the temperature increased. It indicates that lignin is also degraded by heat treatment, but the rate of degradation is much less than that of the hemicelluloses. Huang et al. (2012) reported that the peak at 1465 cm^{-1} in jack pine wood decreased after heat treatment and weathering. Cheng et al. (2013) also reported that the peak at 1462 cm^{-1} in moso bamboo decreased after being heat-treated with three aqueous solutions.

The cellulose crystallinity was also determined using different IR crystallinity ratios. There are two methods to determine the crystallinity, i.e., the first is the ratio of peak areas *A*1370/*A*670, and the second is the ratio of peak heights at *H*1429/*H*897 and at *H*1372/*H*2900 (Åkerholm et al. 2004). Tab. 5 summarizes the result of the measurements.

Tab. 5: Cellulose crystallinity of gmelina and mindi using different IR peak ratios.

Wood species	Temperature (°C)	IR peak ratio		
		A_{1370}/A_{670}	H_{1429}/H_{897}	H_{1372}/H_{2900}
Gmelina	Control	7.50	1.67	0.14
	180	8.33	1.75	0.19
	200	8.80	2.00	0.20
	220	8.93	1.60	0.55
Mindi	Control	8.05	1.25	0.12
	180	8.25	1.00	0.14
	200	8.46	1.67	0.58
	220	8.48	1.50	0.60

The ratio of the peak areas (*A*1370/*A*670) at 1370 and 670 cm^{-1} increased with increasing temperature in gmelina wood whereas the rate increased slightly in mindi wood. Then the values of *H*1429/*H*897 and *H*1372/*H*2900 showed a tendency to increase with increasing temperature in both species. These results indicate that the crystallinity of both woods increased as temperature increased. It is well matched with the result of X-ray diffraction analyses. Akgül et al. (2016) reported that the crystallinity in *Pinussylvestris* and *Abiesnordmanniana* wood increased after heat treatment. They explained that the increase in crystallinity might be due to the re-crystallization of cellulose molecules in quasi-crystalline amorphous region. Yildiz and Gümüskaya (2007) reported that all of the IR peak ratios in spruce and beech woods increased with increasing temperature from 150 to 200°C.

CONCLUSIONS

The oil-heat treatment process of gmelina and mindi wood were investigated to clarify their characteristics before and after treatment. The vessel lumen area and diameter in radial and tangential direction increased with increasing temperature. The fiber lumen area and the fiber total area decreased and the fiber wall area increased with increasing temperature. Oil heat-treatment at 180°C and 200°C led to considerable weight gain for mindi wood but only slight weight gain for gmelina wood. Both wood species lost weight after treatment at 220°C. The dimensions of specimens in tangential direction were increased by the oil-heat treatment. The degree of swelling decreased with increasing temperature. The relative crystallinity of the heat-treated woods was measured by the XRD and FTIR methods increased with

increasing temperature. In FTIR analyses, the peaks from carbohydrate changed after the oil-heat treatment, mainly due to the degradation of hemicellulose.In this study, there were considerable changes in the anatomical, physical, and chemical properties of both wood species after the oil-heat treatment. Mindi wood showed greater changes in the properties than that of gmelina. The results suggest that in the process of heat treatment, species characteristics may be important for the evaluation of the final products.

ACKNOWLEDGMENT

This research was supported by the Basic Science Research Program through the National Research Foundation of Korea (NRF) which is funded by the Ministry of Education (NRF-2016R1D1A1B01008339), Basic Science Research Program through NRF funded by the Ministry of Education (NRF-2018R1A6A1A03025582) and Science and Technology Support Program through the National Research Foundation of Korea (NRF) and funded by the Ministry of Science and ICT (MSIT) (NRF-2019K1A3A9A01000018). This research was also supported by the Indonesian Ministry of Research, Technology, and Higher Education through Post-Doctoral Research Grant in 2019 (Contract No. 065/SP2H/LT/DRPM/2019).

REFERENCES

1. Akgül, M., Gümüskaya, E., Korkut, S., 2007: Crystalline structure of heat-treated Scots pine (*Pinussylvestris* L.) and Uludag fir (*Abiesnordmanniana* (Stev.) subsp. Bormuelleriana (Mattf.)) wood. Wood Science and Technology 41: 281-289.
2. Andersson, S., Serimaa, R., Vaananen, T., Paakkari, T., Jamsa, S., Viitaniemi, P., 2005: X-ray scattering studies of thermally modified Scots pine (*Pinussylvestris* L.). Holzforschung 59: 422–427.
3. Awoyemi, L., Jones, P.I., 2011: Anatomical explanations for the changes in properties of western red cedar (*Thujaplicata*) wood during heat treatment. Wood Science and Technology 45: 261–267.
4. Åkerholm, M., Hinterstoisser, B., Salmén, L., 2004: Characterization of the crystalline structure of cellulose using static and dynamic FT-IR spectroscopy. Carbohydrate Research 339: 569–578.
5. Bal, B.C., 2015: Physical properties of beech wood thermally modified in hot oil and in hot air at various temperatures.Maderas. Ciencia y tecnología 17(4): 789 – 798.
6. Batista, D.J., Paes, J.B., Muniz, G.I.B.D., Nisgoski, S., Oliveira, J.T.D.S., 2015: Microsturctural aspects of thermally modified *Eucalyptus grandis* wood. Maderas. Ciencia y tecnologia 17(3): 525-532.
7. Bernabei, M., Salvatici, M.C., 2016: In situ ESEM observations of spruce wood (*Piceaabies* Karst.) during heat treatment. Wood Science andTechnology 50: 715-726.
8. Biziks, V., Andersons, B., Belkova, L., Kapaca, E., Militz, H., 2013: Changes in the microstructure of birch wood after hydrothermal treatment. Wood Science and Technology 47: 717-735.
9. Boonstra, M.J., Rijsdijk, J.F., Sander, C., Kegel, E., Tjeerdsma, B.F., Militz, H., Van, A.J., Stevens, M., 2006: Microstructural and physical aspects of heat treated wood. Part 1. softwoods. Maderas. Cienca y tecnología 8: 193–208.

10. Bui, T.P., Ly, L.K., Do, P.T., Nguyen, N.H., Nguyen, P.V., Tran, Q.H., Pham, N.B., Chu, H.H., 2019: Improvement of biomass production in transgenic *Melia azedarach* L. plants by the expression of a GA20-oxidase gene. Turkish Journal of Botany 43: 281-289.
11. Burton, A.W., Ong, K., Rea, T., Chan, I.Y., 2009: On the estimation of average crystallite size of zeolites from the Scherrer equation: A critical evaluation of its application to zeolites with one-dimensional pore systems. Microporous and Mesoporous Materials 117(1): 75-90.
12. Cheng, S., Huang, A., Wang, S., Zhang, Q., 2016: Effect of different heat treatment temperatures on the chemical composition and structure of Chinese fir wood. BioResources 11(2): 4006-4016.
13. Cheng, D., Jiang, S., Zhang, Q., 2013: Effect of hydrothermal treatment with different aqueous solutions on the mold resistance of moso bamboo with chemical and FTIR analysis. BioResources 8(1): 371-382.
14. Dubey, M.K., Pang, S., Walker, J., 2013: Changes in chemistry, color, dimensional stability and fungal resistance of *Pinusradiata* D. Don wood with oil heat-treatment. Holzforchung 66(1): 49-57.
15. Dvorak, W.S., 2004: World view of *Gmelinaarborea*: opportunities and challenges. New Forest 28: 111-126.
16. Esteves, B., Marques, A.V., Domingos, I., Pereira, H., 2013: Chemical changes of heat treated pine and eucalypt wood monitored by FTIR. Maderas. Cienc y tecnología 15: 245-258.
17. Febrianto, F., Pranata, A.Z., Septiana, D., Arinana, Gumilang, A., Hidayat, W., Jang, J.H., Lee, S.H., Hwang, W.J., Kim, N.H., 2015: Termite resistance of the less known tropical woods species grown in West Java, Indonesia. Journal of the Korean Wood Science and Technology 43(2): 248–257.
18. Hidayat, W., Jang, J.H., Park, S.H., Qi, Y., Febrianto, F., Lee, S.H., Kim, N.H., 2015: Effect of temperature and clamping during heat treatment on physical and mechanical properties of okan (*Cylicodiscusgabunensis* (Taub.) Harms) wood. BioResources 10(4): 6961-6974.
19. Hidayat, W., Qi, Y., Jang, J.H., Febrianto, F., Lee, S.H., Kim, N.H., 2016: Effect of treatment duration and clamping on the properties of heat-treated Okan wood. BioResources 11(4): 10070-10086.
20. Huang, X., Kocaefe, D., Kocaefe, Y., Boluk, Y., Pichette, A., 2012: Changes in wettability of heat-treated wood due to artificial weathering. Wood Science and Technology 46: 1215-1237.
21. Kim, Y.K., Kwon, G.J., Kim, A.R., Lee, H.S., Purusatama, B.D., Lee, S.H., Kang, C.W., Kim, N.H., 2018: Effects of heat treatment on the characteristics of royal paulownia (*Paulownia tomentosa* (Thunb.) Steud.) wood grown in Korea. Journal of the Korean Wood Science and Technology 46(5): 511-526.
22. Kocaefe, D., Poncsak, S., Dore, G., Younsi, R., 2008: Effect of heat treatment on the wettability of white ash and soft maple by water. HolzalsRoh- und Werkstoff66: 355–361.
23. Kubojima, Y., Okano, T., Ohta, M., 1998: Vibrational properties of Sitka spruce heat-treated in nitrogen gas. Journal of Wood Science 44: 77-37.
24. Lee, S.H., Ashaari, Z., Lum, W.C., Halip, J.A, Ang, A.F., Tan, L.P., Chin, K.L., Tahir, P.M., 2018: Thermal treatment of wood using vegetable oils: A review. Construction and Building Materials 181: 408–419.
25. Lin, B.J., Colin, B., Chen, W.S., Petrissans, A., Rousset, P., Petrissans, M., 2018: Thermal degradation and compositional changes of wood treated in a semi-industrial scale reactor in vacuum. Journal of Analytical and Applied Pyrolysis 130: 8-18.

26. Ling, Z., Ji, Z., Ding, D., Cao, J., Xu, F., 2016: Microstructural and topochemical characterization of thermally modified poplar (*Populuscathayaha*) cell wall. BioResources 11(1): 786-799.
27. Mburu, F., Dumarcay, S., Huber, F., Petrissans, M., Gerardin, P., 2007: Evaluation of thermally modified *Grevillarobusta* heartwood as an alternative to shortage of wood resource in Kenya: Characterisation of physicochemical properties and improvement of bio-resistance. Bioresource Technology 98: 3478-3486.
28. Sailer, M., Rapp, A.O., Leithoff, H., Peek, R.D., 2000: Upgrading of wood by application of an oil heat treatment. HolzalsRoh- und Werkstoff58: 15–22.
29. Schwanninger, M., Rodrigues, J.C., Pereira, H., Hinterstoisser, B., 2004: Effects of short-time vibratory ball milling on the shape of FT-IR spectra of wood and cellulose. Vibrational Spectroscopy 36: 23-40.
30. Segal. L., Creely, J.J., Martin, A.E., Conrad, C.M., 1959: An empirical method for estimating the degree of crystallinity of native cellulose using the X-ray diffractometer. Textile Research Journal 29(10): 786-794.
31. Tang, T., Chen, X., Zhang, B., Liu, X., Fei, B., 2019: Research on the physico-mechanical properties of moso bamboo with thermal treatment in tung oil and its influencing factors. Materials 12(4): 599.
32. Tjeerdsma, B.F., Militz, H., 2006: Chemical changes in hydrothermal treated wood: FTIR analysis of combined hydrothermal and dry heat-treated wood.HolzalsRoh- und Werkstoff63: 102–111.
33. Traoré, M., Kaal, J., Cortizas, A.M., 2018: Differentiation between pine woods according to species and growing location using FTIR-ATR. Wood Science and Technology 52: 487-504.
34. Wang, J.Y., Cooper, P.A., 2005: Effect of oil type, temperature and time on moisture properties of hot oil-treated wood. HolzalsRoh- und Werkstoff63: 417–422.
35. Wang, X.H., Fei, B.H., Liu, J.L., 2014: Effect of vacuum heat treatment temperature on physical and mechanical properties of *Eucalyptus pellita* wood. Wood and Fiber Science. 46(3): 368-375.
36. Welzbacher, C.R., Wehsener, J., Rapp, A.O., Haller, P., 2008: Thermo-mechanical densification combined with thermal modification of Norway spruce (*Piceaabies* Karst.) in industrial scale– Dimensional stability and durability aspects. HolzalsRoh- und Werkstoff66: 39–49.
37. Welzbacher, C.R., Rassam, G., Talaei, A., Brischke, C., 2011: Microstructure, strength and structural integrity of heat-treated beech and spruce wood. Wood Material Science and Engineering 6: 219-227.
38. Yildiz, S., Gümüskaya, E., 2007: The effects of thermal modification on crystalline structure of cellulose in soft and hardwood. Building and Environment 42: 62-67.
39. Yun, H., Tu, D., Li, K., Huang, J., Ou, L., 2015: Variation and correlation of heat-treated wood's crystalline structure and impact toughness. BioResources 10(1): 1487-1494.

Intan Fajar Suri, Byantara Darsan Purusatama,
Seung Hwan Lee, Nam Hun Kim*
Kangwon National University
College Of Forest And Environmental Sciences
Department Of Forest Biomaterials Engineering
Chuncheon 24341
Republic Of Korea
*Corresponding author: kimnh@kangwon.ac.kr

Wahyu Hidayat
University Of Lampung
Faculty Of Agriculture
Department Of Forestry
Bandar Lampung 35145
Indonesia

Shalehudin Denny Ma'ruf
University Of Lampung
Environmental Science Master Study Program
Bandar Lampung 35145
Indonesia

Fauzi Febrianto
IPB University
Faculty Of Forestry
Department Of Forest Products
Bogor 16680
Indonesia

WOOD RESEARCH
e-ISSN 2729-8906
66(3):2021 379-390 pp.
doi.org/10.37763/wr.1336-4561/66.3.379390

ECO-DESIGN: IMPACTS OF BLEACHING CHEMICALS AND VARNISHES ON THE AMOUNT OF CARBON DIOXIDE IN THE COMBUSTION OF ORIENTAL BEECH (*FAGUS ORIENTALIS* LIPSKY)

Ahmet C. Yalinkilic
Kutahya Dumlupinar University
Turkey

Eyup Aksoy
Afyon Kocatepe University
Turkey

Musa Atar, Hamza Cinar, Hakan Keskin
Gazi University
Turkey

(Received June 2020)

ABSTRACT

This study was carried out to determine the effects of bleaching chemicals and varnishes on the amount of carbon dioxide (CO_2) in the combustion of oriental beech (*Fagus orientalis* Lipsky). For this purpose, samples of Oriental beech prepared according to ASTM D 358 contain 18% R_1 = ($NaOH + H_2O_2$), R_2 = ($NaOH + Ca(OH)_2 + H_2O_2$), R_3 = ($Na_2S_2O_5 + H_2C_2O_4$), R_4 = ($NaSiO_3 + H_2O_2$), R_5 = ($KMnO_4 + Na_2S_2O_5 + H_2O_2$) solution groups, after bleaching with solution groups, water based, synthetic, polyurethane and acrylic varnish were applied according to ASTM D 3023 and combustion tests were carried out in accordance with ASTM E 160-50. Gas measurements were made with the SIGMA 74172 NSU flue gas device during the combustion process. As a result, in respect to the burning types; the highest amount of CO_2 (ppm) was found in the self-combustion (8.468 ppm) while the lowest was obtained from the flame combustion source (4.599 ppm). In respect to the types of bleaching; the highest in R_5 (7.458 ppm) and the lowest in R_3 (4.059 ppm) were found. According to the varnish types; the highest value was found in the synthetic varnish (8.261), and the lowest value was found in the acrylic varnish (4.772 ppm). According to combustion type + bleaching solution + varnish type interaction, the highest values were found for without flame combustion (II) + R_3 + Sn (18.40 ppm) and lowest for flame source combustion (I) + R_5 + Pu (0.600 ppm). Consequently, the highest values for combustion gases were found in samples of oriental beech wood samples treated with water-based varnish with R_1 solution. According to this, in terms of human health and life safety, possibility of fire in places, R_3 solution and acrylic varnish may be used in the related industries.

KEYWORDS: Combustion, carbon dioxide, bleaching, varnishing, oriental beech wood.

INTRODUCTION

Eco-design is identified in both academic and policy makers as a point of intervention in the lifecycle assessment of a product to keep in mind environmental performance (Cinar 2005). The benefit of eco-design is enhanced by rooting it firmly within theoretical design principles and establishing 'sustainability' as a functional requirement within a regulatory framework. As argued by Deutza et al. (2013), formulating such an innovative approach requires first understanding current practices of eco-design in industry. Globally, consumption of wood materials has greatly increased to high levels for the production of wood-based boards which are commonly used in the related sectors driven mostly by demands from building and furniture industries in recent years. Besides, growing environmental concerns during the last decades, coupled with public pressure and stricter regulations change the ways how people do the business across the world (Cinar and Erdogdu 2018, Cinar 2018, Cinar et al. 2018). This affects the forest and furniture industries which bring a critical question concerning environmental aspects.

From the argument drawn, for the construction of natural houses, wood is one of the healthiest building materials in contrast to composite materials. It is a natural regulator of indoor climate; it breathes and assists ventilation; it stabilizes humidity and filters and purities the air. It also does not disturb the nature (Pearson 1994). However, wood is an organic compound and consists of 50% carbon. It is one of the natural materials that play an effective role in the absorption of carbon dioxide, and in the case of combustion it releases carbon dioxide gas at a significant level. Wood material is worn out due to environmental conditions and its components are degraded by chemical and biological means. Drying against these drawbacks, impregnation and surface treatment are applied (Highley and Kicle 1990). Although it is an environmentally friendly product used in many areas such as wood, furniture, and building sector, it is very weak and needs to be protected against physical and chemical events. This is of particular importance to the environmental effects of fire and preservatives such as paints and varnishes. With the effect of the chemicals used on the wood material, the fire causes an increase in harmful gases such as carbon dioxide which adversely affects the environment.

Although wood production and wood quality are of utmost importance in forest industry, in environmental aspects, few studies have examined the impact of elevated CO_2 on wood and forest industry. CO_2 is produced by all aerobic organisms when they metabolize carbohydrates and lipids to produce energy by respiration. It is also produced during the processes of decay of organic materials, the fermentation of sugars in bread, beer winemaking and combustion of wood including with other organic materials and fossil fuels such as coal, peat, petroleum and natural gas. It is returned to water via the gills of fish and to the air via the lungs of air-breathing land animals, including humans. It is a colourless, odourless and hazardous gas that is vital to life on Earth. In addition, carbon dioxide is the most significant long-lived greenhouse gas in Earth's atmosphere. Since the Industrial Revolution anthropogenic emissions - primarily from use of fossil fuels and deforestation - have rapidly increased its concentration in the atmosphere, leading to global warming. CO_2 also causes ocean acidification because it dissolves in water to form carbonic acid. The study of Ceuleman et al (2002) demonstrates that larger stem volume production during the first years of exposure to elevated CO_2 resulted from increased ring width, early wood growth in particular and, specifically, larger tracheids. In terms of wood quality, mechanical strength was reduced after three years of CO_2 enrichment, but wood density was not significantly altered.

The physical characteristics (smell, taste, colour, pattern, etc.) of wood species are different. Wood discoloration injuries in live wood, dead knot formation, oxidation of certain chemicals

in the wood next to reasons such as illness or heartwood of the older generation or tannic wood of metals result of contact occurs with the formed bleaching (Banks and Miller 1982). In addition, colour differences may occur due to the intensity of the annual growth of the wood material (summer wood, spring wood). The colour of furniture is as important as shape, size, form and balance. It is desired that the carpet, curtains and textile used in the interior decorations are compatible with the walls, ceilings and floor coverings (Atar 1999).

Colouring or bleaching of woods are carried out for reaching to desired visual aspects. Common laundry bleach or chlorine will effectively remove stain or dye color from wood, but will not affect the wood's natural color. They cause a chemical reaction that creates bleach that will blanch the stain color and can also alter the color of the wood itself. While wood dyes usually add superficial colour to wood, the bleaching chemicals create a deep light colour and shine. Bleaching chemicals are generally reactive compounds acting on the wood material side intermesh of whitening without destroying the main colour and pattern of the woods (Wagner and Kiclighter 1986).

It has been found that boron compounds used to protect wood from biotic and abiotic pests significantly reduce burning in alder wood (Uysal 1998). The combustion properties of the oak wood turned red using $C_2O_4H_2$, NaOH, H_2O_2, NH_3 and HCI solutions were investigated. The highest weight loss was achieved with NaOH, with the highest temperature increase and the highest amount of CO_2 with CO_4H_2 and NaOH (Ozçifci 2001). Uludag fir is a material produced by using 3 layers of impregnated phenol formaldehyde impregnated with most strength zinc chloride from the materials impregnated with $(NH_3)_2$, $Al_2(SO_4)_3$, K_2CO_3, CaCl, $ZnCl_2$ (Uysal and Kurt 2006). Another study (Ozçifci et al. 1999) shows that boron compounds increased combustion resistance of wood and that water-repellent agents (paraffin, styrene, methyl methacrylate and impregnated with isocyanate) reduced combustion enhancing effects in a certain way. In line with the literature summary, wood is exposed to be treated with different chemicals used in impregnations, varnishes and coatings to protect against physical and biological formation and to increase its visual perception. This study carries out to determine the effects of bleaching chemicals and varnishes on the amount of carbon dioxide in the combustion of Oriental beech wood material.

MATERIAL AND METHODS

Wood

Oriental beech wood (*Fagus orientalis* Lipsky) was selected according to TS EN 1476 (1984) without any defects; rots, knots, cracks and with annual rings perpendicular to the surface and sapwood sections. The density of beech was 0.66 g.cm-3. The samples of beech were supplied from the region of Siteler Ankara of Turkey.

Varnishes

Four types of commercial varnishes; water-based (Wb), synthetic (Sn), polyurethane (Pu) and acrylic (Ac) were used for the experiment. The application of varnishes was carried out in accordance with the specification of the producer. Some characteristics of varnishes are given in Tab. 1 (Atar et al. 2010).

Tab. 1: Technical properties of the measured varnishes.

Type of varnish	pH value	Density ($g \cdot cm^{-3}$)	Viscosity (snDINCup / 4mm)	Amount applied ($g \cdot m^{-2}$)	Nozzle gap (mm)	Air pressure (bar)
Pu (filler)	5.94	0.98	18	125	1.8	2
Pu (finishing)	4.01	0.99	18	125	1.8	2
Sn	-	0.94	18	100	-	-
Wb (primer)*	9.17	1.014	18	100	1.3	1
Wb (filler)**	9.30	1.015	18	67	1.3	1
Wb (finishing)***	8.71	1.031	18	67	1.3	1
Ac (filler)	4.30	0.95	18	125	1.8	2
Ac (finishing)	4.60	0.97	18	125	1.8	2

ASTM D 17*, ASTM D 65**, ASTM D 45***.

Bleaching chemicals

Sodium hydroxide (NaOH), hydrogen perhydroxide (H_2O_2), sodium sulfate ($Na_2S_2O_5$), calcium hydroxide $Ca(OH)_2$), hydrochloric acid ($H_2C_2O_4$), sodium silicate ($NaSiO_3$) and potassium permanganate ($KMnO_4$) were used as bleaching chemicals. Some characteristics of bleaching chemicals are given in Tab. 2.

Tab. 2: Bleaching solution groups.

Bleaching chemicals	Neutralization materials
$NaOH + H_2O_2$ (R_1)	Distilled water Acetic acid
$NaOH + Ca(OH)_2 + H_2O_2$ (R_2)	
$NaSiO_3 + H_2O_2$ (R_3)	
$Na_2S_2O_5 + H_2C_2O_4$ (R_4)	
$KMnO_4 + Na_2S_2O_5 + H_2O_2$ (R_5)	

According to the properties of bleaching chemicals, the weight (Mg) or volume (Vml) was prepared as 18% solution. The equation was used as (Atar 1999):

$$M_g = \frac{M_ç .\% M/M}{\%S}$$

where: Mg - the desired amount of solution (g), Mç - preparation of the desired amount of solution (g), %M/M - percentage by weight of the desired solution, %S - impurity ratio of chemical substance (%).

For liquids; the equation was used (Atar 1999):

$$V_{ml} = \frac{V_ç .\%V / V}{\%S.d}$$

where: V_{ml} - amount of solution desired (ml), $V_ç$ - amount of solution desired to be prepared (ml), %V/ V - percent volume of desired solution, d - the density of the solution ($g \cdot cm^{-3}$).

Preparation of test samples

720 test samples were prepared according to ASTM E 160-50, and were cut with 13 x 13 x 76 mm and conditioned at a temperature of (20 ± 2)°C and (65 ± 3)% relative humidity till they reached 12% humidity distribution.

Implementation of samples

Test samples were bleached with 18% solutions of $NaOH + H_2O_2$, $NaOH + Ca(OH)_2 + H_2O_2$, $NaSiO_3 + H_2O_2$, $Na_2S_2O_5 + H_2C_2O_4$, $KMnO_4 + Na_2S_2O_5 + H_2O_2$. The bleaching solutions were applied to the test samples with sponge, parallel to the fibers first, then perpendicular to the fibers and parallel to the fibers, (100 ± 10) $ml \cdot m^{-2}$. The substances forming the solution were applied separately and the second solution was applied after 1-3 min to increase the effect of the first applied substance. After the bleaching process was completed, the samples were left at room temperature for 2 days and neutralized with acetic acid and sterilized water. After these processes, the samples were allowed to air-dry (12%) until the moisture reached. Prior to varnishing, the surfaces of samples were sanded with a 200 sand paper and were varnished in accordance with the provision of ASTM D 3023 (1988).

Application of varnishes

After the dusts were taken, their weights were weighted on a sensitive analytical balance with the accuracy of ± 0.01 g, varnishes were carried out. For each type of varnishes, three layers were applied. The layers for water-based varnish, acrylic and polyurethane were applied by a spray-gun, and for synthetic varnish by a brush in accordance with manufacturer's recommendation. After the application of first layer, the samples were kept in room temperature for 24 hours and surfaces of the samples were subjected to be sanded with 220 grit. Following that the second layer was applied to the surfaces and sanding was carried out with 400 grit and after 24 hours, the second layers were applied to surfaces to reach a smooth surface. Then, the top coat was applied. The varnished samples were kept for 3 weeks in conditioning chambers in (20 ± 2)°C and (65 ± 3)% relative humidity.

Combustion test

Combustion tests were carried out in accordance with the provision of ASTM E 160-50 with combustion test device. Before carrying out the combustion test, the bleached and varnished samples were conditioned at 27°C and 30% relative humidity in a conditioning room until reaching to 7% relative humidity. Fire distance from maker type outlet at the lower bound of funnel was fixed to (25 ± 1.3) cm. When the device was empty, the gas pressure was fixed to 0.5 $kg \cdot cm^{-2}$. During the burning, temperature was set at (315 ± 8)°C in the funnel. Flame source was centered below sample pile and flame source combustion (FSC) was continued for 3 min. After extinguishing of flame source, without flame source combustion (WFSC) was carried out. In the combustion stages, measurements were made for 15, 30 and 30 sec, respectively; then, CO_2 quantities (ppm) were determined.

Data analysis

CO_2 measurements were determined in three stages; at with flame source, without flame source and cinder combustion. Multivariate analysis (MANOVA) was applied to the data in the MSTAT C statistical evaluation program, and the difference between the mean values was compared with Duncan test when the difference between the groups was significant. Thus, the order of succession of the tested factors was determined by dividing them into homogeneity groups according to the critical value of least significant difference (LSD).

RESULTS AND DISCUSSION

CO_2 amounts according to combustion, varnishing and bleaching

The average CO2 amounts according to combustion, varnishing and bleaching substance were given in Tab. 3.

Tab. 3: CO2 amounts according to combustion, varnishing and bleaching substance.

COMBUSTION TYPE*	X	HG
(I) Flame source combustion	4.599	B
(II) Without flame combustion	8.468	A
(III) Glowing combustion	5.414	B
BLEACHING CHEMICALS**		
(Rc) (Control)	6.440	A
(R_1) ($NaOH+H_2O_2$)	6.908	A
(R_2) ($NaOH+Ca(OH)_2+H_2O_2$)	5.928	A
(R_3) ($NaSiO_3+H_2O_2$)	4.059	B
(R_4) ($Na_2S_2O_5+H_2C_2O_4$)	6.170	A
(R_5) ($KMnO_4+Na_2S_2O_5+H_2O_2$)	7.458	A
VARNISH TYPE***		
(Vc) Control	7.695	A
(Wb) Water based varnish	4.828	B
(Sn) Synthetic varnish	8.261	A
(Pu) Polyurethane varnish	5.246	B
(Ac) Acrylic varnish	4.772	B

*LSD = ± 1.09, **LSD = ± 1.55, ***LSD = ± 1.42, X - arithmetic mean, HG - homogeneity group.

The amount of CO_2, in terms of combustion variety, the highest result was obtained in without flame combustion samples (8.468 ppm), the lowest result was obtained in flame source combustion samples (4.599 ppm). The bleaching chemicals yielded the highest result for R_5 (7.458 ppm) while the lowest for R_3 (4.059 ppm). For varnishes, the highest values were obtained in synthetic varnish (8.261 ppm) and the lowest result was obtained in acrylic varnishes (4.772 ppm). The amounts of CO_2 according to the interaction between combustion type + varnishes, combustion type + bleaching chemicals and bleaching chemicals + varnishes were given in Tab. 4.

Tab. 4: Average CO2 values according to the bilateral interaction.

Process type	**X**	**HG**	**Process type**	**X**	**HG**	**Process type**	**X**	**HG**
Combustion type + Varnish type *								
I+Vc	6.289	B	II+Vc	10.42	A	III+Vc	6.372	B
I+Wb	4.903	BCD	II+Wb	7.431	B	III+Wb	2.150	E
I+Sn	5.933	BC	II+Sn	11.47	A	III+Sn	7.375	B
I+Pu	3.178	CDE	II+Pu	7.081	B	III+Pu	5.481	BC
I+Ac	2.692	DE	II+Ac	5.931	BC	III+Ac	5.694	BC
Combustion type + Bleaching chemicals**								
I+Rc	5.150	DEF	II+Rc	8.740	ABC	III+Rc	5.430	DEF

$I+R_1$	6.251	CDE	$II+R_1$	9.503	AB	$III+R_1$	4.970	DEF
$I+R_2$	3.327	EF	$II+R_2$	7.443	BCD	$III+R_2$	7.013	BCD
$I+R_3$	2.330	F	$II+R_3$	5.197	DEF	$III+R_3$	4.650	DEF
$I+R_4$	4.843	DEF	$II+R_4$	8.727	ABC	$III+R_4$	4.940	DEF
$I+R_5$	5.693	CDE	$II+R_5$	11.20	A	$III+R_5$	5.483	DEF
Bleaching chemicals + Varnish type ***								
Rc	11.37	AB	R_4+Wb	6.317	CDEFGH	R_2+Pu	7.933	BCDEF
R_1	6.501	CDEFG	R_5+Wb	7.956	BCDEF	R_3+Pu	0.000	I
R_2	4.178	EFGH	Sn	7.439	BCDEF	R_4+ Pu	4.600	EFGH
R_3	6.456	CDEFGH	R_1+Sn	2.339	HI	R_5+Pu	2.528	GHI
R_4	9.450	BC	R_2+Sn	10.02	BC	Ac	0.000	I
R_5	8.211	BCDEF	R_3+Sn	13.84	A	R_1+Ac	7.978	BCDEF
Wb	8.417	BCDE	R_4+Sn	6.328	CDEFGH	R_2+Ac	7.506	BCDEF
R_1+Wb	6.278	CDEFGH	R_5+Sn	9.600	BC	R_3+Ac	0.000	I
R_2+Wb	0.000	I	Pu	4.972	DEFGH	R_4+Ac	4.156	FGH
R_3+Wb	0.000	I	R_1+Pu	11.44	AB	R_5+Ac	8.994	BCD

*LSD = ± 2.456, **LSD = ± 2.691, ***LSD = ± 3.474, X - arithmetic mean, HG - homogeneity group.

The amount of CO_2, combustion type and varnish interaction in terms of the highest without flame combustion + synthetic varnish (11.47 ppm), the lowest flame source combustion + water-based varnish (2.150) was found. The amount of CO_2, combustion type and bleaching chemicals with regard to the interaction highest without flame combustion + R_5 (11.20 ppm), the lowest values in flame source combustion + R_3 (2.33 ppm) was obtained. The amount of CO_2; varnishes and bleaching solution with regard to the interaction highest R_3 + Sn (13.84 ppm), the lowest R_1 + Sn (2.339 ppm) detected. In some cases, the gas measurement was at level 0. The results of multivariate analysis on the effect of combustion type, bleaching chemicals and varnish type on the amount of CO_2 are given in Tab. 5.

Tab.5: MANOVA of CO2 effects of combustion type, bleaching and varnish type.

Source	Degrees of freedom	Sum of squares	Mean square	F-value	P < %5 (SİG)
Factor A	2	748.657	374.329	26.7226	0.0000
Factor B	4	610.489	152.622	10.8954	0.0000
AB	8	256.923	32.115	2.2927	0.0232
Factor C	5	305.587	61.117	4.3631	0.0009
AC	10	219.930	21.993	1.5700	0.1187
BC	20	2788.943	139.447	9.9549	0.0000
ABC	40	827.074	20.677	1.4761	0.0458
Error	180	2521.428	14.008		
Total	269	8279.032			

Factor A: combustion type, Factor B: varnish type, Factor C: bleaching chemicals

The effect of combustion type, bleaching solution and varnish type on the amount of CO_2 was statistically significant (α = 0.05). Significant differences in the groups in which it is important to determine DUNCAN tests were conducted. The Duncan test results for the combustion and varnish type interaction are given in Tab. 6.

Tab.6: Duncan test results (ppm).

Process type	X	HG	Process type	X	HG
I	7.783	CDEFGHIJKLMNOP	II+R_3+Sn	18.40	A
I+R_1	7.553	CDEFGHIJKLMNOPQ	II+R_4+Sn	9.117	BCDEFGHIJKLMN
I+R_2	5.150	GHIJKLMNOPQ	II+R_5+Sn	14.03	ABCD
I+R_3	3.233	JKLMNOPQ	II+Pu	6.167	EFGHIJKLMNOPQ
I+R_4	6.417	DEFGHIJKLMNOPQ	II+R_1+Pu	16.03	AB
I+R_5	7.600	CDEFGHIJKLMNOPQ	II+R_2+Pu	9.567	BCDEFGHIJKLM
I+Wb	7.250	CDEFGHIJKLMNOPQ	II+R_3+Pu	0.000	Q
I+R_1+Wb	8.450	BCDEFGHIJKLMNO	II+R_4+Pu	7.900	CDEFGHIJKLMNOP
I+R_2+Wb	0.000	Q	II+R_5+Pu	2.817	KLMNOPQ
I+R_3+Wb	0.000	Q	II+Av	0.000	Q
I+R_4+Wb	7.667	CDEFGHIJKLMNOPQ	II+R_1+Av	9.667	BCDEFGHIJKL
I+R_5+Wb	6.050	EFGHIJKLMNOPQ	II+R_2+Av	8.900	BCDEFGHIJKLMN
I+Sn	8.400	BCDEFGHIJKLMNO	II+R_3+Av	0.000	Q
I+R_1+Sn	1.900	LMNOPQ	II+R_4+Av	4.050	HIJKLMNOPQ
I+R_2+Sn	2.450	KLMNOPQ	II+R_5+Av	12.97	ABCDEF
I+R_3+Sn	8.417	BCDEFGHIJKLMNO	III	12.70	ABCDEFG
I+R_4+Sn	6.150	EFGHIJKLMNOPQ	III+R_1	2.783	KLMNOPQ
I+R_5+Sn	8.283	CDEFGHIJKLMNOP	III+R_2	1.467	NOPQ
I+Pu	2.317	KLMNOPQ	III+R_3	8.550	BCDEFGHIJKLMNO
I+R_1+Pu	8.150	CDEFGHIJKLMNOP	III+R_4	10.10	BCDEFGHIJK
I+R_2+Pu	4.767	HIJKLMNOPQ	III+R_5	2.633	KLMNOPQ
I+R_3+Pu	0.000	Q	III+Wb	5.233	FGHIJKLMNOPQ
I+R_4+Pu	3.233	JKLMNOPQ	III+R_1+Wb	1.067	OPQ
I+R_5+Pu	0.600	PQ	III+R_2+Wb	0.000	Q
I+Av	0.000	Q	III+R_3+Wb	0.000	Q
I+R_1+Av	5.200	FGHIJKLMNOPQ	III+R_4+Wb	0.550	PQ
I+R_2+Av	4.267	HIJKLMNOPQ	III+R_5+Wb	6.050	EFGHIJKLMNOPQ
I+R_3+Av	0.000	Q	III+Sn	2.783	KLMNOPQ
I+R_4+Av	0.750	OPQ	III+R_1+Sn	1.783	MNOPQ
I+R_5+Av	5.933	EFGHIJKLMNOPQ	III+R_2+Sn	14.78	ABC
II	13.63	ABCDE	III+R_3+Sn	14.70	ABC
II+R_1	9.167	BCDEFGHIJKLMN	III+R_4+Sn	3.717	IJKLMNOPQ
II+R_2	5.917	EFGHIJKLMNOPQ	III+R_5+Sn	6.483	DEFGHIJKLMNOPQ
II+R_3	7.583	CDEFGHIJKLMNOPQ	III+Pu	6.433	DEFGHIJKLMNOPQ
II+R_4	11.83	ABCDEFGH	III+R_1+Pu	10.15	BCDEFGHIJK
II+R_5	14.40	ABC	III+R_2+Pu	9.467	BCDEFGHIJKLM
II+Wb	12.77	ABCDEFG	III+R_3+Pu	0.000	Q
II+R_1+Wb	9.317	BCDEFGHIJKLM	III+R_4+Pu	2.667	KLMNOPQ
II+R_2+Wb	0.000	Q	III+R_5+Pu	4.167	HIJKLMNOPQ
II+R_3+Wb	0.000	Q	III+Av	0.000	Q
II+R_4+Wb	10.73	BCDEFGHIJ	III+R_1+Av	9.067	BCDEFGHIJKLMN
II+R_5+Wb	11.77	ABCDEFGH	III+R_2+Av	9.350	BCDEFGHIJKLM
II+Sn	11.13	ABCDEFGHI	III+R_3+Av	0.000	Q
II+R_1+Sn	3.333	IJKLMNOPQ	III+R_4+Av	7.667	CDEFGHIJKLMNOPQ
II+R_2+Sn	12.83	ABCDEFG	III+R_5+Av	8.083	CDEFGHIJKLMNOP

HG* = 6.017.

The amount of CO_2, the highest value of II + R_3 + Sn (18.40 ppm) and the lowest value of I + R_5 + Pu (0.600 ppm) were found in the triple interaction of the combustion type + bleaching chemicals + varnish type. The graph of CO_2 changes according to the process is given in Fig. 1.

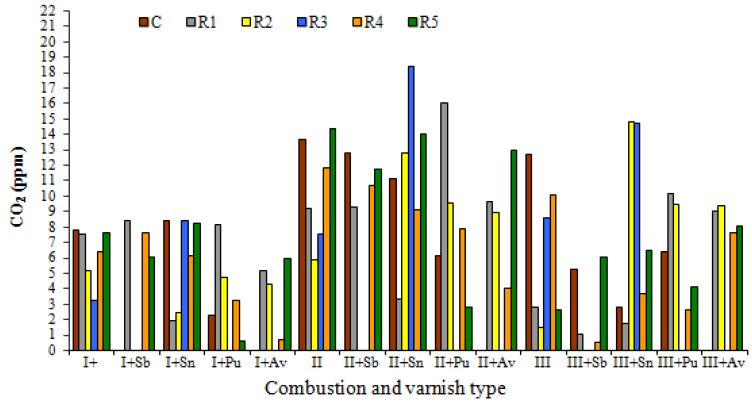

Fig. 1: CO2 changes according to process type

CONCLUSIONS

In this study, the burning properties of wood materials varnished with water-based and synthetic varnishes were investigated after the colour whitening process with some colour-bleaching chemicals. The amount of CO_2 and without flame combustion yielded 46% higher than flame source combustion and 36% from glowing combustion. This can be due to the fact that the ignition is fully realized during the self-combustion phase. As a matter of fact, in the literature, the highest amount of CO_2 was obtained in the without flame combustion stage in cedar, spruce and chestnut woods after being impregnated with Tanalith-E and Wolmanit-CB and then combustion tests were carried out with synthetic and water based varnishes (Yasar et al. 2016a). The amount of CO_2 has shown a decreasing effect except the results of synthetic varnish. This result is supported by the study of Ozcifci (2001) and Fidan et al. (2016b). According to them, the amount of CO_2 in synthetic varnish was higher than water-based varnish. In respect to the results, it is possible to argue that the most suitable varnish is acrylic for combustion.

The amount of CO_2 was found to be different in the bleaching materials. R5 yielded the highest, while the lowest was occurred in R3. The lowest amount of CO2 was found to be in the synthetic varnish (R3) in terms of the combustion type and the bleaching chemicals interaction. This should be taken into account in areas of high fire risk. In terms of varnish type and bleaching chemicals interaction, the amount of CO_2 was found to be the highest for synthetic varnish applications. As a matter of fact, these values were found to be in parallel with the results obtained in the literature (Yasar et al. 2016b, Uysal and Ozcifci 2000). Another argument is made by the study of Qingwen (2004), according to them, Boric acid catalyzes the dehydration and other oxygen-eliminating reactions of wood at a relatively low temperature (100–300°C). It may catalyze the isomerization of the newly formed polymeric materials to form aromatic structures. This contributes partly to the effects of boric acid for promoting charring and fire retardation of wood.

In conclusion, varnishing after the bleaching furniture or implementation of decoration at fire risk should be taken into account as an important factor in the related sectors for public and social concern in terms of human life and property safety.

ACKNOWLEDGMENT

This work was supported by TUBITAK Scientific Research Projects Management Unit with the project numbered 2010 / 109O043.

REFERENCES

1. ASTM D 358, 1983: Wood to be used as panels in weathering test of coating, ASTM Standards, USA.
2. ASTM D 3023, 1988: Practical for determination of resistance of factory applied coatings on wood products of stain and reagents, ASTM Standards, USA.
3. ASTM E 160-50, 1975: Standard test method for combustible properties of treated wood by the crib test, ASTM Standards, USA.
4. Atar, M., 1999: The effects of colour whitening with chemicals on woodworking materials. PhD Thesis. Pp 66-82, Gazi University, Institute of Science and Technology, Ankara (In Turkish).
5. Atar, M., Yalinkilic, A.C., Aksoy, E., 2010: Effect of bleaching on the combustion properties of wood material. TUBITAK Project Final Report, Project Number: 109O043, Ankara, Turkey.
6. Banks, W.B., Miller, E.R., 1982: Chemical aspects of wood technology Sweden. Forest Products Journal 11(4): 57-64.
7. Ceulemans, R., Jach, M.E., Vandevelde, R., Lin, J.X., Stevens, M., 2002: Elevated atmospheric CO_2 alters wood production, wood quality and wood strength of Scots pine (*Pinus sylvestris* Lipsky) after three years of enrichment. Global Change Biology 8: 153-16.
8. Cinar, H., 2005: Eco-design and furniture: Environmental impacts of wood-based panels, surface and edge finishes. Forest Products Journal 55(11): 27–33.
9. Cinar, H., 2018: Effects of temperature and thickness of wood based boards on formaldehyde emission. Wood Research 63(5): 895–908.
10. Cinar, H., Erdogdu, M., 2018: Eco-design: effects of thickness and time in service for wood based boards on formaldehyde emission. Forest Products Journal 68(4): 405-413.
11. Cinar, H., Ozturk, Y., Yildirim, K., 2018: Effects of surface veneering, edge banding, and drilling holes for handles and hinges of wood-based boards on formaldehyde emission. Forest Products Journal 68(3): 264-271.
12. Deutza, P., McGuireb, M., Neighbourb, G., 2018: Eco-design practice in the context of a structured design process: An interdisciplinary empirical study of UK manufacturers Journal of Cleaner Production 39: 117-128.
13. Fidan, M.S., Yasar, S.S., Yasar, M., Atar, M., Alkan, E., 2016a: Characterization of the combustion parameters of impregnated and varnished cedar wood. Forest Products Journal 65(5/6): 290-299.
14. Fidan, M.S., Yasar, S.S., Yasar, M., Atar, M., Alkan, E., 2016b: Effect of seasonal changes on the combustion characteristics of impregnated cedar wood. Construction and Building Materials 106: 711-720.
15. Highley, T.L., Kicle, T.K., 1990: Biological degradation of wood. Phytopsthology 69: 1151-1157.
16. Ozcifci, A., Atar, M., Uysal, B., 1999: The effects of the chemicals used on wood materials on surface gloss and adhesion strength of varnishes. TÜBITAK Turkish Journal of Agriculture and Forestry 23(3): 763-770.

17. Ozcifci, A., 2001: Effects of colorants on the combustion properties of stem less oak wood. (In Turkish). Journal of Technology 3(4): 63-72.
18. Qingwen W., Jian, L., Winandy, JE., 2004: Chemical mechanism of fire retardance of boric acid on wood. Wood Science and Technology 38(5): 375–389.
19. TS EN 1476, 1984: To obtain physical and mechanical properties of homodyne, sample trees and laboratory samples, TSE, Ankara.
20. Uysal, B., 1998: Combustion properties of alder wood of various water repellent and fire retardant chemicals. (In Turkish). Journal of Technology 2: 81-89.
21. Uysal, B., Ozçifçi, A., 2000: The combustion characteristics of eastern beech wood (*Fagus orientalis* Lipsky) without flame source, Journal of Technology 3(1): 107-117.
22. Uysal, B., Kurt, S., 2006: Combustion properties of laminated wood materials glued with PF and PVAc glue impregnated with some chemicals. Doğuş University Journal 7(1): 112-126 (In Turkish).
23. Yasar, S.S., Fidan, M.S., Yasar, M., Atar, M., Alkan E., 2016: Determining the effect of seasonal variation in spruce wood treated with various impregnations on combustion resistance. Bioresources 11(4): 9467-9479
24. Yasar, S.S., Fidan, M.S., Yasar, M., Atar, M., Alkan, E., 2016: Influences of seasonal alterations on the burning characteristics of impregnated and surface treated chestnut (*Castanea Sativa* Mill) wood. Wood Research 61(3): 399-412.
25. Wagner, H.W., Kiclighter, E.C., 1986: Finisher and finishing, bleaching and disassembly. Modern Woodworking 169-170, New York, USA.

Ahmet C. Yalinkilic
Kutahya Dumlupinar University
Faculty Of Simav Technology
Industrial Design Engineering Department
43500 Simav – Kütahya
Turkey

Eyüp Aksoy
Afyon Kocatepe University
School Of Afyon Vocational
Design Department
03217 Afyonkarahisar
Turkey

Musa Atar, Hamza Cinar, Hakan Keskin*
Gazi University
Faculty Of Technology
Wood Products Industrial Engineering Department
06500 Ankara
Turkey
*Corresponding author: khakan@gazi.edu.tr

WOOD RESEARCH
e-ISSN 2729-8906
66(3):2021 391-402 pp.
doi.org/10.37763/wr.1336-4561/66.3.391402

FIBER MORPHOLOGY AND PHYSICAL PROPERTIES OF BRANCH AND STEM WOOD OF HAWTHORN (*CRATAEGUS AZAROLUS* L.) GROWN IN ZAGROS FORESTS

Huijun Dong
Nanjing Forestry University
China

Mohsen Bahmani
Shahrekord University
Iran

Miha Humar
University Of Ljubljana
Slovenia

Sohrab Rahimi
University Of British Columbia
Canada

(Received July 2020)

ABSTRACT

This study aims at investigating the effect of three altitude levels (below 1800 m, 1800-2000 m and above 2000 m) on the physical and biometric properties of stem-wood and branch-wood of hawthorn species. Moreover, the relationship between wood dry density and volumetric swelling, fiber length, fiber diameter, cell wall thickness were studied. Results indicated that altitude had significant effects on the dry density, volumetric swelling and fiber length of stem wood while did not significant effects on the density of branch wood. Additionally, some physical and biometric properties had relatively greater correlation coefficients in branch wood than in stem wood whereas others had higher coefficients in stem wood compared to branch wood. Deep understanding of properties this wood species will provide a fresh insight into the relationship between wood properties and environmental factors.

KEYWORDS: *Crataegus* spp., Zagros, dry density, fiber length, correlation, wood.

INTRODUCTION

Iran's forests cover approximately twelve million ha, including five million ha in the mountainous Zagros region (Haidari et al. 2013). The climate in Zagros is mainly affected by westerly disturbances and the Azores high during the cold (November–March) and warm (May–September) season respectively, resulting in a clear distinction between a wet winter and a dry summer. The mean annual temperature of the region is 16°C and mean annual precipitation is 509 mm (Azizi et al. 2012). Zagros forests represents about 40% of Iranian forests and is the most extensive forest areas of the country (Sagheb-Talebi et al. 2004). The main hardwood species in this area are *Quercus* spp. (oaks), *Pistacia mutica* (wild pistachio), *Crataegus* spp. and *Pyrus* spp (Jazirehi and Rostaghi 2003). *Crategus* spp., belonging to the *Rosaceae* family and *Maloideae* sub-family including about 300 species which are grown in Europe, North Africa, West Asia, and North America. The scientific name of hawthorn comes from the Greek word "kràtaigos" which means "strength and robustness" due to its hard and durable wood (Nazhand et al. 2020). *Crataegus* species are small trees, mostly growing up to 15 m. Basic studies in the types of wood species can reveal the possibility of their usage in various applications or lead to create a database of different wood species.

Most studies regarding hawthorn tree species are associated with its distribution and ecological requirements and its physical and fiber biometric properties have not been studied yet. It is indicated that there are variations between wood properties in the stem and branch woods (Kiaei and Roque 2015, Zhao et al. 2018). Several studies have investigated the characteristics of the stem and branch tissue, particularly in terms of anatomical properties, chemical components and physical properties as well as mechanical properties. Dadzie et al. (2018) investigated the density of branch and stem woods in *Entandrophragma cylindricum*, *Entandrophragma angolense* and *Khaya ivorensis* and indicated that the density is significantly higher in branch-wood than stem-wood for all three species. However, Kiaei and Moya (2015) found that the density of stem-wood is higher than that the branch-wood. Zhao et al. (2015) investigated some properties of fiber biometry of root, branch and stem wood of *Populus ussuriensis* Kom. trees and reported there are significant differences between anatomical characteristics in different parts of the trees. Kiaei et al. (2014) evaluated chemical properties of branch and stem-wood of Plum (*Prunus domestica*) wood in Iran. They concluded, that lignin and cellulose in branch-wood is higher than in stem-wood. Kiaei et al. (2014) and Dadzie et al. (2018) evaluated some biometrical properties of wood branches and stem in Plum (*Prunus domestica*) *Entandrophragma cylindricum*, *Entandrophragma angolense* and *Khaya ivorensis*. In general, the results showed that there is a significant difference between the studied parameters. On the other hand, site condition, biotic and edaphic, altitude, aspect and slope of the ground are interacting parameters affecting wood quality (Gava and Goncalves 2008, Murphy et al. 2009, De Micco et al. 2016, Nazari et al. 2020). It is worth mentioning that most studies mainly concentrated on wood properties and ignore the relationship between wood properties and environmental growth variables. To the best of our knowledge, there is no research on the physical and biometrical properties of hawthorn wood (*Crataegus azarolus* L.). Considering the valuable position of hawthorn wood in the Zagros forests of Iran, current study aims to identify the changes of wood density, fiber length, fiber diameter and cell wall thickness of hawthorn wood in branch and stem woods, comparing the respective factors of hawthorn wood achieved from different altitude levels.

MATERIAL AND METHODS

Site area and sample collection

This study was carried out in trees collected from ecosites (three forest sample stands along an altitudinal gradient (below1800-, 2000-2200 and above 2400 m a.s.l.) in the hawthorn forests of Bazoft. In each ecosite, three plots were implemented, accordingly the 27 plots were selected in study area. Trees characteristics at nine different ecosites collected wood are given in Tab 1. In total, 27 healthy trees were selected. Hawthorn forests in the current study area are spread between 1500 and 2400 m in altitude. The mean annual precipitation and temperature of the area are 330 mm and 14°C, respectively (Chaharmahal and Bakhtiari Meteorological Administratio, 2020). Forest stands are relatively uniform in size and age as well as extensively dominated by Persian oak with basal area ranging between 57.70 and 113.23 $m^2.ha^{-1}$. Due to their remote location and the absence of evidence of human impact, it is assumed that all stands have been developed under the influence of natural impacts and disturbances. The maximum rooting depth is frequently limited by a shallow bedrock. In each plot, all live trees of at least 7.5 cm diameter at breast height (DBH, 1.3 m above the root collar) were identified, and their diameter at breast height, height, crown length and perpendicular diameters were recorded within 0.1-hectare plot. The caliper, Vertex and diameter tape were used to measurements of trees diameters, height and crown diameter, respectively. Then in each plot, those dominant trees that healthy with the largest diameters at breast height (DBH) without any defects and reaction wood were sampled and one disk from stem and branch was taken from the tree trunk for the determination of wood properties.

Tab. 1: Trees characteristics at nine different ecosites collected wood in Zagros forests.

Ecosites		1	2	3	4	5	6	7	7	9
Tree-level variables	[2]DBH	58.67 (11.37)	101.00 (23.52)	69.33 (6.51)	73.33 (12.34)	85.00 (7.00)	109.67 (45.35)	75.33 (16.50)	84.33 (27.02)	84.67 (10.69)
	Height	4.48 (0.36)	8.71 (0.54)	5.13 (0.71)	4.86 (1.63)	6.20 (1.59)	7.25 (3.46)	4.84 (1.44)	5.63 (0.29)	10.76 (5.23)
	Stem basal area	0.28 (0.10)	0.83 (0.37)	0.38 (0.07)	0.43 (0.15)	0.57 (0.09)	1.05 (0.84)	0.46 (0.20)	0.59 (0.36)	0.57 (0.15)
	Stem volume	0.64 (0.27)	3.77 (1.82)	1.00 (0.15)	1.13 (0.66)	1.83 (0.75)	4.78 (5.62)	1.26 (0.83)	1.75 (1.10)	3.28 (2.35)
	[3]ABH	298 (30)	447 (95)	323 (10)	335 (30)	360 (13)	468 (180)	339 (34)	380 (91)	369 (36)
	[4]Crown diameter	2.58 (0.21)	4.65 (0.58)	4.62 (0.39)	5.23 (0.71)	4.25 (0.30)	4.78 (0.58)	4.25 (0.58)	4.77 (1.26)	5.97 (1.08)
	Crown basal area	5.26 (0.83)	17.15 (4.09)	16.81 (2.87)	21.76 (5.94)	14.23 (2.00)	18.14 (4.50)	14.35 (3.82)	18.66 (8.85)	28.56 (10.00)
	[5]MADI (mm)	1.96 (0.19)	2.25 (0.06)	2.14 (0.14)	2.18 (0.16)	2.36 (0.12)	2.33 (0.16)	2.20 (0.27)	2.19 (0.24)	2.29 (0.07)

Notes: 1QMD: quadratic mean diameter; 2DBH: diameter at breast height; 3ABH: age at breast height, 4Crown width in m measured from below the tree in the field; 5MAI: Mean annual diameter increment. Standard deviations are displayed in parentheses.

Physical properties

Wood specimens were prepared from the discs cut from stem and branch woods of hawthorn. In detail, specimens with dimensions of 3 × 2 × 2 cm were prepared in accordance with ISO 13061-14 (2016) for the investigation of oven-dry density and volumetric swelling. Sample dimensions were measured in green (saturated) and oven-dry condition with a slide calliper; oven-dry mass was determined with an electric balance to an accuracy of 0.01 g. Volumetric swelling was calculated using the dimensional change from the green to oven-dry condition. The physical properties were calculated according to the following equations:

$$D_0 = P_0 / V_0 \quad (1)$$

$$\alpha_v = (V_s - V_0)/ V_0 \quad (2)$$

where: D_0 - oven dry density (g·cm^{-3}), α_v - volumetric swelling (%), V_s - volume in the saturate state (cm3), V_0 - volume in state of oven-dry (cm^3), P_0 - weight in state of oven dry (g).

Biometric properties

Separation of individual wood fibre was performed using Franklin (1964) method through which a wood specimens with the dimension of 15 × 10 × 2 mm^3 were saturated in a mixture (1:1) of acetic acid and oxygenized water in test tubes. Afterwards, the specimens were kept in an oven with 65 ± 3°C for 48 h. After maceration, the specimens were washed (2-3 times) in distilled water and then immersed with distilled water. In the next step, shacked and the biometric parameters (fiber length, fiber diameter, and cell wall thickness) were evaluated by light microscopic. From each slice, at least 50 fibers were used for the measurements.

Statistical analysis

In this study, the influence of altitude steps was evaluated on the physical and biometric properties. One-way analysis of variance (ANOVA) performed to determine significant differences using SPSS version 25. Pearson correlation matrix was also applied to determine the correlation between dry wood density with volumetric swelling, fiber length, fiber diameter, cell wall thickness.

RESULTS AND DISCUSSION

Oven-dry density

The average values of dry wood density obtained for hawthorn wood in three different altitudes are shown in Tab. 2. The highest (0.75 g·cm^{-3}) and lowest (0.69 g·cm^{-3}) density values of stem-wood were identified in the intermediate and high altitude, respectively. For branch wood the highest (0.69 g·cm^{-3}) and lowest (0.65 g·cm^{-3}) values were found in the intermediate and low altitude, respectively. It is reported that generally density variations related to the anatomical characteristics, e.g. vessel and fibre morphology, ecological site, moisture content and chemical constitutes (Zobel and van Buijtenen 1989, Preston et al. 2006, Sousa et al. 2018, Bahmani et al. 2018). We were not able to fully elucidate specific reasons for variation in density. However, it is planned to perform more targeted research in one of the future studies. Overall, stem wood (0.71 g·cm^{-3}) showed higher density than branch wood (0.67 g·cm^{-3}). Similar observations were previously reported by Amoah et al. (2012) for *Terminalia ivorensis* and *Milicia excels*, Kiaei and Roque (2015) for *Alnus glutinosa*, Kotowska et al. (2015) for *Theobroma caco* and *Durio zibethinus* and Zhao et al. (2018) for *Populus ussuriensis* Kom. However, Dadzie et al. (2016) mentioned that branch-wood had higher density than stem-wood. The density of hawthorn wood is equal

or relatively higher than that of *Quercus robur* (Wagenführ 1996, 0.69 g·cm^{-3}), Red oak (Zeidler and Borůvka 2016, 0.65 g·cm^{-3} or Pedunculate oak (Zeidler and Borůvka 2016, 0.71 g.cm-3). In contrast to the findings, density of *Q. cerris* (0.75 g·cm^{-3} Pásztory et al. 2014), and *S. torminalis* (0.83 g·cm^{-3} Bahmani et al. 2020) are significantly higher than density of hawthorn wood. The results of ANOVA exhibited that the altitude had significant effects on the density of stem-wood while had no significant effects on the density of branch-wood (Tab. 4).

Volumetric swelling

Tab. 2 shows the mean values of volumetric swelling for hawthorn wood. The highest (21.42%) and lowest (12.70%) values of volumetric swelling of stem-wood were found in the intermediate and in the low altitude, respectively. The same pattern of density variation was also achieved for branch-wood. Generally, swelling and shrinkage is a parameter that strongly related to wood density. Overall, volumetric swelling in stem-wood (0.71 g.cm-3) found out higher than its branch-wood (0.67 g.cm-3). This correlates well with findings reported by Kiaei and Roque (2015). Generally, swelling and shrinkage is a parameter that strongly related to wood density and microfibrillar angle in the S2 layer of secondary. High wood density has proportionately more cell and less lumen volume, and they shrink and swell more due to the unique nature of the microstructures (Schulgasser and Witztum 2015). From the ANOVA test, it can be derived that the effects of altitude levels on volumetric swelling are significant for stem-wood and not significant for branch-wood (Tab. 4).

Tab. 2: The average of physical properties in three different altitudes of hawthorn wood in Zagros forests.

Wood properties	Altitude (m)					
	Below 1800 m (low)		1800-2000 m (intermediate)		Above 2000 m (high)	
	Stem	Branch	Stem	Branch	Stem	Branch
Oven-dry density (g·cm^{-3})	0.69 (0.05)	0.66 (0.04)	0.75 (0.06)	0.69 (0.04)	0.70 (0.07)	0.65 (0.05)
Volumetric swelling (%)	20.31 (0.98)	17.78 (1.43)	21.42 (2.45)	19.45 (1.22)	12.70 (1.34)	11.65 (1.78)

*Values in parenthesis represent standard deviation.

Fiber biometry

Fiber length

Fiber morphology are the key elements responsible for the wood strength and play an important role in determining the qualitative and quantitative wood properties and specific usage of lignocellulosic materials (Panshin and de Zeeuw 1980, Gryc and Vavrčík 2005, Nazari et al. 2021). The mean values of the parameter fiber lengths for hawthorn wood in three different altitude levels are given in Tab. 3. The highest (0.85 mm) and lowest (0.72 mm) values of fiber length in stem-wood were found in the high altitude and in the intermediate altitude, respectively. On the other hand, the highest (0.79 mm) and lowest (0.71 mm) values of fiber length in branch-wood were found in the low altitude and in the intermediate altitude, respectively. Overall, it was observed that stem-wood (0.80 mm) showed that higher fiber length than branch-wood (0.76 g·cm^{-3}). Branch-wood has moderately shorter fibers than its stem-wood in most hardwoods (Bowyer et al. 2003, Samariha et al. 2011). These might be ascribed to the narrower diameter and shorter length longitudinal cells of branch-wood (Antwi-Boasiako and Apreko-Pilly 2016).

The measured values of mean fiber length are lower than those of softwood (2.7-4.6 mm, Tsoumis 1996) and close to most hardwood fibers (0.7-1.6 mm, Horn 1978, Tsoumis 1996). According to Wheeler et al. (1989), fibers are classified into three groups: *(1)* short fibers with a length of less 0.90 mm; *(2)* fibers of medium length between 0.90-1.90 mm such as hawthorn wood with an average fiber length of 0.95 mm; *(3)* fibers longer than 1.90 mm.

There are significant differences in stem-wood fibre length among the three altitude levels, whereas no significant difference in branch-wood fiber lengths found out among the three altitudes (Tab. 4), what is in line with the density measurements as well.

Fiber diameter

A maximum value of 20.93 μm and a minimum value of 19.99 μm for fiber diameter of stem-wood were determined in the low altitude step and in the high altitude, respectively (Tab. 3). For branch-wood, maximum (22.60 μm) and minimum (20.59 μm) were obtained in the intermediate altitude and at the low altitude, respectively (Tab. 2). In total, fiber diameter in branch-wood (21.64 μm) exhibited higher than its stem-wood (20.19 μm). The mean value of fiber diameter of hawthorn wood agree with previous research findings for other hardwood fibers (Atchison 1987, San et al. 2016). Plomion et al. (2001) reported that variations in the fiber diameter could have contributed to the molecular and physiological changes occurring in the vascular cambium as well as in the wood cell walls throughout the tree growth. At 5% significance level, there were significant differences in branch and stem wood fiber diameter among the three altitude levels (Tab. 4).

Cell wall thickness

Cell wall diameter parameter is variable among species, sites, between and within trees as well as highly associated with wood density. The maximum value of the parameter cell wall thickness (5.93 μm) as well as the minimum (5.67 μm) were determined for stem wood trees in the intermediate altitude and at the low altitude, respectively (Tab. 3). The maximum (6.34 μm) and minimum (5.74 μm) values of branch-wood, were acquired in the intermediate altitude and in the low altitude, respectively (Tab. 3). Overall, branch-wood (5.98 μm) showed that cell wall thickness higher than stem wood (5.79 μm). Similar results were obtained by Kiaei et al. (2014) for plum wood and Zhao et al. (2018) for *Populus ussuriensis* Kom. At 5% significance level, there were significant differences in branch and stem wood cell wall diameter among the three altitude levels (Tab. 4).

Tab. 3: The mean parameter of fiber morphology in three different altitudes of hawthorn wood in Zagros forests.

Wood properties	Altitude (m)					
	Below 1800 m (low)		1800-2000 m (intermediate)		Above 2000 m (high)	
	Stem	Branch	Stem	Branch	Stem	Branch
Fiber length (mm)	0.84 (0.04)	0.79 (0.04)	0.72 (0.04)	0.70 (0.04)	0.85 (0.04)	0.78 (0.04)
Fiber diameter (μm)	20.93 (0.04)	21.74 (0.04)	19.99 (0.04)	22.60 (0.04)	20.59 (0.04)	11.65 (0.04)
Cell wall diameter (μm)	5.76 (0.04)	5.85 (0.04)	5.93 (0.04)	6.34 (0.04)	5.67 (0.04)	5.74 (0.04)

*Values in parenthesis represent standard deviation.

Tab. 4: Analysis of variance (ANOVA) of the physical properties of hawthorn wood at different altitude.

Source of variation		Wood properties		Sum of squares	df	Mean square	F value	p value
Altitude	Branch	Oven-dry density	Between groups	0.011	2	0.006	3.190	0.059
			Within groups	0.042	24	0.002		
			Total	0.054	26			
		Volumetric swelling	Between groups	405.091	2	202.546	76.658	0.000
			Within groups	63.413	24	2.642		
			Total	468.504	26			
		Fiber length	Between groups	0.038	2	0.019	1.960	0.163
			Within groups	0.234	24	0.010		
			Total	0.272	26			
		Fiber diameter	Between groups	18.270	2	9.135	4.717	0.019
			Within groups	46.475	24	1.936		
			Total	64.746	26			
		Cell wall thickness	Between groups	1.982	2	0.991	6.524	0.005
			Within groups	3.647	24	0.152		
			Total	5.629	26			
	Stem	Oven-dry density	Between groups	0.019	2	0.009	4.561	0.021
			Within groups	0.049	24	0.002		
			Total	0.068	26			
		Volumetric swelling	Between groups	387.735	2	193.868	38.871	0.000
			Within groups	119.698	24	4.987		
			Total	507.434	26			
		Fiber length	Between groups	0.100	2	0.050	3.024	0.067
			Within groups	0.397	24	0.017		
			Total	0.497	26			
		Fiber diameter	Between groups	7.960	2	3.980	3.474	0.047
			Within groups	27.499	24	1.146		
			Total	35.459	26			
		Cell wall thickness	Between groups	0.294	2	0.147	3.925	0.034
			Within groups	0.898	24	0.037		
			Total	1.191	26			

Tabs. 5 and 6 present the correlation matrixes of the relationships among density and the various characteristics of stem wood, and those among density in branch wood. Results of Pearson matrix correlation showed that the cell wall thickness had significant relationships (i.e. $p < 0.05$) with wood density (Tab. 5).

Tab. 5: Correlation matrix for the interrelationships between density and the morphological feathers of stem wood of the hawthorn species.

Stem wood	1	2	3	4	5
1. Density	1				
2. Volumetric swelling	0.300	1			
3. Fiber length	-0.126	-0.240	1		
4. Fiber diameter	-0.056	0.280	-0.029	1	
5. Cell wall thickness	0.201	0.417*	0.030	-0.070	1

*Correlation is significant at the 0.05 level.

As can be seen in Tab.6, fiber diameter and cell wall thickness had significant relationships (i.e. $p < 0.05$) with wood density of branch-wood (Tab. 5).

Tab. 6: Correlation matrix for the interrelationships between density and the biometric feathers of branch wood of the hawthorn species.

Branch wood	**1**	**2**	**3**	**4**	**5**
1. Density (kg·m^{-3})	1				
2. Volumetric swelling	0.251	1			
3. Fiber length	0.162	-0.276	1		
4. Fiber diameter	0.265	0.473*	-0.171	1	
5. Cell wall thickness	0.166	0.469*	-0.148	0.112	1

* Correlation is significant at the 0.05 level.

Some biometric properties had moderately higher correlation coefficients in branch-wood than in stem wood whereas others had higher coefficients in stem wood than branch wood (Tabs. 4 and 5). For example, fibre length correlated positively but insignificantly ($r = 0.162$, $p > 0.05$) with branch-wood density but inversely and insignificantly ($r = -0.126$, $p > 0.05$) with stem-wood density.

CONCLUSIONS

This study inspected the influence of different altitude levels on wood physical properties (dry density and volumetric swelling) and biometric properties (fiber length, fiber diameter, cell wall thickness) of hawthorn wood in southwest of Iran. The following results have been obtained: *(1)* The results of ANOVA indicated that different altitude levels had a significant effect on physical and fiber biometry of both stem and branch woods. *(2)* There are significant statistical differences of the studied parameters between stem and branch woods. *(3)* The highest mean values of physical properties (dry density, volumetric swelling) of both stem and branch woods are found in the intermediate altitude. *(4)* The highest mean values of fiber length, fiber diameter, and cell wall thickness of stem-wood are found in high, low and intermediate altitude, respectively. However, the mentioned properties of branch-wood are found in low and intermediate altitudes above sea level. *(5)* Pearson matrix correlation indicated that fiber diameter and cell wall thickness have significant relationships with wood density.

REFERENCES

1. Amoah, M., Appiah-Yeboahand, J., Okai, R., 2012: Characterization of physical and mechanical properties of branch stem and root wood of iroko and emire tropical trees. Research Journal of Applied Sciences, Engineering and Technology 4(12): 1754–1760.
2. Antwi-Boasiako, C., Apreko-Pilly, S., 2016: Termite resistivity of the stem and branch woods of *Aningeria robusta* and *Terminalia ivorensis*. African Journal of Wood Science and Forestry 4(2): 231–237.
3. Atchison, J.E., 1987: Data on non-wood plant fibers. In: The Secondary fibers and non-wood pulping (3. ed. Hamilton F and B Leopold). TAPPI Press, Atlanta, USA, 391 pp.

4. Azizi, G., Arsalani, M., Bräuning, A., Moghimi, E., 2013: Precipitation variations in the central Zagros Mountains (Iran) since AD 1840 based on oak tree rings. Palaeogeography, Palaeoclimatology, Palaeoecology 386: 96-103.
5. Bahmani, M., Saeedi, S., Humar, M., Kool, F., 2018: Effect of tree diameter classes on the properties of Persian oak (*Quercus brantii* lindl.) wood. Wood Research 63(5): 755-762.
6. Bahmani, M., Fathi, L., Koch, G., Kool, F., Aghajani, H., Humar, M., 2020: Heartwood and sapwood features of *Sorbus torminalis* grown in Iranian forests. Wood Research 65(2): 195-204.
7. Bowyer, J., Shmulsky, R., Haygreen, J.G., 2003: Forest products and wood science: An introduction. Fourth edition. Ames, IA: Blackwell Publishing Professional, 478 pp.
8. Dadzie, P.K., Amoah, M., Ebanyenle, E., Frimpong-Mensah, K., 2018: Characterization of density and selected anatomical features of stemwood and branchwood of *E. cylindricum*, *E. angolense* and *K. ivorensis* from natural forests in Ghana. European Journal of Wood and Wood Products 76(2): 655-667.
9. Dadzie, P.K., Amoah, M., 2015: Density, some anatomical properties, and natural durability of stem and branch wood of two tropical hardwood species for ground applications. European Journal of Wood and Wood Products 73(6): 759-773.
10. De Micco, V., Campelo, F., De Luis, M., Bräuning, A., Grabner, M., Battipaglia, G., Cherubini, P., 2016: Intra-annual density fluctuations in tree rings: how, when, where, and why? IAWA Journal 37(2): 232-59.
11. Gava, J.L., Goncalves, J.L.M., 2008: Soil attributes and wood quality for pulp production in plantations of *Eucalyptus grandis* clone. Journal of Agriculture Science 65(3): 306-313.
12. Gryc, V.L., Vavrčík, H.A., 2005: Effect of the position in a stem on the length of tracheids in spruce (*Picea abies* (L.) Karst.) with the occurrence of reaction wood. Journal of Forest Science 51: 203-212.
13. Haidari, M., Namiranian, M., Gahramani, L., Zobeiri, M., Shabanian, N., 2013: Study of vertical and horizontal forest structure in Northern Zagros Forest (Case study: West of Iran, Oak forest). European Journal of Experimental Biology 3(1): 268-278.
14. ISO 13061-14, 2016: Physical and mechanical properties of wood. Test methods for small clear wood samples. Part 14. Determination of volumetric shrinkage. Geneva, Switzerland.
15. Jazirehi, M.H., Rostaghi, E.M., 2003: Silviculture in Zagros. University of Tehran Press, Tehran, 520 pp.
16. Kiaei, M., Roque., R.M., 2015: Physical properties and fiber dimension in stem, branch and root of alder wood. Fresenius Bulletin 24(1b): 335-342.
17. Kiaei, M., Tajik, M., Vaysi, R., 2014: Chemical and biometrical properties of plum wood and its application in pulp and paper production. Maderas. Ciencia y tecnología 16(3): 313-322.
18. Kotowska, M.M., Hertel, D., Rajab, Y.A., Barus, H., Schuldt, B., 2015: Patterns in hydraulic architecture from roots to branches in six tropical tree species from cacao agroforestry and their relation to wood density and stem growth. Frontiers in Plant Science 6: 1-17.
19. Murphy, G., Brownlie, R., Kimberley, M., Beets, P., 2009: Impacts of forest harvesting related soil disturbance on end-of-rotation wood quality and quantity in a New Zealand radiata pine forest. Silva Fennica 43(1): 147-160.
20. Nazari, N., Bahmani, M., Kahyani, S., Humar, M., Koch, G., 2020: Geographic variations of the wood density and fiber dimensions of the Persian oak wood. Forests 11(9): 1003.

21. Nazari, N., Bahmani, M., Kahyani, S., Humar, M., 2021: Effect of site conditions on the properties of hawthorn (*Crataegus azarolus* L.) wood. Journal of Forest Science 67(3): 113-124.
22. Nazhand, A., Massimo, L., Alessandra, D., Massimo, Z., Santo, C., Selma B. Souto, A.M., Silva, P.S., Eliana B.S, Antonello, S., 2020: Hawthorn (*Crataegus* spp.): An updated overview on its beneficial properties. Forests 11(5): 564.
23. Panshin, A.J., Zeeuw, C.D., 1980: Textbook of wood technology. Volume I. Structure, identification, uses, and properties of the commercial woods of the United States and Canada, 3rd ed. McGraw-Hill, New York, USA, 391 pp.
24. Pásztory, Z., Börcsök, Z., Ronyecz, I., Mohácsi, K., Molnár, S., Kis, S., 2014: Oven dry density of sessile oak, turkey oak and hornbeam in different region of Mecsek Mountain. Wood Research 59(2): 683-694.
25. Plomion, C., Leprovost, G., Stokes, A., 2001: Wood formation in trees. Plant Physiology 127(4): 1513-1523.
26. Preston, K.A., Cornwell, W.K., DeNoyer, J.L., 2006: Wood density and vessel traits as distinct correlates of ecological strategy in 51 California coast range angiosperms. New Phytologist 170(4): 807-818.
27. Sagheb-Talebi, K., Sajedi, T., Yazdian, F., 2004: Forests of Iran. Research Institute of Forests and Rangelands. Forest Research division 339: 28.
28. Samariha, A., Kiaei, M., Talaeipour, M., Nemati, M., 2011: Anatomical structural differences between branch and trunk in *Ailanthus altissima* wood. Indian Journal of Science and Technology 4(12): 1676–1678.
29. San, H.P., Long, L.K., Zhang, C.Z. Hui, T.C., Seng, W.Y., Lin, F.S., Hun, A.T., Fong, W.K., 2016: Anatomical features, fiber morphological, physical and mechanical properties of three years old new hybrid paulownia: Green Paulownia. Journal of Forest Research 10(1): 30-35.
30. Schulgasser, K., Witztum, A., 2015: How the relationship between density and shrinkage of wood depends on its microstructure. Wood Science and Technology 49: 389–40.
31. Sousa, V.B., Louzada, J.L., Pereira, H., 2018: Variation of ring width and wood density in two unmanaged stands of the Mediterranean Oak *Quercus faginea*. Forests 9(1): 44.
32. Tsoumis, G., 1996: Science and technology of wood: structure. Properties and utilization, Van Nostrand Reinhold, New York. USA, 268 pp.
33. Vaysi, R., Yosefi, F., 2008: An investigation on the production possibility of NSSC pulp and fluting papers from Kiwi residues. Journal of Sciences and Techniques in Natural Resources 3(1): 51-64.
34. Wagenführ, R., Scheiber. C., 1974: Holzatlas. Leipzig, Fachbuchverlag, 690 pp.
35. Wheeler, E.A., Baas, P., Gasson, P.E (eds), 1989: IAWA list of microscopic features for hardwood identification. IAWA Bulletin n.s. 10(3): 219–332.
36. Zeidler, A., Borůvka, V., 2016: Wood density of northern red oak and pedunculate oak grown in former brown coal mine in the Czech Republic. Bioresource 11(4): 9373-9385.
37. Zhao, X., 2015: Effects of cambial age and flow path-length on vessel characteristics in birch. Journal of Forest Research 20(1): 175-185.
38. Zhao, X., Guo, P., Zhang, Z., Wang, X., Peng, H., Wang, M., 2018: Wood density and fiber dimensions of root, stem, and branch wood of *Populus ussuriensis* Kom. Trees. BioResources 13(3): 7026-7036.
39. Zobel, B.J., van Buijtenen, J.P., 1989: Wood variation: Its causes and control. Springer-Verlag, Berlin, Heidelberg, New York, 378 pp.

Huijun Dong
Nanjing Forestry University
College Of Material Science And Engineering
Nanjing 210037
China

Miha Humar
University Of Ljubljana
Department Of Wood Science
Biotechnical Faculty
1501 Ljubljana
Slovenia

Sohrab Rahimi
University Of British Columbia
Department Of Wood Science
Vancouver, BC V6T 1Z4
Canada

Mohsen Bahmani*
Shahrekord University
Department Of Natural Resources And Earth Science
Shahrekord 64165478
Iran
*Corresponding author: mohsen.bahmani@sku.ac.ir

WOOD RESEARCH
e-ISSN 2729-8906
66(3):2021 403-414 pp.
doi.org/10.37763/wr.1336-4561/66.3.403414

CHARACTERIZATION OF AROMATIC FIBERBOARDS

Wei Wang[1,2], Hui Shen[1], Haiqiao Zhang[1], Yang Zhang[1,2],
Yanji Zhou[1], Danyang Zhao[1]
[1]Nanjing Forestry University
China
[2]University Of Tennessee
Usa

(Received August 2020)

ABSTRACT

For use as decoration panels, wood fiber was used to prepare a new type of aromatic fiberboard using hot-press technology that mixes spices and adhesives. Experiments showed that the use of different proportions of two kinds of spices, wormwood and lavender, mixed with waterborne acrylic adhesives, had a slight influence on the curing time and viscosity of the glue. The different mixtures equally affected the physical and mechanical properties of the fiberboard and the smells similarly affected brain wave frequencies. The experimental results showed that a 20% proportion of lavender and wormwood was optimal compared with 5%, 10%, and 15%, and this amount also provided the best health-care effect. This work provides the experimental data and a theoretical basis to achieve pharmacological and health-care effects for the development of aromatic and other special kinds of fiberboard for industrial applications.

KEYWORDS: Spices, aromatic fiberboard, waterborne acrylic acid, smell, brain wave.

INTRODUCTION

Increasing prosperity has led to increased consumer expectations of material goods. Natural products are especially desired for use in all aspects of life, with a strong desire for items related to nature and ecology (Gouveia et al. 2018). Compared to other products processed from raw materials, wood can be made into boards (Pan and Jiang 2019, Liu et al. 2019b,c) for use in the construction of homes and other buildings (Guan and Guo 2009, Liu et al. 2019d,e). Consumers value wood products that retain the features of the original wood, including texture, traits of specific varieties of wood, and the aroma of wood (Xie 2001). Processed, artificial boards lack some of the superior material qualities of the original wood, such as the ability to inhibit bacteria, repel mosquitoes, and purify air, and pleasing qualities such as delicate touch and wood texture (Yerlikaya and Karaman 2020, Kulman et al. 2019, Cinar 2018). Thus, specific processing and production technologies have been developed to make boards that more closely resemble the virgin wood.

Aromas can mask unpleasant smells in rooms and make people feel happy and relaxed (Liu et al. 2019a). Special aromas from spices, such as wormwood (Gu et al. 2018), lavender, citrus, and mint, also may have medicinal effects to promote mental and physical health (Wang 2008). Among the many available household products, aromatic fiber products (Huo 2004) were originally developed in the 1980s and are made using processing and production techniques including microcapsule and blend spinning methods. These products are becoming increasingly popular among consumers (Yuan and Ye 2007). Aromatic fiber textile technology can be used to produce artificial panels with specific effects. Although the preparation of specialized products can be expensive, aromatic fiberboard can be prepared more economically by the addition of spices into the wood fiberboard.

With increasing demands for wood, the expansion of the timber industry, and an increase in the per capita income, the domestic timber market import and export volume has gradually expanded with increased industrial production, house building, and manufacture of daily consumer goods. However, domestic timber resources are limited and there is growing consumer demand for high quality wood for use in houses with an emphasis on ecological design (Antov et al. 2020, Zeng et al. 2018). Continued efforts to improve ecological design and develop new wood materials will allow the continued development of China's timber industry with increased application of indoor wood materials with greater durability. In this work, spices were added during the production of wood fiber sheets than were then combined using glue via hot-press technology. The goal was to prepare materials with spices that could exhibit pharmacological effects such as improving the sensation of well-being (Zhu and Cui 2004). Therefore, a production and processing strategy was applied to prepare aromatic fiberboard for indoor use. The performance of the prepared aromatic fiberboard was tested and the effects of the smell of the prepared materials on brain wave activity were investigated.

MATERIAL AND METHODS

Materials

Wood fiber was obtained from the fiberboard workshop of the Junyi Mineral Products Processing Factory in Lingshou County (Shijiazhuang, China) (Fig. 1a). The water content of the wood fiber was ≤ 5%, the length was 0.5 mm to 1.0 mm, the ash content was ≤ 10%, and the bulk density was approximately 25-29 $g \cdot cm^{-1}$.

Fig. 1: (a) Wood fiber, (b) wormwood, and (c) lavender dry grain.

Wormwood was provided by Jinan Zhongsheng Wormwood Products Technology Co., Ltd. (Jinan, China) (Fig. 1b). Lavender was provided by the Sixty-Five Group of Fragrance Lavender Processing Plant in Huocheng County, Yili, Xinjiang, China (Fig. 1c). Chemical and physical properties of lavender and wormwood provided from producers are listed in Tab. 1.

Tab. 1: Basic properties of lavender and wormwood (data sheets).

	Wormwood	**Lavender**
Main ingredients	Camphor	Linalyl acetate, linalool
PH value	5.3	5.6
Viscosity (cp. 20°C)	11.3	11.8
Odour characteristics	Chinese herbal medicine, tastes strong	Floral, tastes strong
Spice effect	Medicinal, refreshing, plant dye, deworming	Medicine, sleep aid, soothe the nerves, plant dye

Non-toxic waterborne acrylic resin which contents methyl methacrylate (99%) (MMA), soybean protein (99%), ammonium persulfate (98%) (APS), polyvinyl alcohol (analytically pure, PVA), vinyl acetate (analytically pure, VAc) was used as an adhesive to prepare the aromatic fiberboard. Water and acrylic acid were mixed and stirred in a beaker at a mass ratio of 1:1 (water: acrylic acid = 1: 1). The proportion of each component contained in acrylic resin: 3.8% soybean protein, 15.4% PVA, 24.6% VAC, 55.4% MMA, 0.7% APS. The curing performance was tested after the waterborne acrylic acid was mixed with spices.

Aromatic fiberboard manufacturing process

Aromatic fiberboard manufacturing was performed using an electric blast drying oven (model OGH-101-2B, manufactured by Shaoxing Shangyu District Huyue Instrument Equipment Factory, Shaoxing, China); a 250 kN flat vulcanizing machine, manufactured by Huzhou Shunli Rubber Machinery Manufacturing Co., Ltd., Huzhou, China); a multi-functional mixer (model BH-25, manufactured by Daqing Tianyi Food Machinery Co., Ltd., Daqing, China); an electronic balance, model JN-B-5, manufactured by Guangzhou Yuhua Instrument Co., Ltd., Guangzhou, China; sheet mold, dimensions of 50 mm × 50 mm × 300 mm, manufactured by the Nanjing Forestry University artificial board laboratory, Nanjing, China; and a 20 kN control electronic universal testing machine (manufactured by Shenzhen Sansi Technology Co., Ltd., Shenzhen, China).

The dried fiber was sized and added spices at concentrations of 0%, 5%, 10%, 15%, and 20%, respectively, relative to the amount of wood fiber, regarding groups 0 through 4. Then the wood fiber and spices were mixed with acrylic resin (150 $kg \cdot m^{-3}$), and paved. The continuously formed mat was prepressed before being loaded into the hot press. The hot-pressing temperature was 125°C, the pressure was 2.5 MPa, and the hot-pressing time was 4 min. The sheet thickness was

10 mm and the density was 0.7 g·cm^{-3}. After hot-pressing, samples were cooled for 24 h before the physical and mechanical properties of the material were tested.

Extract analysis

The selected spices have special aromas caused by their ingredients. In order to investigate their effective constituents, the spices were subjected to distillation (Li et al. 2019). Impurities and hard branches were first removed from the dry spice granules, then 100 g spice samples were weighed and placed into a 1000 mL glass flask. The flask was connected to a water vapor generating device and the condensing pipe at both ends, and the condensing pipe was connected with a water oil separator for essential oil extraction. Distillation was performed for 7 h, and the extracts were collected. The extracts were mixed with Na2SO4, and the yield was calculated after the removal of water. The essential oils were stored via cryopreservation for further chemical detection and analysis.

The distillation equipment used in the study included an electronic balance (model JN-B-5, manufactured by Guangzhou Yuhua Instrument Co., Ltd., Guangzhou, China) and a digital thermostatic water bath (model HH series-1, manufactured by Qingdao Juchuang Environmental Protection Equipment Co., Ltd., Qingdao, China).

The extract components were detected by gas chromatography (GC) (6890N; Agilent Technologies Inc., Santa Clara, CA, USA) and gas chromatography-mass spectrometry (GC-MS) (S6890/5973N; Agilent Technologies Inc., Santa Clara, CA, USA) using a hue-mass spectrometer (Agilent Technologies, Beijing, China). The chromatographic conditions were as follows: vaporization chamber temperature of 250°C; Supelco 18275-06 A PTE-5 Capillary column (30 m × 0.25 mm × 0.25 μm); injection amount of 0.2 μL; nitrogen as carrier gas, the flow rate was 0.9 mL·min^{-1}, and the shunt ratio was 70:1. The temperature was set to 80 °C and maintained for 15 min, increased to 190°C at a rate of 2°C·min^{-1} and maintained for 15 min, and then increased to 300°C at a rate of 15°C·min^{-1}, and held at 300°C for 15 min.

Mass spectrometry conditions were as follows: Agilent Db-5MS (50 m × 0.25 mm × 0.25 μm) column with a flow rate of 1.1 mL·min^{-1}; multiplier tube voltage of 1623 V; scanning range of 45 AMU to 450 AMU; EI ionization mode; ion voltage of 70 eV; ion source temperature of 230°C; interface temperature of 290°C; and quadrupole rod temperature of 160°C.

Scent-smelling tests on brainwaves

A Model EK brainwave tester was used (Xuzhou Zhongma Diagnostic Apparatus Co., Ltd., Xuzhou, China). In this experiment, 70 adult subjects (equal numbers of men and women, and age range of 25 to 50 years old) participated in measurements of brainwaves after smelling different prepared materials. Before entering the test room, each volunteer was instructed on laboratory safety operation specifications and completed a personal health assessment.

This test was performed in the laboratory of artificial boards at Nanjing Forestry University. During the test, each subject maintained a free and comfortable sitting posture. Brain signals were detected using electrodes. Utilizing Fourier transform, the brain's electric wave, in the form of power and frequency, showed four kinds of curves (α, β, δ, and θ) (Wang et al. 2010). An 18-lead brainwave tester was used and volunteers were asked to keep a calm and relaxed state to enable accurate display and recording of brainwave data.

The goal of these spice-containing materials is that they will give off pleasing aromas (Wang et al. 2015). Medium-density fiberboard (MDF) without spices was used as the blank control group and samples prepared with 20% wormwood or 20% lavender, were tested. During the experiment, each samples of aromatic fiberboard (50 mm × 50 mm × 10 mm) was placed in

a sealed bag of the same volume, and identifying label information was concealed. The experiment was conducted such that the subjects were encouraged to relax. New groups were brought in every 6 min, each cycle lasted 7 days, with a 3-day interval in the middle as a cycle, and the trial period for each subject of two months.

RESULTS AND DISCUSSION

Waterborne acrylic resin properties

The purpose of this experiment was to understand the effect of the addition of spices on the performance of the adhesive. Tests were conducted of four groups plus a blank control group, where the four groups included wood samples prepared with 5%, 10%, 15%, or 20% of spices. The results showed slight differences in the effects of wormwood and lavender, with only a small effect on the curing time of waterborne acrylic acid. Tang (2017) reported the experimental effect of adding water-based acrylic to wood, and using this method, the curing time is shorter. As shown in Tab. 2, a trend in the effect of spice addition ratio on the curing properties of the glue can be seen. After addition of 20% of wormwood and lavender, due to the weak acidity of waterborne acrylic acid (Li et al. 2015), decreased curing time was observed.

Tab. 2: Analysis of the effect of four different spices' addition ratios on the curing time of glue.

Experimental group→ Curing time (s) ↓	Blank control	Wormwood				Lavender		
		G.1	G.2	G.3	G.4	G.1	G.2	G.3
Test 1	70	73	74	75	69	79	64	63
Test 2	74	74	74	70	72	76	68	69
Test 3	75	71	68	72	68	73	69	70
Test 4	75	73	68	70	70	72	69	71
Mean values	73.5	72.8	71.0	71.8	69.8	75.0	67.5	68.3

GC-MS detection and analysis

As shown in Tab. 3, the extracts from wormwood consisted of 32 components, with 1,8-eucalyptol (15.36%), camphor (13.21%), 4-terpineol (5.26%), and chamomile (4.35%) present at the highest concentrations. The components present at concentration greater than 1.00% included terpenes (1.12%), β-myrcene (1.29%), γ-terpinene (1.61%), artemisia ketone (1.13%), artemisia alcohol (2.31%), 2-cyclohexan-1-ol (1.62%), borneol (2.89%), trans-caryophyllene (2.74%), big root geranyl-D (1.56%), trans-carvacrol (2.74%), eugenol (1.12%), and Spartan (3.25%). Components present at less than 1.00% included α-Pinene (0.95%), β-Pinene (0.45%), and Linalool (0.91%).

Tab. 3: Main ingredients of wormwood extract.

Keep time (min)	Compound	Relative content (%)
13.23	α-Pinene	0.95
16.25	β-Pinene	0.45
18.26	Camphene	1.12
21.33	β-Myrcene	1.29
24.12	γ-terpinene	1.61
25.33	1,8-Cineole	15.36
26.15	Artemisia ketone	1.13

29.38	Artemisia alcohol	2.31
34.26	Linalool	0.91
39.71	2-cyclohexen-1-ol	1.62
40.12	Borneol	2.89
43.12	Camphor	13.21
44.02	Terpineol-4	5.26
45.08	Trans-caryoophyllene	4.81
48.71	Germacrene-d	1.56
51.22	Trans-carveol	2.74
51.31	Eugenol	1.12
53.26	Spathulenol	3.25
54.13	Azulene	4.35

Tab. 4 shows that the extracts from lavender contained 42 components, with lavender acetate (15.51%), linalool (20.56%), and linalyl acetate (24.61%) present at the highest concentrations. Components present at more than 1.00% included 1,8-eucalyptol (1.35%), cis-ocimene (2.51%), neryl acetate (1.52%), octene acetate-1-ester (2.94%), α-santalene (1.85%), borneol (2.31%), lavender alcohol (4.35%), α-terpineol (1.92%), geranyl acetate (1.91%), oleoresin (5.89%), benzoic (2.13%), and geraniol (2.35%). Components present at less than 1.00% included α-pinene (0.23%), β-pinene (0.08%), camphene (0.35%), β-myrcene (0.41%), limonene (0.26%), α-terpinene (0.22%), butanoic acid, hexylester (0.41%), 1-octen-3-ol 9 (0.27%), nerol oxide (0.41%), camphor (0.44%), bomyl acetate (0.82%), β-bisabolene (0.15%), cuminaldehyde (0.81%), nerol (0.83%), and α-cadinol (0.94%).

Tab. 4: Main ingredients of lavender extract.

Keep time (min)	**Compound**	**Relative content (%)**
15.23	α-Pinene	0.23
18.66	β-Pinene	0.08
19.56	Camphene	0.35
22.39	β-Myrcene	0.41
25.36	Limonene	0.26
26.36	1,8-Cineole	1.35
27.58	cis-Ocinmene	2.51
31.22	α-Terpinene	0.22
36.56	Octen-1-ol acetate	2.94
38.45	Butanoic acid, hexylester	0.41
40.35	1-Octen-3-ol	0.27
42.12	Nerol oxide	0.41
43.22	Camphor	0.44
45.65	Linalool	20.56
46.12	Linalyl acetate	24.61
49.35	α-Santalene	1.85
53.22	Bomyl acetate	0.82
53.45	Lavandulyl acetate	15.51
51.55	Borneol	2.31
57.54	Lavandulol	4.35
57.72	α-Terpineol	1.92
58.65	Neryl acetate	1.52

58.92	β-Bisabolene	0.15
60.33	Geranyl acetate	1.91
61.52	Cuminaldehyde	0.81
62.11	Nerol	0.83
63.56	Geraniol	2.35
64.44	Caryophyllene oxide	5.89
70.23	Benzoic acid	2.13
71.39	α-Cadinol	0.94

Jiang et al. (2019) showed that wormwood extract has a significant physiological effect on the treatment of human diseases. Tang et al. (2014) reported that the extract of lavender has a good regulating effect on the balance of the human body. The extracts from wormwood and lavender mainly included monoterpene alcohol, with a low content of oxides. The linalool, linalyl acetate, lavender acetate, and other ingredients in lavender essential oil (Yang et al. 2010) can calm nerves (Re et al. 2000) and promote sleep (Hu et al. 2019). Lavender is relaxing (Lü et al. 2016), can reduce fatigue (Spesyvyi et al. 2019), and inhibit bacteria (Xu 2006). Monitoring brain wave frequencies can reveal if chemical components affect human physiology.

Analysis of physical and mechanical properties of aromatic fiberboard

Xu et al. (2011) found that adding plant flavors such as sandalwood or jasmine during wood hot pressing can improve the mechanical properties of fiberboard (Xu 2011). In this experiment, the mechanical properties of the aromatic fiberboard made by lavender and wormwood differed from those of common hot-pressed fiberboard. To assess if the prepared material could meet the requirements of GB/T 11718 (2009) specifying the mechanical properties of fiberboard given the effect on the curing performance of the acrylic resin, the aromatic fiberboard with 20% of added spices was selected for testing.

The spices were weighed precisely by an electronic balance and mixed with glue (waterborne acrylic acid) and wood fiber. The results (as shown in Tab. 5) showed that material prepared with 20% addition of spices improved the internal bond strength of the aromatic fiberboard compared to that with no spices, with 0.57 MPa for wormwood and more than 0.62 MPa for lavender. The addition of lavender somewhat increased the static bending strength of the aromatic fiberboard. Addition of wormwood improved the elastic modulus and the average water absorption thickness expansion rate of the aromatic fiberboard, and this trend was opposite when lavender was added. According to these results, there were relatively small negative impacts on the fiberboard from the addition of spices, so the overall effect was positive.

Tab. 5: Experimental variables of adding 20% wormwood and lavender.

Related variables	Component ratio (%)	Group1	Group2	Group3	Group4	Average
Internal bond strength (MPa)	0%	0.55	0.49	0.51	0.52	0.52
	20% Wormwood	0.59	0.51	0.59	0.57	0.57
	20% Lavender	0.61	0.63	0.62	0.63	0.62
Bending strength (MPa)	0%	19.23	19.11	20.01	19.12	19.37
	20% Wormwood	20.12	20.08	19.98	20.31	20.12
	20% Lavender	19.35	19.95	20.05	20.16	19.88
Elastic modulus (MPa)	0%	2128.25	2109.56	2125.33	2018.21	2117.84
	20% Wormwood	2209.11	2308.91	2318.36	2309.55	2286.48
	20% Lavender	2219.32	2255.99	2289.16	2291.36	2263.96

Water absorption thickness expansion rate (%)	0%	11.38	11.37	11.44	11.31	11.38
	20% Wormwood	12.38	12.83	12.92	12.81	12.74
	20% Lavender	12.21	12.39	12.56	12.53	12.42

Brain wave test comparison

To compare the stimulation and physiological effects on the human brain after smelling the odors emitted from aromatic and common fiberboard samples, brain response was monitored (Li 2010). Sowndhararajan Kandhasamy and Kim Songmun proposed that the influence of odor stimuli on human brain waves indirectly demonstrates the great influence of odor on the body's physiological response, emotions, and social behavior (Sowndhararajan et al. 2016). An odor induction experiment was used by Murali and Kulish (2007), who observed that inhaling a gas with a special odor can produce a corresponding stimulation response in the brain. Thus, electroencephalogram (EEG) analysis was performed for 70 volunteers who smelled wood samples with added wormwood and lavender, and the results are shown in Tab. 6. In the group that smelled the material with added wormwood, the proportion of α wave in the subjects was 45.64% ± 6.75% and the percentage of β wave was 26.44% ± 3.27%. Both were higher than the brainwave frequencies for the blank groups. In the group that smelled the material with added lavender, the α wave to β wave ratio was increased compared with the ratio in the blank group. The δ wave ratio in the two groups of added wormwood and lavender were 14.74% ± 2.75% and 14.54% ± 2.81%, respectively, indicating a downward trend. The θ wave ratios in these two groups were 17.51% ± 2.89% and 17.79% ± 2.85%, respectively, indicating an upward trend.

Tab. 6: Four types of brain wave frequency ratio/ $\bar{x} \pm s$.

Experimental classification	Spice ratio (%)	α wave (%)	β wave (%)	δ wave (%)	θ wave (%)
Blank control	0	45.51 ± 6.10	25.55 ± 3.33	15.52 ± 3.10	17.23 ± 2.60
Wormwood	20	45.64 ± 6.75	26.44 ± 3.27	14.74 ± 2.75	17.51 ± 2.89
Lavender	20	46.75 ± 6.56	26.56 ± 3.68	14.54 ± 2.81	17.79 ± 2.85

*X: average, S: standard deviation.

As shown in Tab. 7, experiments were conducted to evaluate preference for different addition ratios of spices using 70 recruited experimental volunteers. The results showed that a 20% spice addition was the most popular, with approximately 48% of participants preferred 20% wormwood addition and 46% preferred 20% lavender addition. This shows that the higher content of spices was preferred.

Tab. 7: Acceptance of spices' addition ratio.

Experimental classification	Addition ratio (%)	Acceptance (%)
Wormwood	5	30
	10	29
	15	45
	20	48
Lavender	5	40
	10	45
	15	35
	20	46

CONCLUSIONS

In this study, new aromatic fiberboard was prepared and tested. The test results showed that the addition of spices had few effects on board performance, but exhibited stimulating effects on human body function. Different proportions of wormwood and lavender spices were tested for effects on the curing time of waterborne acrylic acid. Higher ratios of added wormwood or lavender had greater effects on the adhesive curing time. Comparison of boards made with addition of the same amount of wormwood or lavender, the aromatic fiberboard prepared with lavender exhibited better mechanical properties. The average internal bond strength of the aromatic fiberboard containing wormwood was 0.57 MPa, and the average internal bond strength of the fiberboard containing lavender was greater than 0.62 MPa, with increased emission of fragrance. The results showed increased brain wave frequency with smell, with a faster increase for aromatic fiberboard prepared with lavender. Overall, the results show that the inclusion of spices in aromatic fiberboard had positive effects for stimulation of the human brain.

ACKNOWLEDGMENTS

The authors gratefully acknowledge the financial support of the project funded by the Jiangsu Government Scholarship for Overseas Studies, the National Natural Science Foundation of China Youth Project (51608271), and the China Postdoctoral Science Foundation (2016M601820).

REFERENCES

1. Altgen, M., Uimonen, T., Rautkari, L., 2018: The effect of de- and re-polymerization during heat-treatment on the mechanical behavior of Scots pine sapwood under quasi-static load. Polymer Degradation and Stability 147: 197-205.
2. Antov, P., Savov, V., Neykov, N., 2020: Sustainable Bio-Based Adhesives for Eco-Friendly Wood Composites. A Review. Wood Research 65 (1): 51-62.
3. Chen, G., Zhao, X.J., Xing, J., Yao, Y.H., Zheng, J.J., 2014: Preparation of mixed stationary phase of cellulose and polysiloxane ionic liquid for gas chromatography.Chinese Journal of Chromatography 32(10):1117-1123.
4. Cinar H., 2018: Effects of temperature and thickness of wood based boards on formaldehyde emission. Wood Research 63(5): 895-908
5. GB/T 11718, 2009: Medium density fibreboard. Standardization Administration of China. Beijing, China.
6. Gouveia, S., Otero, L.A., Fernandez-Costas, C., Filgueira, D., Sanromán, A., Moldes, D., 2018: Green binder based on enzymatically polymerized eucalypt kraft lignin for fiberboard manufacturing. A preliminary study. Polymers 10(6): 642.
7. Gu, H.K., Liu, G.J., Cheng, Z.L., Song, W., Xiao, Z.Q., Xu, Y., Song, M.F., 2018: Application of wormwood to basic research and development. Journal of Anhui Agricultural Sciences 46(9): 22-25, 35.
8. Guan, X., Guo, M.H., 2009: Wood texture strengthening technology. Furniture 5(174): 42-45.
9. Hu, D.Y., Xu, D.M., Chu, M.L., Zhang, C.C., Gan, W.X., 2019: Overview of the main chemical components of camphor tree essential oil. China Forest Products Industry 56(11): 61-64.

10. Huo, Y., 2004: Production and application of aromatic fibers. Synthetic Fiber Industry 27(4): 56-57.
11. Jiang, Z.H., Chang, X.M., Zhang, Z.R., Qu, Y.C., Tian, C., Gu, L.B., Zhang, S.Q., 2019: Research progress on the chemical constituents and pharmacological effects of wormwood. Chinese Journal of Veterinary Drug 53(2) 76-85.
12. Kulman, S., Boiko, L., Gurová, D.H., Sedliačik J., 2019: Prediction of the fatigue life of wood-based panels. Wood Research 64(3): 373-388.
13. Li, J., 2010: Ecological properties of wood - wood is a contributor to human health in a green environment. Journal of Northeast Forestry University 38(5): 1-8.
14. Li, Y.D., Liu, X.M., Qiu, J.F., Yin, K.Y., Xia, J.J., Yang, Y., Duan, Y.Q., 2019: Comparison and analysis of Damascus rose essential oil components from different producing areas. China Food Additives 30(7): 64-72.
15. Li, Z., Li, W.G., Gao, L., Yu, Z.Q., 2015: Preparation and properties of aqueous acrylate adhesive for lithium ion battery. China Adhesives 24(12):40-45.
16. Liu, J., Liu, Q.D., Wu, S.S., 2019a: Study on properties of aromatic microcapsule viscose fiber and its perfume retention properties. Shanghai Textile Science & Technology 47(9): 14-17.
17. Liu, X.Y., Liu, M., Lv, M.Q., Lv, J.F., 2019b: Photodegradation of three hardwood species by sunlight and xenon light sources. Bioresources 14(3): 6909-6922.
18. Liu, X.Y., Timar, M.C., Varodi, A., 2019c: Effects of artificial UV and natural ageing on the colour and surface chemistry of waxes finished surfaces. Journal of Photochemistry and Photobiology B: Biology, article number 111607.
19. Liu, X.Y., Lv, M.Q., Liu, M., Lv, J.F., 2019d: Repeated humidity cycling's effect on physical properties of three kinds of woodbased panels. Bioresources 14(4): 9444-9453.
20. Liu, X.Y., Lv, M.Q., Liu, M., Wu, Z.H., Lv, J. F., 2019e: Characterization and identification of lacquer films from the Qin and Han Dynasties. Bioresources 14(4): 9509-9517.
21. Lü, D., Wang, D.X., Xie, X.Y., Zhang, G.G., 2016: Study on volatile components of terpenes released from *Pinus tabulaeformis*. Journal of Northwest Forestry University 31(1): 231-237.
22. Murali, S., Kulish, V., 2007: Analysis of fractal and fast Fourier transform spectra of human electroencephalograms induced by odors. International Journal of Neuroscience 117(10): 1383-1401.
23. Pan, L.W., Jiang, Y., 2019: Evaluating the effects of KCl on thermal behavior and reaction kinetics of medium density fiberboard pyrolysis. Materials 12(11): 1826.
24. Re, L., Barocci, S., Sonnino, S., Mencarelli, A., Vivani, C., Paolucci, G., Scarpantonio, A., Rinaldi, L., Mosca, E., 2000: Linalool modifies the nicotinic receptor–ion channel kinetics at the mouse neuromuscular junction. Pharmacological Research 42(2): 177-181.
25. Sowndhararajan, K., Kim, S., 2016: Influence of fragrances on human psychophysiological activity: with special reference to human electroencephalographic response. Scientia pharmaceutica 84(4): 724-751.
26. Spesyvyi, A., Španěl, P., Sovová, K., 2019: Styrene radical cations for chemical ionization mass spectrometry analyses of monoterpene hydrocarbons. Rapid Communications in Mass Spectrometry 33(24): 1870-1876.
27. Tang, X.H., 2017: Application research progress of water-based adhesives. Journal of Henan Institute of Education (Natural Science Edition) 26(2): 8-12.
28. Tang, Y., Cao, W.X., Chen, Y., 2014: Research progress of lavender essential oil and

its application in daily necessities. China Cleaning Industry 2014(10): 70-73.
29. Wang, C.L., Hu, Z.H., Shen, H., Leng, P.S., 2015: Health benefits of volatile compounds in aromatic plants. Northern Horticulture 39(15): 171-177.
30. Wang, H.F., Zhu, P., Dong, C.H., 2007: Preparation and properties of aromatic cellulose fibers. Artificial Fibers 37(6): 6-9.
31. Wang, Y.M., 2008: Chinese aromatic plants. Science Press. Beijing, China, 221 pp.
32. Wang, Y.Q., Sun, Y. J., Shi, Y.E., 2010: The chemical constituents and pharmacological activities of lavender essential oil. Foreign Pharmacological Plants 11(9): 5-8.
33. Xie, L.S., 2001: Room environment and wood smell. Furniture and Interior Decoration 2001(3): 13-15.
34. Xu, X.W., 2011: Aromatic fiberboard manufacturing process. China Forestry Science and Technology 25(4): 93-95.
35. Xu, Y.P., 2006: Aromatic fiber and its application. Synthetic Fiber in China 2006(1): 23-26.
36. Yang, Y., Li, J.X., Shi, X.L., Wang, L., Chen, J., Li, G., Fu, J., 2010: Effects of lavender essential oil on blood pressure in rats. Chinese Journal of Hypertension 18(9): 848-849.
37. Yerlikaya, N.C., Karaman A., 2020: Effect of the fabric reinforcement of structural holes in wood based panels. Wood Research 65(3): 485-496.
38. Yuan, X.H., Ye, Y.J., 2007: Preparation of aromatic fibers and textile development. Progress in Textile Science and Technology 2007(3): 14+17.
39. Zeng, Q., Lu, F., Zhou, Y., Chen, N., Rao, J., Fan, M., 2018: Circular development of recycled natural fibers from medium density fiberboard wastes. Journal of Cleaner Production 202: 456-464.
40. Zhu, Y.Z., Cui, Y.H., 2004: Development and application of aromatic home textiles. Shandong Textile Science and Technology 45(6): 43-45.

Wei Wang[1,2*], Hui Shen[1], Haiqiao Zhang[1], Yang Zhang[1,2],
Yanji Zhou[1], Danyang Zhao[1]
[1]Co-Innovation Center Of Efficient Processing
And Utilization Of Forest Resources
College Of Furnishing And Industrial Design
Nanjing Forestry University
Academy Of Chinese Ecological Progress And Forestry Studies
Nanjing Forestry University
Longpan No.159, Nanjing
China
[*]Corresponding author: weiwang1912@163.com

[2]Center For Renewable Carbon
University Of Tennessee
2506 Jacob Drive, Knoxville, TN, 37996
USA

WOOD RESEARCH
e-ISSN 2729-8906
66(3):2021 415-426 pp.
doi.org/10.37763/wr.1336-4561/66.3.415426

A COMPARATIVE STUDY ON THE PHYSICAL AND MECHANICAL PROPERTIES OF DAHURIAN LARCH AND JAPANESE LARCH GROWN IN KOREA

Seong Hyun Kim, Do Hoon Kim, Jae Ik Jo, Jong Ho Kim, Seung Hwan Lee
Jung Kee Choi, Nam Hun Kim
Kangwon National University
Republic Of Korea

(Received July 2020)

ABSTRACT

To compare the wood quality of Dahurian larch and Japanese larch growing in Korea, the physical and mechanical properties were examined using the Korean standards. The proportion of heartwood was 82% and 72% in Dahurian and Japanese larch, respectively. The percentage of latewood was 42% in Dahurian larch and 35% in Japanese larch. The growth ring width of Dahurian larch was narrower than that of Japanese larch. Dahurian larch showed about 20% higher green moisture content compare to Japanese larch wood. Density and shrinkage of Dahurian larch were higher than Japanese larch. Axial compression strength, young`s modulus in compression, and shearing strength in heartwood of Dahurian larch were 11 MPa, 686 MPa, and 2.3 MPa, respectively, showing higher value than Japanese larch. The hardness was in the range of 13.8–38.7 MPa in Dahurian larch and 17.7–48.4 MPa in Japanese larch. The compression strength parallel to the grain and shearing strength in both species were significantly correlated with oven-dried density. Besides, the hardness in Dahurian larch was significantly correlated with latewood percentage and oven-dried density. In conclusion, the differences in the properties of both species were revealed and the results can be used for quality indices of both wood species.

KEYWORDS: Dahurian larch, Japanese larch, physical and mechanical properties, quality indices, wood quality.

INTRODUCTION

The *Larix* species is a deciduous tree belonging to the *Pinaceae* family and is distributed worldwide with about 10 species in the Northern Hemisphere's major regions, such as Alaska, Russia, Mongolia, China, Japan, and Korea (LePage and Basinger 1995). In Korea, there are two species: Dahurian larch (*Larix gmelinii*), which is native to the Korean Peninsula, and Japanese larch (*Larix kaempferi*), introduced from Japan. The wood of *Larix* species has high value as a wood resource because of its excellent quality and straight stem forms. It is used for various purposes, such as post and timber of buildings, flooring, furniture, deck, laminated veneer lumber (LVL), medium density fiberboard (MDF), oriented strand board (OSB), and railroad ties (Chauret et al. 2002, Hwang et al. 2008). The Dahurian larch is sparsely distributed in the mountainous areas of North Korea and in a limited area of South Korea (Hwang and Park 2007). A few studies have been undertaken on the properties of Dahurian larch wood as building material (Hwang and Park 2007, Hwang et al. 2008), its wood characteristics (Chauret et al. 2002) and its physical and mechanical properties of lumber (Zhou et al. 2015, Ishiguri et al. 2019, Han et al. 2019) for its effective utilization. Japanese larch, first introduced in Korea in 1904, is one of the major afforestation species and the most valuable domestic wood material in Korea. It is commonly known as an allied species to the Dahurian larch (Shin and Kim 2003, Jung and Park 2008). Japanese larch is usually used as an alternative to the Dahurian larch as building members, structural materials, and wood pellets, among other uses. There are many studies on the properties of Japanese larch wood for its value-added utilization, such as wood quality (Kwon et al. 2004, Ishikura et al. 2012), enhancing properties for wood-based materials (Wang et al. 2017, Song and Hong 2018), fuel characteristics for wood pellets (Kim et al. 2015) and characteristics of preservation (Choi et al. 2011).

To date, however, there have been few comparative studies on the wood quality of Dahurian larch and Japanese larch growing in Korea (Han et al. 2017). Therefore, in this study, the physical and mechanical properties of these two species were investigated and compared to provide basic data that can be used as wood quality indices for their efficient utilization.

MATERIAL AND METHODS

Material

Design principle

Three trees for each species of both Dahurian larch and Japanese larch were harvested from the research forest of Kangwon National University, Chuncheon, Korea (N 37°77`, E 127°81`). Discs of about 7 to 9 cm thickness were collected from breast height. The characteristics of the wood samples are shown in Tab. 1.

Tab. 1: Basic information of the sampled trees.

Common name	Botanical name	Age (years)	Height (m)	D.B.H. (cm)
Dahurian larch	*Larix gmelinii* (Rupr.) Kuzen.	72	20-22	32-33
Japanese larch	*Larix kaempferi* (Lamb.) Carriere	38	20-22	34-36

Note: D.B.H. – Diameter at breast height.

Methods

Measurement of physical properties

The heartwood proportion was obtained using the following Eq. 1:

$$HP = \frac{Wt-Wh}{Wt} \times 100 \quad (\%) \qquad (1)$$

where: w_t - weight of the original discs (g), w_h - weight of heartwood proportion (g).

Growth ring width and latewood percentage in four directions on the discs were measured by KS F 2202 (2016). Moisture content (KS F 2199, 2016), density and specific gravity (KS F 2198, 2016), and shrinkage of woods (KS F 2203, 2004) were measured in sapwood and heartwood. In each test of physical properties, defect-free wood specimens of 38 pieces in Dahurian larch and 40 pieces in Japanese larch were used.

Measurement of mechanical properties

According to the axial compressive properties (KS F 2206, 2004) and shearing strength (KS F 2209, 2004), test specimens were manufactured in the size of 20(T)×20(R)×30(L) mm in sapwood and heartwood of both species. The specimens for hardness were manufactured in the size of 30 (T) ×30 (R) ×15 (L) mm in sapwood and heartwood of both species (KS F 2212, 2004). The specimens were stored in a constant temperature and humidity chamber (20 ± 2°C, 65 ± 3%) for 5 weeks. Compressive properties and shearing strength were measured using an Instron U.T.M. (Model No. 4482) under a load speed of 1.5 mm·min^{-1}. In the shear test, the shear fracture was a tangential section. The number of specimens used in the compression and shear tests were 40 and 44 pieces in Dahurian larch and 48 and 40 pieces in Japanese larch, respectively. Hardness was measured by the Brinell method at 6 points per section using an Instron U.T.M. (Model No. 4482) under a load speed of 0.5 mm·min^{-1}. The number of specimens used in the hardness test were 72 in Dahurian larch and 66 in Japanese larch.

Statistical analysis

One-way ANOVA and Duncan's multiple tests were undertaken using the IBM SPSS Statistics 24.0, 2016 software to check the significance of the test results of the physical and mechanical properties between the two species. In the correlation analysis, a p-value less than or equal to 0.05 indicated significance.

RESULTS AND DISCUSSION

Physical properties

Heartwood proportion, growth ring width, and latewood percentage

The heartwood proportion, growth ring width, and latewood percentage of Dahurian larch and Japanese larch wood are shown in Tab. 2. The heartwood proportions were 82% and 72% in Dahurian and Japanese larch wood, respectively. The growth ring widths were 2.5 mm and 4.3 mm for Dahurian larch and Japanese larch wood, while the latewood percentages were 42% and 35%, respectively. Dahurian larch wood showed higher heartwood proportion and latewood percentage, and narrower growth ring width than Japanese larch wood. Pazdrowski et al. (2007) described the heartwood proportion of European larch (*Larix decidua*) wood as 57-70% which was a little smaller than this study. Hwang et al. (2008) and Hwang and Park (2007) reported the growth ring width of Dahurian larch wood as 0.6–1.5 mm. Han et al. (2017) also reported the growth ring width and latewood percentage of Dahurian larch wood as 1.02 mm and 40.3%,

and those of Japanese larch wood as 2.09 mm and 31.9%, respectively. In addition, Kwon et al. (2004) explained the growth ring width of Japanese larch wood as 2.83 mm which was like the results of this study.

Tab. 2: Macroscopic characteristics of the sample wood species.

Species	Heartwood proportion (%)	Growth ring width (mm)	Latewood percentage (%)
Dahurian larch	82 ± 2	2.5 ± 1.7	42 ± 9
Japanese larch	72 ± 1	4.3 ± 1.9	35 ± 11

Green moisture content and density

The results of the green moisture content and density of Dahurian larch and Japanese larch wood are shown in Tab. 3. The green moisture content in sapwood and heartwood of Dahurian larch wood was 85.3% and 61.8%, and that of Japanese larch wood was 74.1% and 35.7%, respectively. As a result, both sapwood and heartwood in Dahurian larch wood had higher green moisture content than that in Japanese larch wood. Shin and Kim (2003) reported that the green moisture content in Japanese larch wood was 80–109.7% in sapwood and 34.1–38.1% in heartwood, with a similar result as ours.

There was a considerable difference in green, air-dried, and oven-dried densities between the two species, as shown in Tab. 3. The green density of Dahurian larch wood was 1.06 $g \cdot cm^{-3}$ is remarkably higher than that of Japanese larch wood, which had a density of 0.79 $g \cdot cm^{-3}$. There was no difference between sapwood and heartwood in the green density of Dahurian larch wood, but Japanese larch wood showed a large difference with 0.90 $g \cdot cm^{-3}$ in sapwood and 0.69 $g \cdot cm^{-3}$ in heartwood. In Dahurian larch wood, the air-dried and oven-dried densities in heartwood of 0.84 $g \cdot cm^{-3}$ and 0.75 $g \cdot cm^{-3}$ were higher than those in sapwood of 0.66 $g \cdot cm^{-3}$ and 0.64 $g \cdot cm^{-3}$. Contrasting this, for Japanese larch wood, there was no difference in air-dried and oven-dried densities between sapwood and heartwood. As a result, the green, air-dried, and oven-dried densities of Dahurian larch wood were larger than those of Japanese larch wood. Hwang et al. (2008) reported the air-dried and oven-dried densities of Dahurian larch wood as 0.73 $g \cdot cm^{-3}$ and 0.70 $g \cdot cm^{-3}$, respectively. Jung and Park (2008) presented the green density, air-dried, and oven-dried densities of Japanese larch wood as 0.79 $g \cdot cm^{-3}$, 0.61 $g \cdot cm^{-3}$, and 0.56 $g \cdot cm^{-3}$, respectively. In addition, Han et al. (2017) reported that the oven-dried densities in Dahurian larch and Japanese larch wood were 0.72 $g \cdot cm^{-3}$ and 0.60 $g \cdot cm^{-3}$, respectively. As mentioned above, the previous findings on green moisture content and densities showed a trend that is like our findings.

Tab. 3: Green moisture content and density of the sample wood species.

Properties	Species	Sapwood	Heartwood	Average
Green Moisture content (%)	Dahurian larch	85.3 ± 5.7	61.8 ± 2.7	73.4 ± 13.2
	Japanese larch	74.1 ± 1.5	35.7 ± 1.4	55.0 ± 22.1
Green density (M_g/V_g) ($g \cdot cm^{-3}$)	Dahurian larch	1.04 ± 0.02	1.07 ± 0.06	1.06 ± 0.06
	Japanese larch	0.90 ± 0.03	0.69 ± 0.03	0.79 ± 0.13
Air-dried density (M_a/V_a) ($g \cdot cm^{-3}$)	Dahurian larch	0.66 ± 0.05	0.84 ± 0.04	0.75 ± 0.10
	Japanese larch	0.57 ± 0.01	0.58 ± 0.02	0.58 ± 0.02
Oven-dried density (M_o/V_o) ($g \cdot cm^{-3}$)	Dahurian larch	0.64 ± 0.04	0.75 ± 0.03	0.70 ± 0.06
	Japanese larch	0.57 ± 0.01	0.56 ± 0.02	0.56 ± 0.02

Note: M_g - green weight; M_a - air-dried weight; M_o - oven-dried weight; V_g - green volume; V_a - air-dried volume; V_0 - oven-dried volume.

Shrinkage

The results of the shrinkages in the volumetric, radial, and tangential directions and the coefficients of shrinkage anisotropy of Dahurian larch and Japanese larch wood are presented in Tab. 4. There were significant differences in the shrinkages and the coefficients of shrinkage anisotropy between the species. The volumetric, radial, and tangential shrinkage and the coefficient of shrinkage anisotropy in Dahurian larch wood were slightly higher than those in Japanese larch wood. There was little difference between sapwood and heartwood in the shrinkage values of Dahurian larch and Japanese larch wood. Chauret et al. (2002) reported the radial and tangential shrinkages of Dahurian larch wood grown in Canada as 3.9% and 9.7%, the coefficient of shrinkage anisotropy as 2.5, and volumetric shrinkage as 13.30%. The differences in the shrinkage and coefficient of shrinkage anisotropy of both the species have been earlier reported in agreement with our findings (Bao et al. 2001, Jung and Park 2008). Bao et al. (2001) reported that the radial and tangential shrinkages of Japanese larch wood grown in China were 4.3–4.9% and 6.5–6.8%, respectively, and those of Dahurian larch wood were 3.24–4.51% and 8.01–9.13%, respectively. Further, the coefficient of shrinkage anisotropy was 1.72–2.25 in Japanese larch wood and 1.79–2.78 in Dahurian larch wood. Jung and Park (2008) also reported that the radial and tangential shrinkages of Japanese larch wood were 4.67% and 8.44%, respectively.

Tab. 4: Shrinkage of the sample wood species.

Shrinkage	Species	Sapwood	p-value	Heartwood	p-value	Average	p-value
S_{lo} (%)	Dahurian larch	0.02 ± 0.01	0.008*	0.05 ± 0.04	0.000*	0.04 ± 0.02	0.000*
	Japanese larch	0.30 ± 0.15		0.24 ± 0.07		0.27 ± 0.10	
S_{ro} (%)	Dahurian larch	4.96 ± 0.13	0.123	4.22 ± 0.21	0.162	4.61 ± 0.39	0.015*
	Japanese larch	4.26 ± 0.37		4.03 ± 0.36		4.14 ± 0.27	
S_{to} (%)	Dahurian larch	8.44 ± 0.26	0.045*	8.38 ± 0.24	0.000*	8.38 ± 0.19	0.000*
	Japanese larch	7.09 ± 0.46		6.49 ± 0.42		6.74 ± 0.50	
S_{vo} (%)	Dahurian larch	12.95 ± 0.20	0.043*	12.25 ± 0.33	0.000*	12.65 ± 0.37	0.000*
	Japanese larch	11.00 ± 0.80		10.30 ± 0.66		10.63 ± 0.65	
S_{to}/S_{ro}	Dahurian larch	1.70	0.368	1.99	0.000*	1.84	0.006*
	Japanese larch	1.66		1.62		1.64	

Note: * difference was significance at level 0.05%. S_{lo} - total shrinkage in longitudinal direction; S_{ro} - total shrinkage in radial direction; S_{to} - total shrinkage in tangential direction; S_{to}/S_{ro} - coefficient of shrinkage anisotropy; S_{vo} - Volumetric shrinkage.

Mechanical properties

Compressive properties and shearing strength

The compressive properties and shearing strength of Dahurian larch and Japanese larch wood are shown in Tab. 5. The average values of axial compressive strength and Young's modulus of the two species showed little difference, but there were significant differences in the compression strength parallel to the grain and the Young's modulus between sapwood and heartwood in both species. In heartwood, the compression strength parallel to grain and Young's modulus of Dahurian larch wood were higher than those of Japanese larch wood. However, in sapwood, the compression strength parallel to grain of Dahurian larch wood was lower than that of Japanese larch wood, and the Young's modulus showed insignificant differences between the two species. Hwang et al. (2008) and Hwang and Park (2007) reported the compression

strength parallel to grain of Dahurian larch wood as 60.6 MPa and 66.7 MPa, respectively. Jung and Park (2008) reported the compression strength parallel to grain of Japanese larch wood as 52.1 MPa. Kwon et al. (2004) described the compression strength parallel to grain and Young's modulus of Japanese larch wood as 58.8 MPa and 1960 MPa, respectively, which were lower values than those in this study. The average values in shearing strength of the two species showed little difference, but there was a significant difference in the shearing strength of heartwood of both species, i.e., in heartwood, the shearing strength of Dahurian larch wood was higher than that of Japanese larch wood. Hwang et al. (2008) and Hwang and Park (2007) reported the shearing strength of Dahurian larch wood as 13.3 MPa and 11.5 MPa. Furthermore, Jung and Park (2008) and Kwon et al. (2004) reported the shearing strength of Japanese larch wood as 10.8 MPa and 8.4 MPa, respectively, which are similar to the values obtained in this study. As a result, there were no significant differences in the compressive properties and shearing strengths between the two species. Nevertheless, the compressive properties and shearing strengths were significantly different between sapwood and heartwood in both species at the 5% level, except for the Young's modulus and shearing strength in sapwood (Tab. 5).

Tab. 5: Compressive properties and shearing strength of the sample wood species.

Properties	Species	Sapwood	p-value	Heartwood	p-value	Average	p-value
Compression strength parallel to grain (MPa)	Dahurian larch	60.2 ± 3.3	0.002*	83.2 ± 4.3	0.001*	70.6 ± 12.5	0.910
	Japanese larch	68.2 ± 3.4		72.2 ± 3.7		70.2 ± 3.9	
Young`s modulus in compression (MPa)	Dahurian larch	2,419 ± 579	0.589	3,335 ± 140	0.015*	2,928 ± 607	0.127
	Japanese larch	2,559 ± 316		2,649 ± 514		2,604 ± 415	
Shearing strength (MPa)	Dahurian larch	9.1 ± 1.4	0.668	12.1 ± 2.6	0.043*	10.6 ± 2.5	0.157
	Japanese larch	8.8 ± 1.5		9.8 ± 1.8		9.3 ± 1.7	

Note: * difference was significance at level 0.05%.

Hardness

The hardness results of Dahurian larch and Japanese larch wood are shown in Tab. 6. The average values of hardness in the cross and radial sections between the two species were significantly different.

Tab. 6: Hardness of the sample wood species.

Sections	**Species**	**Sapwood**	**p-value**	**Heartwood**	**p-value**	**Average**	**p-value**
Cross (MPa)	Dahurian larch	32.1 ± 3.0	0.002*	45.3 ± 3.5	0.025*	38.7 ± 7.7	0.030*
	Japanese larch	42.9 ± 2.2		53.0 ± 3.4		48.4 ± 6.5	
Radial (MPa)	Dahurian larch	10.2 ± 1.3	0.000*	17.6 ± 1.9	0.553	13.8 ± 4.4	0.048*
	Japanese larch	16.8 ± 0.9		18.6 ± 2.2		18.2 ± 1.9	
Tangential (MPa)	Dahurian larch	8.2 ± 1.2	0.003*	19.6 ± 1.6	0.262	13.9 ± 6.4	0.211
	Japanese larch	17.5 ± 4.2		17.8 ± 1.6		17.7 ± 2.8	

Note: * difference was significance at level 0.05%.

In both sapwood and heartwood, the hardness of Japanese larch wood was mostly higher than that of Dahurian larch wood. In addition, the hardness of heartwood in the two species was higher than that of sapwood. In the three sections, the hardness of the cross section was the largest, and those of the radial and tangential sections were similar. Tsoumis (1991) explained that the hardness is higher-up to about double in the cross section than radial and tangential sections. Chauret et al. (2002) reported the hardness in the cross-section of Dahurian larch wood grown in Canada as 44.3 MPa. Jung and Park (2008) reported the hardness of Japanese larch wood as 77.4 MPa in the cross-section, 21.6 MPa in the radial section, and 16.7 MPa in the tangential section.

Relationship between physical and mechanical properties

The relationships between the mechanical properties and growth ring width in both wood species are shown in Fig. 1. There was a negative correlation between growth ring width and Young's modulus in compression, however, a positive correlation was found between growth ring width and hardness in the cross section (Fig. 1). It seems that there was no correlation between growth ring width and compression strength parallel to grain and shearing strength (not shown here). In addition, there was little correlation between the compressive properties and shearing strength and latewood percentage (not shown here). On the other hand, there was a significant positive correlation in compression strength parallel to grain and shearing strength to oven-dried density (Fig. 2). Zhang (1995) reported that the mechanical properties of softwood and hardwood species are significantly correlated with growth ring width. Tsoumis (1991) explained that the latewood percentage in softwood tends to decrease with increasing growth ring width, that fast-growing trees produce low strength wood, and that density is the best and simplest index of wood strength, which increases with increasing strength. Kollmann and Côté (1968) reported that the compressive strength and shearing strength in pine and ash woods increased with increasing density. Koizumi et al. (2003) and Jelonek et al. (2009) reported that axial compressive strength of *Larix* species has a high correlation with density. In addition, Riyanto and Gupta (1996) reported that the shearing strength of Douglas-fir has a positive correlation with oven-dried density, showing a tendency similar to that in this study.

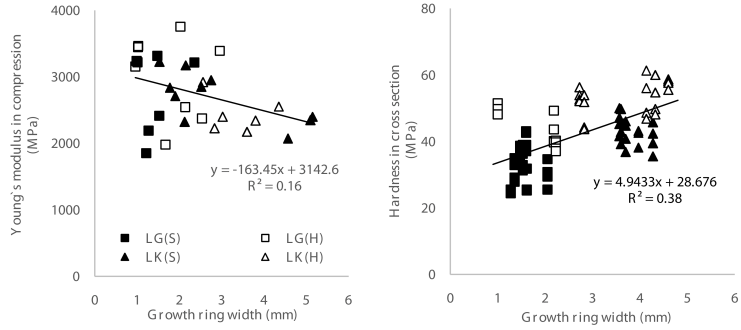

Fig. 1: Relationship between mechanical properties and growth ring width in the sample species: LG - Larix gmelinii; LK - Larix kaempferi; (S) - sapwood; (H) – heartwood.

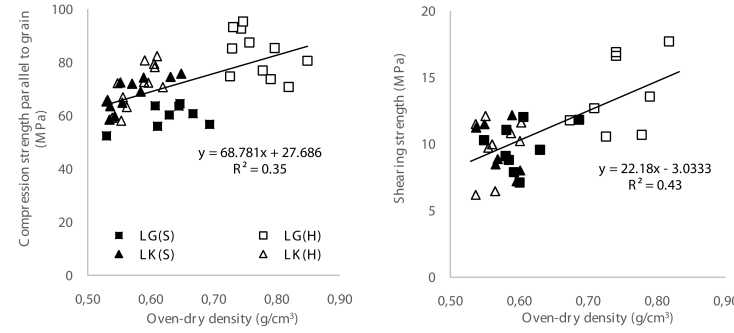

Fig. 2: Relationship between mechanical properties and oven-dried density in the sample species.

The relationships between the physical properties and hardness in the three sections of both wood species are presented in Figs. 3-5. In Dahurian larch wood, there was a positive correlation between the hardness of the three sections and both latewood percentage and oven-dried density. In particular, the hardness in the tangential section showed a relatively high correlation with the latewood percentage and oven-dried density. In Japanese larch wood, however, there was no correlation between hardness and physical properties (not shown in this paper). Tsoumis (1991) explained that the relationship between density and hardness varies with species, but in most cases it is linear. In addition, linear relationships between density and hardness have been reported using Scots pine (Holmberg 2000) and birch species (Heräjärvi 2004). Kollmann and Côté (1968) described that the hardness value in air-dried American wood species showed a proportional relationship with density. Mikkola and Korhonen (2013) reported that the hardness of Scots pine had a positive correlation with latewood percentage, which was similar to the trend observed in this study.

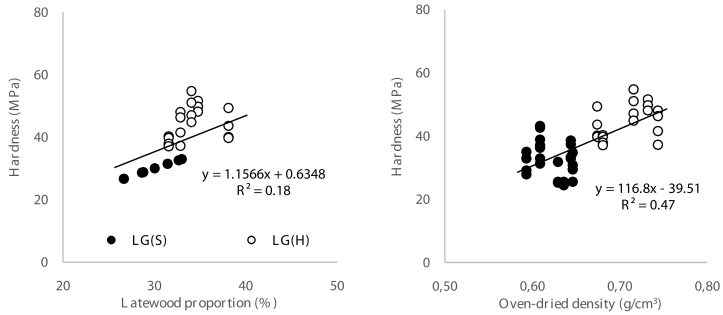

Fig. 3: Relationship between physical properties and hardness in the cross-section of Dahurian larch.

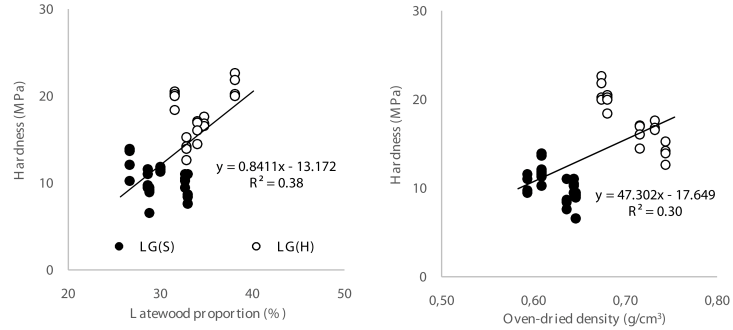

Fig. 4: Relationship between physical properties and hardness in the radial section of Dahurian larch.

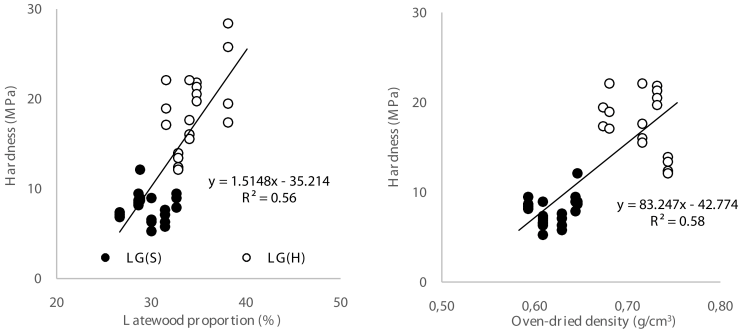

Fig. 5: Relationship between physical properties and hardness in the tangential section of Dahurian larch.

CONCLUSIONS

(1) The heartwood proportion and latewood percentage of Dahurian larch wood were higher than those of Japanese larch wood. The growth ring width in Japanese larch wood was wider than that in Dahurian larch wood. *(2)* The green moisture content and density of Dahurian larch wood were higher than those of Japanese larch wood. In particular, the green density in Japanese larch wood and the air-dried and oven-dried density in Dahurian larch wood showed a large difference between sapwood and heartwood. *(3)* The shrinkage properties of Dahurian larch wood were higher than those of Japanese larch wood. *(4)* The compressive properties and shearing strength between Dahurian larch and Japanese larch wood showed little difference. However, there were significant differences in the heartwood of the two species. *(5)* Japanese larch wood had a higher hardness than Dahurian larch wood. The hardness in the cross and radial sections between the two species was significantly different. Further, the hardness of heartwood in the two species was higher than that of sapwood. *(6)* The compressive properties and shearing strength in both wood species were significantly correlated with oven-dried density compared to growth ring width and latewood percentage. The hardness of Dahurian larch wood showed a significant correlation with latewood percentage and oven-dried density.

ACKNOWLEDGMENT

This study was carried out with the support of the Research Project on Development of Thinning Effect Model and Long-term Monitoring for Major Species in National Forest (Project No. 120180621) funded by Korea Forest Service in 2017, Basic Science Research Program through NRF funded by the Ministry of Education (No. 2018R1A6A1A03025582), and also Basic Science Research Program through the National Research Foundation of Korea (NRF) funded by the Ministry of Education (NRF-2016R1D1A1B01008339).

REFERENCES

1. Bao, F.C., Jiang, Z.H., Jiang, X.M., Lu, X.X., Luo, X.Q., Zhang, S.Y., 2001: Differences in wood properties between juvenile wood and mature wood in 10 species grown in China. Wood Science and Technology 35(4): 363-375.
2. Chauret, G., Zhang, T., Lévesque, Y., 2002: Wood characteristics and end-use potential of two fast-growing exotic larch species (*Larix gmelinii* and *Larix sibirica*) grown in Ontario. Forint Canada Corporation, Report Project: 3563.
3. Choi, Y.S., Oh, S.M., Kim, G.H., 2011: Evaluation of pretreatment moisture content and fixation characteristics of treated wood for pressure treatment of Japanese red pine and Japanese larch skin timber with ACQ, CUAZ and CuHDO. Journal of The Korean Wood Science and Technology 39(6): 481-489.
4. Han, L., Zhao, X., Zhou, H., Luo, X., 2019: Reliability analysis on compression strength property of Chinese larch visually-graded dimension lumber. Wood Research 64(3): 471-482.
5. Han, Y.J., Kim, M.J., Lee, H.M., Kang, J.T., Eom, C.D., 2017: Comparison of cellular anatomical, physical and mechanical properties between Dahurian larch and Japanese larch. Journal of the Korean Wood Science and Technology 45(5): 525-534.

6. Heräjärvi, H., 2004: Variation of basic density and Brinell hardness within mature Finnish *Betula pendula* and *B. pubescens* stems. Wood and Fiber Science 36(2): 216-227.
7. Holmberg, H., 2000: Influence of grain angle on Brinell hardness of Scots pine (*Pinus sylvestris* L.). Holz als Roh-und Werkstoff 58(1-2): 91-95.
8. Hwang, K.H., Park, B.S., 2007: Strength properties of old Korean larch pile. Journal of The Korean Wood Science and Technology 35(6): 23-30.
9. Hwang, K.H., Park, B.S., Park, M.J., 2008: Wood quality and strength properties of old structural members. Journal of the Korean Wood Science and Technology 36(1): 36-44.
10. Ishiguri, F., Iki, T., Otsuka, K., Takahashi, Y., Nezu, I., Tumenjargal, B., Ohshima, J., Yokota, S., 2019: Wood and lumber properties of *Larix gmelinii* var. olgensis planted in Japan. BioResources 14(4): 8072-8081.
11. Ishikura, Y., Matsumoto, K., Ohashi, Y., 2012: Radial variation in partial compression properties perpendicular to the grain of Japanese larch (*Larix kaempferi*). Journal of Wood Science 58(5): 399-407.
12. Jelonek, T., Pazdrowski, W., Tomczak, A., Spława-Neyman, S., 2009: The effect of biological class and age on physical and mechanical properties of European larch (*Larix decidua* Mill.) in Poland. Wood Research 54(1): 1-14.
13. Jung, S.H., Park, B.S., 2008: Wood properties of the useful tree species grown in Korea. Pp 215-218, Korea Forest Research Institute.
14. Kim, S.H., Yang, I., Han, G., 2015: Effect of sawdust moisture content and particle size on the fuel characteristics of wood pellet fabricated with *Quercus mongolica*, *Pinus densiflora*, and *Larix kaempferi* sawdust. Journal of The Korean Wood Science and Technology 43(6): 757-767.
15. Koizumi, A., Takata, K., Yamashita, K., Nakada, R., 2003: Anatomical characteristics and mechanical properties of *Larix sibirica* grown in south-central Siberia. IAWA Journal 24(4): 355-370.
16. Kollmann, F.F.P., Côté, W.A., 1968: Principles of wood science and technology: I Solid Wood. Pp 342-343 and 404, Springer-Verlag, Berlin•Heidelberg. Germany.
17. KS F 2198, 2016: Determination of density and specific gravity of wood.
18. KS F 2199, 2016: Determination of moisture content of wood.
19. KS F 2202, 2016: Determination of average width of annual rings for wood.
20. KS F 2203, 2004: Method of shrinkage test for wood.
21. KS F 2206, 2004: Method of compression test for wood.
22. KS F 2209, 2004: Method of shear test for wood.
23. KS F 2212, 2004: Method of hardness test for wood.
24. Kwon, S.M., Hwang, W.J., Kwon, G.J., Kim, N.H., 2004: Wood quality of *Pinus koraiensis* and *Larix kaempferi*. Journal of Forest and Environmental Science 20: 170-181.
25. LePage, B.A., Basinger, J.F., 1995: The evolutionary history of the genus *Larix* (*Pinaceae*). USDA, Forest Service, Intermountain Research Station, GTR-INT, 319: 19-29.
26. Mikkola, M.T., Korhonen, R.K., 2013: Effect of latewood proportion on mechanical properties of Finnish pine wood modified with compression drying. Wood and Fiber Science 45(4): 335-342.
27. Pazdrowski, W., Jelonek, T., Tomczak, A., Stypuła, I., Spława-Neyman, S., 2007: Proportion of sapwood and heartwood and selected biometric features in larch trees (*Larix decidua* Mill.). Wood Research 52(4): 1-16.
28. Riyanto, D.S., Gupta, R., 1996: Effect of ring angle on shear strength parallel to the grain of wood. Forest Products Journal 46(7/8): 87-92.

29. Shin, H.H., Kim, B.R., 2003: Studies on variability in wood quality in stem of *Larix leptolepis*-green moisture content and shrinkage between heartwood and sapwood. Journal of Korea Forestry Energy 22(1): 1-7.
30. Song, Y.J., Hong, S.I., 2018: Performance evaluation of the bending strength of larch cross-laminated timber. Wood Research 63(1): 105-116.
31. Tsoumis, G.T., 1991: Science and technology of wood: structure, properties, utilization. Pp 171-175, Van Nostrand Reinhold press. New York.
32. Wang, Z., Sun, B.L., Liu, J.L., 2017: Investigation of volatile products released during vacuum heat treatment of larch wood. Wood research 62(5): 773-782.
33. Zhang, S.Y., 1995: Effect of growth rate on wood specific gravity and selected mechanical properties in individual species from distinct wood categories. Wood Science and Technology 29(6): 451-465.
34. Zhou, H., Han, L., Ren, H., Lu, J., 2015: Size effect on strength properties of Chinese larch dimension lumber. BioResources 10(2): 3790-3797.

Jung Kee Choi
Kangwon National University
College Of Forest And Environmental Sciences
24341 Chunchoen
Republic Of Korea

Seong Hyun Kim, Do Hoon Kim, Jae Ik Jo, Jong Ho Kim, Seung Hwan Lee
Nam Hun Kim*
Kangwon National University
College Of Forest And Environmental Sciences
Department Of Forest Biomaterials Engineering
24341 Chunchoen
Republic Of Korea
*Corresponding author: kimnh@kangwon.ac.kr

WOOD RESEARCH
e-ISSN 2729-8906
66(3):2021 427-436 pp.
doi.org/10.37763/wr.1336-4561/66.3.427436

STUDY ON CONCENTRATIONS OF ACIDS AND ALCOHOLS EMITTED BY *PINUS RADIATA* DURING HIGH-TEMPERATURE DRYING

Jiangyi Chu[1], Jinghui Jiang[1], Chusheng Qi[2], Yongdong Zhou[1]
[1]Chinese Academy Of Forestry
China
[2]Beijing Forestry University
China

(Received September 2020)

ABSTRACT

The purpose of this paper is to investigate the influence of kiln temperature, relative humidity and wood moisture content on the content of acid and alcohol released in the drying process of high temperature kiln by studying the radiated pine sawn timber of 40mm thickness. The drying temperature was between 101°C and 115°C, the relative humidity in the drying kiln was reduced from 86.1% to 39.6%, the moisture content of the lumber was reduced from 106.16% to 11.98%, and gas extraction was executed nine times with an extraction speed of 1.0 L•min^{-1} and a sampling time of 30 min. The concentrations of acids and alcohols were analyzed by HPLC. The results showed that the concentrations of formic acid, acetic acid, and methanol emitted in the kiln during drying were 215.6-748.2, 4148.8-16803.2, and 6381.9-15648.9 mg•m^{-3}, respectively, and these concentrations were significantly higher than the relevant standards. The concentrations of the emitted formic acid and acetic acid were proportional to the drying temperature, the concentrations of the emitted formic acid and acetic acid were inversely proportional to the relative humidity in the kiln and the moisture content of the lumber. The concentration of the emitted methanol was independent of the drying temperature, relative humidity in the kiln, and moisture content of the lumber. It is therefore suggested that formic acid, acetic acid, and methanol be separately recovered during the high-temperature drying of *Pinus radiata* lumber.

KEYWORDS: Lumber, *Pinus radiata*, high-temperature drying, emission of acid and methanol, relative humidity, moisture content.

INTRODUCTION

High-temperature drying is defined as an artificial drying process during which the temperature of the drying medium (wet air, superheated steam) is 100-140°C (Zhou and Li 2005). During this process, large amounts of volatile organic compounds (VOCs) such as aldehydes, acid alcohols, and terpenes are emitted (Long and Lu 2008). VOCs refer to compounds that contain carbon and are involved in atmospheric photochemical reactions, excluding CO, CO_2 and other compounds specified in the federal regulations (Milota 2000). VOC volatilization is affected by tree species, wood structure, drying medium temperature and humidity and moisture content (Shmulsky 2000). VOC in wood drying can be divided into two categories. One is terpene and terpene compounds, and the other is non-terpene volatile compounds, mostly organic acids such as formic acid, acetic acid and propionic acid (Lavery 1998). VOC in wood drying comes from some volatile components in wood itself - extractions. Studies showed that the volatiles of pine wood during drying accounted for 25% to 50% of the total extract content in the wood, while the volatiles of spruce accounted for 10% - 50% (Englund and Nussbaum 2000). The aldehydes released by wood mainly come from the oxidative decomposition of unsaturated fatty acids (Makowski et al. 2005, Back and Allan 2000). Softwoods emit the highest concentrations of wood VOCs. The main emission from softwood is terpenes (Risholm-Sundman et al. 1998, Pohleven. et al. 2019). According to China's emission standard of air pollution (GB 16297: 1996) and the design specifications of the environmental protection of wood-based panel engineering, (GB/T 50887: 2013) the monitored concentration limits of formaldehyde and formic acid emissions without organization are 0.25 and 0.20 $mg \cdot m^{-3}$, respectively. Terpene compounds can react with nitrogen oxides under ultraviolet light, resulting in ozone and other photochemical oxides (Risholm-Sundman et al. 1998) that will generate photochemical smog, thus affecting human health and the environment (Long 2012). The concentration limit of terpene suggested by the German committee for health-related evaluation of building products is 1.5 $mg \cdot m^{-3}$ (Däumling et al. 2005). However, although they are also hazards to the environment and human health, little attention has been paid to acids and alcohols in VOCs emitted during drying. Acid, water or methanol, ketone, ether, carbon dioxide and aromatics are the main gaseous products during wood drying (He et al. 2019). Among these polar volatiles, methanol vapor has a strong stimulating effect on the respiratory tract mucosa and can cause dizziness, headache, fatigue, insomnia, and turbidity of consciousness. Formic acid is six times as harmful as methanol, and formaldehyde is 30 times as harmful as methanol. Acetic acid is irritating to the nose, eyes, and respiratory tract. Sometimes the components of volatile organic wood can interact with each other under certain conditions and form secondary pollutants, thus affecting human health and ecological environment (Granstrom 2003). VOCs detection methods often used in wood drying process include: direct measurement method, weighing method and condensation impact method (Tong 2009). At present, the commonly used measurement method is US EPA method 25A, which belongs to the direct measurement method (Wu et al. 1999). In addition, it is an indirect measurement method, which is expressed by the VOC difference of the sample before and after drying. This method is widely used in large commercial drying kilns (Dallons et al. 1993). Standards have been established to determine the limits of the average concentrations and restrictions for short-term exposure to methanol, formic acid, and acetic acid in the air and in the workplace. Examples include the "Occupational exposure limits for hazardous factors in the workplace, part 1: Chemical hazardous factors" (GBZ 2.1-2019, National Standards of China), the Workplace Exposure Standard (New Zealand 2001), Occupational Safety and Health Regulations (OSHA, USA), and the Technical regulations on hazardous substances

(TRGS 900, 2011). However, few studies in this field have been reported. During the drying of *Cunninghamia lanceolat* at a constant temperature of 120°C, the concentrations of formic acid and acetic acid emissions are higher than the limits set by China's standards (Long et al. 2007).

Acetaldehyde is a carcinogen that irritates human skin and mucous membranes (IARC 1999). Similarly, during the drying of *Eucalyptus urophylla* at 90 and 120°C, the concentrations of formic acid, acetic acid, and methanol emissions exceed the limits set by China's standards; the concentration of methanol emissions even exceeds the maximum allowable emission concentration in China's "Comprehensive emission standards for air pollutants. " Drying is executed at constant temperatures, and the concentrations of formic acid, acetic acid, and methanol emitted by sawn wood are dependent on the tree species. The release of high concentration acid is also related to high mass loss, large mechanical property loss, low luminosity and low hue (Bror 2004). Therefore, it is necessary to investigate the concentrations of formic acid, acetic acid, and methanol emitted during the high-temperature drying of sawn timber to provide references for the recovery of drying exhaust at different stages.

In this study, *Pinus Norway* lumber was selected as the research object; it was dried by a high-temperature drying process, and the exhaust was collected at different stages to investigate the effects of the drying stage, temperature, moisture content of the sawn timber, and other factors on the concentrations of formic acid, acetic acid, and methanol in the exhaust.

MATERIAL AND METHODS

Materials and drying experiments

Pinus Norway lumber was obtained from New Zealand and cut into 36 samples of 900 × 120 × 40 mm (L × W × T) in size. The initial moisture content of the samples was 106.16%, and the samples were dried until the moisture content reached 12%, as presented in Fig. 1.

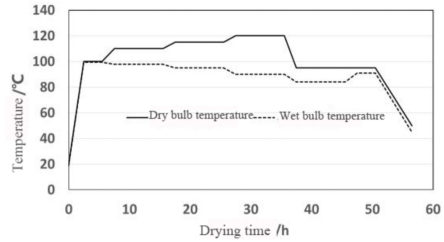

Fig. 1: Schedule of high-temperature drying.

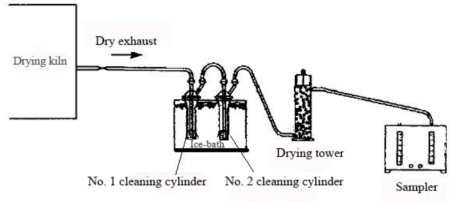

Fig. 2: Diagram of acid and methanol collection during lumber drying.

Collecting acid and methanol

Organic volatiles of acids and alcohols were collected via an ice water bath; 40 mL of distilled water was injected into two 200 mL gas bottles, which were connected and placed in an ice tank to fully dissolve the acids and alcohols. A dryer and sampler were then connected, as illustrated in Fig. 2. The temperature detection hole of the drying kiln was employed as the sampling hole, and a double-channel sample collector was used to collect the VOCs generated at nine sampling times during drying. During sampling, the temperature and humidity in the kiln were stable, the sampling rate was 1.0 L•min^{-1}, and the sampling time was 30 min. The concentrations of formic acid, acetic acid, and methanol in the gas bottles were analyzed by high-performance liquid chromatography (HPLC). The amounts of acids and alcohols emitted were then calculated according to the volume of liquid in the cylinder. The total volume of collected gas was the sum of the volume of gas converted from the liquid increment in the cylinder under the kiln conditions at that time and 30.0 L of gas collected by the sample collector. The concentrations of acids and alcohols in the kiln were calculated according to the amounts of acids and alcohols emitted and the total volume of collected gas. After each sampling cycle, the moisture content testing board was removed from the kiln and the moisture content of the sawn timber was measured. The results are summarized in Tab. 1.

Tab. 1: Dry-bulb and wet-bulb temperatures, relative humidity in the kiln, and moisture content of the lumber.

Sampling time	**1**	**2**	**3**	**4**	**5**	**6**	**7**	**8**	**9**
Dry/wet bulb temperatures (°C)	101/97	103/98	105/97	105/97	105/97	105/97	105/97	113/93	115/90
Relative humidity (%)	86.10	83.10	74.30	74.30	74.30	74.30	74.30	47.90	39.60
Moisture content of lumber (%)	106.16	103.00	99.00	93.00	80.28	71.93	53.72	22.43	11.98

RESULTS AND DISCUSSION

The concentrations of formic acid, acetic acid, and methanol emitted during the high-temperature drying of *Pinus Norway* lumber were 215.6-748.2, 4148.8-16803.2, and 6381.9-15648.9 mg•m^{-3} (Tab. 2), respectively, which are significantly higher than the TWA and STEL values specified in relevant standards (Tab. 3). The results are consistent with concentrations of formic acid, acetic acid, and methanol emitted during the drying of Masson's pine wood at 120°C. The gas emitted during the high-temperature drying of *Pinus Norway* lumber should be recycled and treated.

Tab. 2: Concentrations of formic acid, acetic acid, and methanol emitted during high-temperature drying.

Sampling time	**1**	**2**	**3**	**4**	**5**	**6**	**7**	**8**	**9**
Formic acid (mg·m^{-3})	285.2	500.0	215.6	251.3	473.7	661.4	547.5	752.3	748.2
Acetic acid (mg·m^{-3})	4481.6	5191.4	4148.8	4928.0	9381.5	11803.6	11636.2	12777.7	16803.2
Methanol (mg·m^{-3})	7462.3	13059.7	15648.9	7719.5	6381.9	10897.5	12166.3	6505.6	10119.9

Tab. 3: Concentration limits of formic acid, acetic acid, and methanol in the workplace.

Standard	Formic acid ($mg \cdot m^{-3}$)		Acetic acid ($mg \cdot m^{-3}$)		Methanol ($mg \cdot m^{-3}$)	
	TWA	STEL	TWA	STEL	TWA	STEL
GB Z-2002	10	20	10	20	25	50
New Zealand standard	9.4	19	25	37	262	328
OSHA regulations			-	-	260	-
TRGS 900			25	-	-	-

Note: TWA (Time-weighted average), STEL (Short term exposure limit).

Influences of drying temperature on the concentrations of acid and alcohol emissions

The temperature of high-temperature drying ranged from 101 to 115°C. The average concentrations of formic acid, acetic acid, and methanol of the third to the seventh samples dried at 105°C were calculated. As shown in Fig. 3, the concentrations of formic acid and acetic acid increased linearly with the drying temperature, and the determination coefficients (R2) were 0.9046 and 0.9621, respectively. The drying temperature had no significant effect on the concentration of methanol emitted within the drying temperature range observed in this study. The concentration of emitted methanol ranged from 6381.9 to 15648.9 $mg \cdot m^{-3}$ with an average of 9995.7 mg^{-3}.

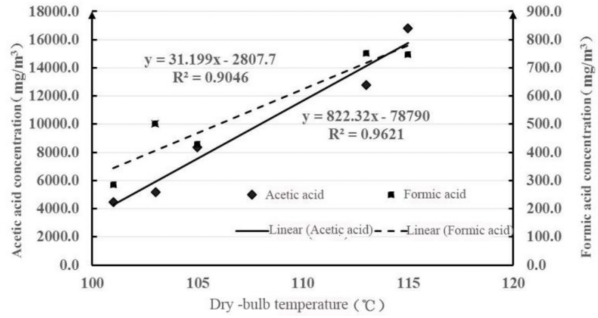

Fig . 3: Temperature vs. concentrations of formic acid and acetic acid.

When the drying temperature was less than 120°C, the hemicelluloses and cellulose in wood had not yet reached the degradation stage, and lignin degradation was also rare. In other words, the degradation of the three components of wood produces negligible amounts of acids and alcohols. Hence, acids and alcohols may primarily be produced by the thermal decomposition of wood extracts, which is similar to the production mechanism of aldehyde substances (Schafer and Roffael 2000). At a constant drying temperature, the concentrations of acids and alcohols emitted from Norway pine lumber had been found to be significantly higher than those from plantation Chinese fir lumber. The VOC emission from high-temperature drying of Chinese fir was much higher than that from conventional drying. Because the drying time is long despite the low VOC release concentration at low temperature, there was little difference in the total VOC release between high-temperature and conventional drying (Ingram et al. 2000). The release rate of methanol, acetic acid and formic acid was significantly higher than that of aldehydes and terpenes (Long and Lu 2008).

This can be attributed to the fact that the extract contents of benzyl alcohol in the Norway pine heartwood and sapwood were 30.01% and 7.31%, respectively, while that of the plantation Chinese fir was 2.90% (Bao and Jiang 1998); additionally, the content of Norway pine lumber heartwood was high. Indeed, the extract content of radiate pine may be 10 times higher than that of Chinese fir.

Influence of relative humidity on the concentrations of acid and alcohol emissions

During the high-temperature drying of the timber samples, the relative humidity in the kiln ranged from 86.10% to 39.60%. Similarly, the average concentrations of formic acid, acetic acid, and methanol of the third to seventh drying samples dried at 105°C were determined. As presented in Fig. 4, the concentrations of formic acid and acetic acid decreased linearly with the relative humidity, and the determination coefficients were 0.8632 and 0.9738, respectively.

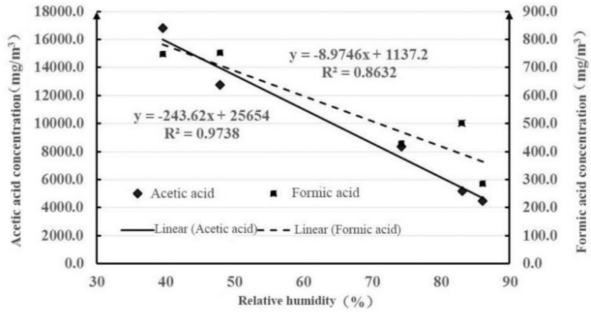

Fig. 4: Relative humidity vs. concentrations of formic acid and acetic acid.

The relative humidity had no significant effect on the concentration of methanol emitted. However, it was found that the relative humidity was inversely proportional to the drying temperature. Additionally, the concentrations of formic acid and acetic acid were inversely proportional to the relative humidity in the kiln, which may be attributed to the negative correlation between the relative humidity and temperature. It is also possible that, at a specific drying temperature, the concentrations of formic acid and acetic acid emitted remained unchanged, and the low relative humidity led to a low water vapor content, thus resulting in high concentrations of formic acid and acetic acid. Future research may focus on the effects of constant drying temperature and relative humidity on the concentrations of acid and alcohol emitted.

Influence of moisture content of sawn timber on the concentrations of acid and alcohol emissions

Some studies have shown that the volatilization amount of VOCs increases with the decrease of the final moisture content of wood, regardless of the drying temperature (Shmulsky and Ingram 2000). During the drying process, the moisture content of the lumber decreased from 106.16% to 11.98%. As the moisture content of the lumber decreased, the concentrations of the formic acid and acetic acid emitted gradually increased, as shown in Fig. 5. The determination coefficients were 0.8521 and 0.9591, respectively. At a drying temperature of 105°C, as the drying proceeded, the moisture content of the lumber decreased from 99.00% to 53.72%, while the concentrations of emitted formic acid and acetic acid increased linearly, as shown in Fig. 6.

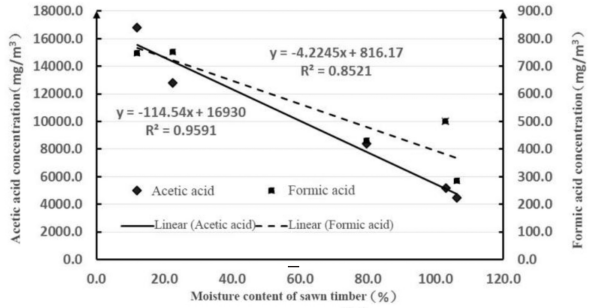

Fig. 5: Concentrations of formic acid and acetic acid vs. moisture content of lumber.

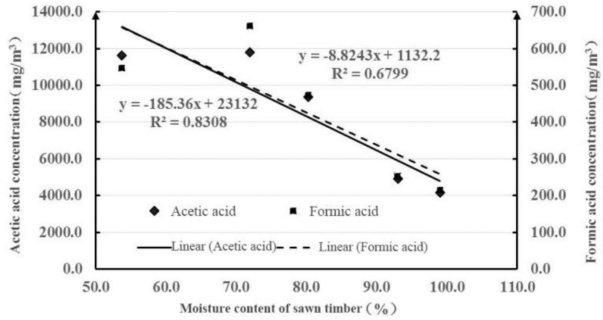

Fig. 6: Concentrations of formic acid and acetic acid vs. moisture content of lumber during drying at 105°C.

The determination coefficients were 0.6799 and 0.8308, respectively. In other words, the concentrations of formic acid and acetic acid emitted were inversely proportional to the moisture content of the lumber. However, the moisture content had no significant effect on the concentration of methanol emitted.

The dry-bulb temperature was also 105°C. From the third to the seventh sampling, the moisture content of the lumber decreased as the drying time increased, resulting in increasing concentrations of formic acid and acetic acid. In contrast, the concentration of methanol emitted did not vary significantly with the moisture content of the lumber. Therefore, the influence of the moisture content of the lumber on the concentrations of acids and alcohols emitted was further confirmed.

CONCLUSIONS

The results of this study indicate that the concentrations of formic acid and acetic acid emissions are proportional to the drying temperature, while they are inversely proportional to the relative humidity and the moisture content of the lumber. The determination coefficients of all cases were found to be greater than 0.6799. In addition, the concentration of methanol

emissions was found to be independent of the drying temperature, the relative humidity, and the moisture content of the lumber. The concentrations of formic acid, acetic acid, and methanol emissions exceeded the threshold values set by the China's national emission standards.

Hence, the recovery of exhausts during the high-temperature drying of wood is strongly recommended. Future studies should explore the effects of relative humidity on the concentrations of acid and alcohol emitted at a constant drying temperature. In addition, the emission mechanisms of acids and alcohols during high-temperature drying should be investigated.

ACKNOWLEDGMENTS

The author extends gratitude to Dr. Fan Zhou, Dr. Fu Zongying and Dr. Gao Xin for their support of this study. Parts of this work were financially supported by National Natural Science Foundation of China (Grant No. 31870536).

REFERENCES

1. Back, E.L., Allan, L.H., 2000: Pitch control, wood resin and deresination. Pp 77-101, Tappi Press, Atlanta , GA.
2. Bao, F.C., Jiang, Z.H., 1998: Wood properties of main tree species from plantation in China, Beijing: China forestry publishing house, 98 pp.
3. Sundqvist, B., 2004: Colour changes and acid formation in wood during heating. Luleå University of Technology 10: 1402-1544.
4. Dallons, V.C., Lamb, L.M., Peterson, M.R. , 1993: An alternate method for estimating VOC emissions from lumber dry kilns. Aiche Symposium. Series 90(302) : 19-32.
5. Däumling, C., Brenske, K.R., Wilke, O., Horn, W., Jann, O., 2005: Health-related evaluation procedure of VOC and SVOC emissions from building products. A contribution to the European construction products directive. Gefahrstoffe Reinhaltung Der Luft 65(3): 90-92.
6. Englund, F., Nussbaum, R.M., 2000: Monoterpenes in Scots pine and Norway spruce and their emission during kiln drying. Holzforschung 54(5): 449-456.
7. Granström, K., 2003: Emissions of monoterpenes and VOCs during drying of sawdust in a spouted bed. Forest Products Journal 53(10): 48-55.
8. He, Z., Wang, Z., Qu, L., Qian, J., Yi, S., 2019: Gaseous decomposition products from wood degradation via thermo gravimetric and Fourier transform infrared analysis during thermal modification of beech and pine woods. Bioresources14(3): 6883-6894.
9. IARC, 1999: Acetaldehyde. IARC Summary and evaluation 71: 319.
10. Ingram, L., Shmulsky, R., Ashlie, T.D., Taylor, F.W., Templeton, M.C., 2000: The measurement of volatile organic emissions from drying southern pine lumber in a laboratory-scale kiln. Forest Products Journal 50(4): 91-94.
11. Pohleven. J., Burnard, M.D., Burnard, Kutnar, A., 2019: Volatile organic compounds emitted from untreated and thermally modified wood. A review. Wood and Fiber Science 51(3): 232-254.
12. Lavery, M.R., 1998: Hydrocarbon emissions from lumber dry kilns. M.S. thesis. Oregon St ate University, Corval-lis, 133 pp.

13. Long, L., Liu, X.X., Zhang, Z.H. 2007: Study on VOC emission during *Eucalypt usurophylla* drying. China Forest Products Industry 34 (4): 8-13.
14. Long, L., Lu, X.X., 2008: VOC emission from Chinese fir (*Cunninghamia lanceolata*) drying. Scientia Silvae Sinicae 44: 107-116.
15. Long, L., 2012: Evaluate on VOC emission wood and wood products. China science publishing, Beijing, 157 pp.
16. Long, L., Lu, X.X., 2008: Release of organic volatiles during Chinese fir drying. Forestry science 01: 107-116.
17. Makowski, M., Ohlmeyer, M., Meier, D., 2005: Long-term development of VOC emissions from OSB after hot-pressing. Holzforschung 48(5): 339-523.
18. Milota, M.R., 2000: Emissions from wood drying. Forest Products Journal 50(6): 10-20.
19. Risholm-Sundman,M., Lundgren,M., Vestin,E., Herder, P., 1998: Emissions of acetic acid and other volatile organic compounds from different species of solid wood. Holz Als Roh-und Werkstolt 56: 125-129.
20. Schafer, M., Roffael, E., 2000: On the formaldehyde release of wood. Holz als Roh-und Werkstoff 58 (4): 259-264.
21. Shmulsky, R., Ingram, L.L., 2000: Empirical prediction of VOC emissions from drying southern yellow pine lumber. Forest Products Journal 50(6): 61-63.
22. Shmulsky, R., 2000: Influence of lumber dimension on voc emissions from kiln-drying loblolly pine lumber. Forest Products Journal 50(3): 63-66.
23. Tong, L.Z., 2009: Research status and development trend of VOCs in wood drying process. Wood Processing Machinery 02: 38-41.
24. Wu, J., Milota, M. R. , 1999: Effect of temperature and humidity on total hydrocarbon emission from douglas-fir lumber. Forest Products Journal 49(6): 52-60.
25. Zhou, Y.D., Li, X.L., 2005: Comparison of high- temperature drying and conventional drying of Chinese fir lumber. Journal of Beijing Forestry University 27(Supp.): 18-21.

Jiangyi Chu, Jinghui Jiang*, Yongdong Zhou
Chinese Academy Of Forestry
Research Institute Of Wood Industry
Wan Shou Shan, Haidian
Beijing
China
*Corresponding author: jiangjh@caf.ac.cn

Chusheng Qi
Beijing Forestry University
Materials Science And Technology
Shuangqing Road, Haidian
Beijing
China

WOOD RESEARCH
e-ISSN 2729-8906
66(3):2021 437-448 pp.
doi.org/10.37763/wr.1336-4561/66.3.437448

EFFECTS OF HOT PRESSING PARAMETERS ON THE PROPERTIES OF HARDBOARDS PRODUCED FROM MIXED HARDWOOD TREE SPECIES

Petar Antov, Viktor Savov, Nikolay Neykov
University Of Forestry
Bulgaria

Ľuboš Krišťák
Technical University In Zvolen
slovakia

(Received September 2020)

ABSTRACT

In this work, wet-process fibreboards (hardboards) were produced in the laboratory using industrial wood fibres of the species European beech (*Fagus sylvatica* L.) and Turkey oak (*Quercus cerris* L.) at the total volume of 40%, and white poplar (*Populus alba* L.) at 60% volume. The effects of hot pressing pressure (varied from 3.3 MPa to 5.3 MPa) and pressing time (from 255 s to 355 s) on the physical and mechanical properties of hardboards were investigated and optimal values of the parameters for fulfilling the European standard requirements were determined. It was concluded that hardboards with acceptable physical and mechanical properties may be produced from 60% poplar wood waste and residues, combined with 40% hardwood raw materials (beech and oak) by regulating the hot pressing regime only, i.e. pressure and pressing time. The following minimum parameters for producing hardboards from mixed hardwood tree species were determined: a pressure of 4.6 MPa and a pressing time of 280 s.

KEYWORDS: Wood composites, fibreboards, hardboards, mixed hardwood raw material, hot pressing.

INTRODUCTION

The growing need for more sustainable materials and final products and the stricter legislative requirements related to the hazardous formaldehyde emissions from wood-based panels have boosted the scientific and industrial interest towards the production of eco-friendly wood-based composites (Pizzi 2006, Papadopoulou 2009, Ferdosian et al. 2017, Nordström et al. 2017, Mantanis et al. 2018, Bekhta and Sedliačik 2019, Hosseinpourpia et al. 2019, Antov et al. 2020a, Santoso et al. 2020, Papadopoulos 2020a, Taghiyari et al. 2020, Tudor et al. 2020a, Antov et al. 2021a, Antov et al. 2021b, Antov et al. 2021c) and optimal utilization of the available lignocellulosic materials (Ihnát et al. 2015, Réh et al. 2019, Bekhta et al. 2019, Kumar and Pizzi 2019, Lubke et al. 2020, Papadopoulos 2020b, Tudor et al. 2020b, Rammou et al. 2021). Fibreboards, produced by the wet process, are an eco-friendly flat-pressed wood composite panels, consisting of lignocellulosic fibres traditionally bonded without any adhesive by hot-pressing (González-García et al. 2014, Widsten and Kandelbauer 2014, Pizzi 2017). Fibre bonding is achieved by the high density (900-1100 $kg.m^{-3}$) and the high-temperature induced flow of the lignin component of the fibres (Pizzi et al. 2020). These engineered wood panels are characterized by homogeneous thickness, density, uniform appearance and no grain (Widsten et al. 2009). Additives such as paraffin wax can be used to improve certain properties such as abrasion and water resistance (González-García et al. 2011).

Another important advantage of these wood-based panels is the increased utilization of small-sized low quality wood of hardwood tree species, which is otherwise used mainly for energy purposes (Trichkov and Antov 2005, Shulga et al. 2016, Schneider et al. 2019). Despite the high quantitative output, wet process fibreboards have certain disadvantages, namely the presence of small percentage of phenolic binder which hinders the recycling and disposal of hardboards (Smith 2004, González-García et al. 2014, Lubis et al. 2018a, Lubis et al. 2020), and the low added value of the final product (Neykov et al. 2018).

A good solution to overcome this problem are factories producing more than one type of wood-based panels (Neykov et al. 2014), such as the company Welde Bulgaria AD (Troyan, Bulgaria), producing hardboards and plywood. The plywood production technology is characterised by the lowest quantitative output of all technologies for production of wood-based composites. The main raw material used in this company is poplar (*Populus* spp.) and the production process is characterized by considerable amounts of wood waste and leftover materials, which can be further utilized in the production of hardboards. Fibre composites allow the utilization of waste and residues from other processing industries, such as pulp and paper industry (Russ et al. 2013, Tikhonova et al. 2014, Bajpai 2015, Lubis et al. 2018b, Ihnát et al. 2018, Ihnát et al. 2020, Antov et al. 2020a, Antov et al. 2021a). Optimising the utilization of waste wood from the production of plywood will have a significant environmental impact and will enhance the competitiveness of the respective companies (Neykov et al. 2020a, Neykov et al. 2020b). The increased utilization of poplar requires changes in the technological regimes used for the production of hardboards. The hot pressing regime applied is of great importance for engineering the hardboard properties (Carvalho and Costa 2003, Gupta 2007, Gul et al. 2017). This also applies to the production of wet process fibreboards, where the adhesive bonds perform mainly a stabilizing function.

The aim of the research work was to investigate the effect of hot pressing parameters, i.e. pressure and pressing time on the physical and mechanical properties of hardboards produced from mixed hardwood raw materials.

MATERIAL AND METHODS

Hardboard were produced in the laboratory using industrial wood-fibre mat, supplied by Welde Bulgaria AD (Troyan, Bulgaria), and composed of the following tree species: European beech (*Fagus sylvatica* L.) and Turkey oak (*Quercus cerris* L.) at the total volume of 40%, and white poplar (*Populus alba* L.) at 60% volume. The phenol-formaldehyde resin content was 0.5%, based on the dry weight of the fibres. The pulp freeness was 16.98 Ds (Defibrator seconds), as the result of the significant quantity of poplar wood. The wood fibre mass was obtained in factory conditions according to the Asplund method by using the L46 Defibrator (Sweden) equipment. The dry content of the mat was 25%. The hot pressing pressure was varied from 3.3 to 5.3 MPa, and the pressing time from 255 to 375 s, respectively. These values were selected in accordance with the factory regimes used for production of hardboards (a pressure of 4.3 MPa and a pressing time of 315 s). The press temperature used was 200°C. Hot pressing was performed in a laboratory press (Defibrator, Sweden) with dimensions of the platens 480 x 480 mm. The physical and mechanical properties of the hardboards were determined according to European standards EN 310, EN 317, EN 319, EN 322 and EN 323 (European Committee for Standardization). The following physical properties of the hardboards were investigated: density, water absorption and thickness swelling. Thickness swelling and water absorption tests were carried out for 24 h. The mechanical properties of the hardboards produced, i.e. modulus of elasticity (MOE), bending strength (MOR) and internal bond strength, were determined using a universal-material testing machine Zwick/Roell Z010 (Zwick/Roell GmbH, Ulm, Germany). Variational and statistical analyses of the results were carried out by using the specialised software QstatLab version 6.0.

RESULTS AND DISCUSSION

A summary of the physical and mechanical properties of the laboratory-produced hardboard panels at different hot pressing parameters (pressure and pressing time) is shown in Tab. 1 and Tab. 2, respectively. The thickness of the hardboards varied from 2.2 to 2.8 mm.

Tab. 1: Physical properties of the laboratory-produced hardboards.

Panel No.	Pressure P (MPa)	Pressing time τ (s)	Panel thickness (mm)	Density ρ (kg.m^{-3})	Water absorption (24h), A (%)	Thickness swelling (24h), Gt (%)
1.	3.3	255	2.78±0.015	871 ± 14	70.95 ± 1.84	34.14 ± 0.99
2.	3.3	315	2.76±0.008	872 ± 15	59.28 ± 2.70	30.50 ± 1.46
3.	3.3	375	2.72±0.009	877 ± 10	57.34 ± 2.12	28.96 ± 1.42
4.	4.3	255	2.45±0.010	885 ± 12	66.96 ± 2.47	32.67 ± 1.33
5.	4.3	315	2.44±0.005	890 ± 9	58.23 ± 2.07	29.79 ± 0.93
6.	4.3	375	2.40±0.001	896 ± 8	56.77 ± 2.21	28.45 ± 1.37
7.	5.3	255	2.28±0.004	901 ± 5	63.45 ± 3.06	30.05 ± 1.07
8.	5.3	315	2.27±0.006	906 ± 6	51.08 ± 2.20	28.59 ± 1.06
9.	5.3	375	2,23±0.003	914 ± 7	48.85 ± 1.81	26.43 ± 0.78

Tab. 2: Mechanical properties of the laboratory-produced hardboards.

Panel No.	Pressure *P*, (MPa)	Pressing time τ, (s)	Modulus of elasticity (MOE), *Em*, (N.mm^{-2})	Bending strength (MOR), *fm*, (N.mm^{-2})	Internal bond strength *ft*, (N.mm^{-2})
1.	3.3	255	2239 ± 71	30.44 ± 0.89	0.48 ± 0.02
2.	3.3	315	2249 ± 63	33.01 ± 0.62	0.55 ± 0.02
3.	3.3	375	2300 ± 39	33.77 ± 0.52	0.58 ± 0.02
4.	4.3	255	2344 ± 35	33.30 ± 0.53	0.52 ± 0.03
5.	4.3	315	2558 ± 77	36.04 ± 0.68	0.57 ± 0.03
6.	4.3	375	2541 ± 47	36.53 ± 0.86	0.59 ± 0.01
7.	5.3	255	2586 ± 46	36.63 ± 0.72	0.53 ± 0.01
8.	5.3	315	2581 ± 19	39.55 ± 0.36	0.67 ± 0.03
9.	5.3	375	2599 ± 64	36.76 ± 1.02	0.66 ± 0.03

A graphical representation of the effects of hot pressing pressure and pressing time on the density of the fibreboards is presented in Fig. 1.

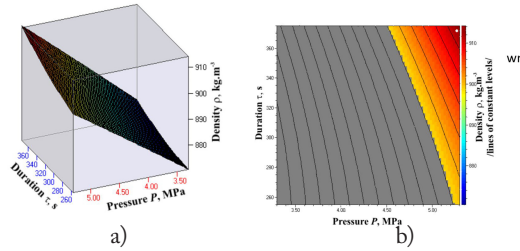

Fig. 1: Variation of the density of hardboard panels depending upon the pressing time (duration) and pressure applied: a) explicit form, and b) optimal value.

The density of the laboratory-produced fibreboards varied from 871 to 914 kg.m-3, hence the variation of the density was 7%. Both studied factors had a positive effect on the density of the panels, i.e. increasing the pressure from 3.3 to 5.3 MPa and pressing time fr om 255 to 374 s, respectively, resulted in higher density values of the fabricated fibreboards. Statistically, the dependence of the density upon both factors is very close to linear. Pressure had almost three times higher effect on the density compared to the pressing time applied. As seen in Fig. 1b, the optimal (maximum) density of the panels of 914 kg.m-3 was obtained at the upper limit factor values. A limitation, i.e. density greater than 900 kg.m-3, required for producing hardboards, was also set (EN 316). As seen in Fig. 1, hardboards can be fabricated from wood-fibre mass, composed of 60% poplar wood and 40% hardwood species (European beech and Turkey oak) at hot pressing pressure of 5.3 MPa and pressing time of 255 s. Hence, the highest output (minimum pressing time) can be achieved at a pressure of at least 5.3 MPa. The minimum pressure for producing hardboards was 4.6 MPa and the pressing time – at least 375 s. A graphical representation of the effects of pressure and pressing time on the modulus of elasticity (MOE) of the fabricated panels is presented in Fig. 2.

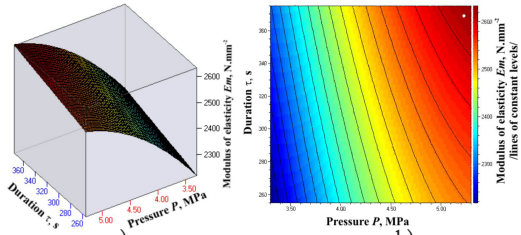

Fig. 2: Variation of the modulus of elasticity (MOE) of hardboard panels depending upon the pressing time (duration) and pressure applied: a) explicit form and b) optimal value.

The MOE of the produced fibreboards improved with the increase of pressure and pressing time. Within the limitations of the experiment the overall improvement of this indicator was 16%. The effect of pressure was of the second degree, with greater improvement observed when the pressure was increased to 4.5 MPa. The dependence of the MOE of the laboratory-produced panels on the pressing time was similar to linear. The pressure had greater effect on the MOE values compared to the pressing time. None of the panels met the standard requirements for fibreboards – use in load-bearing applications (≥ 2700 N.mm^{-2}) (EN 622-2). The maximum MOE value was obtained for fibreboards produced at a pressure of 5.3 MPa and pressing time of 370 s, i.e. close to the upper limit factor values. A graphical representation of the effects of pressure and pressing time on the bending strength (MOR) of the fibreboards is shown in Fig. 3.

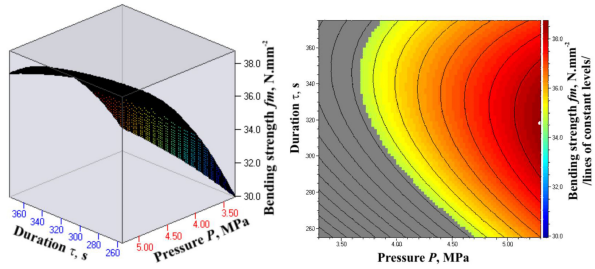

Fig. 3: Variation of the bending strength (MOR) of hardboard panels depending upon the pressing time (duration) and pressure applied: a) explicit form, and b) optimal value.

The increase of pressure applied resulted in increased bending strength (MOR) values of the laboratory-produced panels. Regarding the effect of pressing time on MOR values, it was determined that increasing the pressing time up to 320 s resulted in improved bending strength values, while further increase of pressing time resulted in lower values of the studied indicator. This might be attributed to the initial destructive processes of wood components, occurring due to the extended pressing time. The variation of the MOR values of the produced panels within the standard requirement (≥ 35 N·mm^{-2}) for fibreboards with general application is presented in Fig. 3b. The maximum MOR strength, recorded in this work, i.e. 38.72 N·mm^{-2}, was realised at a pressure of 5.3 MPa and a pressing time of 318 s. A graphical representation of the effects of pressure and pressing time applied on the internal bond strength of fibreboards produced is presented analytically in Fig. 4.

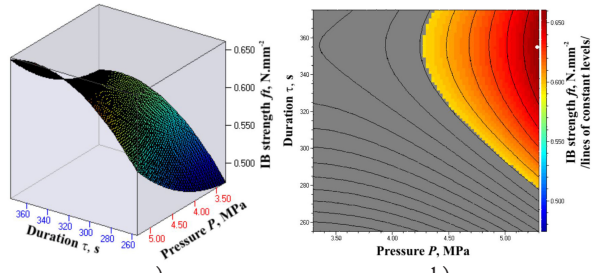

Fig. 4: Variation of the internal bond strength of hardboard panels depending upon the pressing time (duration) and pressure applied: a) explicit form, and b) optimal value.

The increased pressure and extended pressing time resulted in improved IB strength of the laboratory-produced fibreboards. The effect of pressure increased significantly above the value of 4.5 MPa. The pressing time had a stronger effect when extended to 340 s, followed by constant values of the studied indicator. The variation of the IB strength values of the produced panels within the standard requirement (≥ 0.5 N·mm^{-2}) for fibreboards with general application in dry conditions (EN 622-2) is presented in Fig. 4b. The standard requirement can be achieved at pressure values of at least 4.3 MPa and pressing time of at least 280 s. According to the statistical analysis, the optimal value of 0.68 N·mm^{-2} for IB strength was projected at a pressure of 5.3 MPa and 355 s pressing time. A graphical representation of the effects of pressure and pressing time on the thickness swelling of fibreboards is presented in Fig. 5.

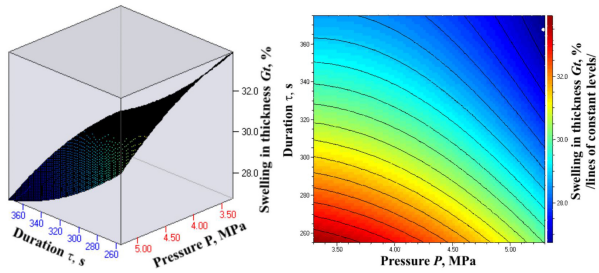

a) b)

Fig. 5: Variation of the thickness swelling of hardboard panels depending upon the pressing time (duration) and pressure applied: a) explicit form, and b) optimal value.

Thickness swelling (TS) and water absorption (WA) are critical physical properties, related to the dimensional stability of wood-based composites (Youngquist 1999, Frihart 2005). The variation of TS values of the fabricated panels was 1.29 times. All laboratory-fabricated panels met the standard requirement for hardboards – general application in dry conditions (TS ≤ 35%) (EN 622-3). The standard requirement for general application in humid environment (TS ≤ 25%) was not achieved. The increased pressure values resulted in improved (lower) TS values, as the most significant improvement was determined at pressure values above 4.25 MPa. Extending the pressing time up to 340 s resulted in relatively gradual improvement of the TS values. The optimal TS value (26.33%) of the panels, produced in this work, can be achieved at a pressure of 5.3 MPa and a pressing time of 366 s. A graphical representation of the effects of pressure and pressing time on the WA of the laboratory-made panels is presented in Fig. 6.

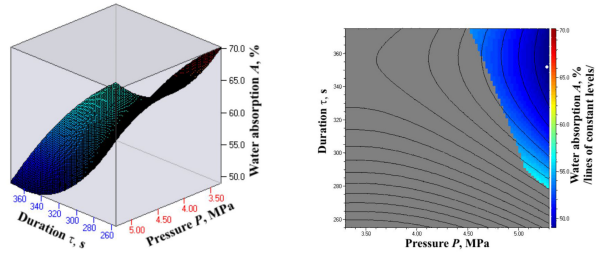

a) b)

Fig. 6: Variation of the water absorption of hardboard panels depending upon the pressing time (duration) and pressure applied: a) explicit form, and b) optimal value.

Improved (lower) WA of the panels was clearly evidenced after increasing the pressure and pressing time. The WA of the laboratory-produced fibreboards varied from 48.85 to 70.95%, a variation of 1.45 times was recorded. Pressure, greater than 4.25 MPa, had a stronger effect on the WA values. Stronger impact of the pressing time on the WA values was determined at values exceeding 310 s. However, further increase of the pressing time above 340 s did not result in lower WA values. WA is not a standardized technical property, hence, the limits related to the other physical and mechanical properties of the panels, were set in Fig. 6b. As seen in Fig. 6, hardboards, meeting the standard requirements, can be produced at a minimum pressure of 4.6 MPa and a pressing time of at least 375 s. The minimum pressing time for producing hardboards was 280 s at a minimum pressure of 5.3 MPa. According to the statistical analysis, the optimal WA value of 48.12% was projected at a pressure of 5.3 MPa and a pressing time of 353 s.

CONCLUSIONS

Hardboards with acceptable physical and mechanical properties according to the EN standards may be produced from 60% poplar wood waste and residues, combined with 40% hardwood raw materials (beech and oak) by regulating the hot pressing regime only, i.e. pressure and pressing time. This facilitates the utilization of residual wood, which is a rather cyclical and irregular process, i.e. the addition of poplar in the composition of hardboards can be successfully implemented when sufficient amount of residual wood and waste is accumulated. The pressure applied had a significantly greater effect on all physical and mechanical properties of the laboratory-produced panels compared to the pressing time. The study revealed that at press temperature of 200°C the pressing time should not exceed 320 s. Otherwise, a deterioration of the strength properties of the panels was determined. The minimum regime parameters for producing hardboards from mixed hardwood tree species were: a pressure of 4.6 MPa and a pressing time of 280 s.

ACKNOWLEDGMENTS

This research was supported by the projects No. НИС-Б-1002/03.2019 '*Exploitation Properties and Possibilities for Utilization of Eco-friendly Bio-composite Materials*', No. НИС-Б-1145/04.2021 '*Development, Properties and Application of Eco-Friendly Wood-Based Composites*' implemented at the University of Forestry, Sofia, Bulgaria, and projects by the Slovak Research and Development Agency under contracts No. APVV-18-0378, APVV-19-0269 and VEGA1/0717/19.

REFERENCES

1. Antov, P., Krišťák, Ľ., Réh, R., Savov, V., Papadopoulos, A.N., 2021a: Eco-friendly fiberboard panels from recycled fibres bonded with calcium lignosulfonate. Polymers 13(4): 639.
2. Antov, P., Mantanis, G.I., Savov, V., 2020a: Development of wood composites from recycled fibres bonded with magnesium lignosulfonate. Forests 11(6): 613.
3. Antov, P., Savov, V., Krišťák, Ľ., Réh, R., Mantanis, G.I., 2021b: Eco-friendly, high-density fiberboards bonded with urea-formaldehyde and ammonium lignosulfonate. Polymers 13(2): 220.

4. Antov, P., Savov, V., Mantanis, G. I., Neykov, N., 2021c: Medium-density fibreboards bonded with phenol-formaldehyde resin and calcium lignosulfonate as an eco-friendly additive. Wood Material Science and Engineering 16(1): 42-48.
5. Antov, P., Savov, V., Neykov, N., 2020b: Sustainable bio-based adhesives for eco-friendly wood composites – a review. Wood Research 65(1): 51-62.
6. Bajpai, P., 2015: Generation of waste in pulp and paper mills. In: Management of Pulp and Paper Mill Waste. Pp 9-17, Springer, Berlin/Heidelberg, Germany.
7. Bekhta, P., Sedliačik, J., 2019: Environmentally-friendly high-density polyethylene-bonded plywood panels. Polymers 11(7): 1166.
8. Bekhta, P., Sedliačik, J., Kačík, F., Noshchenko, G., Kleinová, A., 2019: Lignocellulosic waste fibers and their application as a component of urea-formaldehyde adhesive composition in the manufacture of plywood. European Journal of Wood and Wood Products 77: 495–508.
9. Carvalho, L., Costa, C., 2003: A global model for the hot-pressing of MDF. Wood Science and Technology 37: 241–258.
10. EN 317, 1998: Particleboards and fibreboards. Determination of swelling in thickness after immersion in water.
11. EN 310, 1999: Wood-based panels. Determination of modulus of elasticity in bending and of bending strength.
12. EN 323, 2001: Wood-based panels. Determination of density.
13. EN 622-2, 2004: Fibreboards. Specifications. Part 2: Requirements for hardboards.
14. EN 316, 2009: Wood fibreboards. Definition, classification and symbols.
15. Ferdosian, F., Pan, Z., Gao, G., Zhao, B., 2017: Bio-based adhesives and evaluation for wood composites application. Polymers 9(2): 70.
16. Frihart, C.R., 2005: Wood adhesion and adhesives. In: Handbook of wood chemistry and wood composites (ed. Rowell, RM). Pp 214-278, CRC Press, Boca Raton, FL, USA.
17. González-García, S., Feijoo, G., Heathcote, C., Kandelbauer, A., Moreira, M.T., 2011: Environmental assessment of green hardboard production coupled with a laccase activated system. Journal of Cleaner Production 19(5): 445-453.
18. González-García, S., Feijoo, G., Widston, P., Kandelbauer, A., Zikulnig-Rusch, E., Moreira, M.T., 2014: Environmental performance assessment of hardboard manufacture. International Journal of Life Cycle Assessment 14: 456-466.
19. Gul, W., Khan, A., Shakoor, A., 2017: Impact of hot pressing temperature on medium density fiberboard (MDF) performance. Advances in Materials Science and Engineering, article ID 4056360, 6 pp.
20. Gupta, A., 2007: Modeling and optimization of MDF hot pressing. PhD thesis at the University of Canterbury, 196 pp.
21. Hosseinpourpia, R., Adamopoulos, S., Mai, C., Taghiyari, H. R., 2019: Properties of medium-density fiberboards bonded with dextrin-based wood adhesives. Wood Research 64(2): 185-194 pp.
22. Ihnát, V., Boruvka, V., Lubke, H., Babiak, M., Schwartz, J., 2015: Straw pulp as a secondary lignocellulosic raw material and its impact on properties of properties of insulating fiberboards. Part III. Preparation of insulating fiberboards from separately milled lignocellulosic raw materials. Wood Research 60(3): 457-466.
23. Ihnát, V., Lubke, H., Balberčák, J., Kuňa, V., 2020: Size reduction downcycling of waste wood. Review. Wood Research 65(2): 205-220.

24. Ihnát, V., Lubke, H., Russ, A., Pažitný, A., Borůvka, V., 2018: Waste agglomerated wood materials as a secondary raw material for chipboards and fibreboards. Part II: Preparation and characterization of wood fibres in terms of their reuse. Wood Research 63(3): 431-442.
25. Kumar, R.N., Pizzi, A., 2019: Environmental aspects of adhesives – emission of formaldehyde. In: Adhesives for wood and lignocellulosic materials. Pp 293-312, Wiley-Scrivener Publishing, Hoboken, NJ, USA.
26. Lubke, H., Ihnát, V., Kuňa, V., Balberčák, J., 2020: A multi-stage cascade use of wood composite boards. Wood Research 65(5): 843-854.
27. Lubis, M.A.R., Hong, M.K., Park, B.D., 2018a: Hydrolytic removal of cured urea-formaldehyde resins in medium-density fiberboard for recycling. Journal of Wood Chemistry and Technology 38(1): 1-14.
28. Lubis, M.A.R., Hong, M.K., Park, B.D., Lee, S.M., 2018b: Effects of recycled fiber content on the properties of medium density fibreboard. European Journal of Wood and Wood Products 76: 1515-1526.
29. Lubis, M.A.R., Park, B.D., Hong, M.K., 2020: Tuning of adhesion and disintegration of oxidized starch adhesives for the recycling of medium density fiberboard. BioResources 15(3): 5156-5178.
30. Mantanis, G.I., Athanassiadou, E.T., Barbu, M.C., Wijnendaele, K., 2018: Adhesive systems used in the European particleboard, MDF and OSB industries. Wood Material Science and Engineering 13: 104–116.
31. Neykov, N. Trichkov, N., Koynov, D., 2014: Functional-based and activity-based cost management systems in woodworking enterprises. Specific and perspectives for implementation. Innovation in Woodworking Industry and Engineering Design 1(5): 161-165.
32. Neykov, N., Antov, P., Popova, R., 2018: Competitiveness of woodworking industries in the Balkan countries. Comparative advantages. Eastern European Business and Economics Journal 4(2): 132-142.
33. Neykov, N., Antov, P., Savov, V., 2020a: Circular economy opportunities for economic efficiency improvement in wood-based panel industry. In: Proceedings of the 11th International Scientific Conference "Business and Management 2020". Pp. 8-17, May 7–8, Vilnius, Lithuania.
34. Neykov N., Kitchoukov E., Simeonova-Zarkin T., Halalisan AF., 2020b: Economic efficiency estimation of innovations in combined forestry and wood processing units in Bulgaria through certification in FSC chain of custody. In: Innovation in sustainable management and entrepreneurship (ed. Prostean G, Lavios Villahoz J, Brancu L, Bakacsi G). Pp 695-703, SIM 2019. Springer Proceedings in Business and Economics, Springer, Cham.
35. Nordström, E., Demircan, D., Fogelström, L., Khabbaz, F., Malmström, E., 2017: Green binders for wood adhesives. In: Applied adhesive bonding in science and technology. Pp 47-71, Interhopen Books. London.
36. Papadopoulou, E., 2009: Adhesives from renewable resources for binding wood-based panels. Journal of Environmental Protection and Ecology 10: 1128–1136.
37. Papadopoulos, A.N., 2020a: Advances in wood composites. Polymers 12(1): 48.
38. Papadopoulos, A.N. 2020b: Advances in wood composites II. Polymers 12(7): 1552.
39. Pizzi, A., 2006: Recent developments in eco-efficient bio-based adhesives for wood bonding: opportunities and issues. Journal of Adhesion Science and Technology 20: 829-846.

40. Pizzi, A., 2017: Wood and fiber panels technology. In: Lignocellulosic fibers and wood handbook: Renewable materials for to-day's environment (ed. Belgacem MN, Pizzi A). Chapter 15. Pp 385-406, Scrivener-Wiley, Beverley, MA, USA.
41. Pizzi, A., Papadopoulos, A.N., Policardi, F., 2020: Wood composites and their polymer binders. Polymers 12(5): 1115.
42. Rammou, E., Mitani, A., Ntalos, G., Koutsianitis, D., Taghiyari, H.R., Papadopoulos, A.N., 2021: The potential use of seaweed (*Posidonia oceanica*) as an alternative lignocellulosic raw material for wood composites manufacture. Coatings 11(1): 69.
43. Réh, R., Igaz, R., Krišťák, Ľ., Ružiak, I., Gajtanska, M., Božíková, M., Kučerka, M., 2019: Functionality of beech bark in adhesive mixtures used in plywood and its effect on the stability associated with material systems. Materials 12(8): 1298.
44. Russ, A., Schwartz, J., Boháček, Š., Lübke, H., Ihnát, V., Pažitný, A., 2013: Reuse of old corrugated cardboard in constructional and thermal insulating boards. Wood Research 58(3): 505-510.
45. Santoso, M., Widyorini, R., Prayitno, T.A., Sulistyo, J., Hamidah, N., 2020: Effect of pressing temperatures on bonding properties of sucrose-citric acid for nipa palm fronds particleboard. Wood Research 65(5): 747-756.
46. Schneider, T., Behn, C., Windeisen-Holzhauser, E., Roffel, E., 2019: Influence of thermo-mechanical and chemo-thermo-mechanical pulping on the properties of oak fibres. Holz als Roh- und Werkstoff 77(2): 229-234.
47. Shulga, G., Neiberte, B., Verovkins, A., Jaunslavietis, J., Shakels, V., Vitolina, S., Sedliačik, J., 2016: Eco-friendly constituents for making wood-polymer composites. Key Engineering Materials 688: 122-130.
48. Smith, D.C., 2004: The generation and utilization of residuals from composite panel products. Forest Products Journal 54: 8-17.
49. Taghiyari, H.R., Esmailpour, A., Majidi, R., Morrell, J.J., Mallaki, M., Militz, H., Papadopoulos, A.N., 2020: Potential use of wollastonite as a filler in UF resin based medium-density fiberboard (MDF). Polymers 12(7): 1435.
50. Tikhonova, E., Lecourt, M., Irle, M., 2014: The potential of partial substitution of the wood fibre in hardboards by reject fibres from the paper recycling industry. European Journal of Wood and Wood Products 72: 177–184.
51. Tritchkov, N., Antov, P., 2005: Prospects for developing the production of solid wood products taking into account the raw-material base. In: Proceedings of the COST Action E44 Conference broad spectrum utilisation of wood, issue 9. Pp 131-138, June 14-15, Vienna, Austria.
52. Tudor, E.M., Barbu, M.C., Petutschnigg, A., Réh, R., Krišťák, Ľ., 2020a: Analysis of larch-bark capacity for formaldehyde removal in wood adhesives. International Journal of Environmental Research and Public Health 17(3): 764.
53. Tudor, E.M., Dettendorfer, A., Kain, G., Barbu, M.C., Réh, R., Krišťák, Ľ., 2020: Sound-absorption coefficient of bark-based insulation panels. Polymers 12(5):1012.
54. Widsten P., Kandelbauer., A., 2014: Industrial scale evaluation of cationic tannin as a binder for hardboard. Journal of Adhesion Science and Technology 28(13): 1256-1263.
55. Widsten, P., Hummer, A., Heathcote, C., Kandelbauer, A., 2009: A preliminary study of green production of fiberboard bonded with tannin and laccase in a wet process. Holzforschung 63: 545-550.
56. Youngquist, J.A., 1999: Wood-based composites and panel products. In: Wood handbook: wood as an engineering material. Pp 1-31, USDA Forest Service, Forest Products Laboratory, Madison, WI, USA.

Petar Antov*, Viktor Savov
University Of Forestry
Faculty Of Forest Industry
Department Of Mechanical Wood Technology
10 Kliment Ohridski BLVD.
1797 Sofia
Bulgaria
*Corresponding author: p.antov@ltu.bg

Ľuboš Krišťák
Faculty Of Wood Sciences And Technology
Technical University In Zvolen
960 01 Zvolen
Slovakia

Nikolay Neykov
University Of Forestry
Faculty Of Business Management
10 Kliment Ohridski BLVD.
1797 Sofia
Bulgaria

WOOD RESEARCH
e-ISSN 2729-8906
66(3):2021 449-462 pp.
doi.org/10.37763/wr.1336-4561/66.3.449462

BIOSOCIAL DIVERSITY OF SCOTS PINE (PINUS SYLVESTRIS L.) IN A TREE STAND IN RELATION TO CHOSEN HYDRAULIC CONDUCTIVITY INDICATORS OF THE STEM

Tomasz Jelonek[1], Witold Pazdrowski[1], Joanna Kopaczyk[1,2],
Magdalena Arasimowicz-Jelonek[2], Arkadiusz Tomczak[1]
[1]Poznan University Of Life Sciences
Poland
[2]Adam Mickiewicz University
Poland

(Received October 2020)

ABSTRACT

The research focused in determining the lignification indicator of fresh needled springs and the mass of fresh needles in reference to the lignin content in tracheid walls of peripheral area of the stem (MFT/LC and MFN/LC) of Scots pine differentiated as far as its biosocial position within the community expressed by Kraft's classification. The material for the analysis came from mature pine stands growing on North European Plain, on the territory of Poland. Chemical and structural analyses of wood encompassed the area of mature sapwood, i.e. thickness of the last 10 annual rings located at 1.3 m (DBH). It seems that the noticed differences values of both indicators (MFT/LC and MFN/LC) in pines belonging to the first three Kraft's biological classes are connected with physiological, physical and structural conditionings of water transport with minerals in xylem and are closely connected with competition for sunlight, water, nutrients and living space.

KEYWORDS: *Pinus sylvestris* L., mass of fresh needles, lignin content, tracheid walls, sapwood, peripheral area of stem.

INTRODUCTION

Xylogenesis is multistage process, which leads to the formation of xylem. Each of the stages is regulated by a network of correlations based on positive and negative influences of plant growth regulators. Among numerous tree species, phytohormones, particularly auxins and cytokinins, play a significant role in the process (Fajstavr et al. 2018). They affect certain proteins and genes, and force process, which contribute to the formation of various types of xylem, to take place (Goodwin 1978, Shininger 1979, Sudachkova et al. 2012).

Lignin, whose structure in itself is intriguing, is a significant component of lignified walls, and also above all contributes to the stiffness of cell walls. It is an organic polymer whose basic structural elements are derivatives of phenylpropane. A phenylpropane unit consists of a benzene ring composed of six carbon atoms and propane bonds composed in 3 carbon atoms (Fengel and Wegener 1989). The presence of lignin in the walls of the dead conductive cells of the xylem not only protects the wall against collapse at negative pressure while transporting water with minerals but also offers protection against embolism. Lignification of the cell wall provides a general mechanical resistance and stability of the entire plant organism, especially trees (Barnett and Jeronimidis 2003, Boerjan et al. 2003, Üner et al. 2011, Antonova et al. 2014, Kim and Daniel 2014, Tsuyama and Takabe 2014).

Lignin of deciduous trees in comparison with lignin of coniferous trees is characterised by higher percentage of content of methoxy groups and greater ratio of methoxy groups (-OCH3) to hydroxy groups (-OH) (Fengel and Wegener 1989). In wood, lignin bonds with saccharides and together create lignin-hemicellulose compounds. Chemical bonds: ester, ether, glucosidic, or acetalic (Fengel and Wegener 1989) can occur between these compounds. Furthermore, lignin limits cell wall swelling of anatomical wood elements as well as increases immunity against microorganisms (Austin and Ballaré 2010, Shmulsky and Jones 2011). It also polymerises between polysaccharide components of cell walls and appears after the cell growth or at least a part of a cell wall. Lignin is found in the intercellular layer, primary wall and secondary wall. In dead wood cells such as tracheids, impregnation of the wall with lignin secures the wall polysaccharides against partial hydrolysis (O'Brien 1970). The biosynthesis of lignin was intensively researched over the last few years (Brown 1961, Boerjan et al. 2003, Austin and Ballare 2010, Antonova et al. 2014). Phylogenetic origin of plants conditions various ratios of the three basic units in lignin, i.e. syringic alcohol, coniferyl alcohol, and p-coumaryl alcohol. Lignin which is present in cell walls of Scots pine wood consists of coniferylic units with some admixture of p-coumarylic and syringic units (de Stevens and Nord 1953). The common precursor for all derivatives of phenylpropane is shikimic acid (Tomaszewski 1964). In Scots pine, shikimic acid appears in small amounts as one of the first products of photosynthesis (Hasegawa 1962). By adding the radioactive shikimic acid to callus tissue culture of *Pinus strobus*, Hasegawa et at. (1960) noticed an effective incorporation of this compound into the lignin. Hasegawa (1962) achieved similar results also in reference to tracheids of the Scots pine.

Considering the role and significance of lignin in the functioning of trees and in the lignification process itself, there has been an attempt to determine the manner of shaping the quotient of mass of fresh needled springs and the mass of fresh needles to lignin content in tracheid walls of the peripheral area of the pine stem which represent first three Kraft's classes (I, II, III) which constitute the main tree stand, i.e. predominant trees (I), dominant trees (II) and co-dominant trees (III).

MATERIAL AND METHODS

The research encompassed mature pine stands which had been growing in optimal habitat conditions for this greenwoodogenic species on North European Plain. The sample areas were located over four stands of Scots pine (*Pinus sylvestris* L.) which were within the limits of natural habitats for that particular species in Europe. All the research areas were located in the North of Poland, and the research itself encompassed 36 sample trees, at the ages between 89 and 91. In each tree stand a 1-hectare sample area was established, where the measures of diameter at breast height (DBH) were taken among all pines and simultaneously they were divided into three Kraft's biosocial classes (Kraft 1884). The trees were classified into predominant, dominant and co-dominant categories. In each Kraft's biosocial class, the trees' heights were measured according to their number in the assumed 2 cm stages of thickness. The measurements of the sample trees were determined on the basis of their thickness class following the dendrometric method (Van Laar and Akça 2007). In each sample area 9 sample trees were selected and felled, hence a total of 36 model trees was harvested. From each sample tree, material for research, i.e. a disc-shaped sample was cut at DBH level (1.3 m). In the next step, for each of the tree, the annual volume was determined, as well as, the mass of fresh needled springs and the mass of fresh needles which was done through direct weighing process. The purpose of the disc was to ascertain the sapwood area (*S*a) and the area of earlywood in sapwood (*E*as).

The material used to mark lignin in tracheid walls was collected from the last 10 thickness increments, i.e. from the sapwood which is physiologically active. The measurements of the sapwood area (*S*a) and the area of earlywood was conducted by using increment borer Preisser Digi-Met and a computer programme "Grube Comm". In the sapwood area, the width of earlywood in each annual ring was measured. The areas of earlywood in the peripheral area of the stem (sapwood) was determined as the total area of all annual rings. In addition, the data concerning the mass of fresh needles (*N*mass) from sample tress and sapwood area (*S*a) as well as the area of earlywood in sapwood zone (*E*as) was used to determine a relative efficiency of conductive surface of the analysed tree samples. This was achieved by dividing sapwood area and the area of earlywood tracheids in the cross-sectional area of the trunk by the mass of fresh needles (Eqs. 1 and 2):

$$S_a/N_{mass}\ (mm^2 \cdot kg^{-1}) \quad (1)$$

$$E_{as}/N_{mass}\ (mm^2 \cdot kg^{-1}) \quad (2)$$

The lignin content *Lc* ($mg \cdot g^{-1}$) of dry mass) was marked spectrophotometrically (in three repetitions) following Doster's method (1988). At the first, the wood of the last 10 annual rings was treated with methanol for 48 hours, the adopted ratio was 1 ml of methanol per 1 g of xylem, and next it underwent the drying process. From each variant, i.e. Kraft's class, 20 mg of dry xylem was collected and was mixed with 5 ml of 2 N HCL and 0.5 ml of thioglycolic acid (Sigma-Aldrich). The samples underwent incubation at the temperature of 95°C for over 4 hours, next they were centrifuged at 3000 g for 20 min. The achieved precipitate was washed with deionised water and incubated with 5 ml 0.5 N NaOH over 18 hours in room temperature. After centrifuging at 15000 g, NaOH extraction was collected, and the precipitation was washed with 4 ml of deionised water and centrifuged once more. The obtained supernatant was mixed with NaOH extraction, 1 ml of concentrated HCL was acidified and left overnight at 5°C. The obtained precipitation after centrifuging (15000 g) was dissolved in 5 ml 0.5 N NaOH,

it was centrifuged (15000 g) and the absorbance of the solution was measured at the wavelength of 380 nm using the UV-1202 Shimadzu spectrophotometer. The lignin content was expressed in relative units of absorbance. With the data concerning the mass of fresh needled springs, mass of fresh needles and lignin content in tracheid walls from last ten annual increment thickness from the peripheral area of trunks of chosen pines, it was possible to calculate the quotient of fresh needled springs mass divided by lignin content in tracheid walls as well as the quotient of fresh needles mass to the lignin content in tracheid walls in the last ten annual rings.

The research also determined the mean volume increase of the analysed standing trees by adopting volume tables, prepared in 1908. Moreover, the basic statistical characteristics of the analysed variables and correlations between them were established. The obtained empirical material was analysed by adopting the methods of mathematical statistics by using Statistica 13.0 statistical kit.

RESULTS AND DISCUSSION

The manner of shaping the measures of location and spread of relative conductivity surface (S_a /N_{mass} and E_{as} /N_{mass}) of pine which represent different biosocial classes were depicted in Tab. 1.

Tab. 1: The characteristics of hydraulic conductivity indicators (S_a/N_{mass}, E_{as}/N_{mass}) of Scots pine (Pinus sylvestris L.) depending on the biosocial position of the tree in the tree stand.

S_a / Nmass ($mm^2 \cdot kg^{-1}$)

Kraft's class	Mean	STD	Min	Max	CV (%)
I	1297.48	295.51	736.97	1668.37	22.78
II	1212.64	428.23	486.17	1983.84	35.31
III	1657.67*	668,06	751.71	3335.65	40.30
Total	1389.26	513.45	486.17	3335.65	36.96

E_{as} / N_{mass} ($mm^2 \cdot kg^{-1}$)

Kraft's class	Mean	STD	Min	Max	CV (%)
I	767.26	160.81	510.06	995.92	20.96
II	750.26	295.70	294.43	1327.79	39.41
III	1015.56*	437.30	497.33	2246.90	43.06
Total	844.36	332.92	294.43	2246.90	39.43

**Statistically significant differences at the level of p < 0.05.*

The relative area of hydraulic conductivity of the stem was expressed by the quotient of sapwood area (S_a) divided by the fresh needles mass (N_{mass}) and the quotient of the earlywood area in sapwood divided by the fresh needles mass (N_{mass}); it was diversified depending on the biosocial position of the tree in the tree stand. In both cases the relative area of hydraulic conductivity of the stem (S_a / N_{mass} and E_{sa} / N_{mass}) in pines which represent the third Kraft's biosocial class, which was statistically significant higher ($p < 0.05$) in comparison to predominant and dominant pines (Tab. 1). The mean of both indicators in the case of co-dominating pines (III Kraft's class) were respectively 1657.67 ($mm^2 \cdot kg^{-1}$) (S_a / N_{mass}) and 115.36 ($mm^2 \cdot kg^{-1}$) (E_{sa} / N_{mass}); however, in predominant trees it was 1297.48 ($mm^2 \cdot kg$-1) (S_a / N_{mass}) and 767.26 ($mm^2 \cdot kg^{-1}$) (E_{sa} / N_{mass}) and in dominant pines 1212.64 ($mm^2 \cdot kg^{-1}$) (S_a / N_{mass})

and 750.26 ($mm^2 \cdot kg^{-1}$) (E_{sa}/N_{mass}). The lowest variability of the S_a/N_{mass} indicator was noticed in pines from Kraft's I class (22.78%) and the highest in tress from Kraft's II class (tab. 1). In the case of the case of the indicator (E_{sa}/N_{mass}) the lowest coefficient of variability was among predominant trees and the highest was among dominant pines (Tab. 1).

Tab. 2: Statistical characteristics of MFT/LC and MFN/LC coefficients in Scots pine (Pinus sylvestris L.) depending on the biosocial position of the tree in the tree stand.

MFT/LC ($g \cdot (mg \cdot g^{-1})^{-1}$)

Kraft's class	Mean	STD	Min	Max	CV (%)
I	226.43*	65.50	122.16	327.83	28.93
II	158.95*	48.64	96.16	253.70	30.60
III	99.64*	36.18	52.73	165.16	36.31
Total	161.67	72.54	52.73	327.83	44.87

MFN/LC ($g \cdot (mg \cdot g^{-1})^{-1}$)

Kraft's class	Mean	STD	Min	Max	CV (%)
I	147.95*	40.97	83.11	208.46	27.69
II	102.33*	26.55	63.49	146.35	25.95
III	67.73*	23.41	37.92	109.34	34.56
Total	106.00	45.07	37.92	208.46	42.52

**Statistically significant differences at the level of $p < 0.05$.*

Statistical characteristics of the quotient of fresh moisture springs mass divided by lignin content in tracheid walls in the peripheral area (MFT/LC) and the quotient of fresh needles mass divided by the lignin content in tracheid walls of the peripheral area of the stem (MFN/LC) was presented in Tab. 2. The lowest mean value (226.43 $g \cdot (mg \cdot g^{-1})^{-1}$)) of the indicator (MFT/LC) was noticed in predominant trees representing I Kraft's class, lower (158.95) in pines from II Kraft's class, and the lowest (99.64 $g \cdot (mg \cdot g^{-1})^{-1}$)) in co-dominant pines (Tab. 2). The variable expressed by the coefficient of variability in the case of (MFT/LC) and the lowest value was noticed in predominant trees (28.93%), in dominant pines (30.60%) and in co-dominant trees (36.31%) (Tab. 2). As far as the quotient of fresh needles mass divided by the lignin content in tracheid wall of ten annual rings of the peripheral area of the stem in concerned, the highest value of the indicator (MFN/LC) was observed in pines from I Kraft's class (147.95 $g \cdot (mg \cdot g^{-1})^{-1}$), lower (102.33 $g \cdot (mg \cdot g^{-1})^{-1}$) in trees from II class whereas the lowest (67.73 $g \cdot (mg \cdot g^{-1})^{-1}$)) in co-dominant pines (Tab. 2). The standard variation ranged between 23.40 $g \cdot (mg \cdot g^{-1})^{-1}$ to 40.97 $g \cdot (mg \cdot g^{-1})^{-1}$ (Tab. 2). The coefficient of variability of the described indicators was in the range 25.94% to 34.55% (Tab. 2). The statistical characteristics of the mean increase of the volume in pine trunks which represent the main tree stand, i.e. predominant trees, dominant trees and co-dominant trees have been collected and presented in Tab. 3. The highest value of mean increase of tree volume was noticed in trees from I Kraft's class (predominant trees); however, as the biosocial position progressively deteriorates in the tree stand, the value of mean increment of trees clearly lowers (Tab. 3). The standard deviation and coefficient of variability have also indicated this regularity (Tab. 3). The standard ranged from 0.0009 to 0.0025 whereas the coefficient of variability was from 19.40% to 25.25%.

Tab. 3: Statistical characteristics of the mean increment of the pine stems in each Kraft's biosocial class.

Kraft's class	Mean	STD	Min	Max	CV (%)

I	0.0098*	0.0025	0.0057	0.0136	25.25
II	0.0069*	0.0015	0.0047	0.0089	21.58
III	0.0048*	0.0009	0.0033	0.0065	19.40
Total	0.0072	0.0027	0.0033	0.0136	37.72*

** Statistically significant differences at the level of p < 0.05.*

On the basis of the conducted statistical analyses, it was observed that there is a clear relationship between hydraulic conductivity indicators (S_a / N_{mass} and E_{as} / N_{mass}) and the quotient of the mass of fresh needled springs divided by the lignin content in tracheid walls of the peripheral area of the stem (MFT/LC), and the quotient of the fresh needles mass divided by the lignin content in the tracheid walls in the peripheral area (MFN/LC) and the annual increase of stem volume of the trees from the main tree stand. The mean volume increase is a dependent variable whereas the hydraulic conductivity indicators (S_a / N_{mass} and E_{sa} / N_{mass}) and (MFT/LC and MFN/LC) indicators are independent variables.

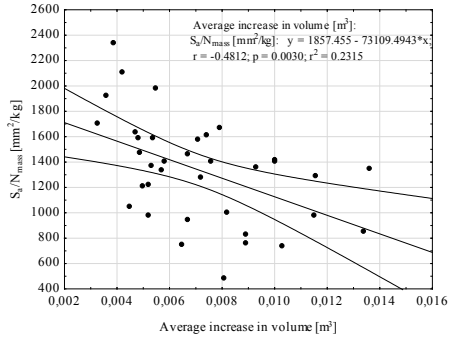

Fig. 1: The mean increase in volume of pine stems in reference to hydraulic conductivity indicator expressed by the quotient S_a / N mass.

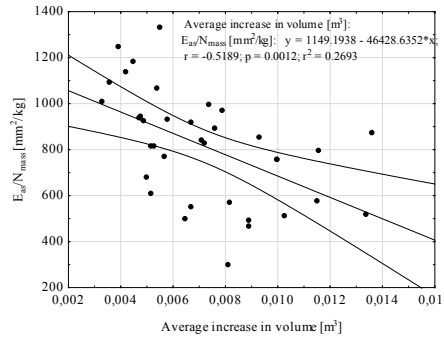

Fig. 2: The mean increase in volume of pine stems in reference to hydraulic conductivity indicator expressed by the quotient E_{as} / N mass.

The mean increase in volume of the pine stems from the sapwood area which referred to the mass of fresh needles (S_a / N_{mass}) correlated negatively. The correlation coefficient assumed the values on the significance level p < 0.05 value r = - 0.4812 (Fig 1). The earlywood area in sapwood was referred to the mass of fresh needles (E_{as} / N_{mass}), and it also assumed values on the level of significance p < 0.05 and correlated negatively, and the value of correlation coefficient was r = - 0,5189 (Fig. 2). The mean increase in volume of pine wood in the main tree stand was conditioned significantly by the MFT/LC and MFN/LC coefficients; as a result, the calculated correlation coefficients were r = +0.94852 in the first one and r = +0.95083 in the second case (Figs. 3 and 4).

Discussion

In the introduction it was mentioned that xylogenesis is a multistage transformation process which eventually leads to the formation of secondary xylem. Each of the stages is regulated by a network of interdependencies based on positive, or negative, interactions with growth regulators (Fajstavr et al. 2018). Among the entire range of regulators, phytohormones, especially auxins and cytokinins, play a significant role in growth and development processes of plants, including trees. The influence of some proteins and genes by coercing particular transformations to take

place, which in the end leads to formation of (Little and Pharis 1995). Xylem is optimised to various degrees as far as their functions are concerned, such as tree growth conditions and strategies allowing its survival. As a result, the characteristic features of the formed xylem are, among others, a complex chemical composition and anatomical structure which is characteristic for each tree species, from which the physical and mechanical properties of wood as a material, including building and construction material, directly results (Barnett and Jeronimidis 2003, Jelonek et al. 2012). Even within a single species there can be differences in structure and properties of xylem, for instance resulting from the geographical location (Martínez-Vilalta 2009, Fernandes et al. 2016), habitat conditions (Eilmann et al. 2011, Matisons et al. 2019), age or biosocial position within in the stand (Pazdrowski et al. 1993, Nilsson and Albrektson 1993, Mäkinen 1996, Vanninen and Mäkelä 2000, Eriksson 2006). The growth and increase of tree species are determined, to a great extent, by the size of their crown, which provides information about the size of the transpiration and assimilation apparatus. The mass of leaves or needles, including the participation of the lighted and shaded crown, intensiveness of the assimilation process, fertility of the habitat and access to water rich in minerals determine xylem production. The amount of biomass collected in various tissues, organs or tree components is known as allocation (Litton et al. 2007). It is usually expressed mathematically as a share of the biomass of a given faction (Poorter and Sack 2012, Poorter et al. 2012) or as a ratio of biomass of various components, i.e. above-ground biomass to underground biomass (Poorter and Sack 2012). In Franklin et al. (2012) the five basic theories explaining the biomass allocation process have been distinguished. In forestry, allometric model is widely used, which assumes that the absolute size of the biomass of a single organ is a dimension function of a different one and the relationship is described by power function (Gayon 2000). However, it should be emphasised that allometric relationships do not consider the influence of internal and environmental factors on the biomass allocation including dendromass, which is significantly conditioned by the tree growth factors (Kellomäki 1981, Oleksyn et al. 1999, Poorter et al. 2012).

The article attempts to analyse the process of establishing the relationship between the mass of fresh needled springs to the lignin content in the tracheid walls in the last ten annual increment thickness rings of the peripheral area of the stem of mature Scots pine (*P. sylvestris* L.) and the relationship of mass of fresh needles to lignin content in tracheid walls of the peripheral area of trees of various biosocial position in the tree stand. The volume mass flow of water with minerals takes place through conducting elements of the xylem from the roots to the transpiration and assimilation apparatus, the so-called long-distance transport. Moreover, the short-distance transport, inner water evaporation and transpiration takes place from higher water potential to lower water potential. The long-distance transport of water in xylem, which is against gravitation, results from the under pressure created by transpiration and also from overpressure generated by root pressure supported by cohesion and adhesion as well as capillary action (Steudle 2001).

The growth and tree increment, including wood production, are determined by preserving the equilibrium between the conducing surface of the stem and the surface of transpiration and the assimilation apparatus in specific (optimal) habitat conditions. The issue, in the work, was expressed by hydraulic conductivity indicator which was expressed by the quotient of the sapwood area and the earlywood tracheid area in sapwood divided by the mass of fresh needles of pines S_a / N_{mass} ($mm^2 \cdot kg^{-1}$), E_{as}/N_{mass} ($mm^2 \cdot kg^{-1}$) representing the main tree stand (predominant, dominant and co-dominant trees).

The obtained results indicate a clear differentiation of the relative conductive area *Sa / N* mass ($mm^2 \cdot kg^{-1}$ E_{as}/N_{mass} ($mm^2 \cdot kg^{-1}$in Scots pine (*P. sylvestris* L.) depending from

their biosocial position in the stand. The trees representing Kraft's III class (co-dominant) in both cases indicated the highest value of analysed indicators, however pre-dominating pines (Kraft's I class) and dominating ones (Kraft's II class) had definitely lower values. It means that in the trees from Kraft's III class, for 1kg of fresh needles falls unequivocally the largest conducive area of sapwood (1491.00 mm^2) and the conducive area of tracheid in earlywood in sapwood (932,22 mm^2) than in predominating and dominating pines. In the former ones, the values of the discussed indicators were respectively (1297.48 mm^2) and (767.26 mm^2) and in the latter ones (1212.64 mm^2) and (750.26 mm^2). The matter can be explained with Pipe Model Theory as described by Shinozaki et al. (1964a,b), which holds that in a physiologically healthy tree the optimisation of the xylem's conductive surface is closely correlated with the size and efficiency of the assimilation and transpiration apparatus of the tree, as well as its height (Jelonek et al. 2008). Analysing the quotient values of the mass of fresh needled springs divided by the lignin content in tracheid wall of the peripheral area of the stem (MFT/LC) and the quotient value of mass of fresh needled divided by the lignin content in tracheid walls of the peripheral area (MFN/LC), clearly reveals the differentiation of values in both indicators in pines belonging to the first Kraft's biosocial class. The predominating trees (Kraft's I class) in the case of both indicators showed their highest value, which was MFT/LC – 226.43 $g\cdot(mg\cdot g^{-1})^{-1}$ and MFN/LC – 147.95 $g\cdot(mg\cdot g^{-1})^{-1}$; whereas the values for dominating pines (Kraft's II class) and co-dominating (Kraft's III class) were definitely lower. In the former, the values of the discussed indicators were respectively (158.95 $g\cdot(mg\cdot g^{-1})^{-1}$ and 102.33 $g\cdot(mg\cdot g^{-1})^{-1}$); whereas in the latter class it was 99.64 $g\cdot(mg\cdot g^{-1})^{-1}$ and 67.73 $g\cdot(mg\cdot g^{-1})^{-1}$.

The social differentiation of the trees in the tree stand is a result of competition for light and living space. The instances of greenwoodogenic species, including pines, occupy a lower position within the altitudinal structure of a tree stand, hence they suffer more from the lack of sunlight, water and also nutrients. The direct result of the struggle for environment resources is the diversification of tree sizes and the changes in xylem structures, conducting surface in xylem and phloem and also the changes in the tree crown (Mátyás and Varga 2000, Sowiński and Szczepaniak 2015). Mäkinen (1996) has noticed that the spring and needle biomass of Scots pine (*P. sylvestris* L.) decreases with the increase of competition.

A special attention should be paid to the relation between the hydraulic conductive indicator (S_a/N_{mass} and E_{sa}/N_{mass}), and the mean increase in tree cubic volume and the quotient of the mass of fresh needled springs divided by the lignin content in the tracheid walls of peripheral areas of the stem (MFT/LC) and the quotient of mass of fresh needles divided by the lignin content in tracheid walls of peripheral areas of the stem (MFN/LC), and the mean increase in tree volume. In the case of the relative conductive surface, i.e. hydraulic conductivity of stems (S_a/N_{mass} and E_{as}/N_{mass}), the increase in volume correlates negatively in both cases. The value of the calculated correlation coefficients was respectively –0.4812 and –0.5189. However, the MFT/LC and MFN/LC coefficients correlated positively but in the case of the latter the coefficient was +0.9485 and in the case of the former +0.9508. The upturn in hydraulic conductivity indicator's value S_a/N_{mass} and E_{as}/N_{mass} in pines will result in lowering the mean tree volume increase; however, lowering the value of relative conducting area will result in the mean volume increase. In the case of MFT/LC and MFN/LC coefficients, together with their increase in the value, also there was a significant increase in mean volume of pines from the main tree stand, i.e. predominating trees, dominating trees and co-dominating trees.

It seems that the variation in both indictors (MFT/LC and MFN/LC) in pines representing the main tree stand is connected with physiological, physical and structural conditioning of transporting water and minerals in the stem. The trees from Kraft's I class indicated the highest

values of the analysed indicators (MFT/LC and MFN/LC), whose mean value was respectively 226.43 g·(mg·g^{-1})$^{-1}$ and 147.95 g·(mg·g^{-1})$^{-1}$. In pines from Kraft's II class the mean values in both indicators were lower from predominating trees and was 158.95 g·(mg·g^{-1})$^{-1}$ and 102.33 g·(mg·g^{-1})$^{-1}$; whereas in co-dominant individuals it was 99.64 g·(mg·g^{-1})$^{-1}$ and 67.73 g·(mg·g^{-1})$^{-1}$. It can be assumed that this is a result of a significant variability of the mass of fresh needled springs, mass of fresh needles, lignin content in tracheid walls of peripheral areas of the pine stems belonging to different biosocial classes in the tree stand. Moreover, it would seem that the noticed values of both indicators are adjusted to the intensity of the assimilation and transpiration process which may result in diversified efficiency of transporting water with minerals. The pines which occupy lower positions in the altitude structure of the tree stand are considerably more vulnerable to sunlight, water and nutrients deficiency rather than the trees from higher biosocial positions. The direct effect of the struggle over environmental resources is the diversification of tree sizes and changes in crown structure (Mátyás and Varga 2000). Mäkinen (1996) noticed that the biomass of springs and needles of the Scots pine lowers with the increase of competition. Naidu et al. (1998) researched allocation of biomass in *Pinus taeda* tree stands and indicated that in intermediate trees the share of the biomass of the stem (75.9%) of the total tree biomass is higher in comparison to dominating trees (63,4%). Furthermore, the intermediate pines are characterised by a higher ratio of biomass of heterotrophic parts, i.e. roots, stem and springs, than the autotrophic parts (needles). According to research conducted by Kellomäki (1981) concerning the influence of the available sunlight on the structure of the current increment of Scots pine, it appears that with greater access to sunlight there is a considerable shift of the current increment of biomass to the springs at the expanse of the stem and needles. The greatest part of the annual production of biomass reaches the stems of trees which grows in conditions with a moderate access to sunlight, but the trees growing is shade direct their greater part of the increment in assimilation apparatus. Vanninen and Mäkelä (2000), as well as Vanninen (2004) have noticed that in pine tree stands, the intermediate trees most part of their current increment locate in stem biomass in comparison to dominating trees.

CONCLUSIONS

(1) On the basis of conducted research of shaping the quotient of the mass of fresh needled springs, mass of fresh needles divided by the lignin content in tracheid wall of the peripheral area of stem (MFT/LC and MFN/LC) of Scots pine (*Pinus sylvestris* L.) varied as far as the biosocial positioning in the tree stand are concerned, diversification of values of analysed indicators in reference to biosocial class of the tress was observed. *(2)* The predominating tress possessed both indicators (MFT/LC and MFN/LC) which were considerably higher, and whose mean value was respectively 226.43 g·(mg·g^{-1})$^{-1}$ and 147.95 g·(mg·g^{-1})$^{-1}$ than pines representing II and III Kraft's biological class. Both values of the discussed indicators in dominating trees was 158.95 g·(mg·g^{-1})$^{-1}$ and 102.33 g·(mg·g^{-1})$^{-1}$, whereas in co-dominating pines it was 99.64 g·(mg·g^{-1})$^{-1}$ and 67.73 g·(mg·g^{-1})$^{-1}$. *(3)* The noticed differences in the values in both analysed indicators (MFT/LC and MFN/LC) in pines belonging to the first three Kraft's biosocial classes constituting the main tree stand are connected with physiological, physical and structural conditioning of transporting water with minerals in the xylem and are closely related with competition for sunlight, water, nutrients and living space.

REFERENCES

1. Abreu, H.D.S., Do Nascimento, A.M., Maria, M.A., 1999: Lignin structure and wood properties. Wood and Fiber Science 31: 426-433.
2. Antonova, G.F., Varaksina, T.N., Zheleznichenko, T.V., Stasova, V.V., 2014: Lignin deposition during earlywood and latewood formation in Scots pine stems. Wood Science and Technology 48(5): 919-936.
3. Austin, A.T., Ballaré, C.L., 2010: Dual role of lignin in plant litter decomposition in terrestrial ecosystems. PNAS 107(10): 4618-4622.
4. Barnett, J.R., Jeronimidis, G., 2003: Wood quality and its biological basis. Wiley-Blackwell, 226 pp.
5. Boerjan, W., Ralph, J., Baucher, M., 2003: Lignin biosynthesis. Annual Review of Plant Biology 54(1): 519-546.
6. Boudet, A.M., Lapierre, C., Grima-Pettenati, J., 1995: Biochemistry and molecular biology of lignification. New Phytologist 129(2): 203-236.
7. Brown, S.A., 1961: Chemistry of lignification. Science 134(3475): 305-313.
8. de Stevens, G., Nord, F.F., 1953: Investigations on lignin and lignification XII. A study of lignin formation based on the oxidation of native and enzymatically liberated lignins. PNAS 39: 80-85.
9. Doster, M.A., Bostock, R.M., 1988: Quantification of lignin formation in almond bark in response to wounding and infection by Phytophtora species. Phytopathology 78: 473-477.
10. Eilmann, B., Zweifel, R., Buchmann, N., Graf Pannatier, E., Rigling, A., 2011: Drought alters timing, quantity, and quality of wood formation in Scots pine. Journal of Experimental Botany 62(8): 2763-2771.
11. Eriksson, E., 2006: Thinning operations and their impact on biomass production in stands of Norway spruce and Scots pine. Biomass and Bioenergy 30(10): 848–854.
12. Fajstavr, M., Paschová, Z., Giaglim K., Vavrčík, H., Gryc, V., Urban, J., 2018: Auxin (IAA) and soluble carbohydrate seasonal dynamics monitored during xylogenesis and phloemogenesis in Scots pine. IFOREST 11(5): 553–562.
13. Fengel, D., Wegener, G., 1989: Wood - chemistry, ultrastructure, reactions. Walter de Gruyter. Pp 132–181, Berlin, Germany.
14. Fernandes, C., Gaspar, M.J., Pires, J., Silva, M.E., Carvalho, A., Brito, J.L., Lousada, J.L., 2016: Within and between-tree variation of wood density components in *Pinus sylvestris* at five sites in Portugal. European Journal of Wood and Wood Products 75(4): 511–526.
15. Franklin, O., Johansson, J., Dewar, R.C., Dieckmann, U., McMurtrie, R.E., Brännström, Å., Dybzinski, R., 2012: Modeling carbon allocation in trees: a search for principles. Tree Physiology 32(6): 648– 666.
16. Gayon, J., 2000: History of the concept of allometry. American Zoologist 40(5): 748-758.
17. Goodwin, P.B., 1978: Phytohormones and growth and development of organs of the vegetative plant. In: The biochemistry od phytohormones and related compounds: a comprehensive treatise, v.2 (ed. Letham DS, Goodwin PB, Higgins TV). Pp 31-174, Elsevier/ North Holland biomedical press. Amsterdam.
18. Hasegawa, M., Higuchi, T., Ishikawa, H., 1960: Formation of lignin in tissue culture of *Pinus strobus*. Plant and Cell Physiology 1: 173-182.
19. Hasegawa, M., 1962: Alicyclic precursors of polyphenols. In: Wood Extractives and their Significance to the Pulp and Paper Industries (ed. Hillis WE). Pp 263-276, Elsevier. New York, NY.
20. Hatfield, R., Vermerris, W., 2001: Lignin formation in plants. The dilemma of linkage Specificity. Plant Physiology 126(4): 1351-1357.

21. Jelonek, T., Pazdrowski, W., Tomczak, A., Grzywiński, W., 2012: Biomechanical stability of pines growing on former farmland in northern Poland. Wood Research 57(1): 31-44.
22. Jelonek, T., Pazdrowski, W., Tomczak, A., 2008: Biometric traits of wood and quality of timber produced in former farmland. Baltic Forestry 14 (2): 138–148.
23. Kellomäki, S., 1981: Effect of the within-stand light conditions on the share of stem, branch and needle growth in a twenty-year-old Scots pine stand. Silva Fennica 15(2): 130-139.
24. Kim, J.S., Daniel, G., 2014: Distributional variation of lignin and non-cellulosic polysaccharide epitopes in different pit membranes of Scots pine and Norway spruce seedlings. IAWA Journal 35(4): 407-429.
25. Kraft, G., 1884: Beiträge zur Lehre von den Durchforstungen, Schlagstellungen und Lichtungshieben. Pp 85-130, Klindworth, Hannover.
26. Little, C.H.A., Pharis, R.P., 1995: Hormonal control of radial and longitudinal growth in the tree stem. In: Plant stems physiology and functional morphology (ed. Gartner BL). Pp 281-319, Academic Press. San Diego, CA.
27. Litton, C.M., Raich, J.W., Ryan, M.G., 2007: Carbon allocation in forest ecosystems. Global Change Biology 13: 2089–2109.
28. Mäkinen, H., 1996: Effect of inter tree competition on biomass production of *Pinus sylvestris* (L.) half-sib-families. Forest Ecology and Management 86(1): 105-112.
29. Martínez-Vilalta, J., Cochard, H., Mencuccini, M., Sterck, F., Herrero, A., Korhonen, J.F.J., Llorens, P., Nikinmaa, E., Nolè, A., Poyatos, R., Ripullone, F., Sass-Klaassen, U., Zweifel, R., 2009: Hydraulic adjustment of Scots pine across Europe. New Phytologist 184(2): 353–364.
30. Matisons, R., Krišāns, O., Kārkliņa, A., Adamovičs, A., Jansons, Ā., Gärtner, H., 2019: Plasticity and climatic sensitivity of wood anatomy contribute to performance of eastern Baltic provenances of Scots pine. Forest Ecology and Management 452: 117568.
31. Mátyás, C., Varga, G., 2000: Effect of intra-specific competition on tree architecture and aboveground dry matter allocation in Scots pine. Investigacion Agraria - Sistemas y Recursos Forestales. Fuera de Serie 1: 111-119.
32. Naidu, S.L., DeLucia, E.H., Thomas, R.B., 1998: Contrasting patterns of biomass allocation in dominant and suppressed loblolly pine. Canadian Journal of Forest Research 28(8): 1116–1124.
33. Nilsson, U., Albrektson, A., 1993: Productivity of needles and allocation of growth in young Scots pine trees of different competitive status. Forest Ecology and Management 62(1-4): 173-187.
34. O'Brien, T.P., 1970: Further observations on hydrolysis of the cell wall in the xylem. Protoplasma 69(1): 1-14.
35. Oleksyn, J., Reich, P.B., Chałupka, W., Tjoelker, M.G., 1999: Differential above- and below-ground biomass accumulation of European *Pinus sylvestris* populations in a 12-year-old provenance experiment. Scandinavian Journal of Forest Research 14(1): 7-17
36. Pazdrowski, W., Spława-Neyman, S., 1993: Badania wybranych właściwości drewna sosny zwyczajnej (*Pinus sylvestris* L.) na tle klas biologicznych w drzewostanie. (Studies on selected properties of Scots pine (*Pinus sylvestris* L.) wood in view of tree biosocial position in the stand). Folia Forestalia Polonica (Ser. B) 24: 133-145.
37. Poorter, H., Niklas, K.J., Reich, P.B., Oleksyn, J., Poot, P., Mommer, L., 2012: Biomass allocation to leaves, stems and roots: meta-analyses of interspecific variation and environmental control. New Phytologist 193(1): 30-50.
38. Poorter, H., Sack, L., 2012: Pitfalls and possibilities in the analysis of biomass allocation patterns in plants. Frontiers in Plant Science 3(259): 1-10. Shininger, T.L., 1979: The control of vascular development. Annual Review of Plant Physiology 30(1): 313-337.
39. Shinozaki, K., Yoda, K., Hozumi, K., Kira, T., 1964a: A quantitative analysis of plant form - the pipe model theory. I. Basic analyses. Japanese Journal of Ecology 14: 97-105.

40. Shinozaki, K., Yoda, K., Hozumi, K., Kira, T., 1964b: A quantitative analysis of plant form - the pipe model theory. II. Further evidence of the theory and its application in forest ecology. Japanese Journal of Ecology 14: 133-139.
41. Shmulsky, R., Jones, D.P., 2011: Forest products and wood science: An introduction. 6th ed. Pp 426-433, Wiley-Blackwell. West Sussex, UK.
42. Sowiński, P., Szczepaniak, J., 2015: Transport dalekodystansowy u roślin: szlaki, mechanizmy, ewolucja (Long-distance transport in plants: paths, mechanisms, and evolution). Kosmos 64(3): 457-469.
43. Steudle, E., 1994: Water transport across roots. Plant Soil 167(1): 79–90.
44. Sudachkova, N.E., Milyutina, I.L., Romanova, L.I., 2012: Biochemical adaptation of conifers to stressful conditions of Siberia. Pp 98-175, Acad. Publ. House "GEO". Novosibirsk, Russia.
45. Tomaszewski, M., 1964: The mechanism of synergistic effects between auxin and some natural phenolic substances. In: Régulateurs Naturels de la Croissance Végétale. Pp 335-351, Coll. Intern. C.N.R.S. Paris.
46. Tsuyama, T., Takabe, K., 2014: Distribution of lignin and lignin precursors in differentiating xylem of Japanese cypress and poplar. Journal of Wood Science 60(5): 353-361.
47. Üner, B., Karaman, I., Tanriverdi, H., Özdemir, D., 2011: Determination of lignin and extractive content of Turkish Pine (*Pinus brutia* Ten.) trees using near infrared spectroscopy and multivariate calibration. Wood Science and Technology 45(1): 121–134.
48. Van Laar, A., Akça, A., 2007: Forest mensuration. Pp 95-147, Springer. Dordrecht, The Netherlands.
49. Vanninen, P., Mäkelä, A., 2000: Needle and stem wood production in Scots pine (*Pinus sylvestris)* trees of different age, size and competitive status. Tree Physiology 20(8): 527-533.
50. Vanninen, P., 2004: Allocation of above-ground growth in *Pinus sylvestris* – impacts of tree size and competition. Silva Fennica 38(2): 155-166.

Tomasz Jelonek*, Witold Pazdrowski, Arkadiusz Tomczak[1]
Poznan University Of Life Sciences
Faculty Of Forestry
Department Of Forest Utilisation
Wojska Polskiego 71A, 60-625 poznan
Poland
*Corresponding author: tomasz.jelonek@up.poznan.pl

Joanna Kopaczyk[1,2]
[1]Poznan University Of Life Sciences
Faculty Of Forestry
Department Of Forest Utilisation
Wojska Polskiego 71A, 60-625 Poznan
Poland
[2]Adam Mickiewicz University
Faculty Of Biology
Department Of Plant Ecophysiology
Umultowska 89, 61-614 Poznan
poland

Magdalena Arasimowicz-Jelonek
Adam Mickiewicz University
Faculty Of Biology
Department Of Plant Ecophysiology
Umultowska 89, 61-614 Poznan
Poland

WOOD RESEARCH
e-ISSN 2729-8906
66(3):2021 463-476 pp.
doi.org/10.37763/wr.1336-4561/66.3.463476

DATA MINING AND ITS IMPACT ON MARKETING COMMUNICATION – CASE: HEAT-TREATED BIRCH WOOD

Roman Dudík, Vlastimil Borůvka, Marcel Riedl, Tomáš Holeček
Czech University Of Life Sciences Prague
Czech Republic

(Received September 2020)

ABSTRACT

The article presents the results of a marketing survey in the area of customer preferences in the case of different degrees of heat-treated solid wood and birch veneer. Part of the marketing survey was a questionnaire survey, where the respondents, as potential customers, expressed their preferences for individual samples which, at first glance, differed in colour due to the different degrees of heat treatment. The result of the research is a clear preference for the heat-treated samples compared to the reference sample without heat treatment. A more detailed secondary analysis of the data from the questionnaire survey was performed with regard to the gender, age and education of the respondents. Here, too, it is possible to conclude a clear preference for heat-treated samples for these groups of respondents. The article also analyses the possibilities of the marketing strategy with a focus on marketing communication, especially in relation to wood processors and producers.

KEYWORDS: Birch, attractiveness, marketing analysis, questionnaire survey, consumer preferences, heat treatment.

INTRODUCTION

This article builds on the published research results (Borůvka et al. 2019) in the field of investigating the properties of *Betula pendula* wood (Silver birch), which were concluded by marketing analysis (Dudík et al. 2020). The reason for the marketing investigation and the subsequent initial marketing analysis was to determine whether there is the potential for customer interest in heat-treated birch wood. The identified interest of customers can then create a precondition for the greater use of such wood, for example in the furniture industry. A secondary data analysis is also performed, which also relates to a deeper examination of the potential interest of customers in heat-treated birch wood. The article presents unpublished results resulting from this secondary analysis of marketing survey data.

According to Espinoza (2015), the existing literature shows that the technical aspects of the thermal modification of wood have received considerable attention in the past; however, only limited attention has been paid to the market opportunities of thermally modified wood-based products. Accordingly, Militz and Lande (2009) states that modified woods are unknown to the market, and it will take time and effort to educate the market players about the advantages of such new materials. Recently, developer modified woods lack this history and, therefore, many properties that the market normally takes for granted need to be explained when marketing a new material.

For these reasons, this article newly presents the theoretical basis for the communication of these findings both in relation to the end customers (consumers) and especially in relation to professional customers, i.e., processors and furniture companies. As stated by Gamache (2017), thermally modified wood (TMW) has multiple applications and offers an opportunity for high value-added uses for timber resources that are underutilised or affected by invasive species, which can improve the forest health and create economic opportunities in rural communities. This argument is also related to the changing position of birch as a tree in the Czech Republic. The position of birch as a woody plant purposefully grown in the Czech Republic until its felling age has been published before, and there is an obvious shift in the view of the importance of birch from a weed wood to an economically important one in the future (Dudík 2018). Information on the position of birch in the wood processing industry of the Czech Republic has also been described by Borůvka et al. (2019).

As part of the secondary analysis, the article evaluates the extent to which the colour changes of the heat-treated solid wood and birch veneer are interesting for individual customer groups from a marketing point of view. An economic evaluation of the production and processing of heat-treated wood and birch veneers is not solved here. The reason for the secondary analysis is to obtain an initial finding whether it makes any sense from the point of view of individual customer groups to consider the importance and use of colour changes in birch wood. This sequence of steps corresponds to a concept testing phase in the development of a new product and is the starting point for a marketing and business analysis. This then facilitates the successful commercialisation associated with the marketing of the product. Because the demand for wood is a driven demand depending on the situation in other industries, that use wood as a raw material, the development of value added in the wood processing industry might be affected also by situation in these industries (Palátová 2019).

According to Bhuiyan (2011), most decisions about launching new products are preceded by marketing research. In our case, the opinion of customers was ascertained by a questionnaire survey. The aim of the survey was to determine the degree of attractiveness of heat-treated samples of solid wood and veneers for potential customers with regard to their perception in the colour differences of the samples and their related preferences. The sample of respondents was sufficient

for the analysis of the responses using statistical methods and to determine whether it is possible to apply the results of the questionnaire survey to the entire population - this was confirmed by (Dudík et al. 2020). In addition, it should be mentioned that the testing should not be solely restricted to this stage; it must be conducted throughout the new product development process (Ulrich and Eppinger 2007) as stated by Cooper (2019) in building the "voice-of-customer".

Work has previously been published that states that the heat treatment of wood gives it, among other things, an attractive colour, which is important from an aesthetic point of view (Santos et al. 2014, Sedlar et al. 2019, Cademartori et al. 2014). The positive importance of darker wood colours in relation to market preferences is reported by Zanuttini et al. (2020). Thus, a dark colour can give the wood a feeling of higher value in some countries and, from this point of view, can be an important benefit of heat treatment. It follows that the heat treatment of wood can increase the market acceptance of such wood (Jirouš-Rajković and Miklečić 2019). In Czech conditions, the heat treatment of birch wood can be considered an innovation in the processing of the birch wood raw material. According to Loucanova et al. (2017), innovation is an important prerequisite for commercial success in the market. From a macroeconomics point of view, this has a positive impact on the consumption, which is a key driver of an economy (Parobek and Palus 2008). Consumption is influenced by the preferences of the customers' decision-making factors, which also applies to purchasing furniture. The most relevant factors affecting the purchasing decision are the quality, price and design of the furniture (Kaputa and Šupín 2010. The design is then closely linked to the perception of the furniture's colours by the customers.

MATERIAL AND METHODS

Marketing investigation

The starting point for the analysis of the influence of the colour shade of the solid birch wood and birch veneer on the decisions of potential customers is a questionnaire survey on a random sample of 102 people from the population of the Czech Republic. The attractiveness of the colour appearance of real samples of solid birch wood (1 reference sample and 5 samples with different degrees of thermal treatment) and birch veneer (1 reference sample and 4 samples with different degrees of thermal treatment) was analysed. For the solid wood samples, Roman numerals I to VI were used, with the reference sample being I. For the veneer samples, letters of the alphabet A to E were used, with the reference sample being A. The methodology of the production and heat treatment of solid wood and birch veneer samples has been published in the article by Borůvka et al. (2019) and Dudík et al. (2020), where the colour representation of the samples is also given.

The designation and characteristics of the samples:

I. Solid wood - untreated (BR-SW-REF) – the lightest colour shade
II. Solid wood - treated at 160°C/3 h (BR-SW-160-3)
III. Solid wood - treated at 170°C/3 h (BR-SW-170-3)
IV. Solid wood - treated at 180°C/3 h (BR-SW-180-3)
V. Solid wood - treated at 190°C/3 h (BR-SW-190-3)
VI. Solid wood - treated at 200°C/3 h (BR-SW-200-3) – the darkest colour shade

A. Veneer - untreated (BR-REF) – the lightest colour shade
B. Veneer - treated at 170°C/3 h (BR-170-3)

C. Veneer - treated at 190°C/3 h (BR-190-3)
D. Veneer - treated at 190°C/5 h (BR-190-5)
E. Veneer - treated at 200°C/3 h (BR-200-3) – the darkest colour shade.

Aware of the possible subconscious influence of the environment in which the respondents live in on their preferences, the attractiveness of the colour appearance of the samples was examined in two variants. The first variant concerned the determination of the attractiveness of the coloured samples of solid wood and veneer during the first furnishing of a new house / flat with furniture (e.g., living room). The second variant was the purchase of a piece of furniture (e.g., in the living room) to the already existing equipment of the house / flat. The level of attractiveness of each individual sample of the solid wood and birch veneer was also very important information, which was evaluated according to the selected point scale (1 point - the least preferable, 5 points - the greatest preference). In other words, the emotional degree of the attractiveness of individual samples was determined. In addition, the gender, age and educational level of each respondent were surveyed. The full text of the questionnaire is published in the article by Dudík et al. (2020).

The data obtained by the questionnaire survey were processed in the first phase by graphical methods of descriptive statistics. The statistical significance of the differences in the preference between the different groups of respondents was evaluated using the Chi-square Goodness of the Fit Test. The estimation of the proportion of the people in the population preferring the thermal wood treatment was made as an interval estimate of the p-binomial distribution parameter (Wonnacot and Wonnacot 1977), i.e

$$P\left[\frac{x}{n}-u\left(\alpha/2\right)\sqrt{\frac{x/n\left(1-x/n\right)}{n}}<p<\frac{x}{n}+u\left(\alpha/2\right)\sqrt{\frac{x/n\left(1-x/n\right)}{n}}\right]=1-\alpha \qquad (1)$$

The statistical evaluation of the questionnaire survey was performed in the program R Version 3.6.1. (The R Foundation, Austria). The same significance level ($\alpha = 0.05$) was used for the analyses (Dudík et al. 2020).

Marketing strategy

In the case of a new technology, Lane (1999) distinguishes between two basic approaches (Fig. 1).

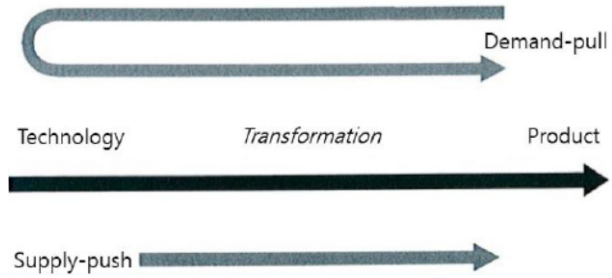

Fig. 1: The push and pull forces initiate the technology transfer (Lane 1999).

In our case, it is a supply-push, where the researchers who used a technology that is not

used in the Czech Republic, in the case of the birch wood, to initiate the technology transfer process (from the left side of Fig. 1) by creating pressure on the use of these innovative technologies by entities that can apply these technologies in products (e.g., wood processing companies, furniture manufacturers, etc.). The market opportunity arises from the fact that the technology supplied demonstrates a feasible solution to an existing problem, or because the desired product demonstrates commercial viability. From the results below, it is clear that from the consumer's point of view, the product, as a material, is sufficiently attractive due to the fact that this technology allows sufficient colour variability based on the fashion and customer requirements. At this stage, it is, therefore, necessary to focus the supply-push marketing strategy on the communication on the relevant links in the value chain. In his article, Choe (2019) analyses the factors influencing the technology transfer performance and presents a more detailed classification of these strategies – in our case, it is a target push (Fig. 2).

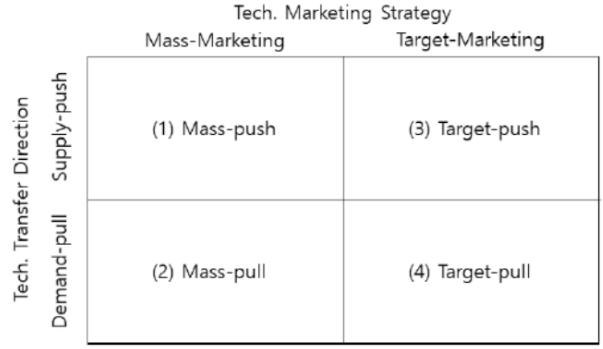

Fig. 2: Research framework: Types of technology transfer (Choe 2019).

One of the main starting points for further managerial decision-making in this area and the implementation of this strategy is a processed SWOT analysis. Details concerning the quality processing of the SWOT analysis of its versatile use are given, for example, by Benzaghta (2021). The processed SWOT analysis and the possibilities of its application are presented at the end of the following chapter.

RESULTS AND DISCUSSION

Initial analysis

The results of the initial analysis of the information obtained from the questionnaire survey (Dudík et al. 2020) show a clear predominant share of potential customers who prefer a variant of heat-treated wood or birch veneer. The share of respondents willing to buy furniture made of wood or birch veneer with thermal treatment is between 0.824 and 0.912. For the calculation of the intervals, a level of significance was chosen at $\alpha = 0.05$, i.e., the resulting intervals cover the actual share of people interested in furniture with a thermal treatment with a probability of 0.95. None of the intervals contains the number 0, so we can reject (at a significance level of 0.05) the hypothesis of zero interest of people in the Czech Republic in furniture with thermally treated wood. In addition, none of the intervals contains a number of 0.5 or less, so it can be estimated that the share of these people in the population is more than half.

The results of the sample preferences, in the case of purchasing a supplemental piece of furniture and new home furnishings, for solid wood and birch veneer samples have already been published (Dudík et al. 2020). The samples of solid birch wood without heat treatment (BR-SW-REF), namely at the level of approx. 9% in the case of new flat furnishing and approx. 11% in the case of purchasing a supplemental piece of furniture, obviously achieved a low preference level. Similarly, the low preference level of birch veneer samples without heat treatment (BR-REF) is evident, at the level of approx. 18% in the case of new flat furnishings and in the case of purchasing a supplemental piece of furniture.

Secondary analysis of the marketing research

As part of the secondary analysis of the data obtained from the questionnaire survey, the structure of information on customer preferences was examined in more detail in terms of gender (men, women), age (younger: under 30, older: 31 and older) and education (up to secondary, university and higher). Tab. 1 shows the proportions of the respondents by gender willing to purchase wooden furniture with a thermal treatment.

Tab. 1: Proportions of respondents by gender willing to purchase wooden furniture with a thermal treatment.

Type of purchase	Type of furniture	Gender	Proportion of respondents	Interval estimate of the share in the population
Furnishing a new flat	Solid wood	Female	0.971	0.914–1.000
		Male	0.882	0.806–0.959
	Veneer	Female	0.824	0.695–0.952
		Male	0.824	0.733–0.914
Purchasing a supplemental piece of furniture	Solid wood	Female	0.882	0.774–0.991
		Male	0.897	0.825–0.969
	Veneer	Female	0.853	0.734–0.972
		Male	0.809	0.715–0.902

For the solid wood furniture for new flat furnishings, we can observe significant differences between men and women. The achieved level of significance is 0.006. Women obviously prefer light shades. The exception is the darkest shade, which is also popular with women (Fig. 3).

In the case of purchasing a supplemental piece of solid wood furniture, the interest in different shades is balanced (Fig. 3). The achieved level of significance is 0.912.

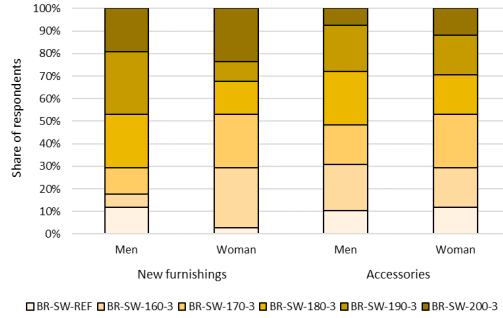

Fig. 3: New flat furnishing and purchasing a solid wood furniture accessory – the differences between women and men.

We did not observe any significant differences between men and women for the new flat furnishings made from veneer. The achieved level of significance is 0.213. Men have the largest share of preferences for the medium colour shade (Fig. 4). In the case of complementary piece of veneer furniture, the interest in different shades is rather balanced (Fig. 4). Again, we did not observe any significant differences. Men, again, have the largest share of preferences for the medium colour shade. The achieved level of significance is 0.140.

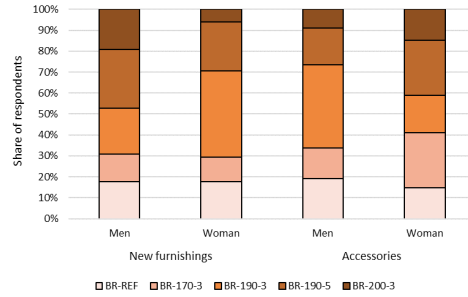

Fig. 4: New flat furnishings and purchasing furniture accessories from veneer – differences between the women and men.

The structure of information on the customer preferences in terms of their age (younger: up to 30 years, older: 31 and more years) is shown in Tab. 2.

Tab. 2: Proportions of respondents according to their age willing to buy wood furniture with a thermal treatment.

Type of purchase	Type of furniture	Age	Proportion of respondents	Interval estimate of the share in the population
Furnishing a new flat	Solid wood	Younger	0.913	0.847 – 0.978
		Older	0.909	0.811 – 1.000
	Veneer	Younger	0.841	0.754 – 0.927
		Older	0.788	0.648 – 0.927
Purchasing a supplemental piece of furniture	Solid wood	Younger	0.870	0.790 – 0.949
		Older	0.939	0.858 – 1.000
	Veneer	Younger	0.797	0.702 – 0.892
		Older	0.879	0.767 – 0.990

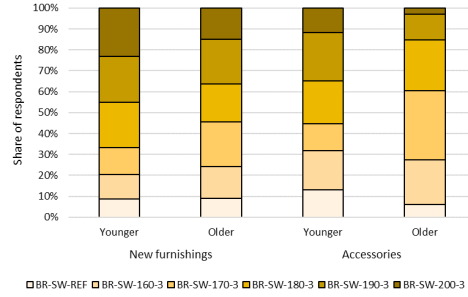

Fig. 5: New flat furnishings and purchasing a solid wood furniture accessory – differences between the age groups.

We did not observe any significant differences between the age groups for veneer furniture for the new flat furnishings. The achieved level of significance is 0.778. The medium dark shade has the largest preference in the older age group (Fig. 6).

In the case of complementary veneer furniture, the interest in the different shades is less balanced (Fig. 6). Nevertheless, the differences between the age groups are not statistically significant. The achieved level of significance is 0.106. Again, the medium dark shade (BR-190-3) has the largest preference in the younger age group.

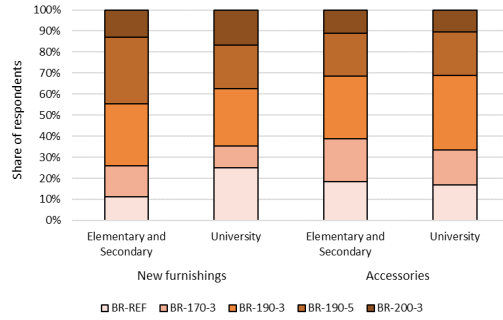

Fig. 6: New flat furnishings and purchasing a supplemental piece of furniture made of veneer – differences between the age groups.

The structure of the information on the customer preferences from the point of view of their education (maximum secondary, university and higher) is shown in Tab. 3.

Tab. 3: Proportions of the respondents according to their education willing to purchase wood furniture with a thermal treatment.

Type of purchase	Type of furniture	Education	Proportion of respondents	Interval estimate of the share in the population
Furnishing a new flat	Solid wood	Elementary and secondary	0.981	0.945 – 1.000
		University	0.833	0.728 – 0.939
	Veneer	Elementary and secondary	0.889	0.805 – 0.972
		University	0.750	0.628 – 0.872
Purchasing a supplemental piece of furniture	Solid wood	Elementary and secondary	0.833	0.734 – 0.933
		University	0.958	0.902 – 1.000
	Veneer	Elementary and secondary	0.815	0.711 – 0.918
		University	0.833	0.728 – 0.939

For the solid wood furniture for the new flat furnishings, we observed significant differences between the groups with the different education. The achieved level of significance is 0.021. The obvious preference for darker shades among the respondents with a maximum secondary education is interesting (Fig. 7).

With the supplemental solid wood furniture, we again observed significant differences between the groups with the different education. The achieved level of significance is 0.002. The darker shade (BR-SW-180-3) has the largest preference in the group of respondents with a university education (Fig. 7).

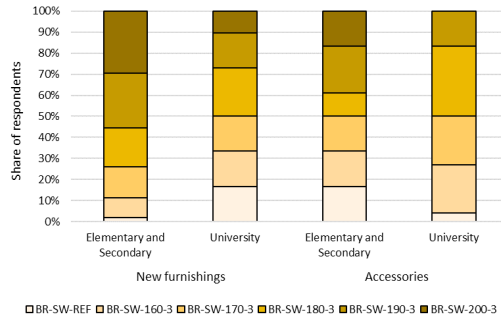

Fig. 7: New flat furnishings and purchasing a solid wood furniture accessory – differences between the groups with the different education.

We did not observe significant differences between the veneer furniture for new flat furnishings between the groups with the different education. The achieved level of significance is 0.337. The darker shade (BR-190-5) had the largest preference in the group of maximum secondary education (Fig. 8).

We also did not observe significant differences between the groups for complementary veneer furniture. The achieved level of significance is 0.972. The medium dark shade (BR-190-3) had the largest preference in the group of respondents with a university education (Fig. 8).

We also did not observe significant differences between the groups for complementary veneer furniture. The achieved level of significance is 0.972. The medium dark shade (BR-190-3) had the largest preference in the group of respondents with a university education (Fig. 8).

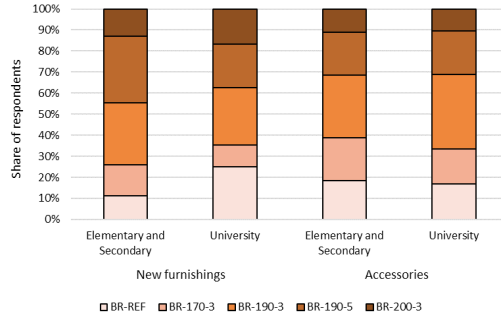

Fig. 8: New flat furnishings and purchasing furniture accessories made from veneer – differences between the groups with the different education.

The secondary analysis of the results of the questionnaire survey confirmed a higher level of attractiveness of the heat-treated samples of the solid wood and birch veneer for individual groups of customers differentiated according to their gender, age and education. The heat-

treated samples represent darker shades. The results of the survey point to the fact that darker colours could be more preferred by the market. Similar results were obtained by Zanuttini et al. (2020). Wood colour is an important parameter for the identification, use and determination of its market value with regard to aesthetic factors (Rosu et al. 2010). In this respect, similar results were obtained by Candelier et al. (2016) because they considered the colour of the wood to be an important property for the final consumer. The reason is that the aesthetic aspect prevails for some end customers. A number of retail chains with interior furnishings offer these interior furnishings in lighter shades - an example is the so-called "bleached oak", etc. The results of the analysis of the questionnaire survey in the Czech Republic indicate a likely change in colour preferences of potential customers towards "warmer" darker colours. However, to confirm this hypothesis, it would be appropriate to conduct a further investigation, preferably using samples of specific pieces of furniture, which would be made from raw birch wood material modified with different degrees of heat treatment.

Marketing strategy

As mentioned in the previous methodological part, a detailed SWOT analysis is a necessary prerequisite for the further decision-making and planning regarding the use of thermally treated wood technology (Tab. 4). In this case, it includes the results of our own research, an analysis of the environment and an analysis of other sources (Espinoza et al. 2015).

Tab. 4: SWOT analysis.

Strengths	**Weaknesses**
• TMW looks more attractive, even luxurious, if it resembles tropical woods. • Improved water properties; resulting in greater dimensional stability. • Longer material life with the possibility of outdoor use. • From the customers' point of view, an „ecological" colour change - without the use of chemicals / paints. • Preservation of the possibility of material processing. • The possibility of reusing the material at the end of its economic life.	• Deterioration of some wood properties (e.g., hardness). • Expenditure related to heat treatment. • Customers often do not know that TMW exists and can request it. • Little used material - deeper operational experience is lacking.
Opportunities	**Threats**
• The price of TMW birch is usually lower than the price of a visually similar tropical wood. • Reducing pressure to use tropical timber, contributing to forest conservation. • It is still a matter of using a renewable natural resource. • Potential use of birch wood in products with higher added value - in the conditions of the Czech Republic, a change in the attitude of forest owners to a positive view of birch and its greater representation in forests.	• Heat treatment represents energy consumption, which can worsen the carbon footprint of a product - it can be perceived negatively by customers. • In the Czech Republic, customers' distrust of TMW as a novelty. • Reluctance of manufacturers to invest in the related technologies enabling heat treatment. • TMW represents the incurrence of costs reflected in the price of products, and the customer may not want to accept this price increase. • Existence of competing materials, e.g., wood-plastic composite.

The promotional strategy for TMW should consider that awareness among both the consumers and the end professional customers is very low in the Czech Republic, and those potential customers are unfamiliar with the TMW's performance and attributes. The most commonly used promotional channel for the current TMW producers is through company websites (Espinoza et al. 2015).

Customer satisfaction is one the most important factor in a successful business (Parobek et al. 2015). It will be important for the TMW industry promotion to include a mixture of stimulating demand to create awareness and increase knowledge, as well as enhance the industry image through advertising, personal selling, and sales promotion, which includes displays at trade shows (Shupe and Vlosky 2010). The systematic application of a communication mix can prepare the professional customers to successfully pursue any opportunity that arises from a supply push.

CONCLUSIONS

The results of the research point to a greater colour attractiveness of heat-treated wood and birch veneer from the point of view of the potential customers' preference. Overall, a greater preference for darker colours was confirmed compared to light colours or the reference samples without heat treatment. During the secondary analysis of the data obtained from the questionnaire survey, it was found that statistically significant differences in the preferences of potential customers occur between men and women in the case of new flat furnishing with solid wood furniture. Other significant differences were found between groups with a different education, both in the case of new flat furnishings and in the case of purchasing a supplemental piece of furniture.

These results further signal that, in relation to the final customer, heat-treated wood is a sufficiently attractive material, provided that there is a sufficiently wide product range that uses this material. TMW wood has a number of advantages: it does not contain toxic substances, it has a wide range of shades, it is a solid material with extended resistance. In addition, it makes it possible to use local sources of birch wood, which, without this treatment, would have less of an opportunity to use such wood in products with higher added value. As part of the communication strategy, it is necessary to mainly focus on professional customers, i.e., wood processors and furniture manufacturers. There is a need to increase the interest of the wood processing industry in this way to create added value to the products (veneers, lumber, etc.) and to harmonise this process view throughout the value chain. The starting point for this communication strategy is a SWOT analysis and an effective communication mix based on this strategy.

ACKNOWLEDGMENT

The research was supported by the National Agency for Agricultural Research of the Ministry of Agriculture of the Czech Republic [project No. QK1920272 – „Communication as a tool to harmonise the needs of society and the forestry sector"] and by the Grant service Forests of the Czech Republic, state enterprise [project No. 90, contract No. 3/2018].

REFERENCES

1. Benzaghta, M.A., Elwalda, A., Mousa, M.M., Erkan, I., Rahman, M., 2021: SWOT analysis applications: An integrative literature review. Journal of Global Business Insights 6(1): 54-72.
2. Bhuiyan, N., 2011: A framework for successful new product development. Journal of Industrial Engineering and Management 4(4): 746-770.
3. Borůvka, V., Dudík, R., Zeidler, A., Holeček, T., 2019: Influence of site conditions and quality of birch wood on its properties and utilization after heat treatment. Part I. Elastic and strength properties, relationship to water and dimensional stability. Forests 10(2): 189.
4. de Cademartori, P.H.G., Mattos, B.D., Missio, A.L., Gatto, D.A., 2014: Colour responses of two fast-growing hardwoods to two-step steam-heat treatments. Materials Research 17(2): 487-493.
5. Candelier, K., Thevenon, M.F., Petrissans, A., Dumarcay, S., Gerardin, P., Petrissans, M., 2016: Control of wood thermal treatment and its effects on decay resistance: a review. Annals of Forest Science 73: 571–583.
6. Choe, W.J., Ji, I., 2019: The performance of supply-push versus demand-pull technology transfer and the role of technology marketing strategies: The case of a Korean Public Research Institute. Sustainability 11(7): 2005.
7. Cooper, R.G., 2019: The drivers of success in new-product development. Industrial Marketing Management 76: 36-47.
8. Dudík, R., Šišák, L., Riedl, M., 2018: Regeneration of declining spruce stands in the Czech Republic - economic view of an alternative species composition. In: Book of abstracts "Sustainable forest management for the future – the role of managerial economics and accounting". Pp 25-26, Croatia.
9. Dudík, R., Borůvka, V., Zeidler, A., Holeček, T., Riedl, M., 2020: Influence of site conditions and quality of birch wood on its properties and utilization after heat-treatment. Part II. Surface properties and marketing evaluation of the effect of the treatment on final usage of such wood. Forests 11(5): 556.
10. Espinoza, O., Buehlmann, U., Laguarda-Mallo, M.F. 2015: Thermally modified wood: Marketing strategies of US producers. BioResources 10(4): 6942-6952.
11. Gamache, S.L., Espinoza, O., 2017: Marketing strategy recommendations for the U.S. thermally modified wood industry. University of Minnesota, 54 pp.
12. Jirouš-Rajković, V., Miklečić, J., 2019: Heat-treated wood as a substrate for coatings, weathering of heat-treated wood, and coating performance on heat-treated wood – review article. Advances in Materials Science and Engineering, Article ID 8621486: 9.
13. Kaputa, V., Šupín, M., 2010: Consumer preferences for furniture. In: Wood processing and furniture manufacturing: Present conditions, opportunities and new challenges (ed. Paluš, H.). Pp 81-90, WoodEMA, i.a. Zagreb.
14. Lane, J.P., 1999: Understanding technology transfer. Assistive Technology 11(1): 5-19.
15. Loučanová, E., Paluš, H., Dzian, M., 2017: A course of innovations in wood processing industry within the forestry-wood chain in Slovakia: a Q_methodology study to identify future orientation in the sector. Forests 8(6): 210.
16. Militz, H., Lande, S., 2009: Challenges in wood modification technology on the way to practical applications. Wood Material Science and Engineering 4(1-2): 23-29.
17. Palátová, P., 2019: Value added in sawmilling industry in the Czech Republic. Central European Forestry Journal 65(1): 60-65.

18. Parobek, J., Paluš, H., 2008: Modelling of wood and wood products flow in the Slovak Republic. In: COST conference on a European wood processing strategy: Future resources matching products and innovations. Pp 93-99, Ghent University, Belgium.
19. Parobek, J., Loučanová, E., Nosáľová, M., Šupín, M., Štofková, K.R., 2015: Customer window quadrant as a tool for tracking customer satisfaction on the furniture market. In International Scientific Conference: Business Economics and Management (ed. Sujova, A., Krajcirova, L.). Pp 493-499, Book Series: Procedia Economics and Finance.
20. Rosu, D., Teaca, C.A., Bodirlau, R., Rosu, L., 2010: FTIR and color change of the modified wood as a result of artificial light irradiation. Journal of Photochemistry and Photobiology B-Biology 99(3): 144-149.
21. Dos Santos, D.V.B., De Moura, L.F., Brito, J.O., 2014: Effect of heat treatment on color, weight loss, specific gravity and equilibrium moisture content of two low market valued tropical woods. Wood Research 59(2): 253-264.
22. Sedlar, T., Sinković, T., Perić, I., Jarc, A., Stojnić, S., Šefc, B., 2019: Hardness of thermally modified beech wood and hornbeam wood. Šumarski list 143(9-10): 425-433.
23. Ulrich, K.T., Eppinger, S.D., 2007: Product design and development. 4th ed., McGrawHill, New York, 384 p.
24. Shupe, T.F., Vlosky, R.P., 2010: Why and how to market wood products. Louisiana Forest Products Development Center, 10 pp.
25. Wonnacot, T.H., Wonnacot, R.J., 1977: Introductory statistics, 3rd ed., John Wiley, New York, 650 pp.
26. Zanuttini, R., Castro, G., Cremonini, C., Negro, F., Palanti, S., 2020: Thermo-vacuum treatment of poplar (*Populus* spp.) plywood. Holzforschung 74(1): 60–67.

Roman Dudík, Marcel Riedl
Czech University Of Life Sciences Prague
Faculty Of Forestry And Wood Sciences
Department Of Forestry And Wood Economics
Kamýcká 129, 165 00 Praha 6 - Suchdol
Czech Republic

Vlastimil Borůvka*, Tomáš Holeček
Czech University Of Life Sciences Prague
Faculty Of Forestry And Wood Sciences
Department Of Wood Processing And Biomaterials
Department Of Forest Biomaterials Engineering
Kamýcká 129, 165 00 Praha 6 - Suchdol
Czech Republic
*Corresponding author: boruvkav@fld.czu.cz

WOOD RESEARCH
e-ISSN 2729-8906
66(3):2021 477-488 pp.
doi.org/10.37763/wr.1336-4561/66.3.477488

EFFECT OF DIFFERENT WOOD DOWELS ON MECHANICAL PROPERTIES OF TRIANGULAR GIRDER TRUSSES

Liuliu Zhang, Cheng Chang, Shuming Yang,
Tongyu Hou, Yifan Liu, Zeli Que
Nanjing Forestry University
China

(Received July 2020)

ABSTRACT

Static load tests were carried out on three kinds of triangular girder trusses with different diameter wood dowels, and the effects of that on the structure of girder trusses were discussed. It was found that there was a good synergy between the wood dowels and the girder trusses. Among the triangular girder trusses with different diameters, the 16 mm diameters had the best energy dissipation performance increased by 184% and deformation resistance of 0.73 mm; the 20 mm diameters had the best stability performance, the better bearing capacity of 60.42 kN and deformation resistance of 0.82 mm. The bearing capacity of the double girder trusses was 2.06-2.25 times that of two single trusses, which had the ability to 'one plus one is greater than two'.

KEYWORDS: Triangular girder truss, truss joint, anti-deformation capability, load-carrying capacity.

INTRODUCTION

Wood structure building is an important representative of ecological architecture. In order to save energy, reduce emissions, relieve the pressure on the environments and resources in the whole life cycle of buildings and achieve the recycling and sustainable development of materials, the promotion and application of wood structures has become a consensus of the whole society (Yang et al. 2020).

As one of the main forms of modern wood structure, light wood frame construction has excellent dimension lumber processing, certification system and mature prefabricated component manufacturing technology (Madsen 1992) compared with heavy timber construction. Furthermore, it also has the advantages of short construction cycle and low cost (Prochazka et al. 2014). Among them, light wood trusses are one of the main load-carrying components of light wood frame construction. Nowadays, more than 60% of residential buildings in North America use wood trusses, of which about 95% of new residential buildings in Canada are built with wood trusses. In addition, wood trusses have been widely used in Europe, Asia and other regions. With the widespread application of light wood frame construction, the application of wood trusses in modern buildings has become more and more extensive. However, the load-carrying capacity of common triangular wood trusses is limited that the suitable span of Howe type wood trusses with the best mechanical performance is no more than 12 m. This limits the scope of application of light wood frame construction roof system and also hinders the promotion and development of wood trusses to some extent. The appearance of triangular girder trusses has effectively solved these problems. By combining several trusses of common triangular wood trusses into one structural component, the section size of the component could be increased to obtain better load-carrying capacity, deformation resistance and stability, so as to meet the requirements of larger span (Zhang et al. 2012, Yang 2014, Que et al. 2015, He et al. 2015).

At present, researches on wood trusses mostly focus on the repair technology, metal tooth plate connection of single truss and light wood truss system. In contrast, the study of girder trusses has hardly been involved (Gupta et al. 2005, Gupta et al. 2004, Rittenburg et al. 2003, Via et al. 2001, Munafòet et al. 2015, Fauziyah et al. 2016, Underwood et al. 2001, Song et al. 2012, Gupta et al. 2004, Cabrero et al. 2009, Islam et al. 2017, Mohamadzadeh et al. 2015, Guntekin 2007, 2009, Sandanus et al. 2016, Moya et al. 2017) due to the common use of girder trusses in engineering, which has no design value reference. This raises several security issues. In the previous study (Wang et al. 2019, Gao 2017), the team members found that the connection of parallel chord girder trusses connected with wood dowels had a good synergistic effect and could effectively solve the instability problem of a single truss. So in order to explore the connection mode and performance between the trusses with different structural forms, this paper conducts experimental research on triangular girder trusses.

MATERIAL AND METHODS

In order to explore the influence of the mechanical properties of triangular girder trusses with different diameter wood dowels, static loading tests were carried out on the Fink double trusses with 6 m span and 1.5 m height of different connection modes according to GB/T 50329 (2012). The number and identifier of specimens were shown in Tab. 1. Among them, ST stands for single truss, GT for girder truss.

Tab. 1: Number and identifier of trusses.

Type of trusses	Two single trusses	Double girder trusses		
Wood dowel	-	16 mm	18 mm	20 mm
Identifier	ST-1	GT-D16-1	GT-D18-1	GT-D20-1
	ST-2	GT-D16-2	GT-D18-2	GT-D20-2

Materials

The material used in the test was *Larix gemlimii*, imported from Russia. The material grade was class II, section sizes were 38 mm x 89 mm. According to GB/T 50329 (2012), material parameters of the specimen were shown in Tab. 2. The density was 0.657 $g{\cdot}cm^{-3}$, and the moisture content was 17.4%, according to GB/T 1928 (2009). The tooth plates used in the experiment were galvanised and made in China. The performance parameters were shown in Tab. 3.

Tab. 2: Material parameters of specimens (units: MPa).

Modulus of elasticity	Modulus of rupture	Compressive strength along grain	Tensile strength along grain	Transverse compressive strength
12220.9 ± 6.21*	85.32 ± 1.18*	45.15 ± 4.3*	10.21 ± 1.25*	7.6 ± 1.8*

*Standard deviation.

Tab. 3: Performance parameters of tooth plate.

Tooth plate thickness (mm)	Density of plate teeth (each/mm²)	Length of plate teeth (mm)	Elastic modulus of steel (GPa)	Tensile yield strength of steel (MPa)
0.90	0.012	8.6	203	248

Specimen processing

The single truss was connected by tooth plates, which was first positioned manually and then pressed by a flat press with a pressure of 13 MPa. The processing of girder truss was based on two single trusses that were stacked. The joint position was drilled out in advance to ensure that the hole diameter was 0.5 mm smaller than wood dowels, which ensured a tight connection. The location of wood dowels in Fig. 1 was selected according to the mechanical characteristic of the truss joints. On this basis, a pistol drill or bench drill was used to drill wood dowels into the holes to form joints. Among them, The wood dowel was *Fagus sylvatica* with a diameter of 16 mm,18 mm or 20 mm and a length of 80 mm.

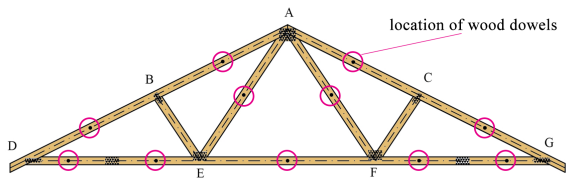

Fig. 1: The dowel joints location.

Loading system and device

The test was carried out based on the method of hierarchical loading test for trusses in the standard for test methods of timber structures GB/T 50329 (2012), and the loading system was shown in Fig. 2, where P_k was calculated according to the Load code for the design of building structures GB 50009 (2012), and the result was P_k = 4.6 kN.

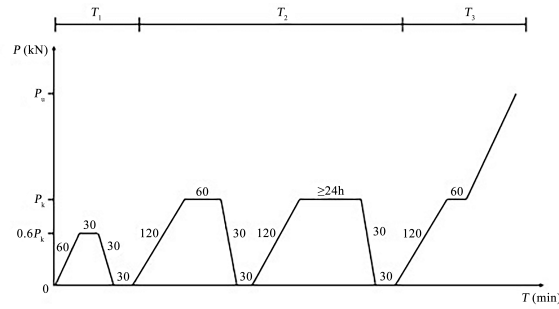

Fig. 2: Continuous loading system according to GB/T 50329 (2012).

The loading procedure was divided into three stages: pre-loading stage T_1, standard loading stage T_2 and destructive loading stage T_3 (Fig. 2). The loading device in Fig. 3 was designed on the basis of the microcomputer-controlled elector-hydraulic servo combined shear wall experimental system. Due to the large span of the truss and its poor stability during loading, o ensure the test, the anti-roll device was essential for the loading of the wood trusses. Based on comprehensive laboratory conditions, this study designed an anti-roll device suitable for this test based on the supporting device that comes with the test machine, as shown in Fig. 3b. The screw was used to connect the anti-rolling wood strip to the support device of the testing machine itself, and to ensure that the wood strip was infinitely close to the truss, so that every part of the truss was laterally supported, ensuring the stability of the entire truss load.

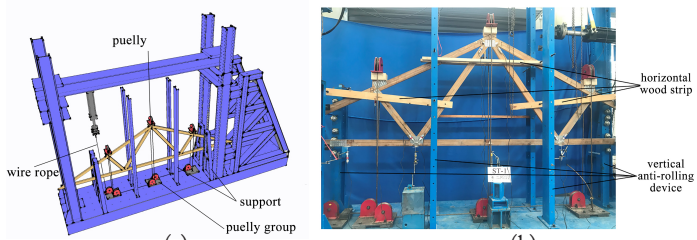

Fig. 3: Loading device: (a) design drawings device, (b) practical setting.

RESULTS AND DISCUSSION

Analysis of experimental phenomena

The trusses under preloading stage T_1 and standard loading T_2 stages all showed good performance. While in the destructive loading stage T_3, the failure modes of trusses were the roughly same. The tooth of the metal tooth plate at the support joints D and G started to separate from the wood, finally occurring the tooth plate separation failure. ST-1 showed no obvious experimental phenomena in preloading stage T_1 and standard loading T_2 stages. When the load increased to about 5.50 kN, G-joint (Fig. 4a) appeared slightly bulging. When the load increased 8.36 kN, G-joint in Fig. 4b showed tooth plate separation failure. GT-D16-1 showed no obvious experimental phenomena in preloading stage T_1 and standard loading T_2 stages. When the load increased to about 12.90 kN, each tooth plate at D-joint (Fig. 5a) appeared slightly bulging. Meanwhile, the tooth plates of the double girder truss between the two single trusses also showed slightly bulging at G-joint (Fig. 5b). With the increase of the load, the tooth plates slightly bulged and gradually evolved into tooth plate separation. When the load reached 19.26 kN, each D-joint tooth plate (Fig. 5c) completely separated from the lower chord.

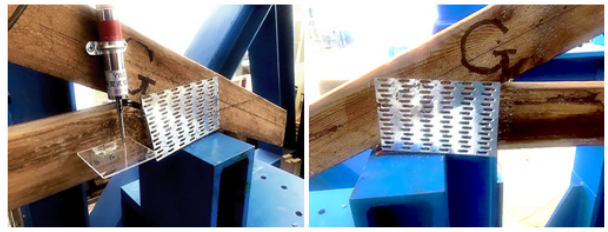

(a) (b)

Fig. 4: The failure phenomena of ST-1: (a) load 5.50 kN, (b) load 8.36 kN.

(a) (b) (c)

Fig. 5: The failure phenomena of GT-D16-1: (a) D-joint at 12.90 kN, (b) G-joint at 12.90 kN, (c) D-joint at 19.26 kN.

However, the test did not stop after the tooth plate separation failure at the support joint. Two single trusses lost the bearing performance, while the girder truss showed wood split failure at B-joint when the load reached about P_k. The phenomenon was shown in Fig. 6. It showed that compared with two single trusses, girder truss had better security performance. At the end of each test, the wood dowels were taken out, as shown in Fig. 7. The figure showed that there were no obvious phenomena in wood dowels. This meant the wood dowel could remain in the elastic range when the final damage occurred, so the coordination between the two single trusses could be maintained very well.

(a) (b)

Fig. 6: Wood tearing failure under loading B-joint: (a) front, (b) back.

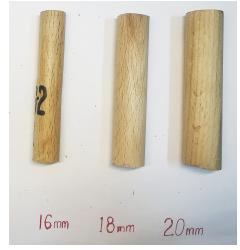

Fig. 7: Three kinds of wood dowels after test.

In summary, all the wood trusses suffered from tooth plate separation failure at the support joints. When it continued loading after the damage, a second failure would occur at the loading point B, indicating that the loading point was the second weakest link of the triangular wood truss. From the analysis of the axial force of single triangular wood truss (Fig. 8) could be seen that the axial forces at the rod ends of BD and CG were the largest, so the rod ends of BD and CG were the weakest part of the truss. The test results were consistent with the theoretical predictions.

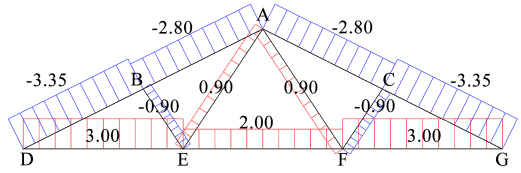

Fig. 8: The axial force of single triangular wood truss.

Stability performance of truss

As shown in Fig. 9, the mid-span deflection of the lower chord of each truss was obtained, showing that GT-D20 truss had the lowest degree of dispersion, which indicated that the performance of this kind was more stable. It was not difficult to find from the figure that the four types of trusses all showed normal test conditions, and had good consistency in first two stages, and the variability of wood made different types of trusses had different results in the third stage. From the mid-span load-deflection curves of T_1 and T_2 stages (Fig. 10) can be seen that the degree of dispersion of the curve was GT-D18 > GT-D16 > GT-D20 within the girder trusses. Combining the two curves found that the stability performance of 20 mm dowel-connected girder truss was the best.

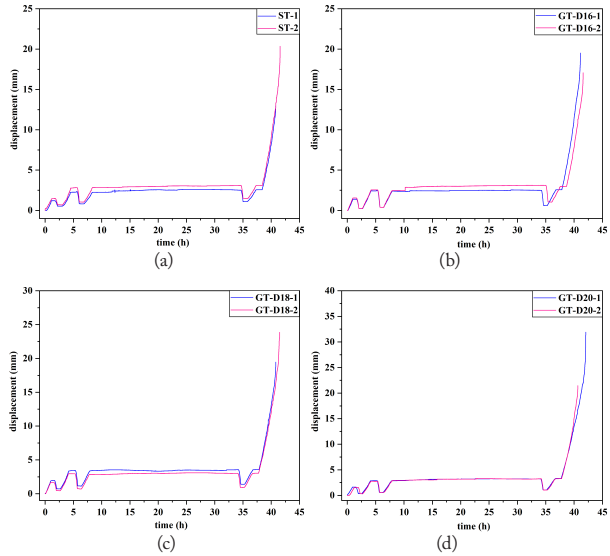

Fig. 9: Displacement variation in the middle of the lower chord span of each truss: (a) ST, (b) D16, (c) D18, (d) D20.

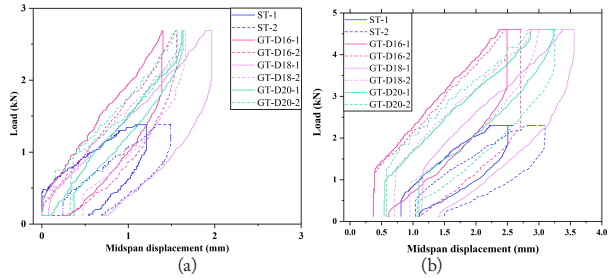

Fig. 10: The mid-span load-displacement curves: (a) T1 stage, (b) T2 stage.

Energy dissipation performance of truss

The area covered by the load-displacement curve in stage T_2 could be obtained, as shown in Tab. 4. The area represented the energy dissipation performance of the truss. From Tab. 4, it could be seen that the area covered by load displacement curve of GT-D16 truss was the largest, which showed the energy dissipation performance of the 16 mm dowel-connected triangular girder truss was the best. Compared with the energy dissipation performance of ST, GT-D16 increased by 184%, GT-D18 increased by 165%, and GT-D20 increased by 110%. When the standard load had completed, each truss entered the stage of elastic recovery. After unloading and 30 minutes of no-load, each truss had plastic deformation. The elastic recovery size and the percentage of the recovery size to the end deflection of the continuous load were shown in Tab. 5. As could be seen, the elastic recovery capacity of double girder trusses was stronger than two single trusses, and all were above 60%.

Tab. 4: Area wrapped in load-displacement curve of truss joints.

Identifier of truss	Area wrapped in load-displacement curve (joints /mm^2)						
	Node A	Node B	Node C	Mid-span	Node E	Node F	Average
ST	1.29	1.25	1.26	1.96	1.22	1.19	1.36
GT-D16	3.77	4.37	3.60	5.21	2.91	3.30	3.86
GT-D18	4.31	3.81	3.53	4.06	3.08	2.79	3.60
GT-D20	2.01	3.06	2.51	4.70	2.53	2.34	2.86

Tab. 5 : Elastic recovery of truss after unloading.

Identifier of truss	Elastic recovery size of lower chord (joints/mm)			
	Mid-span	Node E	Node F	Average
ST-1	1.42 (55.3)	1.13 (59.2)	1.16 (65.9)	1.34(56.2)
ST-2	1.62 (52.1)	1.42 (56.3)	1.24 (52.5)	
GT-D16-1	1.89 (73.5)	1.60 (71.4)	1.60 (71.7)	1.64(66.9)
GT-D16-2	1.68 (56.4)	1.53 (63.8)	1.51 (64.3)	
GT-D18-1	2.16 (60.5)	1.85 (60.3)	1.70 (70.0)	1.74(62.2)
GT-D18-2	2.07 (67.9)	1.57 (54.5)	1.74 (59.8)	
GT-D20-1	2.16 (64.9)	1.92 (69.6)	1.67 (75.9)	1.95(70.3)
GT-D20-2	2.20 (67.3)	2.12 (67.9)	1.67 (75.9)	

*Values in brackets represent % of the recovery size to the end deflection of the continuous load.

Residual deformation of truss

The residual deformation of the truss after unloading could be obtained from the second part of the load-displacement diagram of stage T2, as shown in Tab. 6. It could be seen from the table that the residual deformation of GT-D16 was the smallest, but only 0.09 mm different from that of GT-D20 truss. Therefore, the creep-resistant deformation ability of 16 mm dowel-connected girder trusses were similar to 20 mm dowel-connected girder truss, but the former was better.

Ultimate bearing capacity of truss

The residual deformation of the truss after unloading could be obtained from the second part of the load-displacement diagram of stage T_2, as shown in Tab. 6. It could be seen from the table that the residual deformation of GT-D16 was the smallest, but only 0.09 mm different from that of GT-D20 truss. Therefore, the creep-resistant deformation ability of 16 mm dowel-connected girder trusses were similar to 20 mm dowel-connected girder truss, but the former was better.

Tab. 6: Residual deformation of truss lower chord after T2 unloading (units: mm).

Identifier of truss	Mid-span	Node E	Node F	Average
ST	1.29	0.93	0.9	1.04
GT-D16	0.82	0.66	0.70	0.73
GT-D18	0.97	1.12	1.04	1.04
GT-D20	1.05	0.85	0.55	0.82

Ultimate bearing capacity of truss

In the destructive loading stage T_3, all trusses suffered from tooth plate separation failure at the bearing joints. However, the maximum bearing capacity of each truss was different due to the different performance of trusses and the influence of wood variability. The ultimate bearing capacity of various truss tests was shown in Fig. 11. The maximum bearing capacity of ST, GT-D16, GT-D18 and GT-D20 was 26.91 kN, 55.68 kN, 57.96 kN and 60.42 kN respectively. It could be seen that the ultimate bearing capacity of truss was GT-D20 > GT-D18 > GT-D16 > ST. The bearing capacity of the double girder trusses was 2.06-2.25 times that of two single trusses. According to the relationship between wood dowel diameter and ultimate bearing capacity of truss, they were proportional. The results showed that the bearing capacity of the triangular girder truss connected by 20 mm wood dowels was the strongest.

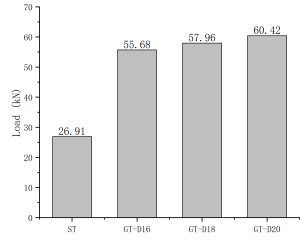

Fig. 11: Ultimate bearing capacity of various types of trusses.

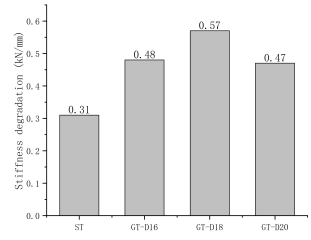

Fig. 12: Stiffness degradation.

Stiffness of truss

The stiffness of the two-stage truss was obtained from the load-displacement diagrams of stage T_2 and stage T_3, respectively, as shown in Tab. 7 and Tab. 8. From Tab. 8, it could be seen that the stiffnesses of girder trusses were GT-D16 > GT-D18 > GT-D20 > ST. From Tab. 7 and Tab. 8, it could be seen that the stiffness degradation of the two stages trusses was obvious, and the degradation sizes were shown in Fig. 12. The stiffness degradation of GT-D18 was the greatest among the wood dowel-connected girder trusses, while GT-D16 and GT-D20 were smaller, which indicated that GT-D16 and GT-D20 had good synergy.

Tab. 7: Curve stiffness during loading in T2 stage (units: kN·mm^{-1}).

Identifier of truss	Mid-span	Node E	Node F	Average
ST	1.11	1.27	1.44	1.27
GT-D16	1.88	2.22	2.27	2.12
GT-D18	1.66	1.99	2.34	2.00
GT-D20	1.62	1.66	2.15	1.81

Tab. 8: Curve stiffness during loading in T3 stage (units: kN.mm-1).

Identifier of truss	Mid-span	Node E	Node F	Average
ST	0.80	1.03	1.04	0.96
GT-D16	1.44	1.74	1.75	1.64
GT-D18	1.25	1.49	1.55	1.43
GT-D20	1.15	1.37	1.50	1.34

Discussion

Researches on wood trusses mostly focus on the repair technology, metal tooth plate connection of single truss and light wood truss system. In contrast, the study of girder trusses has hardly been involved (Gupta et al. 2005, Gupta et al. 2004, Rittenburg et al. 2003, Via et al. 2001, Munafò et al. 2015, Fauziyah et al. 2016, Underwood et al. 2001, Song et al. 2012, Gupta et al. 2004, Cabrero et al. 2009, Islam et al. 2017, Mohamadzadeh et al. 2015, Guntekin 2007, 2009, Sandanus et al. 2016, Moya et al. 2017) due to the common use of girder trusses in engineering, which has no design value reference. This raises several security issues. In the previous study (Wang et al. 2019, Gao 2017), the team members found that the connection of parallel chord girder trusses connected with wood dowels had a good synergistic effect and could effectively solve the instability problem of a single truss. So in order to explore the connection mode and performance between the trusses with different structural forms, this paper conducts experimental research on triangular girder trusses. It could be seen from the pre-loading stage that the residual deformation of the wood dowel-connected girder trusses were much smaller than that of the common wood trusses in previous research. The deflection value of corresponding joints at the loading stage of standard load was larger than that at the pre-loading stage, indicating that the increase of holding load would affect the deflection value, and the greater the holding load, the greater the deflection value. Under the same load, the length of load holding time had a certain influence on the deflection of truss during load holding period.

The support joint was the weak link of truss. The separation of the teeth started from the metal tooth plate at the support joint, then evolved into partial separation failure, and finally occurred complete separation failure. There was no significant failure phenomenon at other joints,

and the load during the separation of the teeth was about two-thirds of the maximum load. After the separation failure of the support joint, loading continued. The second failure occurred for wooden trusses after they were loaded to the size of P_k, which was the split failure of the wood at joint B, indicating that the girder trusses had good safety.

Except for an indentation on the surface of the dowel with a diameter of 16 mm, there was no obvious phenomenon in the other two kinds. The results showed that compared with two single trusses, the dowel-connected girder had better synergies. In the multiple wood trusses connected with wood dowels, the stiffness was inversely proportional to the ultimate bearing capacity, and inversely proportional to the diameter of the wood dowels.

CONCLUSIONS

Above all static loading tests were carried out on triangular girder truss with different diameter wood dowels. The following conclusions were obtained by analysing the experimental phenomenon of various types of trusses in the destructive loading stage T_3 and the experimental data of preloading stage T_1, standard load loading T_2 and destructive loading stage T_3. From failure mode, the wood dowel joints still had structural load-carrying capacity after the first failure, and the second failure occurred when the continuous loading reached the P_k value, which indicated that the girder truss connected by wood dowels had better safety. At the same time, there was a good synergy between the wood dowels and the girder trusses. The 20 mm wood dowel-connected girder truss had the best stability performance, the better bearing capacity of 60.42 kN and deformation resistance of 0.82 mm. From the ultimate bearing capacity of truss, the bearing capacity of the double girder trusses was 2.06-2.25 times that of two single trusses, which had the ability to 'one plus one is greater than two'. The energy dissipation performance of girder truss connected with 16 mm diameter wood dowel increased by 184% was the best and deformation resistance of 0.73 mm, slightly better than the 16 mm one. From the comprehensive performance, the 20 mm wood dowel-connected girder truss had the best connection effect in the triangular girder trusses.

ACKNOWLEDGMENTS

This work was supported by the Special Fund for National Natural Science Foundation of China(Project No. 31670566) and National Key Technology Research and Development Program for the 12th Five-year Plan of China(No. 2015BAD14B05).

REFERENCES

1. Cabrero, J.M., Gebremedhin, K.G., 2009: Finite element model for predicting stiffness of metal-plate-connected tension-splice and heel joints of wood trusses. Transactions of the Asabe 52(2): 565-573.
2. Que, Z., Li, Z., Wang, F., Wang, Y., Wang, Y., 2015: Influence of high salinity environment on shear strength of wood frame structures. Industrial Construction 45(9): 81-85.
3. Fauziyah, S., Soesilohadi, R.C.H., Retnoaji, B., Alam, P., 2016: Dragonfly wing venous cross-joints inspire the design of higher-performance bolted timber truss joints. Composites Part B 87: 274-280.

4. Gao, Y., 2017: Design and optimization of girder truss joints. Pp 20-41, Nanjing Forestry University.
5. GB/T 50329, 2012: Standard for test methods of timber structures. Profession standards of the People's Republic of China.
6. GB 50009, 2012: Load code for the design of building structures. Profession standards of the People's Republic of China.
7. Gupta, R., Miller, T.H., Kittel, M.R., 2005: Small-scale modeling of metal-plate-connected wood truss joints. Journal of Testing and Evaluation 33(3): 139-149.
8. Gupta, R., Miller, T.H., Redlinger, M.J., 2004: Behaviour of metal-plate-connected wood truss joints under wind and impact loads. Forest Products Journal 54(3): 76-84.
9. Gupta, R., Miller, T.H., Freilinger, S.M.W., 2004: Short-term cyclic performance of metal-plate-connected wood truss joints. Structural Engineering and Mechanics 17(5): 627-639.
10. Guntekin, E., 2007: Bending moment capacity of metal plate connected wood-splice joints constructed with red pine (*Pinus brutia* Ten.) lumber. Turkish Journal of Agriculture and Forestry 31(3): 207-212.
11. Guntekin, E., 2009: Performance of Turkish calabrian pine (*Pinus brutia* Ten.) timber joints constructed with metal plate connectors. Wood Research 54(3): 99-108.
12. He, S., Shang, P., Yang, B., Jiang, T., Yan, W., Zhu, Y.,2015: Influence of corrosion inducing treatment on shear behavior of bamboo nail and steel nail. China Forestry Science and Technology 29(2): 90-94.
13. Islam, A.K.M.A., Phillips, D., 2017: An experimental analysis of a timber Howe truss. Structures 10:39-48.
14. Madsen, B., 1992: Structural behavior of timber. Engineering Ltd. Vancouver, 10 pp.
15. Mohamadzadeh, M., Hindman, D.P., 2015: Analysis of metal plate connected wood truss assemblies under out-of-plane loads. Structures Congress 2015: 2021-2031.
16. Prochazka, J., Bohm, M., Svitak, M., 2014: Diverse influence of user-economic aspects to truss and rafter roof systems and their comparison. Wood Research 59(3): 449-458.
17. Rittenburg, K.A.W., Kunnath, S.K., 2003: Deflection of metal plate connected wood trusses with nontriangulated openings. Journal of Structural Engineering-ASCE 129(11): 1546-1558.
18. Moya, R., Tenorio, C., 2017: Strength and displacement under tension and compression of wood joints fastened with nails and screws for use in trusses in Costa Rica. Wood Research 62(1): 139-155.
19. Munafò P., Stazi F., Tassi C., Davì F., 2015: Experimentation on historic timber trusses to identify repair techniques compliant with the original structural–constructive conception. Construction and Building Materials 87(15): 54-66.
20. Underwood, C.R., Woeste, F.E., Dolan, J.D., Holzer, S.M., 2001: Permanent bracing design for MPC wood roof truss webs and chords. Forest Products Journal 51(7-8): 73-81.
21. Song, X., Lam, F., 2012: Stability analysis of metal-plate-connected wood truss assemblies. Journal of Structural Engineering 138(9): 1110-1119.
22. Sandanus, J., Sogel, K., Slivansky, M., 2016: Results of rheological test on timber trusses. Wood Research 61(2): 235-242.
23. Via, B.K., Zink-Sharp, A., Woeste, F., Dolan, J.D., 2001: Influence of specific gravity on embedment gaps in metal-plate-connected truss joints. Forest Products Journal 51(10): 88-92.

24. Wang, F., Teng, Q., Gao, Y., Chen, Q., Wang, C., Que, Z., 2019: Static load test and bearing capacity of timber girder truss. Journal of Civil and Environmental Engineering 41(2): 86-92.
25. Zhang, J., Zhong, Y., Zhao, R., Zhou, H., 2012: Reviews of mechanical properties for timber bolted joints. China Wood Industry (04): 39-42.
26. Yang, X.J., Zhao, Q., Hao, D., Wang, J.Y., Fu, S., Ma, L., 2020: Flexural behavior of OSB reinforced wood truss. Wood Research 65(2): 245-256.
27. Yang, L., 2014: The influence on properties of wood structure in high temperature high humidity and high salinity. Pp 15-36, Nanjing Forestry University.
28. GB/T 1928, 2009: General requirements for physical and mechanical tests of wood. Profession standards of the People's Republic of China.

Liuliu Zhang, Cheng Chang, Shuming Yang,
Tongyu Hou, Yifan Liu, Zeli que*
Nanjing Forestry University
College Of Material Science And Engineering
Nanjing 210037
P.R. China
*Corresponding author: zelique@njfu.edu.cn

WOOD RESEARCH
e-ISSN 2729-8906
66(3):2021 489-504 pp.
doi.org/10.37763/wr.1336-4561/66.3.489504

AXIAL COMPRESSION TESTING OF BAMBOO PLYWOOD-ENCASED THIN-WALLED STEEL TUBE/STONE DUST CONCRETE COLUMNS

Weifeng Zhao
Guangdong Construction Polytechnic
China

Weifeng Zhao, Zongjian Luo, Yajun Li
Xiangtan University
College Of Civil Engineering And Mechanics
China

Jing Zhou
South China University Of Technology
China

(Received November 2020)

ABSTRACT

A novel structural member, the bamboo plywood-encased thin-walled **s**teel tube/stone dust concrete composite **c**olumn (BSDCC), was investigated in this study. Axial compression tests were conducted on 10 BSDCC specimens; their failure characteristics and modes were examined, and the effects of the stone-dust concrete content ratio and strength, specimen slenderness ratio, cross-sectional composition and binding bar confinement pattern, and binding bar spacing ratio on the bearing capacity and deformation of the columns were investigated. Two main compressive failure modes were observed: *(1)* adhesive failure by cracking and debonding between the bamboo plywood boards and between the bamboo plywood and the steel tube and *(2)* compressive-flexural failure of the bamboo plywood between the binding bars in the middle of the specimen. For specimens with the same cross-sectional dimensions, the cross-sectional content ratio of the stone dust concrete impacted the deformation and failure mode but did not significantly affect the ultimate bearing capacity. The bearing capacity decreased with increasing specimen slenderness and binding bar spacing ratio and increased with increasing stone dust concrete strength and bamboo plywood constraint (in terms of the cross-sectional composition and binding bar restraint pattern). A model for the ultimate bearing capacity of BSDCCs was established through regression analysis.

KEYWORDS: Bamboo plywood, thin-walled steel tube, stone dust concrete, composite column, axial compression testing.

INTRODUCTION

The dwindling engineering wood supply and growing acceptance of sustainably developed green building materials have resulted in the widespread use of bamboo as a renewable biomass material in the civil engineering field (Sharma et al. 2015, Zhang et al. 2015, He et al. 2015). In particular, the successful development of laminated bamboo has broadened the application of bamboo in engineering (Reynolds et al. 2016, Kumar et al. 2016). Tian et al. (2019) studied the compressive behaviour of sprayed composite mortar-original bamboo columns and found that their ultimate load and ductility are 1.5 and 2.6 times higher than those of the original bamboo column, respectively. Li et al. (2017) reported that the axial load bearing capacities and the initial stiffness of both concrete-filled and cement-mortar-filled bamboo columns are much higher than those of conventional bamboo columns. Moroz et al. (2014), Siddika et al. (2017), and Nayak et al. (2013) considered the use of bamboo-reinforced concrete members as an alternative to the use of steel members. Li et al. (2015, 2016, 2019) investigated the mechanical performance of laminated bamboo columns under axial and eccentric compression over a wide range of slenderness ratios and eccentricities. Wei et al. (2016) investigated the eccentric compression performance of a novel bamboo column and proposed a calculation method. Zhao et al. (2019, 2020) proposed a novel structural member: a thin-walled steel tube/bamboo plywood composite column with binding bars (SBCCB). The compression damage of a SBCCB was found to primarily occur by breaking of the bamboo plywood and adhesive failure between the matrix interfaces at the end and middle of the column between the binding bars.

There are very few studies on the application of stone dust. Aliabdo et al. (2014) studied the performance of concrete in which marble stone dust was used to replace cement or river sand. Kandolkar et al. (2015) used recycled stone dust as an admixture in the construction of bamboo or steel-reinforced concrete walls. Arel et al. (2016) conducted experiments to determine how replacing cement with stone dust affected the mechanical properties of a concrete. Singh et al. (2016) replaced a portion of river sand with stone dust and investigated the durability of the resulting concrete. Febin et al. (2019) found that the compressive and splitting strengths of cement blocks were significantly improved by the incorporation of stone dust. However, studies on the application of stone dust are still scarce (Zheng et al. 2017). Because the use of stone dust in large amounts as concrete admixtures decreases the strength of the concrete, research on the applications of stone dust could have enormous social and economic benefits.

In the present study, a novel bamboo plywood-encased thin-walled steel tube/stone dust concrete composite column (BSDCC) was proposed to integrate the utilization of stone dust waste and bamboo plywood. The composite column in this study is clearly different from the bamboo plywood and thin-walled steel tube hollow-core column (the SBCCB) proposed by Zhao et al. (2019, 2020). In a BSDCC, the square thin-walled steel tube is filled with low-strength stone dust concrete, which not only disposes of a large amount of industrial solid waste but also promotes the recycling and reuse of waste resources; the resulting composite column has a steel tube/concrete configuration, which has better and more stable mechanical properties than those corresponding to the SBCCB configuration because the new form changes the force failure mechanism. The new type of composite column adopts a cross-sectional configuration of bamboo plywood and a thin-walled steel tube to constrain the stone dust concrete. The thin-walled steel tube plays the role of not only a lining but also a water barrier between the stone dust concrete and the bamboo plywood; at the same time, including binding bars can result in a good hoop effect, increase the horizontal restraint force, and improve the integrity of the composite column. Axial compression tests were carried out on 10 BSDCC specimens to examine the failure characteristics

and modes of the specimens and investigate the effects of the bearing capacity and deformation of the specimen on the failure characteristics and modes.

MATERIAL AND METHODS

Specimen preparation

Ten BSDCC specimens were subjected to axial compression tests. The parameters of the specimens are listed in Tab. 1, the cross-sectional compositions and binding bar confinement patterns are shown in Fig. 1, and the configuration is shown schematically in Fig. 2a. Specimens AC-1, AC-2, and AC-3 were compared to examine the effects of the cross-sectional content ratios of stone dust concrete and bamboo plywood. Specimens AC-2, AC-4, and AC-5 were compared to investigate the influence of the slenderness ratio λ. Specimens AC-4, AC-6, and AC-7 were compared to study the effect of the cross-sectional composition and binding bar confinement pattern. Specimens AC-5, AC-8, and AC-9 were compared to study the effect of the binding bar spacing ratio (r_1). Specimens AC-6 and AC-10 were compared to examine the influence of the stone dust concrete strength. The λ, stone dust concrete content ratio (ρ), and r_1 of a specimen were calculated using the following formulas:

$$\lambda = L/B \quad (1)$$

$$\rho = A_c/A \quad (2)$$

$$r_1 = s/B \quad (3)$$

where: L is the length of the specimen, B is the side length of the cross-section, A is the cross-sectional area of the specimen, A_c is the cross-sectional area of the stone dust concrete, and s is the spacing between the binding bars.

Tab. 1: Parameters of the specimens.

Specimen number	λ	Concrete strength (MPa)	Confinement patterns	Section of steel tube (mm)	Bamboo plywood layers	r_1	Bamboo plywood content ratio/%	Steel tube content ratio (%)	ρ (%)	L/mm
AC-1	8	9.0	□	60×60×2	4	2	81.6	1.2	17.2	1120
AC-2	8	9.0	□	80×80×2	3	2	67.3	1.6	31.1	1120
AC-3	8	9.0	□	100×100×2	2	2	49.0	2.0	49.0	1120
AC-4	12	9.0	□	80×80×2	3	2	67.3	1.6	31.1	1680
AC-5	16	9.0	□	80×80×2	3	2	67.3	1.6	31.1	2240
AC-6	12	9.0	□	80×80×2	3	2	67.3	1.6	31.1	1680
AC-7	12	9.0	□	80×80×2	3	2	67.3	1.6	31.1	1680
AC-8	16	9.0	□	80×80×2	3	1	67.3	1.6	31.1	2240
AC-9	16	9.0	□	80×80×2	3	3	67.3	1.6	31.1	2240
AC-10	12	14.2	□	80×80×2	3	2	67.3	1.6	31.1	1680

Material properties

Moso bamboo plywood, from the same batch, with dimensions of 2440 × 1220 × 10 mm^3 (length × width × thickness) was used in this work. The moisture content was 9%, the transverse and longitudinal static bending strengths were 52 MPa and 83 MPa, respectively, the transverse and longitudinal moduli of elasticity were 7.4 GPa and 8.3 GPa, respectively, and the longitudinal compressive strength was 24 MPa. Seamless thin-walled square steel tubes with a thickness of 2 mm and fully threaded Ø8 binding bars were used to create the specimens. The properties of the binding bars and thin-walled steel tubes were tested according to the GB/T228.1 standard (2011). The yield strength and elastic modulus of each steel tube were 350 MPa and 190 GPa, respectively. The yield strength and elastic modulus of each binding bar were 260 MPa and 193 GPa, respectively. EP120 epoxy resin AB glue (Ausbond, China) was used as an adhesive, which has a shrinkage ratio < 1%, tensile strength > 10 MPa, and shear strength < 12 MPa. The dust powder was provided by the Foshan Ceramics Plant and was air-dried and used as an admixture. The dust powder was incorporated as a cementitious material into concrete at a certain ratio to produce low-strength dust-powder-containing concrete. Uniaxial compressive strength tests were performed on the cubic specimens as per the GB/T50081 standard (2019). The stone dust concrete was designed to have compressive strength values of 9.0 MPa and 14.2 MPa and elastic moduli of 16.4 GPa and 21.7 GPa.

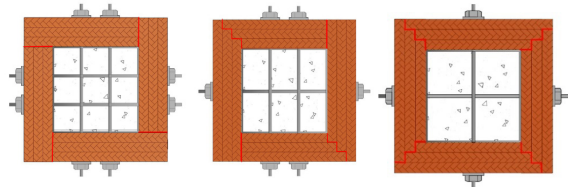

(a) *(b)* *(c)*

Fig. 1: Cross-sectional composition and binding bar confinement patterns: (a) pattern I; (b) pattern II; (c) pattern III.

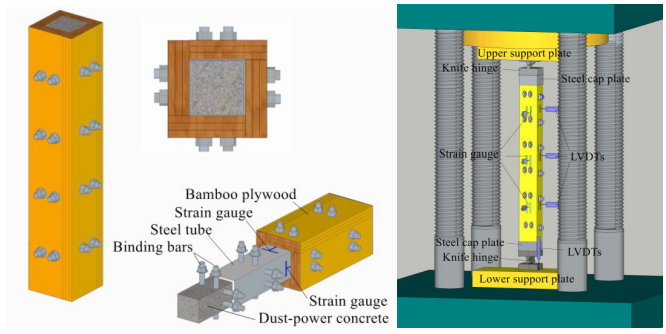

(a) *(b)*

Fig. 2: Schematic: (a) BSDCC components; (b) test device.

Test method

The test apparatus and measuring point arrangement are shown in Fig. 2b. Vertical loads were transferred to both ends of the specimen through unidirectional knife hinges. A steel cap plate with a depth of 40 mm was placed between the column end and the knife hinge plate to constrain the bamboo plywood at the column end, and a thin layer

of high-strength plaster was applied inside the steel cap plate for levelling. The longitudinal deformation of the specimen was measured by displacement gauges installed on the pressing plates of the testing machine. A total of six horizontal displacement gauges were placed on the upper, middle, and bottom surfaces of two adjacent sides of the specimen to measure the lateral deformation. The transverse and vertical strains of the thin-walled steel tube and bamboo plywood were measured by strain gauges arranged on the two adjacent sides of the thin-walled steel tube and bamboo plywood. The test loads, displacements, and strains were collected automatically by a static data acquisition system. The load was applied uniformly at a slow rate under displacement control. The test was terminated when the specimen underwent considerable cracking or its deformation increased rapidly, and the corresponding peak load was taken as the ultimate bearing capacity of the specimen.

RESULTS AND DISCUSSION

Phenomena and failure characteristics

The failure processes of all the specimens exhibited similar mechanical behaviour, while their failure modes had different characteristics due to the different parameters considered. At the initial stage of loading, the specimen was basically in an elastic stage. When the loading reached 50% to 60% of the ultimate load, intermittent short, faint cracking sounds were detected, and fine cracks occurred in the bamboo plywood between the binding bars, indicating adhesive cracking due to the shear stress and the normal tensile stress between the bamboo plywood boards exceeding the bond strength. As the load reached approximately 70% of the ultimate load, a loud cracking sound occurred, the original cracks gradually developed further, the bamboo plywood locally bulged outwardly, and the axial compressive deformation increased. At this time, the binding bars were tightened, and the bamboo plywood near the binding bars remained intact. As the peak load was approached, the cracks developed rapidly and approached the binding bars. A relatively loud cracking sound occurred, and the bamboo plywood between the binding bars in the middle of some specimens completely deboned, bulged, and failed under compression and flexure. In the failure zone, the bamboo plywood basically stopped resisting the load, and the stone dust concrete-filled steel tube bore the load alone. Due to its small cross-sectional dimensions, the concrete-filled steel tube had a limited lateral stiffness; hence, the lateral deflection in the middle of the column increased rapidly, causing the loss of the vertical bearing capacity and the overall failure of the specimen. The binding bars of each specimen were in a stable stress state and did not exhibit significant shear deformation or failure. The binding bars and the stone dust concrete-filled steel tube produced a confinement effect, which inhibited the development of adhesive cracking in the bamboo plywood, strengthened the deformation compatibility of various matrices, and improved the integrity of the composite column. The failure modes of the specimens are presented in Fig. 3, and Fig. 4 shows the failure process using specimen AC-3 as an example.

AC-1 AC-2 AC-3 AC-4 AC-5 AC-6 AC-7 AC-8 AC-9 AC-10

Fig. 3: Failure modes of all the specimens.

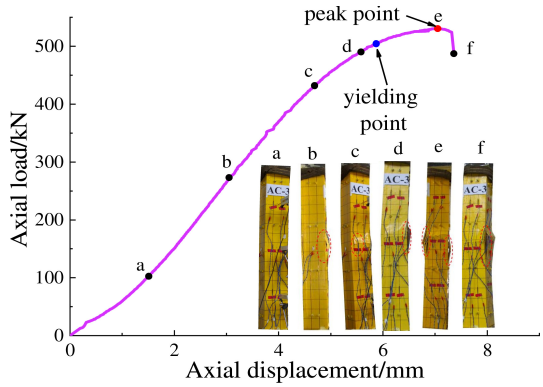

Fig. 4: Damage process of specimen AC-3.

As revealed by the test phenomena, the failure modes of the specimens differed to various degrees and can be divided into three main types, namely, the adhesive cracking and debonding of the bamboo plywood and thin-walled steel tube between the binding bars in the middle of the specimen, adhesive cracking between bamboo plywood boards, and bamboo plywood material failure under compression and flexure. In the compressive-flexural failure zone of the bamboo plywood, the thin-walled steel tube buckled at the corresponding location (Fig. 5c). The typical compressive failure modes are as follows: *(1)* Compressive-flexural failure of bamboo plywood on one side. For specimens AC-5, AC-8, and AC-9, which had relatively high slenderness ratios, the bearing surface was not perpendicular to the axis of the specimen due to inevitable material nonuniformities. Hence, the second-order effect of flexure occurred on the weak side of the specimen during the axial compression process and generated an additional bending moment, which led to nonuniform compression of the cross-section, causing compressive-flexural failure of the bamboo plywood on the side with a high compressive stress. *(2)* Compressive-flexural failure of bamboo plywood in a barrel shape. For specimens AC-1, AC-2, and AC-3, which had relatively low slenderness ratios, the second-order effect of flexure was relatively weak. During the loading process, each specimen was basically in an axial compression state, and the cross-section was relatively uniformly stressed. When the axial compression load was close to the ultimate bearing capacity, the bamboo plywood on each of the four sides of the core column basically reached the ultimate strength, thereby resulting in compressive-flexural failure of the bamboo plywood in a barrel shape, and the material strength was fully utilized

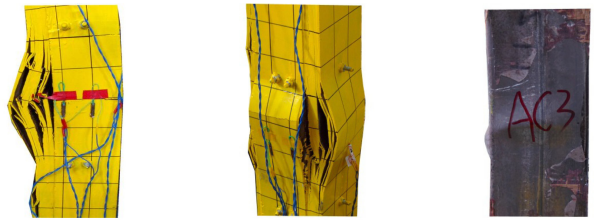

(a) *(b)* *(c)*

Fig. 5: Specimen failure modes: (a) bamboo plywood failure on one side of the specimen, (b) barrel-shaped bamboo plywood failure, and (c) buckling of the steel tube.

Load-displacement/strain responses

Effect of cross-sectional material content ratio

Fig. 6 compares the load-displacement/axial compressive strain curves of specimens AC-1, AC-2, and AC-3, which have different stone dust concrete and bamboo plywood content ratios. The three specimens had the same cross-sectional dimensions but had different net cross-sectional areas of stone dust concrete, bamboo plywood and thin-walled steel tubes, as shown in Tab. 1.

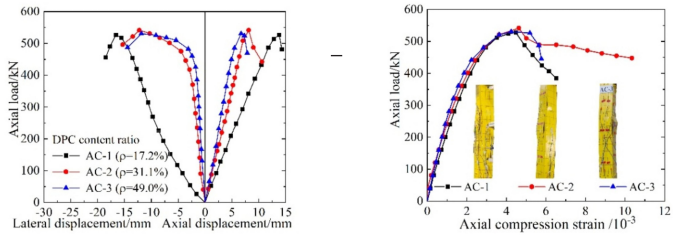

(a) *(b)*

Fig. 6: Effect of the material content ratio: (a) load-displacement curves and (b) bamboo plywood load-strain curves.

The three specimens differed little in ultimate bearing capacity (with a ratio of 1:1.03:1.01) but differed substantially in axial and lateral deformation. Specimen AC-1 had a low net cross-sectional ratio of stone dust concrete (17.2%) and a high net cross-sectional ratio of bamboo plywood (81.6%). Since the compressive strength and flexural stiffness of the stone dust concrete were higher than those of the bamboo plywood, specimen AC-1 had low overall axial and lateral stiffnesses and hence high axial and lateral deformation. The axial and lateral deformation values of specimen AC-2 were only slightly greater than those of specimen AC-3, indicating that overall, the two specimens had comparable axial and lateral stiffnesses. Specimen AC-3 had a greater net cross-sectional ratio of stone dust concrete (49.0%); thus, more dust powder waste could be utilized, but the load bearing capacity tended to decrease. Before the peak load was reached, the vertical strains of the three specimens were basically the same, whereas after the peak load, the vertical strain of the bamboo plywood in specimen AC-2 was the most fully developed, indicating that the bamboo strength was fully utilized. Overall, the cross-sectional material content ratio of a specimen had an important influence on its compression performance. The proportions of different components can be adjusted to obtain the optimized stiffness and bearing capacity to maximize the use of material strength.

Effect of the stone dust concrete strength

The load-displacement/axial compressive strain curves of specimens AC-6 and AC-10, which had different stone dust concrete strengths, are compared in Fig. 7. The compressive strength values of the stone dust concrete were 9.0 MPa and 14.2 MPa, respectively. The axial and lateral deformations of the two specimens were not significantly different, but the bearing capacity of specimen AC-6 was significantly lower than that of AC-10 (with a bearing capacity ratio of 1:1.14), indicating that the specimen with a high stone dust concrete strength had a relatively high bearing capacity. The stone dust concrete of specimen AC-10 had a greater elastic modulus; in the elastic deformation stage and under the same axial compression as that of specimen AC-6, the strain in specimen AC-10 developed more slowly, and the adhesive cracking and debonding failure of the bamboo plywood was delayed, thus resulting in a higher ultimate

bearing capacity. The vertical strain of the bamboo plywood in specimen AC-6 developed more thoroughly, indicating that the strength of the bamboo plywood material in AC-6 was better utilized and that the bamboo plywood resisted a greater portion of the vertical load. In the present study, only two specimens were designed to examine the influence of the stone dust concrete strength. More tests and numerical simulation analyses are needed further investigate the trend of the influence of stone dust concrete strength on the deformation compatibility and bearing capacity of such composite columns.

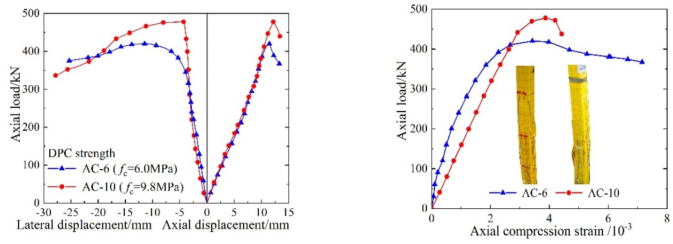

a) *(b)*

Fig. 7: Effect of the stone dust concrete strength: (a) Axial load-displacement curves; (b) bamboo plywood load-strain curves.

Effect of slenderness ratio

Fig. 8 shows the load-displacement/axial compressive strain curves of specimens AC-2, AC-4, and AC-5, which had different slenderness ratios (λ). λ had a significant impact on the ultimate compressive bearing capacity and deformation of the specimen, and the basic pattern was that a low λ corresponded to a high ultimate bearing capacity and low vertical and lateral deformations. The three specimens had the same cross-sectional dimensions and material composition ratios and hence the same axial compressive stiffness, but the specimen with a low λ underwent a relatively small compressive deformation ($\Delta L=NL/EA$, which is only related to the length of the specimen, where N is the axial load and EA is the stiffness of the specimen under axial compression). In addition, the specimen with a low λ had a high ultimate axial compressive strain of bamboo plywood, indicating that the material strength was more fully utilized. For example, specimen AC-2 (λ = 8) had a small axial compressive deformation, and its ultimate compressive strain was significantly greater than that of specimen AC-5 (λ = 16). According to the Euler principle, AC-5, with a high λ, had a lower ultimate bearing capacity, a relatively short linear elastic stage, and a reduced stability under axial compression than those of specimens AC-2 and AC-4, and specimen AC-5 was more sensitive to the second-order effect of flexure, leading to an increase in lateral deformation. The bearing capacities of specimens AC-2, AC-4, and AC-5 were at a ratio of 1:0.81:0.73, indicating that the bearing capacity decreased as λ increased. Specimen AC-4 (λ = 12) underwent the largest lateral deformation, probably because the local initial imperfection of bamboo plywood caused the earlier occurrence of the second-order effect of flexure. The vertical strain curve of the bamboo plywood in specimen AC-4 shows relatively fast development, with a difference from that of the other two specimens even in the initial stage and a long elastoplastic stage before the peak load.

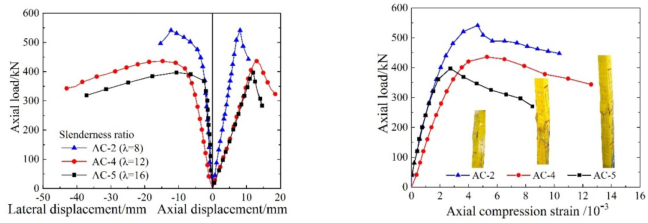

a) *(b)*

Fig. 8: Effect of the slenderness ratio: (a) Axial load-displacement curves; (b) bamboo plywood load-strain curves.

Effect of the cross-sectional composition and binding bar confinement pattern

Fig. 9 compares the load-displacement/axial compressive strain curves of specimens AC-4, AC-6, and AC-7, which had different cross-sectional composition and binding bar confinement patterns. As Fig. 9(a) shows, specimen AC-7 (pattern III) had the highest bearing capacity, specimen AC-4 (pattern I) and specimen AC-6 (pattern II) had similar bearing capacities, and the ultimate bearing capacities of AC-4, AC-6, and AC-7 had a ratio of 1:0.96:1.11, indicating that the bamboo plywood composition with a layer-staggered interlocking pattern and an increase in the number of transverse binding bars could improve the overall compressive bearing capacity. The composition effect was closely related to the interlocking of the inner and outer bamboo plywood boards at the bonding interface and the confinement by the binding bars. As shown in Fig. 1, if a single piece of bamboo plywood on the cross-section of the specimen had a width of *b*, the bonding interface at the end of specimen AC-7 (pattern III) had a length of 20*b*. The layer-staggered interlocking outer bamboo plywood suppressed the adhesive cracking failure of the inner bamboo plywood. The bonding interface at the end of specimen AC-4 (pattern I) had a length of 12*b*. Although there was no staggered interlocking confinement at the end of AC-4, this specimen had one additional binding bar compared to those of specimen AC-7 (pattern III) in each of the two directions of its cross-section. The binding bars and the concrete-filled steel tube in the core zone played the role of transverse stirrups, which produced a confinement effect and thus achieved the same composition effect. Specimen AC-6 (pattern II) was a combination of the construction of specimen AC-4 and specimen AC-7, clearly achieving an improved result. The development of the vertical strain in the bamboo plywood of specimen AC-7 was relatively short, indirectly indicating that the inner bamboo plywood, thin-walled steel tube, and stone dust concrete play a considerable role in the performance of this specimen.

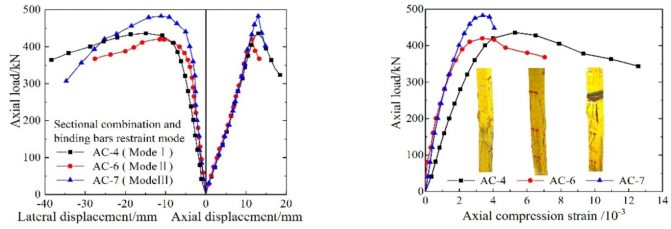

a) *(b)*

Fig. 9: Effect of the cross-sectional composition and binding bar restraint mode: (a) axial load-displacement curves; (b) bamboo plywood load-strain curves.

Effect of the binding bar spacing ratio

Fig. 10 compares the load-displacement/axial compressive strain curves of specimens AC-5, AC-8, and AC-9, which had binding bar spacing ratios (r_1) of 2, 1, and 3, respectively. The ultimate bearing capacities of these specimens exhibited a ratio of 1:0.89:0.94, so specimen AC-5 had the highest ultimate bearing capacity. The parameter r_1 directly affected the local adhesive cracking failure. A reasonable binding bar spacing could effectively improve the local buckling strength of the thin-walled steel tube and bamboo plywood. Through the confinement of the lateral deformation of the thin-walled steel tube and bamboo plywood, the failure mode of the specimen changed, and the bearing capacity improved. It can be seen from the comparison of the failure modes of the three specimens that the local cracking of the specimen significantly increased with r_1. The binding bars with a low r_1 worked with the thin-walled steel tube to produce a confinement effect, which effectively inhibited the local adhesive cracking and debonding of the bamboo plywood and enhanced the integrity of the composite specimen. In addition, the deformation and strain compatibility of the bamboo plywood and thin-walled steel tube increased, changing the compressive failure mode and thereby improving the compression and deformation resistance of the specimen. As shown in Fig. 10c, specimen AC-8, which had a low r_1, exhibited synchronized vertical strains in the bamboo plywood and thin-walled steel tube, indicating that the two materials could work together. For specimen AC-9, in the early stage of loading, the difference between the strains of the bamboo plywood and thin-walled steel tube was relatively small; as the axial load increased further, the vertical strains of the two materials became very different, resulting in a continuous decrease in the axial stiffness of the specimen. In addition, compared to AC-5 and AC-8, AC-9 had significantly low ultimate strains in these two materials, indicating that their material strengths were not fully utilized.

In specimen AC-8, local adhesive cracking failure occurred relatively late, and the axial compressive strain of the bamboo plywood was fully developed. However, its bearing capacity was not much different from that of specimen AC-9, which might be due to the deviation in the materials used for specimen preparation as well as in the installation process, a topic that needs to be further investigated in the future. Considering the product manufacturing process, a lower r_1 value does not lead to better structural performance. An r_1 value of 2 can be used to obtain a reasonable design.

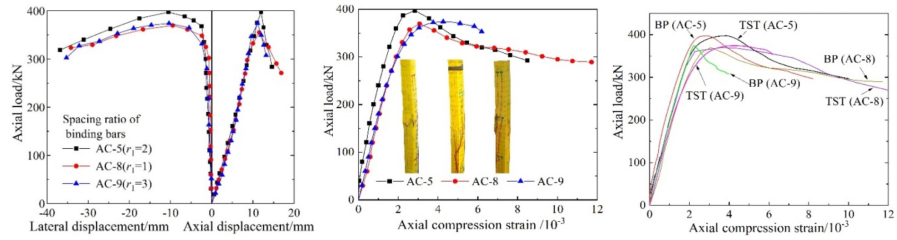

(a) *(b)* *(c)*

Fig. 10: Effect of the binding bar spacing ratio: (a) axial load-displacement curves, (b) bamboo plywood load-strain curves; (c) comparison of strain curves.

Characteristic points and ductility

Tab. 2 shows the characteristic points of the axial compressive load-deformation curves and the corresponding axial compression deformation ductility factors. In the ascending part of an axial compressive load-axial deformation curve, the equivalent energy method is

used to determine the yield load (N_y) and the yield displacement (Δ_y). In the descending part of the curve, the displacement corresponding to the time when the load drops to 85% of the peak load is taken as the ultimate displacement (Δ_u). The axial deformation ductility factor is defined in Eq. 4:

$$\mu = \Delta_u/\Delta_y \quad (4)$$

Bamboo has a high elastic deformation capacity but does not exhibit favourable elastoplastic or plastic deformation behaviours. For the BSDCCs studied here, the proportion of bamboo plywood in the cross-section was relatively large, and the stone dust concrete had a lower elastic modulus than ordinary concrete. Therefore, overall, the BSDCC specimens exhibited mechanical behaviour similar to that of bamboo. Compared to other concrete composite columns (Liu et al. 2015), the specimens tested in the present study exhibited higher axial compression yield displacement ratios (Δ_y/L) but did not have higher axial compression plastic displacement ratios ($(\Delta_u-\Delta_y)/L$). In particular, the bearing capacity of a specimen declined rapidly after the peak load, and the plastic deformation development stage was very short, indicating that the specimen did not demonstrate advantageous plastic deformation behaviour and underwent brittle failure. Hence, overall, the corresponding axial compression deformation ductility factor was relatively low. In future work, the cross-sectional configuration and the comprehensive performance of the design will need to be optimized in terms of ultimate bearing capacity and plastic deformation, and the cross-sectional content ratio of the stone dust concrete will need to be increased.

To further investigate the influence of the binding bar confinement pattern and the encased stone dust concrete on the axial bearing capacity of the specimen, the ultimate compressive stresses of the specimens tested in the present study are compared with those of thin-walled steel tube/bamboo plywood composite hollow short columns with a single row of binding bars (SBCCBs) (Zhao et al. 2020), as shown in Fig. 11. The average ultimate compressive stress of the SBCCBs is 20.29 MPa, while that of the BSDCCs is 23.23 MPa, amounting to a 14.53% increase. Thus, filling the steel tube with low-strength stone dust concrete significantly increased the average compressive stress of the specimens. Therefore, each BSDCC specimen had a relatively good coupling effect, which determined the failure mode of the specimen and caused the strength of the bamboo plywood to be fully utilized, highlighting the advantages of this new type of composite column.

Tab. 2: Characteristic points and specimen ductility.

Specimen number	N_y (kN)	Δ_y (mm)	Δ_y/L (%)	N_u (kN)	Δ_u (mm)	$(\Delta_u-\Delta_y)/L$ (%)	μ
AC-1	499.12	12.62	1.13	527	14.30	0.15	1.13
AC-2	526.29	7.64	0.68	541.4	9.81	0.19	1.28
AC-3	503.12	5.97	0.53	530.6	7.56	0.14	1.27
AC-4	482.78	12.61	0.75	436.08	16.17	0.21	1.28
AC-5	396.47	11.96	0.53	397.4	13.30	0.06	1.11
AC-6	413.62	11.64	0.69	420.25	13.29	0.10	1.14
AC-7	460.48	13.44	0.80	482.82	14.61	0.07	1.10
AC-8	350.28	11.23	0.50	369.6	15.60	0.20	1.39
AC-9	350.28	11.23	0.50	374.1	12.80	0.07	1.14
AC-10	466.55	12.66	0.75	477.8	13.40	0.03	1.06

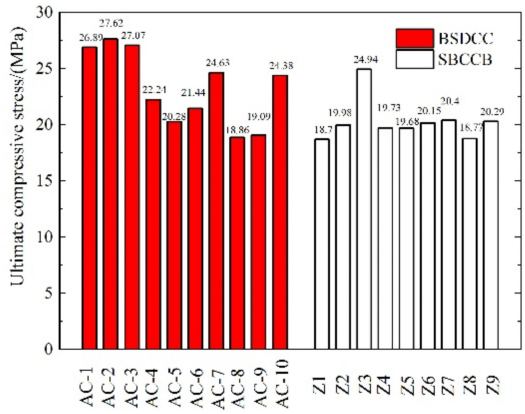

Fig. 11: Comparison of compressive stresses observed in this study with those observed in other studies (Zhao et al. 2020).

Model for estimating bearing capacity under axial compression

The ultimate bearing capacity of a BSDCC is affected by a multitude of factors but generally follows certain patterns. The axial bearing capacity of a BSDCC is not only related to factors such as the specimen slenderness ratio, stone dust concrete strength, and cross-sectional material content ratio but also affected by the cross-sectional composition and binding bar confinement pattern. According to the above analysis, the ultimate bearing capacities of specimens with patterns I and II were not very different, and those of pattern III were relatively high. Comprehensive consideration of the bearing capacity and manufacturing factors shows that the cross-sectional composition of pattern I is recommended; accordingly, the influence of the other patterns is not taken into account. With reference to the timber structure design standard (2017), a model for calculating the ultimate bearing capacity is established based on the superposition principle. The axial compression stability coefficient (φ) is decomposed into the product of the slenderness ratio influence coefficient (φ_λ) and the binding bar influence coefficient (φ_r). The bearing capacity model is constructed as follows:

$$N_u = \varphi_\lambda \varphi_r \left(f_b A_b + f_s A_s + f_c A_c \right) \tag{5}$$

$$\varphi_\lambda = \frac{1}{1+\left(\lambda / \alpha_1 \right)^2} \tag{6}$$

$$\varphi_r = 1 + \frac{\alpha_2 r_2}{r_1} \tag{7}$$

where f_b is the longitudinal compressive strength of the bamboo plywood, f_s is the yield strength of the thin-walled steel tube, f_c is the compressive strength of the stone dust concrete, A_b is the net cross-sectional area of the bamboo plywood, A_s is the net cross-sectional area of the thin-walled steel tube, A_c is the net cross-sectional area of the stone dust concrete, r_1 and r_2 are the relative spacing ratio and number of rows of the binding bars, respectively, and α_1 and α_2 are fitting parameters.

A nonlinear regression analysis was performed to obtain the simplified parameters

α_1 = 16.45 and α_2 = 0.11, with an overall correlation coefficient of R^2=0.85. Tab. 3 compares the test values and the calculation values of the ultimate bearing capacity, which have absolute errors of less than 15%, showing that the calculation results agree well with the test results.

Tab. 3: Comparison of the test and calculated results.

Specimen number	Test results N_{u1} (kN)	Calculated results N_{u2} (kN)	$(N_{u1}- N_{u2})/N_{u1}$ (%)
AC-1	527	522.2	0.91
AC-2	541.4	533.5	1.46
AC-3	530.6	534.0	-0.64
AC-4	436.08	440.9	-1.10
AC-5	397.4	342.1	13.92
AC-6	420.25	440.9	-4.91
AC-7	482.82	440.9	8.68
AC-8	369.6	375.9	-1.71
AC-9	374.1	339.1	9.36
AC-10	477.8	463.2	3.06

The bearing capacity calculation model was used to estimate the proportion of the bearing capacity provided by each material, as shown in Fig. 12. The bamboo plywood had a high cross-sectional content ratio and provided a large proportion of the bearing capacity. By comparison, the thin-walled steel tube had a low cross-sectional content ratio but a high strength and hence contributed a large proportion of the bearing capacity. Although the stone dust concrete had a high cross-sectional content ratio, its proportion of the bearing capacity was small due to the low strength of the stone dust concrete material. The stone dust concrete played a role in determining the failure mode of the specimen under stress, improved the compression stability, and decreased deformation of the specimen. As revealed by comparison, the further optimization of the cross-sectional content ratio of stone dust concrete or an appropriate increase in the strength of stone dust concrete is expected to optimize the comprehensive performance of this new type of composite column in terms of its compressive bearing capacity and deformation capacity.

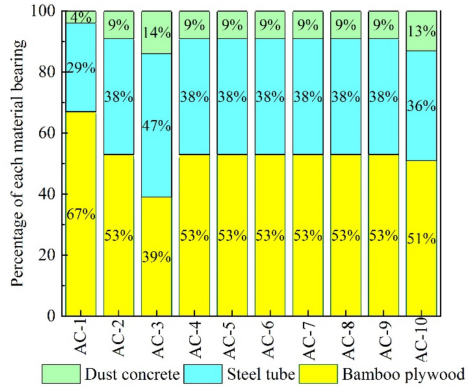

Fig. 12: Proportion of the bearing capacity.

CONCLUSIONS

Experimental investigations of the performance of BSDCC specimens in compression were conducted in this study. The following conclusions were drawn from the results: (1) The axial compressive failure modes of the new type of BSDCC mainly included the adhesive cracking and debonding failure between the bamboo plywood boards and between the bamboo plywood and the steel tube and the compressive-flexural failure of the bamboo plywood between the binding bars in the middle of the specimen. The thin-walled steel tube in the bamboo plywood compressive-flexural failure zone buckled locally. (2) The ultimate bearing capacity of the BSDCC decreased as the specimen slenderness ratio and binding bar spacing ratio increased and increased with increasing stone dust concrete strength. The stronger the confinement of the bamboo plywood due to the cross-sectional composition and binding bar confinement pattern, the higher the ultimate bearing capacity. For the specimens considered in the present study, the cross-sectional content ratio of stone dust concrete had no significant effect on the ultimate bearing capacity of the BSDCC. (3) The encased low-intensity stone dust concrete could interact with the thin-walled steel tube and binding bars to improve the compressive stiffness and stability of the BSDCC specimens, thereby controlling the axial compressive failure mode and deformation capacity of the composite column. (4) The model for calculating the ultimate bearing capacity of such a composite column under axial compression is proposed on the basis of the test results and has an absolute error of less than 15%. The calculation model can be used as a reference in future engineering applications.

ACKNOWLEDGMENTS

The authors acknowledge the financial support from the Science and Technology Planning Project of Guangzhou City (grant no. 201904010108) and the National Natural Science Foundation of China (grant no. 51708476).

REFERENCES

1. Arel, H.Ş., 2016: Recyclability of waste marble in concrete production. Journal of Cleaner Production 131:179-188.
2. Aliabdo, A.A., Abd Elmoaty, A.E.M., Auda, E.M., 2014: Re-use of waste marble dust in the production of cement and concrete. Construction and Building Materials 50: 28-41.
3. Febin, G.K., Abhirami, A., Vineetha, A., Manisha, V., Ramkrishnan, R., Sathyan, D., Mini, K., 2019: Strength and durability properties of quarry dust powder incorporated concrete blocks. Construction and Building Materials 228: 1-9.
4. GB/T228.1, 2010: Metallic materials-tensile testing: Method of test at room temperature.
5. GB 50005, 2017: Standard for design of timber structures.
6. GB/T 50081, 2019: Standard for test methods of concrete physical and mechanical properties.
7. He, M., Li, Z., Sun, Y., Ma, R., 2015: Experimental investigations on mechanical properties and column buckling behavior of structural bamboo. Structural Design of Tall and Special Buildings 24(7): 491-503.
8. Kumar, A., Vlach, T., Laiblova, L., Hrouda, M., Kasal, B., Tywoniak, J., Hajek, P., 2016: Engineered bamboo scrimber: Influence of density on the mechanical and water absorption properties. Construction and Building Materials 127: 815-827.
9. Kandolkar, S.S., Mandal, J.N., 2015: Behavior of reinforced stone dust walls under strip loading. Advances in Civil Engineering Materials 4(1):1-30.

10. Li, H.T., Chen, G., Zhang, Q.S., Ashraf, M., Xu, B., Li, Y., 2016: Mechanical properties of laminated bamboo lumber column under radial eccentric compression. Construction and Building Materials 121: 644-652.
11. Li, H.T., Liu, R., Lorenzo, R., Wu, G., Wang, L.B., 2019: Eccentric compression properties of laminated bamboo columns with different slenderness ratios. Proceedings of the Institution of Civil Engineers-Structures and Buildings 172:315-326.
12. Li, H.T., Su, J.W., Zhang, Q.S., Deeks, A.J., Hui, D., 2015: Mechanical performance of laminated bamboo column under axial compression. Composites Part B: Engineering 79: 374-382.
13. Li, W.T., Long, Y.L., Huang, J., Lin, Y., 2017: Axial load behavior of structural bamboo filled with concrete and cement mortar. Construction and Building Materials 148: 273–287.
14. Liu, Y., Guo, Z.X., Xu, P.H., Jia, L., 2015: Experimental study on axial compression behavior of core steel reinforced concrete. Journal of Building Structures 36(4): 68-74.
15. Moroz, J.G., Lissel, S.L., Hagel, M.D., 2014: Performance of bamboo reinforced concrete masonry shear walls. Construction and Building Materials 61: 125–137.
16. Nayak, A., 2013: Replacement of steel by bamboo reinforcement. IOSR Journal of Mechanical and Civil Engineering 8(1): 50–61.
17. Reynolds, T., Sharma, B., Harries, K., Ramage, M., 2016: Dowelled structural connections in laminated bamboo and timber. Composites Part B: Engineering 90: 232-240.
18. Siddika, A., Mamun, M., Siddique, M., 2017: Evaluation of bamboo reinforcements in structural concrete member. Journal of Construction Engineering and Project Management 7(4): 13–19.
19. Singh, S., Nagar, R., Agrawal, V., 2016: A review on properties of sustainable concrete using granite dust as replacement for river sand. Journal of Cleaner Production 126(10): 74-87.
20. Sharma, B., Gatoo, A., Bock, M., Ramage, M., 2015: Engineered bamboo for structural applications. Construction and Building Materials 81: 66-73.
21. Tian, L.M., Kou, Y.F., Hao, J.P., 2019: Axial compressive behaviour of sprayed composite mortar–original bamboo composite columns. Construction and Building Materials 215: 726-736.
22. Wei, Y., Zhou, M.Q., Yuan. L.D., 2016: Mechanical performance of glulam bamboo columns under eccentric loading. Acta Materiae Compositae Sinica 33(2): 379-385.
23. Xiao,Y., Yang, R., Shan, B., et al., 2012: Experimental research on mechanical properties of glubam. Journal of Building Structures 33 (11):150-157.
24. Zhao, W.F., Gu, W., Zhou, J., Long, Z.L., 2016: Eccentric compression behavior of thin-walled steel-tube/bamboo-plywood assembling short hollow column with binding bars. Transactions of Chinese Society of Agricultural Engineering 15(32): 75-82.
25. Zhao, W.F., Yang, B., Zhou, J., 2019: Axial compressive creep behavior of a square steel tube/bamboo plywood composite column with binding bars. Wood Research, 64(2):2230-236.
26. Zhao, W.F., Luo, Z.J., Li, Y.J., 2020: Axial compression testing of bamboo-laminated encased steel tube composite columns. Iranian Journal of Science and Technology-Transactions of Civil Engineering 44(2): 645–655.
27. Zhang, Z.W., Li, Y.S., Liu, R., 2015: An analytical model of stresses in adhesive bonded interface between steel and bamboo plywood. International Journal of Solids and Structures 52: 103–113.
28. Zheng, D., Han, H., Hao, L., 2017: Influence of the amount of recycled dust on cement stabilized crushed stone base. Bulletin of the Chinese Ceramic Society 36(7): 2476-2480.

Weifeng zhao
Guangdong Construction Polytechnic
Guangzhou
China

Weifeng Zhao, Zongjian Luo, Yajun Li
Xiangtan University
College Of Civil Engineering And Mechanics
Xiangtan
China

Jing Zhou*
South China University Of Technology
Key Laboratory Of Subtropical Architecture Science
Guangzhou 510640
China
*Corresponding author: ctjzhou@scut.edu.cn

WOOD RESEARCH
e-ISSN 2729-8906
66(3):2021 505-516 pp.
doi.org/10.37763/wr.1336-4561/66.3.505516

EFFECT OF ADDITION OF DEINKED PULP TO BLEACHED KRAFT PULP ON TISSUE PAPER PROPERTIES

Monika Stankovská, Mária Fišerová, Juraj Gigac, Elena Opálená
Pulp And Paper Research Institute
Slovak Republic

(Received April 2020)

ABSTRACT

The influence of addition of deinked pulps with low and high brightness to bleached eucalyptus and pine kraft pulps on functional tissue paper properties was studied. Deinked pulps with low and high brightness had some different functional properties. Deinked pulp with high brightness has higher bulk, porosity, water absorption after immersion, initial water absorption, bulk softness as well as brightness. On the contrary, the difference in relative bonded area and porosity ε between deinked pulps with low and high brightness was moderate. The mixed pulps laboratory pulp sheets from bleached eucalyptus kraft pulp or bleached pine kraft pulp with addition of 20, 40 and 80% of deinked pulp with low brightness or deinked pulp with high brightness were prepared. The addition of the deinked pulp with high or low brightness to bleached kraft pulp leads to increasing of bulk, bulk softness as well as high water absorption after immersion and initial water absorption. The tensile index rapidly decreased by the addition of deinked pulps with high brightness to bleached eucalyptus and pine kraft pulps. Similarly, the addition of deinked pulp with low brightness to bleached pine kraft pulp led to rapid decreasing of tensile index. On contrary, with the addition of deinked pulp with low brightness to eucalyptus kraft pulp, the decreasing of tensile index was less pronounced. Mixed pulp from bleached eucalyptus kraft pulp with a small content of deinked pulp with low brightness with functional properties suitable for production of tissue papers was found as optimal.

KEYWORDS: Hardwood kraft pulp, softwood kraft pulp, deinked pulp, water absorption, tensile index, bulk softness, optical properties, tissue paper.

INTRODUCTION

Paper production from recycled fibres is environmentally friendly as it saves forests and at the same time eliminates the problem of its disposal. Recycled paper processing is becoming part of companies' environmental strategy. With the repeated use of recycled paper, the properties of paper change with the increase of the recycle number, especially the strength properties due to changes in the morphological structure of the fibres as well as due to interfibre bonding during beating and drying of pulp. Although the use of recycled fibres can significantly reduce the use of raw materials as well as energy consumption in tissue paper production, some toxic substances, such as mineral oils and heavy metals, remain in recycled fibres. When recycled fibres were used in food packaging materials, the contamination of food products was found (Biedermann et al. 2010, Sturaro et al. 2006). Another common practice is to add a fluorescent whitening agent to remove the negative effect of residual ink in the recycled fibres on the brightness of the paper, but fluorescent whitening agent is also toxic (Tirado et al. 2009). Therefore, the use of recycled fibres in the production of tissue paper poses a risk that customers may come into contact with these harmful substances.

Paper production and recycling processes lead to surface and volume changes of cellulosic fibres. The basic effects of recycling on pulp properties have already been presented in detail in works (Howard and Bichard 1992, Howard 1995). Recycled fibres have low swelling ability and wet flexibility, especially dried kraft fibres, which leads to a reduction in inter-fibre bonding and bonded area. Recycled fibres are shorter and have a higher content of fines than the virgin fibres (Hubbe et al. 2007, McKinney 1995). In addition, if kraft fibres are refined before drying during the production of paper, a further greater loss in fibre splicing is expected when the same fibres are recycled (Hubbe et al. 2007). The magnitude of the drying-induced strength loss of recycled fibres varies with the nature of the original fibre. Chemical pulps with very low lignin contents are more susceptible to loss of tensile or bonding strength than other types of pulp. Dry-fiberized newsprint pulp produces paper sheets of low strength due to shortened fibres and a loss of surface fibrillation. Minor and Atalla (1992) attempted to develop a new paper recycling process that required substantially less water than current processes and the water-intensive repulping where paper forming steps were replaced with dry-fiberizing, air-forming, gas-phase ozone and ammonia treatments, and press drying. In the case of mechanical pulps, the recycling process increases the collapse and flexibility of the fibres, leading to better fibre bonding and improved paper strength. It was illustrated (Scallan and Tigerstrom 1992) that high yield pulps such as thermomechanical (TMP) and chemi-thermomechanical pulp (CTMP) can recover the ability to take-up water following a drying treatment, while lower yield pulps cannot. Among the different types of mechanical pulps, CTMP pulp has a faster response to the recycling process than TMP pulp. CTMP pulp has lower fibre wall stiffness than other mechanical pulps (McKinney 1995).

Recycled fibres generally contribute to a reduction in bulk and surface softness compared to the original fibres. Recycled fibres are rigid and are unable to provide the required flexibility needed for good surface softness and strength. Although the recycling process reduces the fibre bonding capacity, recycled fibres have been previously refined and thus have a higher bonding capacity than unrefined fibres from hardwood, leading to a reduction in bulk softness (McKinney 1995). On the other hand, recycled fibres have lower swelling and are stiffer and more dimensionally stable; the results are papers with greater bulk and absorbency (McKinney 1995, Hubbe et al. 2007). Recycled fibres can potentially be used to reduce fibre bonding. Brightness of handsheets made from recycled pulps tested by Ali (Ali 2006) showed that it slightly increased

initially and then decreased with recycling where the initial increase in light reflectance may be attributed to the loss of fines changing the network structure of paper.

To improve the strength of recycled fibres, mechanical refining is a common approach used by paper manufacturers. However, the refining of recycled fibres must be considered carefully. Most recycled fibres have already been refined once, and recycled fibres are expected to be more susceptible to fragmentation than the virgin fibres. Refining of previously dried fibres leads only to a partial recovery of lost strength. Loss of bonding is observed even when recycled fibres are refined to the same degree of refining as they were before their first drying (McKinney 1995, Hubbe et al. 2007). It can be expected that the use of high intensity refining will increase the tensile strength of some fibres, but also increase the number of fines which leads to reduction of the dewatering rate. The using of high consistency refining can be considered as a better alternative as this refining will reduce the contact between the surface of the refiner and the fibres, where fibre fragmentation may occur (de Ruvo and Htun 1983). Another common approach to minimizing the limitations associated with recycled fibres is blending them with flexible and fibrillated virgin fibres. A high pH medium can also be used to restore the swelling and flexibility of the fibres, although this approach will cause significant delignification. Limitations in fibre bonding can also be overcome by the using of additives, e.g. cationic starch to wet end of a paper machine (McKinney 1995, Hubbe et al. 2007).

Improving strength properties of mixture from recycled and virgin fibres pulp is possible with the addition of dry strength agents (Gulsoy and Erenturk 2017). In order to improve the strength properties of recycled old corrugated carton pulp, various polymers as chitosan, cationic starch and polyvinyl alcohol (Hamzeh et al. 2013) as well as blending with virgin fibres of kenaf pulp (Latifah et al. 2009) were used. The bonding ability of borax might help in improving the strength properties of recycled paper from bleached softwood kraft pulp (Devisetti 1999). Restoring strength of recycled fibres from old cardboard, copy paper and newspaper by blending them with oil palm empty fruit bunch was studied (Rushdan 2003). Blending of recovered fibres with unbleached spruce pulp of 30% content showed also improvement of strength properties of paper handsheets (Fišerová et al. 2012).

The objective of the work was to determine the effect of blending of deinked pulps with bleached hardwood or softwood kraft pulp on functional properties of tissue paper.

MATERIAL AND METHODS

Materials

Bleached pine kraft pulp (Pine) – Södra Black was made from juvenile pine trees. Bleached eucalyptus kraft pulp (Eucalyptus) – Pontevedra was made from eucalyptus wood. Deinked pulp with low brightness 59.5% ISO (DIP LB) was prepared in Metsä Tissue Krapkowice mill from 57% of waste papers Group No. 1 "Ordinary grades", 38% of Group No.3 "High grades" according to EN 643: 2014 and 5% of cartons. Deinked pulp with high brightness 73,5% ISO (DIP HB) was prepared in Metsä Tissue Krapkowice mill from 80% of waste papers Group No. 3 "High grades" according to EN 643: 2014 and 20% of broke from production of hygienic paper from bleached pulp. The total lignin content in deinked pulp was 5.8%.

Methods

The bleached softwood and hardwood kraft pulps were beaten to 20°SR in a laboratory Jokro mill according to ISO 5264-3:1979. Low drainage resistance was chosen for pulps as pulp beating

markedly reduces water absorption, bulk softness and brightness (Fišerová et al. 2019). Bleached eucalyptus kraft pulp or bleached pine kraft pulp was mixed with 0, 20, 40 and 80% of deinked pulp with low brightness or deinked pulp with high brightness. The hand sheets (60 $g \cdot m^{-2}$) were prepared in the Rapid Köthen sheet former according to ISO 5269-2:2004.

Analysis

Porosity ε was calculated according to the equation given in literature (Daub et al. 1986). The bulk was calculated from the apparent bulk density determined according to ISO 534: 2012. *Water absorption* after immersion for time of 10 s was determined according to the standard ISO 5637: 1989.

Relative bonded area was calculated according to Equation 1 based on the light scattering coefficient S and S_0. The light scattering coefficient S ($m^2 \cdot kg^{-1}$) was measured on Elrepho 2000 colorimeter according to ISO 9416: 2017. The light scattering coefficient S_0 was evaluated from the linear dependence between the light scattering coefficient S and the tearing index where the light scattering coefficient S_0 was read when the tearing index was extrapolated to zero value. This method was described in work of Ingmanson and Thode (1979).

$$RBA = \frac{S_0 - S}{S_0} \times 100 \quad (\%) \tag{1}$$

where: S - light scattering coefficient for sheet ($m^2.kg^{-1}$) which was prepared in water and thus the interfibre bonds were formed, S_0 - light scattering coefficient of fibres in unbonded states.

Water penetration dynamics were measured by the ultrasound device PDA C.02 (Emtec, Radnor, PA, USA) with a frequency of 2 MHz. Water with a surface energy of 72 $mJ \cdot m^{-2}$ was used as the test liquid. Ultrasound signal intensity (USI) change was obtained at 43 ms - 60 s using the SC algorithm. The algorithm for calculating initial water absorption was designed from the USI drop in 200 ms. A more detailed description of this method as well as an evaluation process of the initial water absorption has already been published (Stankovská et al. 2019).

The tensile index was determined according to ISO 1924-2a (2008). *The bulk softness* was calculated from the bending stiffness determined at 15° and 10 mm distance between the clamp and the knife-edge according to TAPPI T 556 pm-95 method. *The brightness* was determined according to ISO 2470-1: 2016 and *colour coordinate b** according to ISO 5631-1: 2015.

RESULTS AND DISCUSSION

Porosity, bulk and water absorption of mixed pulps

The addition of deinked pulps to bleached kraft pulps results in an increase in porosity ε as shown in Fig.1a. Porosity of deinked pulps was higher than the bleached kraft pulps. By increasing the addition of deinked pulps, the porosity increased evenly. The addition of the deinked pulp with high brightness (full line) changes porosity more markedly than the addition of the deinked pulp with low brightness (dashed line). The bulk of pulp significantly influences the water absorption after immersion and initial water absorption (Stankovská et al. 2019) as well as softness (Morais et al. 2019) of pulp sheet. Deinked pulps had a higher bulk than the bleached kraft pulps. Deinked pulp with high brightness had a higher bulk than the deinked pulp with low brightness (Fig. 1b). Recycled fibres that have been dried in the past are stiffer and less flexible, which results in higher bulk; this is desirable for the production of tissue papers. The addition of deinked pulps to bleached kraft pulps increased significantly the bulk; the shape of the curves is very similar to the shape of the curves of porosity (Fig. 1a). The addition of deinked pulps to bleached

kraft pulps increased significantly the bulk; the shape of the curves is very similar to the shape of the porosity curves (Fig. 1a). As in the case of porosity, the addition of the deinked pulp with high brightness affected the change in bulk more significantly than the addition of the deinked pulp with low brightness.

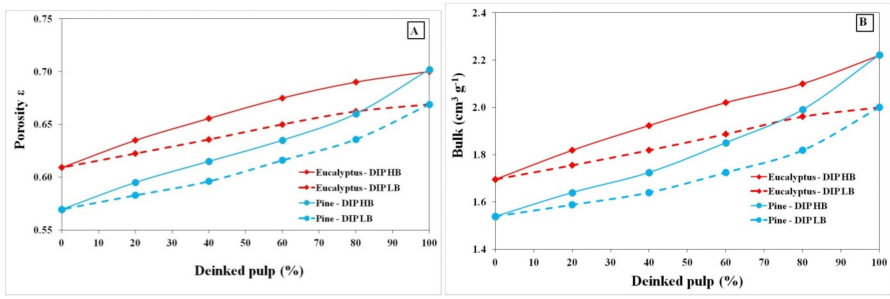

(a) (b)

Fig. 1: Influence of addition of deinked pulp with high brightness (DIP HB) or deinked pulp with low brightness (DIP LB) to bleached eucalyptus kraft pulp (eucalyptus) or to bleached pine kraft pulp (pine) on porosity (a), and bulk (b).

The effect of deinked pulps addition to bleached kraft pulps on the water absorption after immersion is shown in Fig. 2a. Deinked pulp with high brightness had significantly higher water absorption after immersion than deinked pulp with low brightness. The addition of deinked pulp with high brightness to bleached softwood or hardwood kraft pulp increased the water absorption after immersion significantly while the addition of deinked pulp with low brightness has less effect. The initial water absorption of the deinked pulps was significantly higher than the bleached kraft pulps (Fig. 2b). By comparison of deinked pulps, deinked pulp with high brightness had higher initial water absorption (455%) than that of low brightness (387%). With increasing addition of deinked pulps to bleached kraft pulps, the initial water absorption increased. The addition of deinked pulp with high brightness to bleached eucalyptus kraft pulp or bleached pine kraft pulp increased the initial water absorption very significantly, with bleached pine kraft pulp even up to 3-6-times. The addition of deinked pulp with low brightness to bleached pine kraft pulp also increased the initial water absorption significantly. The effect of addition of deinked kraft pulp with low brightness to bleached eucalyptus kraft pulp was less pronounced.

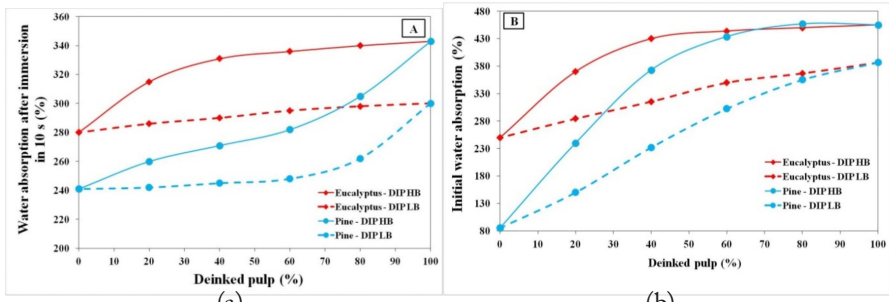

(a) (b)

Fig. 2: Influence of addition of deinked pulp with high brightness (DIP HB) or deinked pulp with low brightness (DIP LB) to bleached eucalyptus kraft pulp (eucalyptus) or to bleached pine kraft pulp (pine) on water absorption after immersion (a), and initial water absorption (b).

Relative bonded area of mixed pulps

The relative bonded area has proved to be suitable tools for prediction of initial water absorption of bleached softwood and hardwood kraft pulps (Stankovská et al. 2019). The relative bonded area between the two types of deinked pulps did not differ significantly (Fig. 3). The addition of deinked pulps to the bleached kraft pulps leads to decreasing of relative bonded area, as the recycled fibres are less flexible than virgin fibres.

With the addition of deinked pulps to bleached eucalyptus kraft pulp, the relative bonded area dropped significantly. The addition of deinked pulp to bleached pine kraft pulp led also to decreasing of relative bonded area, with the addition of 20% deinked pulp with low brightness decline was more moderate.

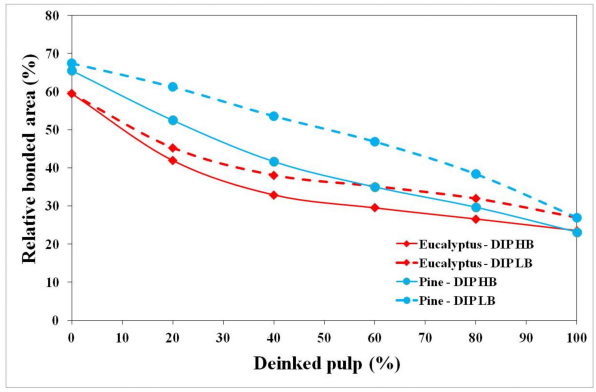

Fig. 3: Influence of addition of deinked pulp with high brightness (DIP HB) or deinked pulp with low brightness (DIP LB) to bleached eucalyptus kraft pulp (eucalyptus) or to bleached pine kraft pulp (pine) on relative bonded area.

A high correlation between the initial water absorption and relative bonded area of the mixture of deinked pulps with bleached eucalyptus and pine kraft pulps has been proven, as shown in Fig.4.

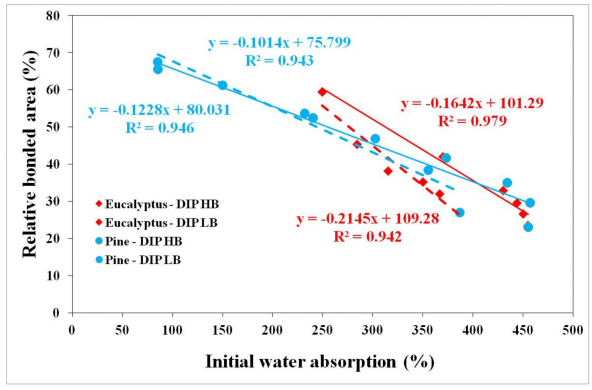

Fig. 4: The relationship between relative bonded area and initial water absorption of mixed pulps from deinked pulp with high brightness (DIP HB) or deinked pulp with low brightness (DIP LB) and bleached eucalyptus kraft pulp (eucalyptus) or bleached pine kraft pulp (pine).

Tensile index and bulk softness of mixed pulps

The effect of addition of deinked pulps with different brightness to bleached kraft pulps on the tensile index is shown in Fig. 5a. The tensile index of deinked pulps was significantly lower than that of bleached kraft pulps. Deinked pulp with high brightness had lower tensile index by 61% (23.2 $Nm \cdot g^{-1}$) than deinked pulp with low brightness (37.3 $Nm \cdot g^{-1}$).

The addition of deinked pulp with low brightness to bleached eucalyptus kraft pulp led to uniform decreasing of tensile index. In the case of addition of deinked pulp with high brightness to bleached eucalyptus kraft pulp, the effect on tensile index was more pronounced. As the content of deinked pulp with low brightness in the mixture with bleached pine kraft pulp increased, the tensile index decreased evenly within 12-43%. The addition of deinked pulp with high brightness to bleached pine kraft pulp led to significant and uneven decline of tensile index reduced by 51-64%. Decreasing of tensile index with addition of deinked pulp can be also significantly affected by the recycle number which may be linked to the reduced bonding ability of repeatedly recycled pulps (Ali 2006).

Deinked pulp with high brightness has higher bulk softness (2.0 $mN \cdot m^{-1}$) than deinked pulp with low brightness (1.85 $mN \cdot m^{-1}$). Both types of deinked pulps have higher bulk softness than bleached eucalyptus kraft pulp (1.39 $mN \cdot m^{-1}$) and bleached pine kraft pulp (1.49 $mN \cdot m^{-1}$). The addition of both types of deinked pulps to bleached pine kraft pulp significantly improved the bulk softness (Fig. 5b). The addition of 20-80% of both types of deinked pulps to bleached eucalyptus kraft pulp leads to increase in bulk softness by 3-33% (deinked pulp with low brightness), respectively by 6-44% (deinked pulps with high brightness). In case of 20-80% addition of both types of deinked pulps to bleached pine kraft pulp, there was an almost uniform increase of bulk softness from 5 to 20%.

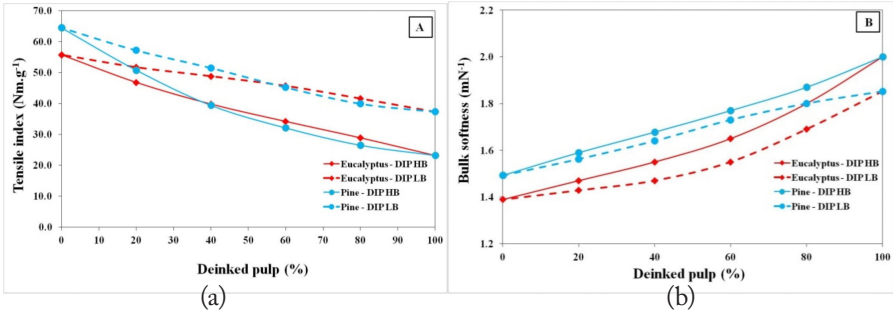

Fig. 5: Influence of addition of deinked pulp with high brightness (DIP HB) or deinked pulp with low brightness (DIP LB) to bleached eucalyptus kraft pulp (eucalyptus) or to bleached pine kraft pulp (pine) on tensile index (a), and bulk softness (b).

Optical properties of mixed pulps

The effect of the addition of deinked pulps to bleached kraft pulps on brightness has been shown to be more pronounced for deinked pulps with low brightness and the shape of the curves is almost identical for bleached eucalyptus and pine kraft pulp (Fig. 6a). With increased addition of deinked pulp with low brightness to bleached pine and eucalyptus kraft pulps, the brightness decreased by 14-28% (pine) and 11-26% (eucalyptus). The effect of deinked pulp addition with higher brightness to bleached eucalyptus and pine kraft pulp was similar, resulted in declination by 5-17%.

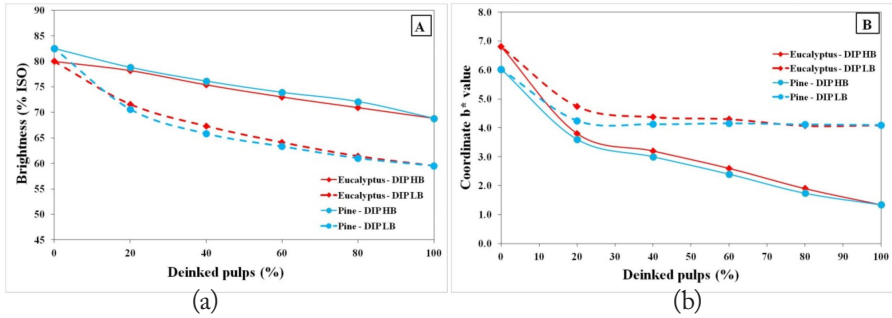

(a) (b)

Fig. 6: Influence of addition of deinked pulp with high brightness (DIP HB) or deinked pulp with low brightness (DIP LB) to bleached eucalyptus kraft pulp (Eucalyptus) or to bleached pine kraft pulp (Pine) on brightness (a), and coordinate b (b).*

Fig. 6b shows the effect of addition of deinked pulps to bleached pine and eucalyptus kraft pulps on the b* coordinate value, which indicates the yellowness of the pulp sheets. The coordinate b* value of bleached eucalyptus kraft pulp is higher (6.80) than that of bleached pine kraft pulp (6.02). There is a significant difference for deinked pulp with different brightness, when fibres with lower brightness were used, a 3-fold higher coordinate b* value was obtained than with using of deinked pulp with higher brightness. The shape of the curves of the dependence of the coordinate b* on the content of deinked pulps with high brightness in the mixture of bleached pine and eucalyptus kraft pulp is identical. With addition of 20% of deinked pulps with high brightness to bleached pine and eucalyptus kraft pulp, the coordinate b* value decreased rapidly. When using of deinked pulps with low brightness, the significant decrease of the coordinate b* value occurred only with addition of 20% and further additions had no more effect.

CONCLUSIONS

Deinked pulp with high brightness had a higher bulk, air permeability, water absorption after immersion, initial water absorption and bulk softness of the pulp sheet than deinked pulp with low brightness. However, the relative bonded area did not differ significantly. The tensile index of deinked pulp with low brightness was higher by 38%. The addition of deinked pulp with low and high brightness to bleached eucalyptus or pine kraft pulp significantly increased the bulk, volume softness as well as the water absorption after immersion and the initial water absorption. The initial water absorption well correlated with relative bonded area of the mixture of deinked pulps with bleached eucalyptus and pine kraft pulps. The addition of deinked pulps to bleached kraft pulp led to decreasing of tensile index. However, in the case of addition of deinked pulps with low brightness to bleached eucalyptus kraft pulp, the declining slope of the curve is less pronounced. The suitability of using deinked pulp for tissue paper was demonstrated when blending of bleached eucalyptus kraft pulp with a 20% addition of deinked pulp with low brightness. By this way, bulk softness and water absorption after immersion increased and tensile index almost unchanged when compared to bleached eucalyptus kraft pulp, and in addition, initial water absorption significantly improved. This type of mixed pulp could be used for the production of tissue products where very high softness and brightness is not required whereas, on the other hand, these papers could have a higher yellowness.

ACKNOWLEDGMENT

This publication is the result of the project implementation: Centre of Excellence of Forest-based Industry, ITMS: 313011S735) supported by the Research & Development Operational Programme funded by the ERDF.

REFERENCES

1. Ali, I., 2012: Study of the mechanical behavior of recycled fibers. Applications to papers and paperboards. Doctoral thesis. Pp 1-241. Université de Grenoble.
2. Biedermann, M., Grob, K., 2010: Is recycled newspaper suitable for food contact materials? Technical grade mineral oils from printing inks. European Food Research and Technology 230(5): 785- 796.
3. Daub, E., Sindel, H., Göttsching, L., 1986: Absorption von Flüssigkeiten in Papier. Das Papier 40(5): 188-197.
4. Devisetti, S.K., 1999: Borax as a strength additive in recycling. Master's Theses 4936. Pp 1-69, Faculty of The Graduate College, Department of Paper and Printing Science and Engineering, Western Michigan University, USA.
5. Fišerová, M., Illa, A., Boháček, Š., Kasajová, M., 2012: Handsheet properties of recovered and virgin fibre blends. Wood Research 58(1): 57-66.
6. Gülsoy, S.K., Erenturk, S., 2017: Improving strength properties of recycled and virgin pulp mixtures with dry strength agents. Starch 69(3-4): 1600035.
7. Hamzeh, Y., Sabbaghi, S., Ashori, A., Abdulkhani, A., Soltan, F., 2013: Improving wet and dry strength properties of recycled old corrugated carton (OCC) pulp using various polymers. Carbohydrate Polymers 94: 577-583.
8. Howard, R.C., Bichard, W., 1992: The basic effects of recycling on pulp properties. Journal of Pulp and Paper Science 18(4): J151-J159.
9. Howard, R.C., 1995: The effects of recycling on pulp quality. In Technology of Paper Recycling Ed. McKinney R.W.J. Pp.180-203, Chapter 6. Blackie Academic & Professional, New York.
10. Hubbe, M.A., 2006: Bonding between cellulosic fibers in the absence and presence of dry strength agents. A review. BioResources 1(2): 281-318.
11. Ingmanson, W.L., Thode, F.T., 1959: Factors contributing to the strength of the sheet of paper. II. Relative bond area. Tappi 42(1): 83-93.
12. STN EN ISO 534: 2012: Paper and board. Determination of thickness, density and specific volume.
13. STN EN ISO 536: 2012: Paper and board. Determination of grammage.
14. ISO 1924-2: 2008: Paper and board. Determination of tensile properties. Part 2: Constant rate of elongation method (20 mm/min).
15. ISO 2470-1: 2016: Paper, board and pulps. Measurement of diffuse blue reflectance factor. Part 1: Indoor daylight conditions (ISO brightness).
16. ISO 5264-3: 1979: Pulps. Laboratory beating. Part 3: Jokro mill method.
17. ISO 5269-2: 2004: Pulps. Preparation of laboratory sheets for physical testing. Part 2: Rapid-Köthen method.
18. ISO 5631-1: 2015: Paper and board. Determination of colour by diffuse reflectance. Part 1: Indoor daylight conditions (C/2 degrees).

19. ISO 5636-5: 2013: Paper and board: Determination of air permeance (medium range) - Part 5: Gurley method.
20. ISO 5637: 1989: Paper and board. Determination of water absorption after immersion in water.
21. ISO 9416: 2017: Paper. Determination of light scattering and absorption coefficients (using Kubelka-Munk theory).
22. Latifah, J., Ainun, Z.M.A., Rushdan, I., Mahmudin, S., 2009: Restoring strength to recycled fibres by blending with kenaf pulp. Malaysian Journal of Science 28(1): 79-87.
23. McKinney, R.W.J., 1995: Technology of paper recycling. Pp 1-401, First Ed., Blackie Academic& Professional, Glasgow.
24. Minor, J.L., Atalla, R.H., 1992: Symposium LA – Materials interactions relevant to recycling of wood-based materials 266. Pp 215-228, TAPPI, Atlanta.
25. Morais, F.P., Bértolo, R.A.C., Curto, J.M.R., Amaral, M.E.C.C., Carta, A.M.M.S., Evtyugin, D.V., 2019: Comparative characterization of eucalyptus fibers and softwood fibers for tissue papers applications. Materials Letters: X4: 100028-100032.
26. Rushdan, I., 2003: Structural, mechanical and optical properties of recycled paper blended with oil palm empty fruit bunch pulp. Journal of Oil Palm Bulletin 15(2): 29-36.
27. Ruvo, A.D., Htun, M.,1983: Fundamental and practical aspects of paper-making with recycled fibers. In: The role of fundamental research in paper making, J. Brander (ed.), Vol. 1. Pp 195-225, Mechanical Engineering Pub., Ltd., London.
28. Scallan, A.M., Tigerstrom, A.C., 1992: Swelling and elasticity of the cell walls of pulp fibers. Journal of Pulp and Paper Science 18(5): 188-193.
29. Stankovská, M., Gigac, J., Fišerová, M., Opálená, E., 2019: Relationship between structural parameters and water absorption of bleached softwood and hardwood kraft pulps. Wood Research 64(2): 261-272.
30. Sturaro, A., Rella, B., Parvoli, G., Ferrara, D., Tisato, F., 2006: Contamination of dry foods with trimethyldiphenylmethanes by migration from recycled paper and board packaging. Journal of Food Additives and Contaminants 23(4): 431-436.
31. TAPPI T 556-95 pm method, 1995: Bending resistance of paper and paperboard (Lorentzen and Wettre type tester).
32. Tirado, L.B.M., Area, M.C., Velez, H.E., 2009: Optimizing alkaline sizing in sugar cane bagasse paper recycling. Cellulose Chemistry and Technology 43(4-6): 179-187.

Monika Stankovská*, Mária Fišerová, Juraj Gigac, Elena Opálená
Pulp And Paper Research Institute
Dúbravská cesta 14
841 04 Bratislava
Slovak republic
*Corresponding author: stankovska@vupc.sk